Predicting Activation Barrier, Reduction Potential and Fluorescence using Molecular Electrostatic Potential: Organic and Organometallic Systems

Thesis Submitted to AcSIR for the Award of the Degree of
DOCTOR OF PHILOSOPHY
in Chemical Sciences

AcSIR

By
Anjali B.
Registration No: 10CC14J39001

Under the Guidance of
Dr. C. H. Suresh

Chemical Sciences and Technology Division
CSIR-National Institute for Interdisciplinary Science and Technology
Thiruvananthapuram-695019, Kerala, India

January 2019

DECLARATION

I hereby declare that the Ph. D. thesis entitled "**Predicting Activation Barrier, Reduction Potential and Fluorescence using Molecular Electrostatic Potential: Organic and Organometallic Systems**" is an original work carried out by me at Chemical Sciences and Technology Division(CSTD), CSIR-National Institute for Interdisciplinary Science and Technology (CSIR-NIIST), Thiruvananthapuram, under the supervision of Dr. C. H. Suresh, Principal Scientist, CSTD, CSIR-NIIST, and it has not been submitted elsewhere for any other degree, diploma or title.

CSIR-NIIST

07/01/2019

Anjali B.

i

Council of Scientific & Industrial Research
National Institute for Interdisciplinary Science and Technology
Thiruvananthapuram-695019, Kerala, India

Dr. C. H. Suresh
Principal Scientist
Chemical Sciences & Technology Division
Tel: +91- 4712515472
E-mail: sureshch@gmail.com
sureshch@niist.res.in

7th January 2019

CERTIFICATE

This is to certify that the work incorporated in this Ph. D. thesis entitled "**Predicting Activation Barrier, Reduction Potential and Fluorescence using Molecular Electrostatic Potential: Organic and Organometallic Systems**" submitted by Ms. Anjali B. to Academy of Scientific and Innovative Research (AcSIR) in fulfillment of the requirements for the award of the Degree of Doctor of Philosophy, embodies original research work done under my supervision. I further certify that this work has not been submitted to any other University or Institution in part or full for the award of any degree or diploma. Research material obtained from other sources has been duly acknowledged in the thesis. Any text, illustration, table, etc. used in the thesis from other sources, have been duly cited and acknowledged.

Anjali B.

(Student)

Dr. C. H. Suresh

(Thesis Supervisor)

Acknowledgments

I would like to extend my heartfelt gratitude to all who have contributed directly or indirectly for the successful completion of my Ph. D thesis.

First of all, I would like to express my deep gratitude towards Dr. C. H. Suresh, research supervisor, for suggesting me an excellent research topic and providing fruitful guidance throughout my Ph. D. work. I admire his intelligence and wisdom, and I strongly motivated by his ability and enthusiasm in scientific and non-scientific endeavours. I am thankful that he has created a beautiful research environment with all the necessary computational facilities.

I would like to express my sincere gratitude to Dr. A. Ajayaghosh, Director, CSIR-NIIST, and former directors, Dr. Suresh Das and Dr. Gangan Pratap for providing the necessary facilities for carrying out my research in this institution.

I am extremely thankful to Dr. R. Luxmi Varma, Head, Chemical Sciences and Technology Division and AcSIR coordinator for her insightful comments and encouragement. She has been available throughout with continued patience and endless support. I also extend my sincere thanks to former HOD Dr. K. R. Gopidas and former AcSIR coordinator Dr. Mangalam S. Nair for all their support and guidance. I must acknowledge that the supportive and friendly nature of both the AcSIR coordinators made the academic procedures easy.

I am grateful to my Doctoral Advisory Committee members, Dr. K. V. Radhakrishnan, Dr. K. K. Maiti, and Dr. Boje Gowd for their valuable suggestions and guidance throughout my Ph. D. work.

I would like to extend my heartfelt gratitude to all the former members of our research group, Dr. Sandhya, Dr. Neetha, Dr. Prabha, Mr. Shyam, Dr. Remya K., Dr. Renjith, Dr. Remya P. R., and Dr. Della for their friendship, timely advice and support. I am thankful to all the present members of our group Rakhi, Remya G. S., Bijina, Divya, Anila and Anjali for all their help, affection and warm friendship.

I am grateful to all my friends, scientific and non-scientific staff at CSIR-NIIST. A special thanks to all the scientists who have taken the AcSIR classes.

I am extremely thankful to my parents, M. Kumaran and E. V. Amutha Bai for being strong pillars in my life. I am thankful to my sister Aswathi, my little guardian; she has been fondly checking whether I am getting fellowship on time, and meeting all my needs throughout my research period.

Words may not be sufficient to describe the care and affection my better half, Anuraj has showered on me. He is always so keen about my well-being and extends every possible support that he can.

I owe my deepest gratitude to all my family members, especially to my mother in law, Usha and to my brother in laws Akhil and Sreeraj for their affection, care and support. I gratefully acknowledge my teachers and friends for their inspiration and support.

I am thankful for this beautiful life.

Thank you all !!

Anjali

CONTENTS

Chapter 1

Introduction

Part A: Molecular Reactivity Descriptors

Part B: Computational Chemistry Methods

Chapter 2

Part A: Predicting Reduction Potentials of Mononuclear Cobalt Catalysts using MESP

Part B: Absorption and Emission Properties of 5-Phenyl Substituted Tris(8hydroxyquinolinato) M(III) Complexes (M = Al, Ga, In) and Correlations with MESP

Chapter 4

Interpreting Oxidative Addition of Ph-X (X = CH$_3$, F, Cl, Br) to Monoligated Pd (0) Catalysts using MESP

List of Figures

B3P86/6-311+G** level of theory.

List of Schemes

List of Tables

List of Abbreviations

AMBER   : Assisted Model Building with Energy Refinement

AO   : Atomic Orbitals

BO   : Born Oppenheimer

CASSCF   : Complete Active Space Self Consistent Field

CBS   : Complete Basis Set

CC   : Coupled Cluster

CPMD   : Car Parrinello Molecular Dynamics

CG   : Contracted Gaussian

CGTO   : Contracted Gaussian-Type Orbitals

CHARMM   : Chemistry at Harvard Macromolecular Mechanics

CI   : Configuration Interaction

CNDO   : Complete Neglect of Differential Overlap

CP   : Critical Point

DFT   : Density Functional Theory

DZ   : Double-Zeta

ECP   : Effective Core Potential

FMO   : Frontier Molecular Orbital

GGA   : Generalized Gradient Approximation

GROMACS   : Groningen Machine for Chemical Simulations

GROMOS   : Groningen Molecular Simulation

GTOs   : Gaussian Type Orbitals

HSAB   : Hard and Soft Acids and Bases

HF   : Hartree-Fock

INDO   : Intermediate Neglect of Differential Overlap

LDA   : Local Density Approximation

LSDA   : Local Spin Density Approximation

MCSCF   : Multi Configurational Self Consistent Field

MD   : Molecular Dynamics

MESP   : Molecular Electrostatic Potential

MM   : Molecular Mechanics

MP   : Moller-Plesset Perturbation

MRCI   : Multiconfiguration Reference Configuration Interaction

NDO   : Neglect of Differential Overlap

NDDO   : Neglect of Diatomic Differential Overlap

PCM   : Polarizable Continuum Model

PES   : Potential Energy Surface

PGTO   : Primitive Gaussian-type Orbital

QM   : Quantum Mechanics

QSAR   : Quantitative Structure Activity Relationship

QZ   : Quadruple-Zeta

RHF   : Restricted Hartree-Fock

SCF   : Self Consistent Field

STOs   : Slater-Type Orbitals

SCRF   : Self Consistent Reaction Field

SMD   : Solvation Model Density

TDDFT   : Time Dependent Density Functional Theory

TZ   : Triple-Zeta

ZDO   : Zero Differential Overlap

PREFACE

Chemical reactivity prediction with the help of computational chemistry is an important area of research. Reactivity descriptors or the reactivity indices are helpful in predicting the perturbations, which stabilize or destabilize the molecule. Electronegativity, electrophilicity index, hardness, etc. are the common reactivity descriptors. These reactivity descriptors are useful in foreseeing the chemical reactivities of the molecule. The molecular electrostatic potential (MESP) is a powerful descriptor of chemical reactivity. MESP is experimentally observable; which makes it unique and advantageous over other reactivity descriptors such as electronegativity. The works of Tomasi, Pullman, Politzer, and Gadre have pioneered the use of the theoretically derived MESP to understand molecular reactivity. The works of Wheeler and Houk have also contributed to the growth in this area; whereas a greater part of MESP based reactivity analysis is limited to small organic molecules. The major objective of the thesis is to computationally predict and tune reactivity parameters such as activation barrier and reduction potential of industrially relevant organic and organometallic systems and to find their relationship with MESP. The thesis consists of MESP based investigation using density functional theory (DFT). The absorbance and fluorescence properties have also been studied using time-dependent density functional theory (TDDFT). The thesis is divided into four chapters.

The first part of **Chapter 1** provides a brief account of reactivity descriptors and an overview of the literature in MESP. An overview of various computational methodologies is presented in the **Part B** of **Chapter 1**.

Chapter 2 is divided into two parts. **Part A** discusses the correlation and prediction of reduction potentials (E^0) of hydrogen evolution mononuclear cobalt electrocatalysts with the use of molecular electrostatic potential (MESP). The selected complexes are designated as **1-X**, **[2-X]$^{2+}$**, **3-X**, **[4-X]$^{3+}$**, **[5-X]$^{3+}$**, and **6-X.** The electron donating/withdrawing effect of various substituents *viz*. CH_3, CN, CF_3, Cl, H, F, OCH_3, OH, and NH_2 on the tetraazamacrocycle to modulate E^0 is reported at solvation effect-included B3P86/6-311+G** level of density functional theory. A strong linear

correlation between the electrostatic potential at the Co nucleus (V_{Co}) and E^0 is observed for all the complexes and the correlation coefficients (r) for **1-X**, **[2-X]$^{2+}$**, **3-X**, **[4-X]$^{3+}$**, **[5-X]$^{3+}$**, and **6-X** are 0.961, 0.978, 0.968, 0.965, 0.967, and 0.980 respectively. The correlation plots between V_{Co} and E^0 provide an easy-to-interpret graphical interpretation and quantification of the effect of ligand environment on the reduction potential. Among all the complexes, **1-X** is found to be the most unique due to its two –O-BF$_2$-O– bridges to make the macrocyclic N-to-N connectivity. In **Part-B** of **Chapter 2**, a systematic investigation on the reduction potentials (E^0) of a large variety of Fischer carbene complexes (FCCs) of chromium using the B3LYP density functional theory has been carried out. The change in *electronic effect of ligands* (*eeL*) is quantified using topographical features of the MESP. The MESP at the chromium centre (V_{Cr}) showed a clear linear dependency with E^0. The change in reduction potential (ΔE^0) due to variations in ligand environment is found to be directly proportional to change in the *eeL* measured as ΔV_{Cr}. In the neutral form, electron density is localized more towards the carbonyl oxygen while its carbene carbon shows electron deficiency. In general, the reduced system shows very high negative MESP than a neutral molecule due to the dominance of the electronic term over the nuclear term. For instance, for a representative system in its neutral form, V_{min} -36.2 kcal/mol is observed at the carbonyl group positioned *trans* with respect to the carbene ligand whereas V_{min} -109.0 kcal/mol observed for its reduced form, almost 3 times more negative than the neutral. This observation holds good for all the reduced systems studied.

Part A of **Chapter 3** discusses the influence of mono- and multiple substituent effect on the reduction potential (E^0) of 1,3,6-triphenyl fulvenes. The MESP minimum at the fulvene π-system (V_{min}) and the change in MESP at any of the fulvene carbon atoms (ΔV_C) for both neutral and reduced forms are used as excellent measures of substituent effect from the *para* and *meta* positions of the 1-phenyl, 3-phenyl, and 6-phenyl moieties. Substitution at 6-phenyl *para* position has led to significant change in E^0 than any other positions. By applying the additivity rule of substituent effects, an equation in ΔV_C is derived to predict E^0 for multiply substituted fulvenes. Further, E^0 is predicted for a set of 2000 hexa-substituted fulvene derivatives where the substituents and their

positions in the system are chosen in a random way. **Part B** of **Chapter 3** discusses the absorption maximum (λ_{abs}) and fluorescence maximum (λ_F) of a series of tris (8-hydroxyquinolinato) M(III) complexes of aluminium, gallium and indium (abbreviated as Mq3). A good linear correlation with experimental fluorescence values calculated using fluorescence spectroscopy with that of time-dependent density functional theory (TDDFT) calculated values is observed. The effect of different substituents *viz*. NMe$_2$, NH$_2$, OH, OCH$_3$, F, H, Cl, OCF$_3$, CHO, COOMe, COMe, CF$_3$, CN on the phenyl ring of ***mer-Mq3-R*** complexes are examined. Substituent effect is found to be predominant in λ_F values whereas the effect is subsidiary in λ_{abs} values. By changing the metal from Al to In, a gradual red-shift in λ_F values is observed. The V_{min} and the electrostatic potential at the metal centre (V_M) exhibit excellent correlations with the λ_F and Stokes shift (λ_F -λ_{abs}) values.

In organometallic complexes, metal center plays the pivotal role in executing a reaction and a single parameter that explains the reactivity of the metal center is yet to be established with respect to a correlation with the activation barrier of the reaction. Further, the question of how the selectivity of a ligand influences the performance of the metal center in the rate-determining step of a reaction remains unanswered. Thus, in **Chapter 4**, we provide a mechanistic interpretation of the oxidative addition of aryl halides to Pd(0) solely based on the MESP at the Pd center which undergoes delicate changes with respect to changes in ligand environment. The chapter discusses the B3LYP density functional theory (DFT) study on the oxidative addition of halogenobenzenes and toluene to monoligated zerovalent palladium catalysts (Pd-L) using the 'L' ligands phosphines, N-heterocyclic carbenes (NHC), alkynes, and alkenes. The electron deficiency of the under-coordinated Pd in Pd-L is quantified in terms of MESP at the metal center (V_{Pd}) which showed significant variation with respect to the nature of the L ligand. Further, a strong linear correlation between ΔV_{Pd} and the activation barrier (E_{act}) of the reaction is established. The correlation plots between ΔV_{Pd} and E_{act} suggests that a priori prediction on the ability of the palladium complex to undergo oxidative addition is possible from V_{Pd} analysis. In general, as the electron donating nature of ligand increases, the suitability of Pd(0) catalyst to undergo

oxidative addition increases. V_{Pd} measures the electron rich/deficient nature of the metal center and provides a quantitative measure of the reactivity of the catalyst. The E_{act} of oxidative addition of substrates follows the order PhF ≈ Ph-Me >> Ph-Cl > Ph-Br. Compared to the strong C-C and C-F bonds, the weaker C-Cl and C-Br bonds cleave with significantly less energy.

Chapter 1

Introduction

Part A

Molecular Reactivity Descriptors

Part B

Computational Chemistry Methods

Part A: Molecular Reactivity Descriptors

1.1 An Overview of Molecular Reactivity Descriptors

Predicting chemical reactivities and understanding how and why they occur is of paramount importance in chemistry.[1-9] The reactivity of different reaction sites within a molecule or the reactivity difference of a single reaction center in the presence of altered substituents or reactants is evaluated using the reactivity indices or reactivity descriptors.[10] The reactivity descriptors furnish an easy way to predict the perturbations which stabilize and destabilize the molecule and in turn, aid to forsee the chemical reactivities of the molecule.[11] The performance and predictive power of the theoretically evaluated reactivity indices can not only be assessed with the direct comparison of theoretically determined parameters but also with appropriate experimental results.

A branch of density functional theory (DFT), termed as "conceptual DFT" by its founding father R. G. Parr, provide qualitative insights into chemical reactivity (thus often known as chemical reactivity theory of DFT). It has been developed since the late 1970s and early 1980s and gives a precise definition to often well known but rather imprecisely defined chemical concepts with the use of electron density relevant concepts and principles.[12,13] DFT based reactivity descriptors are mainly classified as global and local reactivity descriptors. Global reactivity descriptors measure the overall reactivity of a molecule whereas the local reactivity descriptors provide information about the relative reactivities of different sites within a molecule. Some of the global reactivity descriptors are electronegativity, global hardness and softness, electronic chemical potential, electrophilicity index etc. and the local reactivity descriptors include Fukui function, local hardness, local softness etc. Conceptual DFT extends the existing descriptors and use them either as such or within the context of principles such as Sanderson's electronegativity equalization principle, the hard and soft acids and bases (HSAB) principle, and the maximum hardness principle. The reactivity indices are

2

defined based on the functional derivatives of the total electronic energy to the total number of electrons or the external potential.

Conceptual DFT has been effectively used for a better understanding of the nature of aromaticity,[14-16] the intra and intermolecular reactivity,[17-22] regioselectivity,[11,23-33] electrophilicity, and nucleophilicity of organic reactions,[19,21,34-37] and prediction of the reactive site of various molecular systems.[38] It has been invoked to comprehend the reactivities of a large variety of chemical and biological systems.[39-43] The works of Geerling *et al.*[16,30,36,44-52] significantly contributed in this area and since 1980s, an avalanche of papers investigating and utilizing the capacity of conceptual DFT has been appeared in literature.[7,25,31,53,54]

The first partial derivative of energy, E with respect to the number of electrons N under constant external potential $v(\mathbf{r})$ is defined as the chemical potential, μ for a system.[12] The relation of electronegativity (χ) with the the chemical potential (μ) is given in Eq. 1.1. The chemical potential is the escaping tendency of electrons from the system, whereas the electronegativity measures the tendency of the system to attract electrons.

$$\mu = \left(\frac{\partial E}{\partial N}\right)_{v(\mathbf{r})} = -\chi \qquad \text{(Eq. 1.1)}$$

Second order response functions, shown in Eq. 1.2 and Eq. 1.3, are related to the concepts of absolute hardness (η)[55] and the Fukui function, $f(\mathbf{r})$, respectively,

$$\left(\frac{\partial^2 E}{\partial N^2}\right)_{v(\mathbf{r})} = \left(\frac{\partial \mu}{\partial N}\right)_{v(\mathbf{r})} = \eta \qquad \text{(Eq. 1.2)}$$

$$\left(\frac{\partial^2 E}{\partial v(\mathbf{r})\partial N}\right) = \left(\frac{\partial \rho(\mathbf{r})}{\partial N}\right) = f(\mathbf{r}) \qquad \text{(Eq. 1.3)}$$

Local reactivity descriptors contain exactly one differentiation with respect to the external potential. The Fukui function, $f(\mathbf{r})$ is one of the widely used local reactivity descriptors[56] (Eq. 1.3) which quantifies the site selectivity of a reaction. The higher the Fukui function, the softer is the center and lower is the electron localization or the lower is the "resistance" of the electron density to fluctuate from/toward this

center.[33,56,57] Coefficients that contain exactly two or more differentiations with respect to the external potential are called nonlocal reactivity descriptors or reactivity kernels. Nonlocal reactivity descriptors either measure a molecule's polarization with respect to its environment or the change in polarization associated with electron transfer. Nonlocal indices include softness kernel and hardness kernel.[27,53] A brief account of some of the well-known reactivity descriptors such as electronegativity, hardness and softness, electrophilicity index, and the frontier molecular orbital theory is provided.

1.1.1. Electronegativity

The concept of electronegativity is considered almost as old as chemistry whereas an accurate scale of measuring electronegativity (χ) was first introduced by Linus Pauling in 1932.[58-61] Electronegativity is defined as "the power of an atom when in a molecule to attract electrons to itself" by Pauling and it has been used to account molecular processes such as bond formation, electron transfer processes etc. Pauling scale is based on bond dissociation energy calculations of different elements joined by covalent bonds.[62] In 1934, Mulliken proposed electronegativity as an arithmetic average of ionization energy and electron affinity.[63] Other popular electronegativity scales are proposed by Allred-Rochow[64,65] (based on the electrostatic force of attraction between the nucleus and the valence electrons), Allen[66] (based on the average one-electron energy of the valence shell electrons in the ground-state free atoms), Sanderson[67] (a modification of Pauling scale), and Gordy's electrostatic potential scale[68,69] of electronegativity.[59] The works of Iczkowski and Margrave have also given a firm theoretical background and a precise definition to the chemical concepts of electronegativity.[70]

There have been several other intense theoretical works[71-74] which introduced alternative ways to calculate electronegativity. Suresh and Koga,[75] demonstrated an approach where a consistent set of atomic electronegativities of main block and d-block transition elements was derived from the position and value of the molecular electrostatic potential bond critical point of the C-E bond of a methyl-element-hydride system, H_3C-EH_n (E is an element and n = 0, 1, 2, 3, 4, and 5 depending on the position of

E in the periodic table) which exhibited very good agreement with the other popular electronegativity scales. In practice, most modern-day studies use Mulliken's scale of electronegativity.[7] Though electronegativity is an empirical concept that has proven to be very helpful in the context of chemical reactive behaviour, it is not a physical observable.[70] A recent study by Onoda *et al*. attempted the electronegativity determination of individual surface atoms by atomic force microscopy.[76]

1.1.2 Hardness and Softness

The concepts of chemical hardness (η) and softness (S) were introduced in the early 1960s by Pearson, while comparing the stabilities of the reaction products of generalized Lewis acid-base reactions.[77] Pearson made a classification of Lewis acids and bases as hard and soft which is known as his famous hard and soft acids and bases (HSAB) principle, stating that the hard acids prefer to interact with hard bases and similarly soft acids prefer to react with soft bases.[61,77-81] Based on experimental data, Pearson made a classification of Lewis acids in to two groups; class 'a' and class 'b', the acids in class 'a' consist of positively charged small volume acceptor atoms such as H^+, Li^+, Na^+, and Mg^{2+} whereas class 'b' acids consist of acceptor atoms of greater volume such as Cs^+, and Cu^+. The donor atoms of the Lewis bases in terms of increasing electronegativity are given below:

$$As < P < Se < S \sim I \sim C < Br < Cl < N < O < F$$
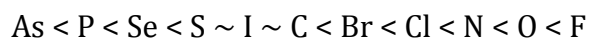
The criterion used was that Lewis acids of class 'a' would form stabler complexes with donor atoms to the right of the series, whereas those of class 'b' would preferably interact with the donor atoms to the left. This classification turns out to be essentially polarizability based, the hardness describes systems of low polarizability, high electronegativity, and that are difficult to oxidize and softness refers to systems of the exact opposite characteristics: high polarizability, low electronegativity, and easily oxidizable. A quantitative treatment was hampered for a long while because of a shortage for quantifying hardness and softness. A breakthrough was reached in Parr and Pearson's seminal work.[55] The work considered chemical hardness as the

difference between the ionization energy (I) and electron affinity (A) of a species in the same spirit as the contribution by Parr and co-workers on the identification of the electronegativity as the negative of the electronic chemical potential. By this means, both the experimental determination and its quantum chemical evaluation have been made possible. Parr, Lee, and Chattaraj[82] presented evidence for the HSAB principle, a more detailed treatment being presented later by Gázquez and Méndez.[83] The hardness is considered as a resistance to charge transfer, while the softness measures the ease of transfer. A local version of the HSAB principle, proposed by Gázquez and Méndez[84] is an alternative description of reactivity using local descriptors. However, it involves the descriptors of both the reacting systems for predicting the reactive sites. This issue and the feasibility of the local HSAB principle have been studied in part by Pal and co-workers,[85] Geerlings and co-workers,[23,86] and Ngyuen and co-workers.[86-89]

1.1.3 Electrophilicity Index

The electrophilicity index (ω), introduced by Parr *et al.*[87] provides the quantitative classification of the global electrophilic nature of a molecule within a relative scale. ω gives insight into the structure, properties, stability, reactivity, interactions, bonding, toxicity, and dynamics of many electron systems in ground and excited electronic states.[88,89] It measures the stabilization in energy when the system acquires an additional electronic charge from the environment. The works of Maynard *et al.*[90] have formed strong foundation for the electrophilicity index, which provided the direct relationship between the rates of reaction and the ability to identify the function or capacity of an electrophile and the electrophilic power of the inhibitors. Chattaraj *et al.* investigated the kinetic and thermodynamic aspects of ω by correlating it with the relative experimental rates of various reactions.[91] A thorough discussion, aided by analytical reasoning, on the thermodynamic and kinetic aspects of ω is provided by Bagaria and Roy.[92] The electrophilic nature of Fischer carbene complexes have been investigated by Frenking *et al.*[93]

ω can be expressed as,

$$\omega = \frac{\mu^2}{2\eta} \qquad\qquad\qquad \text{(Eq. 1.4)}$$

where μ is the chemical potential and η is the hardness. Chemical potential and hardness can be calculated from the HOMO and LUMO orbital energies using the following approximate expressions:

$$\mu = (E_{\text{HOMO}} + E_{\text{LUMO}})/2 \qquad\qquad \text{(Eq. 1.5)}$$

$$\eta = E_{\text{LUMO}} - E_{\text{HOMO}} \qquad\qquad \text{(Eq. 1.6)}$$

1.1.4 Frontier Molecular Orbital (FMO) Theory

Frontier molecular orbital (FMO) theory is considered as a practical way of describing chemical reactivity, which is developed by Kenichi Fukui.[94] Instead of assessing the total electron density, FMO theory analyses the highest occupied and lowest unoccupied molecular orbitals (HOMO and LUMO). In their seminal paper published in 1952, Fukui and co-workers established a quantitative correlation between chemical reactivity and the electron dense region. By studying 15 different hydrocarbons, they found that the electrophilic or oxidizing reagents can readily attack electron dense region. Consequently, they concluded that, compared to other π-electrons the pair of π-electrons occupying the highest orbital, which is referred to as frontier electrons, plays a decisive role in chemical activation of these hydrocarbon molecules. One of the 15 hydrocarbons studied by them is naphthalene, the HOMO and LUMO of naphthalene is provided in Figure 1.1. Similarly, FMO theory predicts that a site, at which the lowest unoccupied orbital is localized, is a good electrophilic site. FMO theory is also helpful in rationalizing the outcomes of cycloaddition reactions and other pericyclic reactions. FMO theory has its own limitations, in the case of molecules with several functional groups or electron delocalization, there are chances that the HOMO orbital is not strictly localized to a particular site but often span a large portion of a molecule, making the interpretation more difficult. The situation will be worse for the case of LUMO. In addition, there are many examples where the reactivity is not

controlled by frontier orbitals. For example, if the HOMO is involved in the aromatic system, it is less likely to react as a nucleophile or a base because this will lead to the loss of resonance stabilization. In other cases, the reactivity is determined by strong electrostatic forces rather than by frontier orbitals.
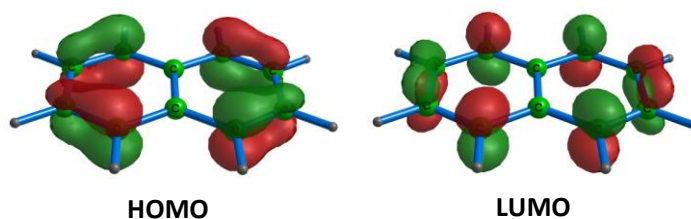
Figure 1.1 HOMO and LUMO of naphthalene molecule.

The energy separation between HOMO and LUMO orbitals (HOMO-LUMO gap)[95] has been widely used as a direct indicator of kinetic stability.[96] A large HOMO-LUMO gap corresponds to high kinetic stability and low chemical reactivity. Pearson demonstrated that the HOMO-LUMO gap constitutes the chemical hardness of a molecule.[14,97] Zhou and Parr explained the chemical reactivity of cyclic conjugated systems with the help of HOMO-LUMO gaps of the reactant and the transition state. There are a number of other studies[14,98-101] which define the chemical reactivity based on the HOMO-LUMO gap of the molecule, especially in the case of semiconductors. The chemical reactivity of C_{60} fullerene is governed by its low HOMO–LUMO gap making it an excellent electron acceptor. As conjugation in a molecule increases, the HOMO–LUMO gap decreases, thus causing a bathochromic shift in absorption spectra (red shift).

All these descriptors provide us with a status to understand experimental observations in an elegant way. Other widely used reactivity descriptors are atomic charges from Mulliken, natural bond orbital (NBO), atoms-in-molecules (AIM), and Hirshfeld population analysis etc.[102] The diverse applications of molecular electrostatic potential (MESP) in explaining direct or indirect aspects of chemical reactivity are described below.

1.1.5 Molecular Electrostatic Potential (MESP) as a Reactivity Descriptor

The molecular electrostatic potential (MESP) at a given point in the vicinity of a molecule is the force acting on a positive test charge (a proton) through the electrical charge cloud generated through the molecules electrons and nuclei. The Coulomb's law is the foundation for deriving MESP equation. It states that the force of attraction or repulsion between two point charges is directly proportional to the product of the charge and inversely proportional to the square of the distance between the charges:

$$F = \frac{q_1 q_2 \hat{\mathbf{r}}}{4\pi\varepsilon_0 \mathbf{r}^2} \qquad \text{(Eq. 1.7)}$$

where q_1 and q_2 are point charges separated by a distance $\mathbf{r}$, a unit vector $\hat{\mathbf{r}}$ joins the position vectors of q_1 and q_2. $4\pi\varepsilon_0$ is the proportionality constant.

The electric field, E produced by a fixed point charge q at a site $\mathbf{r}$ can be written as:

$$E = \frac{q\mathbf{r}}{4\pi\varepsilon_0 |\mathbf{r}|^3} \qquad \text{(Eq. 1.8)}$$

The MESP, V($\mathbf{r}$) at a point r in space is calculated by the following equation,

$$V(\mathbf{r}) = \sum_{A}^{N} \frac{Z_A}{|\mathbf{r} - \mathbf{R}_A|} - \int \frac{\rho(\mathbf{r}')}{|\mathbf{r} - \mathbf{r}'|} d^3\mathbf{r}' \qquad \text{(Eq. 1.9)}$$

where Z_A is the charge on the nucleus A which is located at the position $\mathbf{R}_A$, $\rho(\mathbf{r}')$ is the electron density, and N is the total number of nuclei in the molecule.

The MESP at a nucleus, V_N can be written as:

$$V_N = \sum_{B \neq A} \frac{Z_B}{|\mathbf{R}_B - \mathbf{R}_A|} - \int \frac{\rho(\mathbf{r}')}{|\mathbf{r} - \mathbf{r}'|} d^3\mathbf{r}' \qquad \text{(Eq. 1.10)}$$

The topographical analysis of $V(\mathbf{r})$ is based on locating and characterizing the critical points (CPs). These are points in space at which first-order partial derivatives of the $V(\mathbf{r})$ vanishes. A critical point is represented as an ordered pair consisting of rank and signature which is grouped into (3, +3), (3, -3), (3, +1), and (3, -1). A MESP minimum

9

(V_{min}) corresponds to a (3, +3) CP which represents the potential binding sites for electrophiles and (3, -3) stands for a maximum, while (3, +1) and (3, -1) denote saddle points.

The concept of electrostatic potential was introduced by Scrocco and Tomasi.[103,104] MESP has emerged as a sensitive electronic parameter in the study of molecular reactivity and related phenomena.[105 106-113] The MESP at a given point near a molecule is a measure of the electrostatic energy a unit test positive charge would experience at that point. A negative MESP value corresponds to an attractive interaction with this test charge, while positive MESP value designates repulsion. The most negative valued MESP point of a molecule, designated as V_{min}, symbolizes the sites of electron localization in a molecule. MESP can be experimentally determined from the electron density data derived from X-ray diffraction studies on crystals whereas being a one electron property, its accurate calculation is rather easy with theoretical methods implemented in many of the standard *ab initio*/DFT program packages.[114,115] MESP based electron distribution studies were pioneered by the works of Pullman,[116] Politzer[105,117-121] and Gadre.[122-132] The works of Wheeler and Houk[133-137] and Galabov[102,138,139] have also contributed to the growth of this area. A number of studies by Suresh *et al.* disclosed the usefulness of MESP based analysis to interpret and quantify resonance effect,[140] inductive effect,[141] substituent effects,[142,143] trans influence,[144] cation-π interactions,[145-147] lone pair-π interactions,[148] non-covalent interactions including a large variety of hydrogen bonds,[149] aromatic character of benzenoid hydrocarbons,[150,151] stereoelectronic features of ligands in organometallic/inorganic chemistry[152-157] etc.

1.1.5.1 Substituent, Resonance and Inductive Effect

Quantitative assessment of the substituent effect of a molecular system is of central importance not only to understand the chemical reactivity of that system but also to design new systems with desired properties.[158] MESP has been widely exploited as a powerful tool for the quantification of substituent effect for a variety of systems.[117,133,134,136,143,159-162] Hammett[163] introduced substituent constants which give

a measure of electronic perturbations arising from substitution. The widely used substituent constants or Hammett constants are σ_m and σ_p which are obtained from the dissociation constant data of the *meta* and *para* substituted benzoic acids. Politzer and Murray established the MESP of amine nitrogen as a measure of the total electron-attracting tendencies of substituents where a linear correlation between the V_{min} at N and the Taft substituent constants for 24 NH_2-X molecules were obtained.[164] In another work, Politzer and co-workers demonstrated that, in the case of *para* substituted anilines, the V_{min} associated with the amine lone pairs is a highly sensitive indicator of the electron-donating and electron-attracting tendencies of the para substituents.[165] Haeberlein and Brinck[166] have analyzed the substituent effects in para-substituted phenoxide ions and established a linear correlation between V_{min} observed near the phenoxide oxygen and the gas-phase acidities. Gadre and Suresh[106] studied 13 monosubstituted benzenes to quantify the electronic perturbations offered by the substituents, where the MESP critical points close to *para* carbon and *meta* carbon established good linear correlations between σ_p and σ_m respectively which provided an impetus for the use of MESP topography for explaining substituent effect. Further, they have extended the work to 45 doubly substituted benzenes where the changes due to the different orientations (*para*, *meta*, and *ortho*) and conformations of the substituents and different mechanisms of electron donation or withdrawal found to reflect on the V_{min} values.[167] The V_{min} and σ values of the *ortho* and *meta* disubstituted benzenes showed good linear correlation and a new substituent pair-constants have been introduced respectively for the *para*, *meta*, and *ortho* arrangements which provide a quantitative measure of the simultaneous effect of two substituents over the aromatic nucleus. It is the pair-wise interactions that are excluded in the determination of Hammett constants when applied to multiply substituted benzenes that are mainly responsible for the deviations from the additivity of σ constants. The predictive power of these quantities is checked in the case of some triply substituted benzenes obtained good results. The work provides a simple and practical approach toward a better treatment of multiply substituted benzenes in the area of quantitative structure-activity relationship (QSAR).
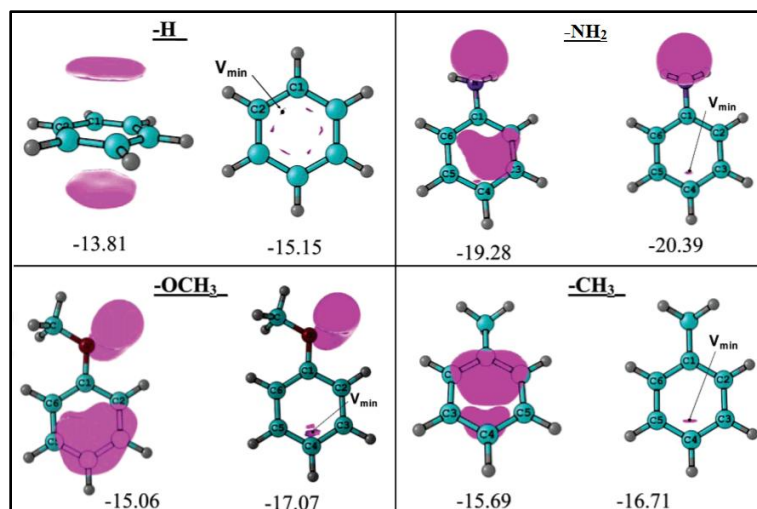
Figure 1.2 Two different MESP isosurface values of benzene and NH_2, OCH_3 and CH_3 substituted benzenes (each isosurface value in kcal/mol is given at the bottom of the structure). Location of the most negative-valued point V_{min} is also depicted.[168]

Galabov, Elieva, and Schaefer[169] carried out a DFT study for a series of 15 monosubstituted benzene derivatives and found excellent linear correlation between σ values and the MESP at the para carbon atom of substituted benzenes. The results underline the usefulness of MESP as a local reactivity descriptor. Several other studies of substituent effect have also been conducted using MESP.[168]

The substituent effect on aryl ring can be transmitted through a number of mechanisms such as π-resonance, inductive (through-σ-bond), and field (through-space) effects and MESP approaches have been used to quantify these effects. Sherrill and co-workers[160,170] characterized the "degree of π-density" in substituted benzenes by exploiting the MESP plots where the electron-withdrawing substituents generally increase the MESP above the aryl ring, while donors lead to a decrease in the MESP, relative to benzene. These MESP maps found to reflect both π-resonance and inductive/field effects. Wheeler and Houk[133,171] demonstrated that through-space effects of substituents dominate on the MESP by taking a series of substituted benzenes and substituted arenes used in drug design, host-guest chemistry, and crystal engineering. It has been suggested that when considering MESPs of substituted analogues of candidate drugs built on aryl frameworks, the role of direct through-space

effects of substituents is potentially significant and must be considered. Hunter and co-workers[172] reported a strong correlation between σ_m and the MESP at the ring centres of *para*-substituted *meta*-xylenes.

Politzer and co-workers have demonstrated the dominant role of inductive/field effects in nitrobenzene with the help of MESP.[173] Inductive and resonance effects aid to elucidate a large number of structure-activity related problems in organic chemistry and Suresh *et al.* performed a quantitative assessment of inductive effect with help of MESP.[174] They have studied three systems (4-substituted bicyclo[2.2.2]octane carboxylic acids, anions of 4-substituted bicyclo[2.2.2]octane carboxylic acids and 4-substituted quinuclidines) for the dependencies between V_{min} and the inductive substituent constant σ_I using 20 different substituents, ranging from electron withdrawing to electron donating nature. By obtaining an excellent linear correlation between V_{min} and σ_I for all the 3 systems they suggested that the calculation of V_{min} parameter in these systems offers a simple and efficient computational approach for the evaluation of inductive substituent constants.

The regiospecific effects of substituents on the aromatic ring of benzene have been explained by Galabov *et al.*[161] Fareed and Suresh employed MESP to study the proximity effects and additive nature of substituents for a series of *ortho*, *meta*, and *para* substituted benzoic acids.[142] It has been found that the V_{min} at the lone pair region of OH on the functional group COOH serves as an excellent descriptor of the substituent effects. They have also suggested the use of V_{min} as an alternate measure for Hammett substituent constants. This approach has shown that, in the case of multiply-substituted systems, the substituent effects largely follow (86.3%) an additive rule. Further, MESP has been applied to define an electrostatic scale of substituent resonance effect.[140] Through-bond (TB) and through-space (TS) substituent effects in substituted alkyl, alkenyl, and alkynyl arenes are quantified individually using MESP topographical analysis.[175] A recent study conducted by Suresh and Remya, quantified the substituent effect in organic molecules based on MESP parameter which is the difference between MESP at the nucleus of the para carbon of substituted benzene and a carbon atom in benzene. Further, using the MESP parameter for a large variety of benzene derivatives,

the transferability and additivity properties of substituent effects in conjugated organic molecules were established.[176]

1.1.5.2 Noncovalent Interactions

MESP has been widely used to investigate and elucidate noncovalent interactions on the molecular surface of chemical and biological systems.[177-179] It gives a straightforward way of approximating the interaction strength and geometry of noncovalent complexes including complex systems, to study protein-ligand, protein-protein, aromatic stacking, and aromatic π-π interactions etc.[137,170,180,181] MESP has applied to predict the sites and directionality of hydrogen bonds in various systems.[182-184] Kollman and co-workers predicted the hydrogen bond energies of a series of hydrogen-bonded dimers with the help of MESP.[182] Galabov *et al.*[138,139,184-186] successfully used MESP at the site of electron donor atom as a reactivity descriptor for the study of hydrogen bonding. Neetha and Suresh quantified the noncovalent interactions in a variety of intermolecular noncovalent complexes using MESP analysis of hydrogen, halogen, and dihydrogen bonds.[149] The electronic changes that accompany the bond formation can be clearly understood by comparing V_{min} values of isolated electron donor (D) and acceptor (A) molecules. MESP plots of a representative set of complexes are given in Figure 1.3 along with their V_{min} values. In the formation of H_2O dimer, one of the H_2O molecules (A) gains electron density at the expense of the other (D) (Figure 1.3(a)). In this case, V_{min-D} and $V_{min-D'}$ are −50.45 and −34.51 kcal/mol, respectively and V_{min-A} and $V_{min-A'}$ are −50.45 and −63.82 kcal/ mol, respectively. ΔV_{min-D} and ΔV_{min-A} are 15.95 and −13.37 kcal/mol, respectively, which indicate that a significant amount of electron density of D has been transferred to A during the formation of the noncovalent complex. The quantity $\Delta\Delta V_{min} = \Delta V_{min-D} - \Delta V_{min-A}$ could be used as a measure of the donor-acceptor strength of the noncovalent interaction. Further, they have obtained a reasonably good linear correlation between $\Delta\Delta V_{min}$ and non covalent interaction energy which suggests that the strength of the noncovalent bond is directly related with the donor-acceptor strength.

14
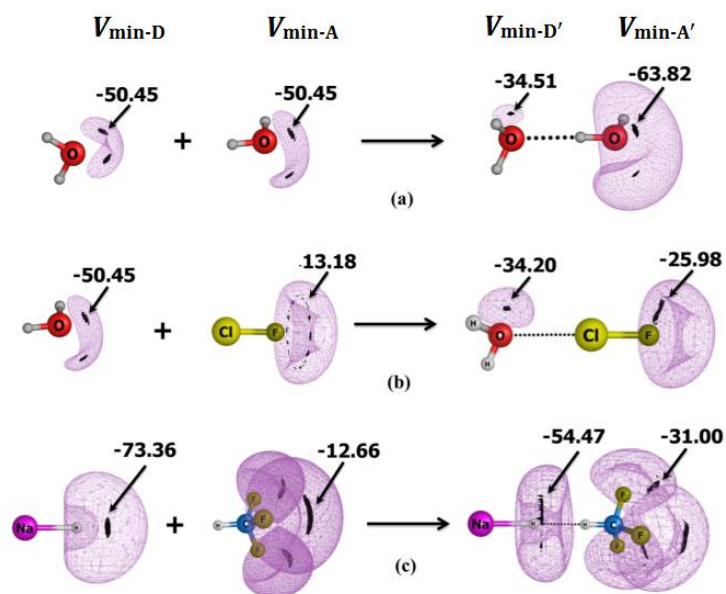
Figure 1.3 Change in V_{min} upon bond formation for (a) $H_2O...H_2O$, (b) $H_2O...ClF$, and (c) $NaH....HCF_3$. The black dots represent the location of the most negative MESP-valued point and the corresponding V_{min} values in kcal/mol are also depicted.[149]

Prediction of most probable interactions in a competitive system can be achieved by a simple electrostatic view of hydrogen-bond strength.[187-193] Kenny demonstrated V_{min} as an excellent predictor of hydrogen bond basicity in a set of heterocycles[190] and also as a tool to provide insight into a number of hydrogen bonding phenomena, including lactam self-association, DNA base pairing, and bioisosterism.[191] Aakeröy and co-workers have studied a series of co-crystallizations between four biimidazole based compounds and nine symmetric aliphatic di-acids and found that MESP can be effectively used to allocate the selectivity in hydrogen-bond based intermolecular interactions.[187] The competition between hydrogen and halogen bonding in co-crystals of supramolecular systems have also been analyzed.[189] Politzer and Murray[188] illustrated that MESP can be complemented to Etter's empirical rules for hydrogen bonding patterns, by providing physical means for identifying and ranking hydrogen bond donating and accepting sites, and also gives greater insight into the mechanism.

One of the popular noncovalent interactions is σ-hole bonding which involves the covalently bonded Group IV–VII atoms interacting attractively in a highly directional manner with negative sites on other molecules (or even within the same molecule), e.g., the lone pairs of Lewis bases. The positive electropotential region is called σ-hole. A Group VII atom interacting with a negative site is called halogen bonding. The σ-hole concept is introduced by Politzer *et al.*[119]
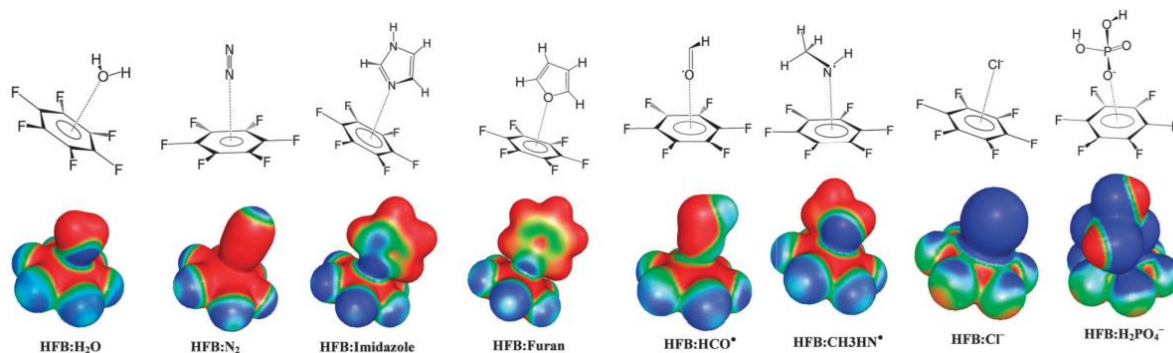
Figure 1.4 Molecular electrostatic potential textured on the 0.003 au electron density surface for HFB–lone pair complexes. Color coding , blue −0.02 au to red 0.02 a.u. for neutral and free radicals and blue −0.14 au to red −0.1 au for anionic species.[148]

Identifying lone pair regions using MESP can greatly help in establishing bonding theories for intermolecular complex formation.[194,195] Gadre and co-workers[196-199] have provided a precise description of electron-rich regions corresponding to lone pairs or π bonds in molecules with the help of the topographical features of MESP. The weak interactions between lone pair containing molecules and π deficient molecular systems have been probed by Gadre, Suresh and co-workers.[148] They have obtained good correlation between the lone pair–π interaction energy (E_{int}) with the V_{min} value of the electron-rich system. The electron density distribution of some of the lone pair containing species interacting with the electron deficient hexafluorobenzene (HFB) is provided in Figure 1.4, which depict MESP textured on to a 0.003 au electron density surface. The MESP maps clearly indicate the interaction of the electron deficient core of HFB (red) with the electron-rich lone pair/anion region (blue) giving rise to lone pair/anion–π interactions.

Dougherty and co-workers have conducted various studies to explore MESP based prediction of cation-π interactions.[200-202] They estimated that the strength of cation-π interactions and the MESP above the center of substituted benzenes can be strongly correlated with σ_m constants than σ_p. MESP based approach has been proposed to quantify the substituent effects on cation-π interactions in complexes of mono-, di-, tri-, and hexa substituted benzenes with Li^+, Na^+, K^+, and NH_4^+.[145] The V_{min} on the π-region of C_6H_5X showed strong linear dependency to the cation-π interaction energy. Substituent effects on cation-π interactions have also been quantified on π systems of the type Φ−X···M$^+$ with a variety of M$^+$ ions and variety of X substituents. The quantification is made based on the ΔV_{min} values, suggesting that the MESP approach to substituent effect is accurate and useful for predicting the interactive behaviour of substituted π-systems with cations.[203]

1.1.5.3 Tuning Stereoelectronic Features of Ligands

In 2002, Suresh and Koga[152] efficiently characterized and quantified the electron-donating power of 33 phosphine ligands with the aid of V_{min} at the lone pair region using DFT. They have suggested that calculating V_{min} at the lone pair region is the simple and easiest way to find the lone pair strength in phosphines. They confirmed this suggestion by illustrating linear correlations of V_{min} with pKa values of the conjugate acids of phosphates ([PR_3H]$^+$), Tolman electronic parameter (the ν-CO values correspond to the asymmetrical stretching frequency of carbonyl groups in $Ni(CO)_3L$), energy (ΔE) of the reactions $Ni(CO)_3$ + PR_3 giving $Ni(CO)_3PR_3$ and ScH_3 + PR_3 giving ScH_3PR_3, the standard reduction potential (E^0) and enthalpy change (ΔH^0) corresponding to the electrochemical couple η-Cp(CO)(PR$_3$)(COMe)Fe$^+$/η-Cp(CO)(PR$_3$)(COMe)-Fe^0. Later in 2006, Suresh[153] extended the MESP based approach for the PR_3 ligands using two-layer ONIOM (B3LYP/6-31G(d,p):UFF) quantum mechanics (QM)-molecular mechanics (MM). By evaluating the steric effects it has been found that the subtle variations in the electron distribution arising from the steric bulkiness as well as the conformational changes in the substituent groups are well reflected in the V_{min} value.[153] Shortly, Suresh and Jomon created a map of phosphine

ligands (Figure 1.5) based on steric (S_{eff}) and electronic (E_{eff}) features derived from V_{min} calculations using a combination of QM and MM approaches where the difference between the V_{min} of unsubstituted PH$_3$ (V_{min} (PH$_3$)) and the V_{min} of PR$_3$ is considered as E_{eff} + S_{eff}.[154] All these MESP based studies helped theoreticians and experimentalists in understanding the stereoelectronic profile of phosphine ligands which led to the rational design of superior ligands.[204,205] A comparative study of various theoretical methods used for predicting net donating ability of phosphine ligands carried out by Olaf Kuhl supported the use of V_{min} for the quantification of the electronic effect of phosphine ligands.[206]
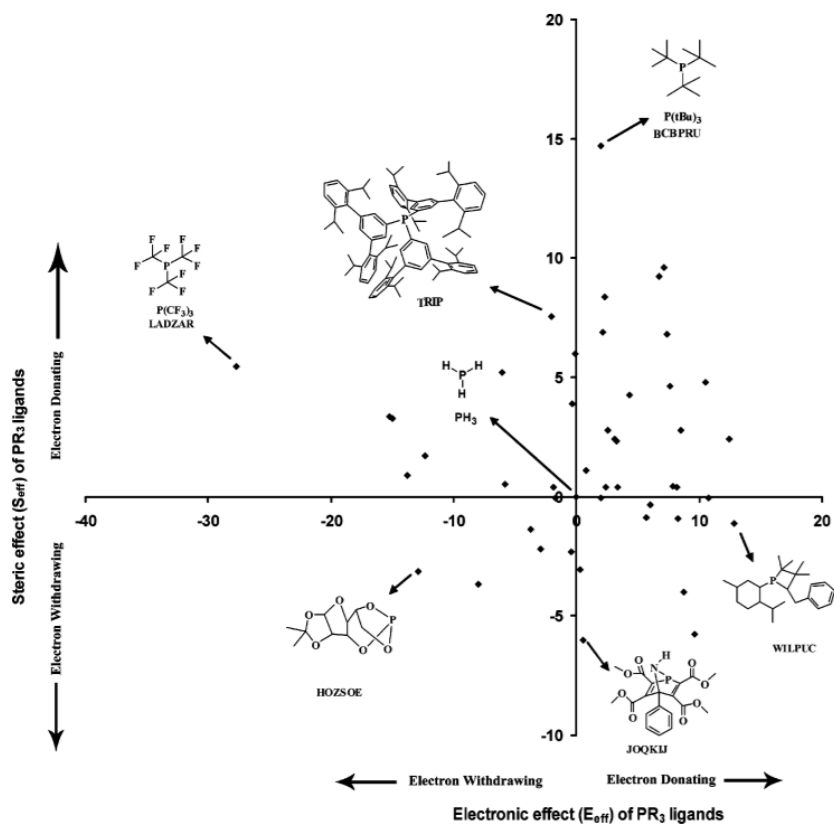
Figure 1.5 Stereoelectronic plot of PR$_3$ ligands.[154]

Quantification of stereoelectronic features of N-heterocyclic carbene (NHC) ligands towards the metal coordination has also been carried out using MESP, where a linear correlation between V_{min} and MESP at carbene carbon[207] with Tolman electronic

18

parameter (TEP) was established.[155] Further, MESP has been employed to investigate several Grubbs first generation olefin metathesis catalysts to understand the role of steric and electronic effects of PR_3 in olefin (ethylene) binding processes as well as in the formation of metallacyclobutane.[156] The MESP at the phosphorus nucleus of the active form of the catalyst, $Cl_2(PR_3)Ru=CH_2$ (**1**) and its ethylene-coordinated complex (**2**) are determined and the change in MESP values of $Cl_2(PR_3)Ru=CH_2$ with respect to $Cl_2(PH_3)Ru=CH_2$ is taken as a measure of combined steric and electronic effect of PR_3 in **1** (V_{SE1}), the corresponding effect of PR_3 in **2** (V_{SE2}) also measured. Also, the frozen structures corresponding to **1** and **2** are located by changing the P-R bonds with P-H bonds. The MESP at the P of a frozen geometry is devoid of the electronic effect of R but having steric effects due to the structural restrictions imposed in the geometry, and denoted as V_{S1} for **1** and V_{S2} for **2**. Thus, the electronic effect of PR_3 in **1** (V_{E1}) is V_{SE1} - V_{S1} and that in **2** (V_{E2}) is V_{SE2} - V_{S2}. Both V_{S1} and V_{S2} showed linear correlations with Tolman cone angle (θ) and the symmetric deformation coordinate (S4′). V_{E1} and V_{S1} showed a linear correlation with the binding energy of ethylene (E_1), suggesting that the steric effect is 1.88 times more dominant than the electronic effect in the olefin binding process. Similarly, both V_{E2} and V_{S2} showed linear correlation with the activation energy (E_2) for the formation of metallacyclobutane. These studies demonstrate that the success of the first-generation Grubbs catalysts is mainly due to the choice of the right mix of steric (bulky R substituents on P) and electronic (electron-donating R substituents on P) effects of the PR_3 ligand. Based on the similar MESP approach, the stereoelectronic features of Grubbs second generation catalysts have also been investigated.[157] The stereoelectronic features of NHCs have been analyzed using V_{min} for its CO_2 fixation ability.[208] V_{min} at the carbene lone pair region of NHC (V_{min1}) as well as at the carboxylate region of the NHC-CO_2 adduct (V_{min2}) are measured. Both V_{min1} and V_{min2} are found to be simple and efficient descriptors of the stereoelectronic effect of NHCs. The work has also proved the additive nature of stereoelectronic effect with N- and C-substitutions.[208]

Sajith and Suresh[144] attempted the quantification of the trans influence of various ligands in hypervalent Iodine (III) complexes of $CF_3[I(X)Cl]$. It has been found

that the V_{min} at the Cl lone pair region gives a sensitive measure of the trans influence (Figure 1.6). Trans and cis influences of various X ligands in two isomeric structures of acyclic hypervalent compound Ph[XI(OH)] and heterocyclic λ^3-iodane Ph[(heterocycle)I(OH)] have also been investigated and V_{min} at the OH lone pair found to be a good parameter for quantifying the trans and cis influences.[209]
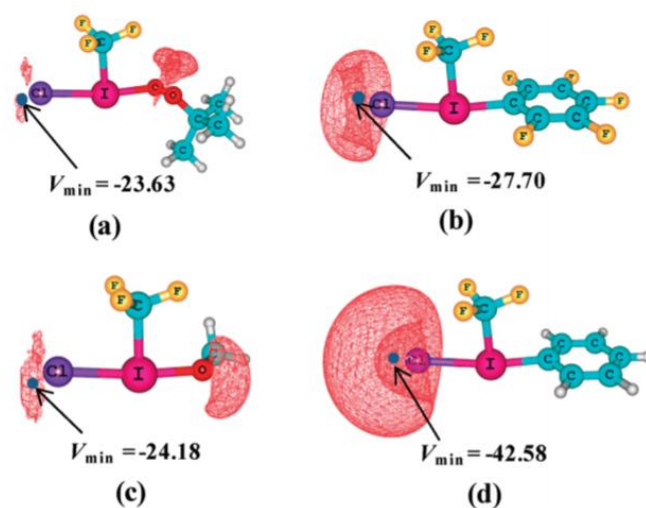
Figure 1.6 Representation of MESP isosurface in $CF_3[I(X)Cl]$ complexes at -23 kcal/mol along with V_{min} in kcal/mol. The ligands X are (a) OOtBu, (b) C_6F_5, (c) OMe, and (d) Ph.[144]

Structure and reactivity of substituted arene-$Cr(CO)_3$ complexes are well explained using MESP topography analysis.[210] Octahedral metal hydride complexes of groups VI, VII and VIII, having significant catalytic applications have been evaluated for its hydridic character using MESP topography.[211] The V_{min} and the MESP value at the hydride nucleus (V_H) found to quantify the hydridic character of the ligand. Since the hydride ligand is negatively charged, the M–H region of a metal hydride complex is expected to be electron rich. Sandhya and Suresh[211] illustrated this using the MESP features of a representative system (Figure 1.7). Here a MESP plane passing through M–H and M–NO bonds. The regions clearly indicate a concentration of electrons around the hydride ligand as well as around the oxygen of the NO ligand. The MESP isosurface depicted in Figure 1.7(b) is useful to obtain a 3D view of the electron concentration

around the hydride ligand. The V_{min} is also noted for the hydride and NO ligands. The negative MESP region around NO can be correlated to the lone pair region of its oxygen.
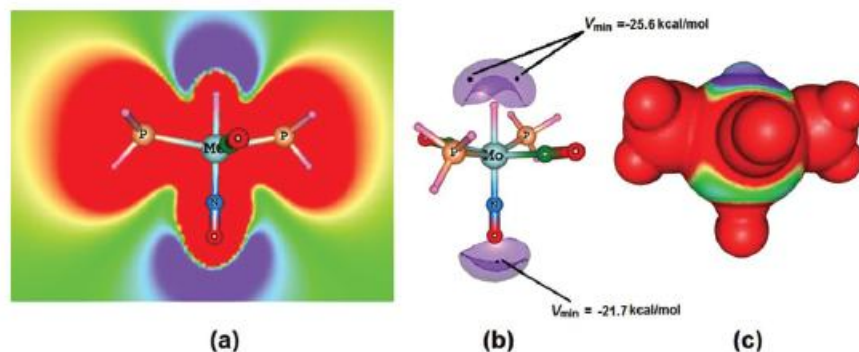
Figure 1.7 Electrostatic potential features of metal hydride complex. (a) MESP plotted on a plane. (b) MESP isosurface plot, value −22.0 kcal/mol. (c) MESP on van der Waals (value range from −0.02 au to 0.02 au).[211]

It is also established that increasing hydridic character favours protonation from organic molecules leading to dihydrogen complex formation. A strong hydridic character of a metal hydride can promote hydrogen release through a water splitting outer sphere mechanism.[212] An assessment of hydridic character and thus the tendency for water splitting reactions were rationalized with the help of V_{min} or V_H values.[211] A correlation between activation energy (ΔE) for H_2 elimination and hydridic descriptor V_{min} of group VI complexes has also been obtained. Activation barrier of water splitting Milstein catalyst of ruthenium (II) pincer hydride has been tuned with the use of MESP.[213] It is found that replacing bulky t-butyl substituent at the P-arm of pincer ligand by either methyl or ethyl group can substantially reduce the activation barrier and also a correlation between V_{min} and activation energy was established.

MESP has also been applied in several other fields to understand various aspects of structure and reactivity. Wang *et al.* investigated the relative stability of two fullerene isomers of C_{50} using MESP topography.[214] Active sites for molecular reactions are located at pentagon-pentagon vertex fusions which provide a reasonable explanation for protonation and alkylation of C_{50} fullerene. Alipour and Mohajeri[215] proposed MESP as an effective approach in predicting the rate constant of etherification reaction of

phenol derivatives due to substituent effect. The etherification rate constant found to be proportional to MESP at the hydrogen and oxygen of phenolic hydroxyl group.

Part B: Computational Chemistry Methods

Quantum theory provides us with a striking illustration of the fact that we can fully understand a connection though we can only speak of it in images and parables.

-Werner Heisenberg

1.2   An Overview of Computational Chemistry

Computational chemistry, as the name suggests, resolve the chemical problems with the help of sufficiently developed mathematical methods implemented on computers. This branch of theoretical chemistry has its roots in the late 19th century and in the first part of the 20th century. In recent years, the experimental characterization of new systems turns out uncomplicated with the use of novel computational approaches which rationalize the structural, energetic, electronic and dynamic features, in turn developing synergic interactions between experimentalists and theoretically-oriented chemists. The development of high computational facilities including supercomputers, the vector/parallel machines, powerful workstations, desktop computers and a variety of software packages elevated the status of applied computational chemistry to one of the major branches of chemistry. Computational chemistry relies on the view that chemistry can be best understood as the materialization of the behaviour of atoms and molecules, and these are real entities rather than merely convenient intellectual models.

Computational chemistry methods range from highly accurate ones feasible only for small systems to very approximate methods for larger systems. One can obtain useful information about the systems containing up to several thousand particles based on the nature of the system under study and the required accuracy. In general, computational chemistry methods are classified as *ab initio* quantum chemical methods, semiempirical methods, density functional theory, molecular mechanics, and

molecular dynamics. Computational methods are helpful in investigating molecular geometries, conformational energies, reaction mechanisms, reaction kinetics, spectroscopic properties such as IR, Raman, UV, NMR etc. The *ab initio* (Latin term for "from the beginning") methods solve the Schrödinger equation by using universal constants such as the speed of light, the masses and charges of electrons and nuclei, Planck's constant etc. with no inclusion of empirical data. Semiempirical methods use experimental values (using parameterization) to find approximate solutions of the Schrödinger equation. Density functional theory uses electron density as a functional to find the total energy of a system. Molecular mechanics is based on the ball and spring model of the molecules (atoms are considered as spherical balls and bonds are considered as springs) and molecular dynamics incorporate Newton's laws of motion.[216]

1.2.1 *ab initio* Quantum Chemical Methods

The Schrödinger equation is the basis for all the quantum chemical methods.[217] The *ab initio* methods solve the electronic Schrödinger equation with the direct use of theoretical principles. In quantum mechanics, the molecules are described in terms of the interactions among nuclei and electrons, and the molecular geometry in terms of the minimum energy arrangements of nuclei. For a system comprising electrons and nuclei the non-relativistic time-independent Schrödinger equation in its simplest form is:

$$H\Psi = E\Psi \qquad\qquad \text{(Eq. 1.11)}$$

where H is the Hamiltonian operator, Ψ is the many-electron wave function and E is the energy eigenvalue of the system. The Hamiltonian operator for a many-body system of N electrons and M nuclei can be written as:

$$H = -\sum_{i=1}^{N}\frac{1}{2}\nabla_i^2 - \sum_{A=1}^{M}\frac{1}{2M_A}\nabla_A^2 - \sum_{i=1}^{N}\sum_{A=1}^{M}\frac{Z_A}{\mathbf{r}_{iA}} + \sum_{i=1}^{N}\sum_{j>i}^{N}\frac{1}{\mathbf{r}_{ij}} + \sum_{A=1}^{M}\sum_{B>1}^{M}\frac{Z_A Z_B}{\mathbf{R}_{AB}} \qquad \text{(Eq. 1.12)}$$

The first and second term accounts for electronic and nuclear kinetic energy operators, third, fourth and fifth terms are the potential energy operators

corresponding to nuclear-electron and electron-electron, and nuclear-nuclear interactions respectively. $\mathbf{R}_A$ and $\mathbf{r}_i$ are the position vector of nuclei and electrons, $\mathbf{r}_{iA}$ is the distance between i^{th} electron and A^{th} nucleus, $\mathbf{r}_{ij}$ is the distance between i^{th} and j^{th} electrons and $\mathbf{R}_{AB}$ is the distance between A^{th} and B^{th} nucleus. M_A is the ratio of mass of the nucleus to the mass of the electron and Z_A is the atomic number.

The exact solution for Schrödinger equation is only possible for hydrogen atom, for all other systems, approximations are needed for its practical applications. The most common and reasonable approximation is the Born Oppenheimer (BO)[218] approximation in which the nuclear motion is neglected, since the nuclei are much heavier and moves much slower than the electrons. Based on this approximation, the nuclear kinetic energy term in Eq. 1.12 becomes zero and the nuclear-nuclear repulsion becomes a constant. The remaining Hamiltonian is H_{elec} which describes the motion of N electrons in the field of M point charges. The electronic Hamiltonian can be written as:

$$H_{\text{elec}} = -\sum_{i=1}^{N} \frac{1}{2} \nabla_i^2 - \sum_{i=1}^{N} \sum_{A=1}^{M} \frac{Z_A}{\mathbf{r}_{iA}} + \sum_{i=1}^{N} \sum_{j>i}^{N} \frac{1}{\mathbf{r}_{ij}} \qquad \text{(Eq. 1.13)}$$

In Eq. 1.13, the third term corresponds to electron-electron interactions; it is challenging to determine the exact solution for this term. To make an approximation we must consider a scheme in which the corresponding terms becomes zero indicating that the N electrons are moving completely independent of each other. Then the total wavefunction will become the product of N electron wavefunctions as below:

$$\Psi = \psi_1(\mathbf{r_1})\, \psi_2(\mathbf{r_2}) \ldots . \psi_N(\mathbf{r_N}) \qquad \text{(Eq. 1.14)}$$

The eigenvalue equation corresponding to the electronic Hamiltonian can be written as:

$$H_{\text{elec}} \Phi_{\text{elec}}(\{\mathbf{r}_i\}; \{\mathbf{R}_A\}) = E_{\text{elec}} \Phi_{\text{elec}}(\{\mathbf{r}_i\}; \{\mathbf{R}_A\}) \qquad \text{(Eq. 1.15)}$$

where, $\{\mathbf{r}_i\}$ accounts for the position of electrons and $\{\mathbf{R}_A\}$ represents the position of nuclei. The solution to Eq. 1.15 gives the electronic wave function which describes the motion of electrons and depends explicitly on the electronic coordinates and parametrically on the nuclear coordinates. BO approximation could effectively separate

electronic and nuclear Hamiltonians and their corresponding wave functions. Thus the molecular wavefunction can be represented as the product of electronic and nuclear counterparts:

$$\Phi(\{\mathbf{r}_i\};\{\mathbf{R}_A\}) = \Phi_{\text{elec}}(\{\mathbf{r}_i\};\{\mathbf{R}_A\})\Phi_{\text{nucl}}(\{\mathbf{R}_A\}) \qquad \text{(Eq. 1.16)}$$

By knowing wave function Ψ from the Schrödinger equation, many properties can be calculated as the expectation value of the appropriate operator. The BO approximation is usually very good. For instance, for the hydrogen molecule (H_2) the error can be in the order of 10^{-4} au, and the approximation becomes better for the systems with heavier nuclei.

1.2.1.1 Hartree-Fock Theory

The Hartree-Fock (HF) method[219] is one of the simplest approximations for solving the many-body Hamiltonian and this *ab initio* calculation uses BO approximation for solving the Schrödinger wave equation.[218,220] It is the basis for most of the electronic structure theory methods. HF method describes the motion of each electron by a molecular orbital and does not depend explicitly on the instantaneous motions of the other electrons. The Hamiltonian of a simpler system containing noninteracting electrons can be represented as:

$$H = \sum_{i=1}^{N} h(i) \qquad \text{(Eq. 1.17)}$$

where $h(i)$ is the operator describing the kinetic energy and potential energy of electron i. Also, the corresponding wave function can be written as the product of individual one electron function called *Hartree Product* (HP),

$$\Psi^{\text{HP}}\left(\boldsymbol{x}_{1,}\boldsymbol{x}_{2,}\dots.,\boldsymbol{x}_{N}\right) = \chi_i(\boldsymbol{x}_1)\chi_j(\boldsymbol{x}_2)\dots.\chi_N(\boldsymbol{x}_N) \qquad \text{(Eq. 1.18)}$$

where χ_i, χ_j, etc. corresponds to the spin orbitals, and $\boldsymbol{x}_1$, $\boldsymbol{x}_2$, etc. corresponds to the combined spatial and spin coordinates of each electron. The major shortcoming of HP is that it fails to satisfy the *antisymmetry principle*. According to Pauli's exclusion principle, no two electrons of an atom can have identical value of all the four quantum

numbers *viz.* n, l, m, and s. Anti-symmetrization can be achieved by arranging the one electron spin-orbital in a determinant form called Slater determinant. Slater determinant for an N-electron wave function can be written as:

$$\Psi(\boldsymbol{x}_1, \boldsymbol{x}_2, \ldots, \boldsymbol{x}_N) = \frac{1}{\sqrt{N!}} \begin{vmatrix} \chi_i(\boldsymbol{x}_1) & \chi_j(\boldsymbol{x}_1) & \cdots & \chi_N(\boldsymbol{x}_1) \\ \chi_i(\boldsymbol{x}_2) & \chi_j(\boldsymbol{x}_2) & \cdots & \chi_N(\boldsymbol{x}_2) \\ \cdot & \cdot & & \cdot \\ \cdot & \cdot & & \cdot \\ \cdot & \cdot & & \cdot \\ \chi_i(\boldsymbol{x}_N) & \chi_j(\boldsymbol{x}_N) & \cdots & \chi_N(\boldsymbol{x}_N) \end{vmatrix}$$

(Eq. 1.19)

where $\frac{1}{\sqrt{N!}}$ is a normalization factor. In this wavefunction, interchanging the coordinates of any two electrons can lead to interchange of two rows of the determinant, which will alter the sign of the determinant. Hence, *antisymmetry principle* is satisfied. Also, all the electrons are indistinguishable, and the motion of electrons with parallel spins is correlated when the many-electron wave function is represented in Slater determinant form.[221-224] The normalized Slater determinant can also be represented with a shorter notation:

$$\Psi(\boldsymbol{x}_1, \boldsymbol{x}_2, \ldots, \boldsymbol{x}_N) = |\chi_i \chi_{j\ldots\ldots} \chi_N \rangle$$

(Eq. 1.20)

According to the variational principle, the best wavefunction is the one which gives the lowest electronic energy. This can be calculated as an expectation value of the Hamiltonian. With the increase in the basis set size, the energy decreases, until a limit, called the Hartree-Fock limit.

$$E_0 = \langle \Psi_0 | H | \Psi_0 \rangle$$

(Eq. 1.21)

The variational flexibility in the wave function (Eq. 1.21) is in the choice of appropriate spin orbitals χ_i. By minimizing E_0, with respect to the spin orbitals, one can derive an eigenvalue equation called Hartree-Fock equation. It determines the optimal spin orbitals and can be written as:

$$f(i)\chi(\boldsymbol{x}_i) = \varepsilon \chi(\boldsymbol{x}_i)$$

(Eq. 1.22)

where *f*(*i*) is an effective one-electron operator, called the Fock operator, of the form:

$$f(i) = -\frac{1}{2}\nabla_i^2 - \sum_{A=1}^{M} \frac{Z_A}{\mathbf{r}_{iA}} + V^{HF}(i) \qquad \text{(Eq. 1.23)}$$

The term $V^{HF}(i)$ is the average potential experienced by the ith electron due to the remaining electrons known as Hartree–Fock potential. It can be written as:

$$V^{HF}(i) = \sum_{i=1}^{N} \sum_{i,j=1}^{N} (J_{ij} - K_{ij}) \qquad \text{(Eq. 1.24)}$$

$$J_{ij} = \iint \psi_i(\mathbf{x}_1)\psi_i^*(\mathbf{x}_1)\frac{1}{\mathbf{r}_{12}}\psi_j^*(\mathbf{x}_2)\psi_j(\mathbf{x}_2)d\mathbf{x}_1 d\mathbf{x}_2 \qquad \text{(Eq. 1.25)}$$

$$K_{ij} = \iint \psi_i(\mathbf{x}_1)\psi_j^*(\mathbf{x}_1)\frac{1}{\mathbf{r}_{12}}\psi_i(\mathbf{x}_2)\psi_j^*(\mathbf{x}_2)d\mathbf{x}_1 d\mathbf{x}_2 \qquad \text{(Eq. 1.26)}$$

where the Coulomb operator J_{ij} represents the Coulombic repulsion between the electrons, and the exchange operator K_{ij} denotes the quantum correlation due to Pauli exclusion principle.

Since the electron repulsion is treated in an average way in HF approximation, the complicated many-electron problem is simplified as a one-electron problem. The Hartree-Fock potential $V^{HF}(i)$, or the field experienced by the ith electron depends on the spin orbitals of the remaining electrons. *i.e.*, the Fock operator depends on its eigenfunctions. Thus the Hartree-Fock equation is nonlinear and must be solved iteratively. The procedure for solving the Hartree-Fock equation is called self-consistent-field (SCF) method. By making an initial guess of the spin orbitals, it calculates the average field (*i.e.*, V^{HF}) experienced by each electron, and then solves the eigenvalue equation (Eq. 1.22) for a set of new orbitals. With the use of new orbitals, one can get the new fields and repeat the procedure until self-consistency is reached. The solution yields a set of orthonormal spin-orbitals, $\{\chi_k\}$ are obtained with a corresponding set of energies, $\{\varepsilon_k\}$. The N spin orbitals with the lowest energies are called the occupied orbitals, and the remaining orbitals are known as virtual or unoccupied orbitals. Though an infinite number of virtual orbitals is possible, the HF equation is usually solved by providing a finite set of K spatial basis functions $\{\phi_\mu(\mathbf{r})| \mu = 1, 2,...., K\}$, corresponding to which, 2K set of spin orbitals are generated. Out of these orbitals, N will be occupied, and 2K-N will be virtual orbitals. With the increase

in the size of the basis set used, the energy expectation value of E_0 = $<\Psi_0|H|\Psi_0>$ decreases until the HF limit is attained. A finite value of K usually yields an energy value above this limit.

For closed shell systems, the derivations of HF equations are developed independently by Clemens C. J. Roothaan and George G. Hall in 1951.[225,226] The HF equation (Eq. 1.22) can be rewritten by considering the spin orbitals as linear combinations of basis functions (Φ_μ).

$$\psi_i = \sum_{\mu=1}^{K} C_{\mu i}\Phi_\mu \qquad\qquad i = 1, 2, \ldots, K \qquad\qquad \text{(Eq. 1.27)}$$

where $C_{\mu i}$ are the coefficients of Φ_μ, and K is the total number of basis functions. The Roothan-Hall equation for closed shell systems is also known as restricted Hartree-Fock theory (RHF). It can be written as a single matrix form:

$$\textbf{FC} = \textbf{SC}\varepsilon \qquad\qquad\qquad \text{(Eq. 1.28)}$$

where **F** is the Fock matrix, **C** is a matrix of coefficients, **S** is the overlap matrix of the basis functions and ε is the matrix of orbital energies.

HF theory constructed using the Roothaan approach results in certain limitations since all the electron correlation is ignored other than exchange. Though the correlation energy can be a small fraction of the total energy, it can be significant in many systems of physical and chemical interest. Also, basis set requires numerical solution of the four index integrals appearing in the Fock matrix elements which is a tedious process. Since each index exceeds the total number of basis functions, there will be N^4 total integrals to be evaluated.

1.2.1.2 Post Hartree-Fock Methods

The major drawback of HF calculations is that it does not consider electron correlation, instead the average affect of electron repulsion (not the explicit electron-electron interaction) is taken into account.[227] The correlation energy is defined as the

difference between the energy in the Hartree-Fock limit (E_{HF}) and the exact nonrelativistic energy of a system (ε_0).

$$E_{corr} = \varepsilon_0 - E_{HF} \qquad \text{(Eq. 1.29)}$$

The approaches which begin with a HF calculation and then correct for correlation are collectively known as post Hartree-Fock methods. The post HF methods includes Moller-Plesset perturbation theory (MPn, where n is the order of correlation), configuration interaction (CI), coupled cluster theory etc.

1.2.1.2.1 Møller-Plesset Perturbation (MP) Theory

In 1934, Christian Møller and Milton S. Plesset[228] published the Møller–Plesset perturbation [72] theory in which the electron correlation effects are added as a perturbation from Hartree-Fock wavefunction.[229,230] The difference between the exact Hamiltonian and the Fock operator is considered as a perturbation. HF becomes a first-order perturbation in mapping the HF wave function onto a perturbation theory formulation, thus a minimal amount of correlation is added by using the second order MP2 method.[231] Third-order (MP3) and fourth-order (MP4) calculations are also frequently used methods. MP5 and higher order methods are not common due to high computational cost (N^{10} complexity or worse).[227] Møller-Plesset calculations are not variational, *i.e.*, calculated energy may be lower than the true ground state energy. In MP method the exact Hamiltonian operator *H* can be written as:

$$H = H_0 + \lambda U \qquad \text{(Eq. 1.30)}$$

where H_0 is the unperturbed or 'zeroth order' Hamiltonian, U is the perturbation and λ is an arbitrary real parameter that varies between 0 and 1. When λ = 0, then $H = H_0$ and when λ = 1, then *H* equals its true value.

1.2.1.2.2 Configuration Interaction (CI)

In configuration interaction (CI) method, the electron correlation effect is incorporated in a simple and easiest way by using a multiple determinant wavefunction. A CI wavefunction considers determinants corresponding to excitation of

electrons from occupied to unoccupied orbitals along with the ground state HF wavefunction. CI uses a variational wave function that is a linear combination of configuration state functions (CSFs) built from spin orbitals and the general form of CI wavefunction can be written as:

$$|\Phi_0\rangle = c_0|\Psi_0\rangle + \sum_{ar} c_a^r|\Psi_a^r\rangle + \sum_{\substack{a<b \\ r<s}} c_{ab}^{rs}|\Psi_{ab}^{rs}\rangle + \sum_{\substack{a<b<c \\ r<s<t}} c_{abc}^{rst}|\Psi_{abc}^{rst}\rangle + \cdots \qquad \text{(Eq. 1.31)}$$

The first term accounts for the Slater determinant corresponding to the HF wave function and all other terms constitute singly, doubly, triply, ..., n-tuply excited determinants with appropriate expansion coefficients. The indices *a*, *b*, *c*, *etc.* correspond to the occupied orbitals and *r*, *s*, *t*, *etc.* are the virtual orbitals in the electron excitations. The CI methods are classified according to the number of excitations made to construct each new determinant. Configuration interaction single-excitation (CIS) calculation gives an approximation to the excited states of the molecule, not changing the ground-state energy. Single and double excited CI method (CISD) provides a ground state energy that has been corrected for correlation. Triple (CISDT) and quadruple (CISDTQ) excitation calculations are used only when very high accuracy is required.

In multi-configurational self-consistent field (MCSCF) calculations orbitals are optimized for use with the multiple-determinant wavefunction. MCSCF calculation provides the most accurate results for a given amount of CPU time. However this method demands technical sophistication from the user. One has to determine which molecular orbital is to be used and also it is important to ensure that the bonding and corresponding antibonding orbitals are correlated. In a complete active space self-consistent field (CASSCF) calculation, all combinations of the active space orbitals are included and this calculation provides the maximum correlation in the valence region. The smallest MCSCF calculation is the two configuration SCF (TCSCF) calculations. In multiconfiguration-reference configuration interaction (MRCI) the CI calculation is initiated with a MCSCF wavefunction instead of an HF wavefunction.[232] The starting wavefunction used in the calculation is called the reference state. This method uses higher number of CI determinants than a conventional CI. MRCI can provide accurate results but it is computationally demanding. An MRCI calculation with single and double

CI excitation out of an MCSCF reference space is denoted as MCSCF+1+2. Similarly, CASSCF+1+2 and GVB+1+2 are also possible. CI calculations are very accurate, but computationally expensive (N^8 times complexity or worse). A CI calculation which considers all possible excitations is known as a full CI. This is rarely done due to the demand of immense amount of computational resources. A full CI calculation can yield exact quantum mechanical results.[227]

1.2.1.2.3 Coupled Cluster (CC) Theory

Coupled cluster theory introduced by Cizek and Paldus provides the most accurate results among the practical *ab initio* electronic-structure theories applicable to moderate-sized molecules.[233-235] The truncated coupled cluster theory is not variational. In CC method, the total wavefunction is described as a linear combination of several determinants similar to CI. However, the method for choosing the wavefunction is different compared to CI. The various orders of CC expansion are CCSD, CCSDT etc. If the excitations are included successively, the energy provided by a coupled cluster method will be variational.

The central principle of CC theory is the full CI wave function, which can be written as:

$$\Psi_{CC} = e^T \Psi_{HF} \qquad \text{(Eq. 1.32)}$$

where Ψ_{CC} is a Slater determinant constructed from HF molecular orbitals and e^T can be written as:

$$e^T = 1 + T + \frac{1}{2}T^2 + \frac{1}{6}T^3 + \cdots = \sum_{k=0}^{\infty} \frac{1}{k!} T^k \qquad \text{(Eq. 1.33)}$$

T is the cluster operator which acts on to produce a linear combination of excited slater determinants:

$$T = T_1 + T_2 + T_3 + \cdots + T_n \qquad \text{(Eq. 1.34)}$$

where n is the total number of electrons, and various T_i operators generate all possible determinants having *i* excitations from the reference. For example,

$$T_2 = \sum_{i<j}^{\text{occ.}} \sum_{a<b}^{\text{vir.}} t_{ij}^{ab} \, \Psi_{ij}^{ab} \qquad \text{(Eq. 1.35)}$$

In Eq. 1.35 the amplitudes t are determined by the constraint that Eq. 1.32 should be satisfied. Considering the double excitation T = T_2, the Taylor expansion of the exponential function in Eq. 1.32 can be written as:

$$\Psi_{\text{CCD}} = \left(1 + T_2 + \frac{1}{2!}T_2^2 + \frac{1}{3!}T_2^3 + \cdots\right)\Psi_{\text{HF}} \qquad \text{(Eq. 1.36)}$$

where CCD (coupled cluster double) corresponds to the coupled cluster with only the double excitation operator. Coupled cluster methods are classified based on the highest number of excitations allowed in the definition of T. The various orders of CC expansion are CCSD, CCSDT, *etc.* where S, D, and T represents single, double and triple excitations. If the excitations are included successively, the energy provided by a coupled cluster method will be variational. Thus, CCSD calculations give variational energy, whereas CCD calculations do not. When many excitation terms are included in the expansion, CC methods become computationally very expensive compared to HF calculations.[218,236] The scaling behavior of CCSD is in the order N^6 and that of CCSDT is N^8. The most robust and most commonly used method is CCSD(T) having the computational scale of N^7.

1.2.2 Semiempirical Methods

Semi-empirical methods revise the Hartree-Fock calculations by introducing functions with empirical parameters.[234] The method is highly demanding for larger systems since the computational cost due to two-electron integrals (Coulomb and exchange) in Hamiltonian is simplified (the N^4 complexity in HF calculation typically reduced to N^2). Since the core electrons do not contribute much towards chemical activity, the core electron functions are neglected from the Hamiltonian calculation. Generally, the entire core (the nucleus and core electrons) of atoms is replaced by a parameterized function and to compensate for the errors caused by these approximations, empirical parameters are introduced into the remaining integrals and calibrated against reliable experimental or theoretical reference data. This will

drastically reduce the complexity of the calculation. Also, in semiempirical methods, only minimum requisite number of basis sets is employed.

John Pople[237] introduced the neglect of differential overlap (NDO) method which is the basis of most of the successful semiempirical methods. The method involves the modification of the HF equation, where the overlap matrix is approximated as a unit matrix. This will make the HF secular equation simpler to calculate. Traditionally, there have been three levels of integral approximations, CNDO (complete neglect of differential overlap), INDO (intermediate neglect of differential overlap), and NDDO (neglect of diatomic differential overlap). In CNDO method, all integrals involving different atomic orbitals are neglected. NDDO is found to be the best of these approximations since it retains the higher multipoles of charge distributions in the two-center interactions.

Over the years, a large number of semiempirical methods have been developed such as ZINDO (the Zerner's INDO or spectroscopic INDO), SINDO1 (symmetrically orthogonalized intermediate NDO), TNDO (typed NDO) etc. Modified neglect of differential overlap (MNDO) approach is one among the popular methods.[238] In this method, parameters are assigned for different atomic types and are fitted to reproduce properties such as heats of formation, geometrical variables, dipole moments, and first ionization energies. The most frequently used versions of the MNDO method include, Austin model 1 (AM1) and the parametric method 3 (PM3). M. J. S. Dewar and coworkers[238] introduced the zero differential overlap (ZDO) approximation which has a similar approach to MNDO in approximating two-electron integrals, but uses a modified expression for nuclear-nuclear core repulsion. ZDO neglects all products of basis functions depending on the same electron coordinates when located on different atoms. Most of the semiempirical methods are used to determine the geometric and energetic features of the molecule. Some methods provide information on dipole moments, heats of reaction and ionization potentials etc. A few methods are parameterized to give specific properties such as NMR chemical shifts and electronic spectra.

1.2.3 Density Functional Theory

The development of density functional theory (DFT) has played considerable role in the advancement of quantum chemistry.[239] The basic idea of DFT is that the energy of an electronic system can be defined using its electron density, $\rho(\mathbf{r})$ rather than wave function which is used in Hartree-Fock theory. A functional is a function of a function.[240] In DFT, the functional is the electron density which is a function of space and time. Determining energy by means of electron density significantly speeds up the calculation since the electron density is only a function of x, y, z coordinates (only three variables), whereas the many-body electronic wavefunction is a function of 3N variables (the coordinates of all N atoms in the system). Despite the number of electrons in the system, the density is always 3 dimensional which broaden the applicability of DFT to much larger systems with hundreds or even thousands of atoms. Further, the density $\rho(\mathbf{r})$ is an observable, while the many-body wave function is an intangible entity.

Though the works of Thomas and Fermi[241,242] in the late 1920s laid the foundation for DFT, the practical use was made possible by the works of Hohenberg, Kohn, and Sham.[243,244] The significance of DFT in understanding the science of molecules is reflected in the 1998 Nobel Prize in Chemistry, where Walter Kohn, the founding father of DFT, and John Pople, who was instrumental in implementing DFT in computational chemistry shared the prestigious award. These days, a majority of electronic-structure calculations in physics and chemistry utilizes DFT, which includes the analysis of electrical, magnetic, and structural properties of materials.[245,246]

In DFT, electron density, ρ, can be defined as the number of electrons in the unit volume around a point in space around $\mathbf{r}$. Electron density, when integrated over all space, gives the total number of electrons, N.

$$N = \int \rho(\mathbf{r})d\mathbf{r} \qquad \text{(Eq. 1.37)}$$

The electronic energy, E is regarded as a functional of the electron density, $E[\rho(\mathbf{r})]$.

1.2.3.1 Thomas-Fermi Model

In 1927, E. Fermi and L. H. Thomas introduced the idea of expressing the energy of a system as a function of the total electron density. In Thomas-Fermi (TF) model[241,242,247] the kinetic energy of the electrons is derived from the quantum statistical theory based on the fictitious substance called jellium (infinite number of electrons moving in an infinite volume of space with uniformly distributed positive charge) also known as the uniform electron gas, but the electron-nucleus and electron-electron interactions are treated classically. In TF model, the kinetic energy of the electron gas, $T_{\text{TF}}[\rho(\mathbf{r})]$ can be written as:

$$T_{\text{TF}}[\rho(\mathbf{r})] = \frac{3}{10}(3\pi^2)^{2/3} \int d\mathbf{r}\, \rho^{5/3}(\mathbf{r}) \qquad \text{(Eq. 1.38)}$$

It is approximated that the kinetic energy of the electrons depends exclusively on the electron density. Thus, a total energy in terms of electron density can be obtained by adding the interaction between electron-nucleus and electron-electron as below:

$$E[\rho(\mathbf{r})] = \frac{3}{10}(3\pi^2)^{\frac{2}{3}} \int d\mathbf{r}\, \rho^{\frac{5}{3}}(\mathbf{r}) - Z\int \frac{\rho(\mathbf{r})}{\mathbf{r}}d\mathbf{r} + \frac{1}{2}\iint \frac{\rho(\mathbf{r}_1)\rho(\mathbf{r}_2)}{|\mathbf{r}_1 - \mathbf{r}_2|}d\mathbf{r}_1 d\mathbf{r}_2 \qquad \text{(Eq. 1.39)}$$

The second term corresponds to electron-nucleus interaction and the third term denotes the electron-electron interactions.

Though Thomas-Fermi kinetic energy functional has an elegant mathematical derivation, it is not accurate enough for the practical application.

1.2.3.2 Hohenberg-Kohn Theorem

The theorem developed by Hohenberg and Kohn[244] in 1964 is the foundation of DFT.[248] The first Hohenberg-Kohn[99] theorem states that the ground state properties of a many-electron system depend only on the electron density and the second HK theorem states that the correct ground state density for a system is the one that minimizes the total energy through the functional. The ground state energy functional can be written

as a sum of two terms:

$$E[\rho(\mathbf{r})] = \int V_{\text{ext}}(\mathbf{r})\rho(\mathbf{r})d\mathbf{r} + F[\rho(\mathbf{r})]$$ (Eq. 1.40)

In Eq. 1.40, the first term represents the interaction of the electrons with an external potential $V_{\text{ext}}(\mathbf{r})$ and $F[\rho(\mathbf{r})]$ is the sum of the kinetic energy of the electrons and the contribution from the interelectronic interactions. The best solution corresponds to the minimum value of energy and in order to minimise the energy a Lagrangian multiplier, μ can be introduced:

$$\frac{\delta}{\delta\rho(\mathbf{r})}\left[E[\rho(\mathbf{r})] - \mu \int \rho(\mathbf{r})d\mathbf{r}\right] = 0$$ (Eq. 1.41)

Eq. 1.41 can be written as:

$$\left(\frac{\delta E[\rho(\mathbf{r})]}{\delta\rho(\mathbf{r})}\right)_{V_{\text{ext}}} = \mu$$ (Eq. 1.42)

Eq. 1.42 is the DFT equivalent of time-independent Schrödinger equation.

1.2.3.3 The Kohn-Sham Equations

Kohn and Sham[243] put forward a practical way to solve the Hohenberg-Kohn theorem. The difficulty in calculating $F[\rho(\mathbf{r})]$ in Eq. 1.40 is simplified by considering the kinetic energy of a *fictitious* system of *non-interacting* electrons with the same density $\rho(\mathbf{r})$ as the real system. Even if the systems share the same density, the non-interacting kinetic energy cannot be equal to the true kinetic energy of the interacting system. Kohn and Sham accounted this problem by introducing the following separation of the functional, $F[\rho(\mathbf{r})]$

$$F[\rho(\mathbf{r})] = E_{\text{KE}}[\rho(\mathbf{r})] + E_{\text{H}}[\rho(\mathbf{r})] + E_{\text{XC}}[\rho(\mathbf{r})]$$ (Eq. 1.43)

where $E_{\text{KE}}[\rho(\mathbf{r})]$ is the kinetic energy of non-interacting electrons, $E_{\text{H}}[\rho(\mathbf{r})]$ is the electron-electron Coulombic energy, and $E_{\text{XC}}[\rho(\mathbf{r})]$ corresponds to the energy contributions from exchange and correlation. The first term,

$$E_{\text{KE}}[\rho(\mathbf{r})] = \sum_{i=1}^{N} \int \Psi_i(\mathbf{r}) \left(-\frac{\nabla^2}{2} \right) \Psi_i(\mathbf{r}) d\mathbf{r} \qquad \text{(Eq. 1.44)}$$

Hartree electrostatic energy,

$$E_{\text{H}}[\rho(\mathbf{r})] = \frac{1}{2} \iint \frac{\rho(\mathbf{r}_1)\rho(\mathbf{r}_2)}{|\mathbf{r}_1 - \mathbf{r}_2|} d\mathbf{r}_1 d\mathbf{r}_2 \qquad \text{(Eq. 1.45)}$$

Combining Eq. 1.44 and Eq. 1.45 and adding electron-nuclear interaction leads to the full expression for the energy of an N-electron system within the Kohn-Sham scheme:

$$E[\rho(\mathbf{r})] = \sum_{i=1}^{N} \int \Psi_i(\mathbf{r}) \left(-\frac{\nabla^2}{2} \right) \Psi_i(\mathbf{r}) d\mathbf{r} + \frac{1}{2} \iint \frac{\rho(\mathbf{r}_1)\rho(\mathbf{r}_2)}{|\mathbf{r}_1 - \mathbf{r}_2|} d\mathbf{r}_1 d\mathbf{r}_2 + E_{\text{XC}}[\rho(\mathbf{r})] - \sum_{A=1}^{M} \int \frac{Z_A}{\mathbf{r} - \mathbf{R}_A} \rho(\mathbf{r}) d\mathbf{r} \qquad \text{(Eq. 1.46)}$$

The exchange-correlation energy functional in Eq. 1.46 not only comprises of the contributions due to exchange and correlation but also a contribution due to the difference between the exact and non-interacting kinetic energy of the system. Kohn and Sham proposed that the electron density of the system can be written as the sum of the square moduli of a set of N one-electron orbitals:

$$\rho(\mathbf{r}) = \sum_{i=1}^{N} |\psi_i(\mathbf{r})|^2 \qquad \text{(Eq. 1.47)}$$

Introducing Eq. 1.47 for electron density and applying the appropriate variational condition leads to the one-electron Kohn-Sham equation:

$$\left\{ -\frac{\nabla_1^2}{2} - \left(\sum_{A=1}^{M} \frac{Z_A}{\mathbf{r}_{1A}} \right) + \int \frac{\rho(\mathbf{r}_2)}{\mathbf{r}_{12}} d\mathbf{r}_2 + V_{\text{XC}}[\mathbf{r}_1] \right\} \psi_i(\mathbf{r}_1) = \varepsilon_i \psi_i(\mathbf{r}_1) \qquad \text{(Eq. 1.48)}$$

where ε_i represent the orbital energies and V_{XC} corresponds to the exchange-correlation potential which is related to the exchange-correlation energy by:

$$V_{\text{XC}}[\mathbf{r}] = \frac{\delta E_{\text{XC}}[\rho(\mathbf{r})]}{\delta \rho(\mathbf{r})} \qquad \text{(Eq. 1.49)}$$

A self-consistent approach is incorporated to solve the Kohn-Sham equations. An initial guess of the density in Eq. 1.48 will derive a set of orbitals, leading to an improved value of density, which is then employed in the second iteration and so on to attain the convergence.

1.2.3.4 Exchange-Correlation Functionals

The exchange-correlation energy, E_{XC} comprises an exchange term E_X (associated with the interaction of electrons of the same spin) and a correlation term E_C (associated with the interaction of electrons of opposite spin). The corresponding functionals are exchange functional and correlation functional:

$$E_{XC}[\rho(\mathbf{r})] = E_X[\rho(\mathbf{r})] + E_C[\rho(\mathbf{r})] \qquad \text{(Eq. 1.50)}$$

The functional dependence of E_{XC} on the electron density is expressed as an interaction between the electron density and an 'energy density' ε_{xc} that is dependent on the electron density, *viz.*

$$E_{XC}[\rho(\mathbf{r})] = \int \rho(\mathbf{r}) \, \varepsilon_{xc}[\rho(\mathbf{r})]d\mathbf{r} \qquad \text{(Eq. 1.51)}$$

ε_{xc} is the sum of individual exchange and correlation contributions. The electron density is a per unit volume density whereas the energy density is a per particle density, within this formalism the Slater exchange energy density is:

$$\varepsilon_x[\rho(\mathbf{r})] = -\frac{9\alpha}{8}\left(\frac{3}{\pi}\right)^{\frac{1}{3}} \rho^{\frac{1}{3}}(\mathbf{r}) \qquad \text{(Eq. 1.52)}$$

For practical applications, DFT methods have been designed by modifying the exchange-correlation potential. Mainly, there are three types of approximations named as local density approximation (LDA), generalized gradient approximation[249,249,250] and meta-GGA[251] methods.

1.2.3.4.1 Local Density Approximation (LDA)

The local density approximation (LDA) is the simplest approach to represent the exchange-correlation functional based on the *uniform electron gas* (a *fictitious* system in which electrons move on a positive background charge distribution such that the total ensemble is electrically neutral). The number of electrons N as well as the volume V of the gas are considered to approach infinity, while the electron density attains a constant value everywhere. LDA assumes that the exchange-correlation energy at any point in

space is a function of the electron density at that point and the exchange function is can be represented as:

$$E_X^{\text{LDA}}[\rho(\mathbf{r})] = -\frac{3}{4}\left(\frac{3}{\pi}\right)^{\frac{1}{3}} \int \rho^{\frac{4}{3}}(\mathbf{r}) d\mathbf{r}$$

(Eq. 1.53)

The local spin density approximation (LSDA) proposed by J.C. Slater,[252] represents a more general application of LDA, which introduces spin densities into the functionals, thereby solving several conceptual problems of LDA. The exchange functional in LSDA approach is given by:

$$E_X^{LDA}[\rho(\mathbf{r})] = -2^{1/3}\left(-\frac{3}{4}\left(\frac{3}{\pi}\right)^{\frac{1}{3}}\right)\int\left(\rho_\alpha^{\frac{4}{3}}(\mathbf{r}) + \int \rho_\beta^{\frac{4}{3}}(\mathbf{r})\right)d\mathbf{r}$$

(Eq. 1.54)

In Eq. 1.54, α and β represent spin up and down, respectively.

The KS orbitals in the LDA are usually similar to Hartree-Fock orbitals. In LDA, the correlation energy E_C per particle is difficult to obtain separately from the exchange energy. Several different formulations for this functional have been developed by Vosko, L. Wilk and M. Nusair known as Vosko-Wilk-Nusair or VWN[253] by incorporating Monte Carlo results.

1.2.3.4.2 Generalized Gradient Approximation (GGA)

Generalized gradient approximation methods (GGAs) assume that the exchange-correlation energies depend not only on the density but also on the gradient of the density, $\nabla\rho(\mathbf{r})$.

$$E_{\text{XC}}[\rho_\alpha(\mathbf{r}), \rho_\beta(\mathbf{r})] \equiv \int \varepsilon_{\text{xc}}(\rho_\alpha(\mathbf{r}), \rho_\beta(\mathbf{r}), \nabla\rho_\alpha(\mathbf{r})\rho_\beta(\mathbf{r})) d^3\mathbf{r}$$

(Eq. 1.55)

The development of GGA methods, follow two main lines; one based on numerical fitting procedures proposed by Becke[254] and a more rational-based one advocated by Perdew.[255,256]

1.2.3.4.3 meta-GGA

Meta-GGA functionals represent a significant improvement over GGA methods and depend explicitly on higher order density gradients which involve derivatives of the occupied Kohn-Sham orbitals. Minnesota functional, developed by Truhlar and coworkers at Minnesota University are based on the meta-GGA approximation.[257-261] The Minnesota functional includes one meta-GGA (M06-L), two meta-NGAs (M11-L and MN12-L), seven global-hybrid meta-GGAs (M05, M05-2X, M06-2X, M08-HX, and M08-SO), one range-separated hybrid meta-GGA (M11) and one screened exchange hybrid meta-NGA (MN12-SX). Among all these, the M06 family is one of the frequently used and most popular methods.

Hybrid density functional (H-GGA) methods combine the exchange-correlation of a conventional GGA method with a percentage of HF exchange. The exact amount of HF exchange is fitted semiempirically from experimental atomization energies, ionization potentials, proton affinities, total atomic energies, and other data, for a representative set of small molecules. Hybrid-meta GGA (HM-GGA) methods represent a new class of density functionals, based on a similar concept of M-GGAs, but start from M-GGAs instead of standard GGAs. These methods depend on HF exchange, the electron density and its gradient and the kinetic energy density. Examples for H-GGA methods are B3LYP, B3P86, B3PW91, B97-1, MPWB1K, and X3LYP *etc*. and B1B95, BB1K, MPW1B95 and TPSS1KCIS *etc*. are comes under HM-GGA methods.

1.2.3.5 Perdew's Jacob's ladder of Density Functionals

J. Perdew and Schmidt[262] introduced the concept of the Jacob's ladder(the famous allusion from the book of Genesis) of density functional in 2001, which is placed in the ground of the Hartree world and ends in the heaven of chemical accuracy.[263] It consists of five different rungs, comprising the five generations of density functionals *viz.* LDA, GGA, M-GGA, H-GGA and HM-HGA, and finally the fully nonlocal description. The accuracy (and also the complexity) of the functional (the exchange correlation part) increases upwards the ladder. The sixth rungs represent generalized random phase approximation, which uses occupied and unoccupied orbitals in the calculation.

Representation of the Jacob's ladder is given in Figure 1.8. Recently, Janesko added a new rung on the Jacob's ladder called "rung 3.5" which is an intermediate between the local and hybrid functional.[264,265]
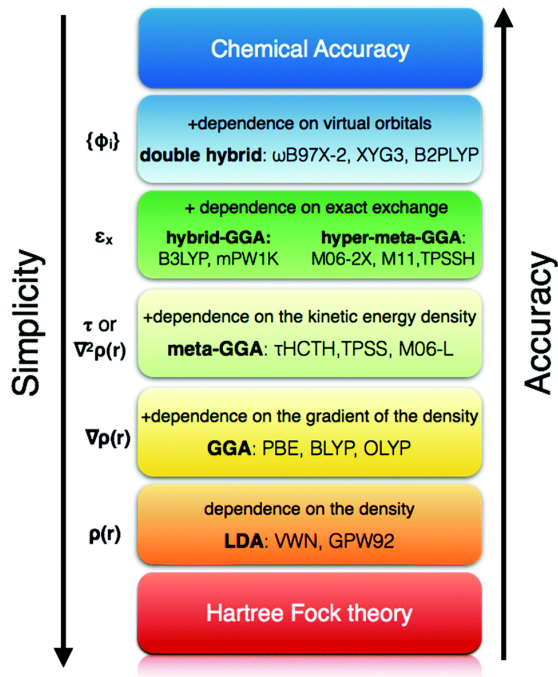
Figure 1.8 Jacob's ladder representing the five generations of density functional from the world of Hartree to the heaven of chemical accuracy, with examples from each class.[266]

1.2.3.6 Dispersion Corrections

The long-range van der Waals type interactions in molecules are incorporated using dispersion corrections.[267-269] The dispersion corrections are added to the KS-DFT functionals and the total energy of the system can be represented as:

$$E_{DFT-D} = E_{KS-DFT} + E_{disp}$$ (Eq.1.56)

where $E_{KS\text{-}DFT}$ accounts for the self-consistent Kohn-Sham energy functional.

The dispersion energy can be written as:

$$E_{disp} = -S_6 \sum_{i=1}^{N_{at}-1} \sum_{j=i+1}^{N_{at}} \frac{C_6^{ij}}{R_{ij}^6} f_{dmp}(\mathbf{R}_{ij}) \tag{Eq.1.57}$$

where N_{at} is the number of atoms in the system, S_6 is a global scaling factor which depends on the dispersion function, C_6^{ij} is the dispersion coefficient for atom pair ij, $\mathbf{R}_{ij}$ is the interatomic distance, and f_{dmp} is the damping function which must be used to avoid near-singularities for small interatomic distance.

1.2.3.7 Time-Dependent Density Functional Theory (TDDFT)

Time-dependent density functional theory (TDDFT) has become a standard tool to calculate the electronically excited states (EESs).[270,271] The structural features of the excited states and absorption and emission spectra can be well-studied using TDDFT wihin a DFT framework. In 1984, Runge and Gross[271] laid the theoretical foundations of TDDFT, they proved the time-dependent analogue of HK theorem and developed a KS scheme for the time-dependent case.

The time-dependent many-body Schrödinger equation is:

$$i\frac{\partial}{\partial t}\Psi(\{\mathbf{r}\}, t) = \hat{H}(\{\mathbf{r}\}, t)\Psi(\{\mathbf{r}\}, t) \tag{Eq. 1.58}$$

where $\hat{H}$ is the Hamiltonian operator, $\{\mathbf{r}\} = \{\mathbf{r}_1..., \mathbf{r}_N\}$ are the spatial coordinates of N electrons. By knowing the state of the system at initial time t_0, one can calculate Ψ at any other time t with the use of Eq. 1.58.

The Hamiltonian can be expressed using three terms:

$$\hat{H}(\{\mathbf{r}\}, t) = \hat{T}(\{\mathbf{r}\}) + \hat{W}(\{\mathbf{r}\}) + \hat{V}_{ext}(\{\mathbf{r}\}, t) \tag{Eq. 1.59}$$

where the first term is the the kinetic energy of electrons, second term represents the electrn-electron interaction and $\hat{V}_{ext}(\mathbf{r}, t)$ is time-dependent external potential.

$$\hat{T}(\{\mathbf{r}\}) = -\frac{1}{2}\sum_{i=1}^{N} \nabla_i^2 \tag{Eq. 1.60}$$

$$\hat{W}(\{\mathbf{r}\}) = \frac{1}{2}\sum_{\substack{i,j=1 \\ i \neq j}}^{N} \frac{1}{|\mathbf{r}_i - \mathbf{r}_j|} \tag{Eq. 1.61}$$

$$\hat{V}_{\text{ext}}(\{\mathbf{r}\}, t) = \sum_{i=1}^{N} v_{\text{ext}}(\mathbf{r}_i, t)$$

(Eq. 1.62)

The Coulomb interaction of the electrons with a set of nuclei can be described as:

$$v_{\text{ext}}(\mathbf{r}, t) = -\sum_{A=1}^{N_n} \frac{Z_A}{|\mathbf{r} - \mathbf{R}_A(t)|}$$

(Eq. 1.63)

where Z_A is the charge and $\mathbf{R}_A$ is the position of the nucleus A, N_n corresponds to the total number of nuclei in the system. The absolute square of the wave-function, $|\Psi(\{\mathbf{r}\}, t)|^2$ is the probability of finding electron at time t, it can be represented as:

$$\rho(\mathbf{r}, t) = N \int d^3 \mathbf{r}_2 \dots d^3 \mathbf{r}_N |\Psi(\mathbf{r}_1, \mathbf{r}_2, \dots, \mathbf{r}_N, t)|^2$$

(Eq. 1.64)

the density $\rho(\mathbf{r}, t)$ is normalized at all times to the total number of electrons, N. This quantity, the electronic density (r, t), is the basic variable in terms of which TDDFT is formulated.

The central theorem of TDDFT is the Runge-Gross theorem, which proves that there is a one-to-one correspondence between the time-dependent external potential, $v_{\text{ext}}(\mathbf{r}, t)$ and the time-dependent electron density, $\rho(\mathbf{r}, t)$ for many-body systems evolving from a fixed initial state. With the external potential the time-dependent Schrödinger equation can be solved, and all properties of the system can be obtained. With the use Runge-Gross theorem a time-dependent Kohn-Sham (KS) scheme can be constructed. The density of the interacting system can be calculated from the KS orbitals and can be written as:

$$\rho(\mathbf{r}, t) = \sum_{i=1}^{N} |\Phi_i^{\text{KS}}(\mathbf{r}, t)|^2$$

(Eq. 1.65)

These KS orbitals, $\phi_i(\mathbf{r}, t)$ obey the time-dependent Kohn-Sham equations,

$$i \frac{\partial \phi_i(\mathbf{r}, t)}{\partial t} = \left(\hat{H}_{\text{KS}}(\mathbf{r}, t) \right) \phi_i(\mathbf{r}, t)$$

(Eq. 1.66)

$$H_{\text{KS}}(\mathbf{r}, t) = -\frac{\nabla^2}{2} + v_{\text{KS}}[\rho](\mathbf{r}, t)$$

(Eq. 1.67)

Just like the KS scheme for the ground-state, the time-dependent KS potential can be written as the sum of three terms:

$$v_{KS}[\rho](\mathbf{r}, t) = v_{ext}(\mathbf{r}, t) + v_{Hartree}[\rho](\mathbf{r}, t) + v_{xc}[\rho](\mathbf{r}, t) \qquad \text{(Eq. 1.68)}$$

In Eq. 1.68, the first term is the external potential and second term accounts for the classical electrostatic interaction between the electrons and the thirs term is the exchange-correlation potential, the second term can be written as:

$$v_{Hartree}[\rho](\mathbf{r}, t) = \int d^3\mathbf{r}' \frac{\rho(\mathbf{r}', t)}{|\mathbf{r} - \mathbf{r}'|} \qquad \text{(Eq. 1.69)}$$

Similar to ground-state density functional theory, this is the only the fundamental approximation in TDDFT.

The TDDFT fluorescence energy can be calculated from the TDDFT singlet excitation energy by optimizing the geometry of the singlet excited state. The corresponding Stokes shift is the difference between the absorption and fluorescence energies.

$$\omega_{STOKES} = \omega_{ABS} - \omega_{FLUO} \qquad \text{(Eq. 1.70)}$$

The vertical absorption and fluorescence energies[272,53] can be written as a function of energy (E) and the geometry (R) of the system at electronically excited state and ground state as below:

$$E^{vert-abso} = E^{EES}R^{GS} - E^{GS}R^{GS} \qquad \text{(Eq. 1.71)}$$

$$E^{vert-fluo} = E^{EES}R^{EES} - E^{GS}R^{EES} \qquad \text{(Eq. 1.72)}$$

Comparison of TDDFT results with accurate spectroscopic information shows that the excited state structures , dipole moments, vibrational frequencies for small systems have equivalent accuracy as that of ground state DFT methods.[273] The use of TDDFT methods are continuously emerging and the use of KS reference over HF reference made TDDFT a reasonable method.[274-278]

1.2.4 Molecular Mechanics (MM)

Molecular mechanics (MM) methods also referred to as force field methods employ the classical laws to determine the structure and energy of very large systems.[279,280] Unlike in quantum mechanical approaches, electrons are not explicitly included, instead atoms are considered as the "building blocks". Molecules are described by a "ball and spring" model, with atoms having different sizes and "softness" and bonds having different lengths and "stiffness".[220] This perspective considers the molecule as a collection of masses that are interacting with each other *via* harmonic forces and the interactions between nuclei is described using potential energy functions.[281] The potential energy is calculated using force field instead of the wavefunction. The equations and parameters that define the energy surface of a molecule are referred to as the force field. Force fields have been steadily evolving over the years and the development of potential energy equations has been an area of important research.[281,282] The force field energy (E) is calculated based on the geometry or conformation of a molecule and it can be written as an algebraic sum of energies arising from bond stretching (E_{str}), bond bending (E_{bend}), rotation around a bond *i.e.*, torsional energy (E_{tor}), and also from non-bonded interaction energies such as van der Waals energy (E_{vdw}), and electrostatic energy (E_{elec}). The total energy can be written as:

$$E_{tot} = E_{str} + E_{bend} + E_{tor} + E_{vdw} + E_{elec} \qquad \text{(Eq. 1.73)}$$

The transferability of parameters from one molecule to a similar structural unit in another is a fundamental assumption in molecular mechanics. This assumption simplifies the force field methods and the success mainly depends on the energy expression and the data used for parameterization. Force fields differ in the number of terms in the energy expression, the complexity of the terms used, and the way in which the constants were obtained. A valence term describes various aspects of molecular shape such as bending, stretching, torsional motion etc. and all force fields have at least one valance term. A cross term describes how one motion of a molecule affects the others. For example, a stretch-bend term describes how equilibrium bond lengths tend to shift with bond angle changes.[220,283]

The calculations using force field methods are quite inexpensive even for very large systems comprising thousands of atoms such as enzymes, DNA, proteins, etc. The first force fields were introduced in the 1960's, to predict the molecular structures, vibrational spectra and enthalpies of isolated molecules. The MM potentials developed by Allinger's group: MM1, MM2 (MMX and MM+ are variations of it) were some of the popular general purpose software used for organic systems.[52,53] Today, most of the software packages for MM methods are built in with specific force fields.[284] The Merck Molecular Force Field (MMFF) uses a generalized Lennard-Jones potential where the exponents and two empirical constants are derived from experimental data for rare gas atoms.[285-287] AMBER (Assisted model building with energy refinement) and CHARMM (Chemistry at Harvard macromolecular mechanics) are the widely used force fields for proteins and nucleic acids.[284,288] The consistent force field (CFF), calculate the strain energy, vibrational spectra and vibrational enthalpy of proteins. There are different versions of CFF such as Ure-Bradley version (UBCFF), valence version (CVFF), Lynghy CFF and quantum mechanically parameterized QMFF. UFF (Universal force field) is a full periodic table force field method and is used for studying systems containing inorganic elements.[250] CHEAT (carbohydrate hydroxyls represented by external atoms) and EFF (Empirical force field) are designed for modeling carbohydrates.[289] GROMOS (Gronien molecular simulation) predict the dynamical motion of molecules and bulk liquids, and modeling of biomolecules.[236] The OPLS (Optimized potential for liquid simulations) force fields are designed to study bulk liquids. The accuracy of MM methods have been extensively documented.[290]

1.2.5 Molecular Dynamics

Molecular dynamics is a widely accepted simulation technique for finding the time dependent behavior (e. g. Brownian motion) of molecular system. MD determines how positions, velocities, and orientations of an interacting molecule changes over the time period by solving the Newton's equation of motion:

$$\mathbf{F}_i = m_i \frac{\mathrm{d}^2 \mathbf{r}_i(t)}{\mathrm{d}t^2} \qquad \text{(Eq. 1.74)}$$

where $\mathbf{r}_i(t)=(x_i(t), y_i(t), z_i(t))$ is the position vector of the ith particle and $\mathbf{F}_i$ is the force acting upon i^{th} particle at time t and m_i is the mass of the particle.

MD techniques can be used to predict thermodynamic, structural and dynamic properties of the molecule such as diffusion coefficients, correlation functions, vibrational motions, and radial distribution etc. The energy of a system at a fixed time is obtained by incorporating the molecular mechanics force field. An initial geometry is selected (not necessarily the optimized geometry) with specified initial position and velocities. Then the momentum and forces acting on each of the atoms is calculated. In the following step, a new position for each atom after a short time interval is determined using Newton's equations for motion. Then the new velocity and forces acting on each atom will be obtained. Further, these iterations are repeated till the system reaches equilibrium. The list of coordinates obtained over time is called a trajectory. The iterations are continued until a data with sufficient accuracy is attained. The MD trajectories are defined by both position and velocity vectors and they describe the time evolution of the system in phase space. Thus, MD is used as a computational "experiment" where a system is defined, allowed to evolve, and then observations made based on its evolution.

The MD methods are generally classified as classical MD and *ab initio* MD (AIMD). Classical MD is computationally inexpensive since there is no involvement of electronic motion in deriving the force acting on the atoms. The classical potentials such as Leonard-Jones, Buckingham etc. are employed in classical MD.[291] In order to determine the local atomic properties like chemical bonding, *ab initio* version of MD is required which simulate the atomic motion using quantum mechanically calculated forces.[292,293] In 1985, Car and Parrinello demonstrated the field of AIMD as a combination of MD with DFT, later it has known as the popular Car Parrinello molecular dynamics (CPMD).[294]

Techniques in which solutions are made by approximating through statistical sampling are termed Monte Carlo simulations.[295,296] MD uses a step by step algorithm to solve Newton's equation of motion using a time scale ranging from picoseconds to nanoseconds. The commonly used algorithm is Verlet algorithm.

1.2.6 Basis Sets

A basis set is a set of mathematical functions used to create the molecular orbitals, which are expanded as a linear combination with coefficients to be determined. In 1930, J. C. Slater developed a set of basis functions which decay exponentially with the distance from the nuclei.[297,298] These are known as Slater type orbitals (STOs).[299] The STOs can be represented as:

$$\Phi_{abc}^{STO}(x,y,z) = Nx^a y^b z^c e^{-\zeta r} \tag{Eq. 1.75}$$

where N is a normalization constant, a, b, c are the components of angular momentum ($L = a+b+c$), r is the radius in angstrom and ζ is the orbital exponent. STOs are primarily used for atomic and diatomic systems where high accuracy is required and in semi-empirical methods where all three- and four-centre integrals are neglected. They can also be employed with DFT methods where the exact exchange is not included and where the Coulomb energy is determined by fitting the density into a set of auxiliary functions.[220] STOs are accurate but it takes longer time to compute integrals using them. A type of orbitals which are easier to compute were introduced by S. F. Boys and it is known as Gaussian type orbitals (GTO).[300,301] GTOs can be represented as:

$$\Phi_{abc}^{GTO}(x,y,z) = Nx^a y^b z^c e^{-\zeta r^2} \tag{Eq.1.76}$$

This is a primitive Gaussian type orbital (PGTO) which is inferior to STO in accuracy. Basis sets assign a group of basis functions to each atom within a molecule to approximate its orbitals. These basis functions are composed of a linear combination of Gaussian functions; such basis functions are called contracted functions, and the component Gaussian functions are referred to as primitives. A basis function with a single Gaussian is called uncontracted. A linear combination of enough GTOs can be used to mimic an STO. A combination of n Gaussians to mimic an STO is often called STO-nG.[302,303] It is important to note that STO-nG is not composed of STOs, but n GTOs that are arranged to look like GTOs. The basis set where the smallest possible number of functions used is known as a minimal basis set (single zeta basis set). The STO-3G is a well-known minimal basis set which contracts 3 Gaussian functions to approximate the

more accurate (but more difficult to compute) STOs. Although a contracted GTO might give a good approximation to an atomic orbital, it lacks any flexibility to expand or shrink in the presence of other atoms in a molecule. Thus single zeta basis is incapable of giving highly accurate results. To solve this it is important to add extra basis functions beyond the minimum number required to describe each atom. If we have twice as many basis functions as in a minimum basis, this is called a double zeta basis set. Hence, a double-zeta basis set for hydrogen would have two functions, and a true double-zeta basis set for carbon would have 10 functions. Furthermore accurate basis sets can be described with three (triple zeta) or more basis functions.[304] Pople and coworkers introduced basis sets where the valence orbitals are represented by multiple zeta and the core orbitals by a single basis function.[305] Such basis sets are called split-valence basis sets; 3-21G, 4-21G, 6-31G, etc. are the examples of split-valence basis sets. In 3-21G basis set, the core electrons are represented as the sum of three gaussian functions and the valence orbitals are represented by two basis functions of which one is a sum of two primitive gaussians and the second one is a single gaussian function.

The additional flexibility can be built in by adding higher-angular momentum basis functions. Since the highest angular momentum orbital for carbon is a p orbital, the polarization of the atom can be described by adding a set of d functions. A hydrogen atom would use a set of 3 p functions as polarization functions. These functions are represented with * or ** [(d) or (d, p)] following G in the notation of the basis sets are called polarization functions. Diffuse basis functions are employed to describe anions, molecules with lone pairs, excited states, and transition states which can be denoted by + or ++ signs.[306] In 6-31+G basis set, s and p diffuse functions are added to non hydrogen atoms and 6-311++G adds diffuse functions to both non-hydrogen and hydrogen atoms.

Increasing the number of contracted gaussians improves the quality of basis sets and using an infinite number of functions lead to a complete basis set. Any molecular orbital can be represented by a complete basis set (CBS), but using infinite functions are not practical for calculations. The CBS can be estimated by a methodical increase in the number of basis functions and extrapolating to an infinite-size basis set limit.[307]

Dunning basis sets (cc-pVDZ, cc-pVTZ, ccpVQZ, *etc.*) are intended to converge smoothly towards the CBS limit by extrapolation.

In order to describe heavier atoms such as transition metals with large inner core, a large number of basis functions are required. This difficulty can be simplified using effective core potentials (ECPs). ECPs can be used to replace the inner (core) electrons of atomic and molecular systems by an effective core potential and treat only the valence electrons explicitly.[220,308,309] This can be effective since only the valence electrons are involved in the bonding. Incorporating ECP substantially reduce the computational cost needed for a calculation involving all the electrons and also allows for an efficient treatment of relativistic effects. There are large core and small core ECP, In large core all orbitals except $(n+1)s$, $(n+1)p$ and nd orbitals are treated as core electrons and in a small core ECP the ns, np, nd and $(n+1)s$ forms the valence orbitals. Some of the frequently employed ECPs are Los Alamos National Laboratory (LANL) ECPs and Stuttgart/Cologne ECPs.

1.2.7 Potential Energy Surface (PES)

In order to mimic the experiment, it is very important to consider not only one structure of a given structural formula, but also all the possible structures.[288,234] A potential energy surface (PES) is a mathematical function that gives the energy of a molecule as a function of its geometry. PES can provide a complete description of all the conformers and isomers possible for a system. Minimum energy structure or optimized geometry is the minima on the PES surface. A PES can have a global minimum and local minima, the global minimum represents a lowest-energy minimum structure, and the local minima represent higher energy conformers or isomers. The transition state of a reaction is marked as a first-order saddle point on the PES whereas the reactants and products are designated as minima. A simple PES can be compared to a mountain landscape with valleys and hills (Figure 1.9).[310-312] Analyses of PES can provide information regarding the molecular system. Reaction rates can be determined from the height and profile of the pathway connecting reactant and product valleys. Analysis of the shape of a valley gives information on the vibrational spectrum of the molecule.

Also, the response of the energy to electric and magnetic fields determines molecular properties such as dipole moment, polarizability, NMR shielding.[251,313]
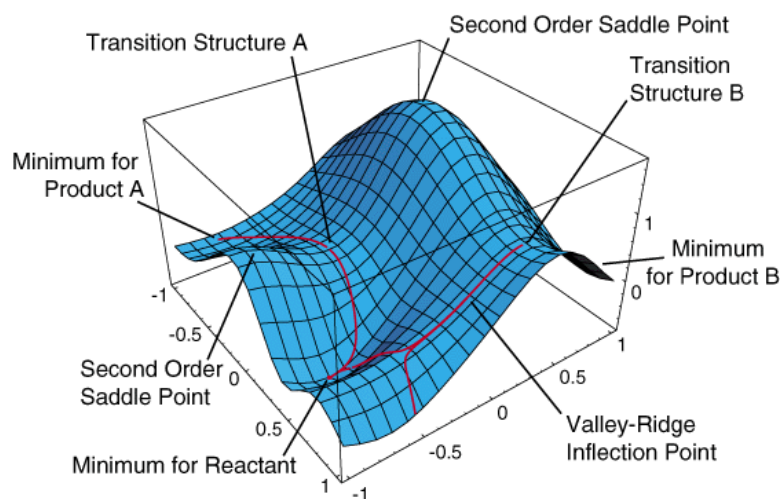
Figure 1.9 A model representation of potential energy surface.

Considering a PES of a chemical reaction, the reactant and products are positioned as minima, and the transition state of the reaction is represented as first-order saddle point. Consequently, compared to minimization, locating a transition state is a complicated job in computational chemistry.[314-317] Finding the transition state is imperative to calculate the reaction barriers and reaction rates. For a first-order saddle point, it should be a maximum in one direction and minimum in all other direction. The synchronous transit-guided quasi-Newton (STQN) method introduced by Schlegel and co-workers is the widely used approach for locating transition state.[318] Two variables of this method are QST2 and QST3 which are available in the Gaussian program suite.[319,320] QST2 requires two molecule specifications, for the reactants and products, as its input, while QST3 requires three molecule specifications: the reactants, the products, and an initial structure for the transition state. The order of the atoms must be identical within all molecule specifications.

1.2.8 Solvation Models

Since most of the reactions take place in solution, it is important to include solvent effects in computational methods. Solvent effect can be incorporated in a

system using two methods, either by implicit solvent method or by explicit solvent method.[321,322] Though the explicit solvation model provides an accurate way of modeling, their application is restricted as they are computationally expensive. Implicit solvation models are also known as continuum solvation models where a solvated molecule is encapsulated in a dielectric medium of the solvent. The electrostatic interaction of a solute with the solvent depends on the charge distribution and polarizability of the solute. A concept for treating solute polarization in solution is the reaction field and iterating that reaction field to self-consistency is called the self-consistent reaction field (SCRF) method.

One of the most frequently used continuum solvation methods is the polarizable continuum model (PCM) introduced by Tomasi and coworkers.[322-324] PCM casts the quantum mechanical SCRF equations into a boundary element problem with apparent surface charges on the solute cavity surface. There are mainly three types of PCM calculations. The original method is known as dielectric PCM (D-PCM),[323,325] an alternative model where the surrounding medium is modeled as a conductor instead of a dielectric is called C-PCM,[326] and the third one is integral equation formalism (IEF-PCM) where the PCM equations are allocated in an integral equation formalism.[327] The PCM model calculates the molecular free energy in solution as the sum over three terms:

$$\Delta G_{sol} = \Delta G_{elec} + \Delta G_{disp} + \Delta G_{cav} \tag{Eq. 1.77}$$

The first term ΔG_{elec} accounts for the electrostatic solute-solvent interaction; ΔG_{disp} is the solute-solvent dispersion and repulsion. ΔG_{cav} is the cavitation energy, needed to form the molecular cavity inside the continuum. All three terms are calculated using a cavity defined through interlocking van der Waals-spheres centered at atomic positions. The reaction field is represented through point charges located on the surface of the molecular cavity (apparent surface charge (ASC) model). A method that is very similar to PCM is the conductor-like screening model (COSMO) developed by Klamt and coworkers. This model assumes that the surrounding medium is well

modeled as a conductor, which simplifies the electrostatics computations, and corrections can be for dielectric behavior.

In solvation model density (SMD) methods the electron density of the solute as a whole is interacting with the solvent rather than its partial atomic charge. SMD is a universal solvation model, since it can be applied to any charged or uncharged solute in any solvent. SMD works similar to PCM but uses specifically parametrized radii to construct the cavity.[328] In SMD the solvation, free energy is the sum of electrostatic and cavity-dispersion term. The first component is due to a self-consistent reaction field treatment that involves the solution of the nonhomogeneous Poisson equation for electrostatics in terms of the integral equation-formalism polarizable continuum model (IEF-PCM). The second component is the contribution arising from short-range interactions between the solute and solvent molecules in the first solvation shell. There are several solvation models available and also the models are getting constant improvisations over the years.

1.3 Conclusions

The first part of Chapter 1 portrayed various aspects of reactivity descriptors used in conceptual DFT. A brief account of some of the reactivity descriptors such as electronegativity, harness and softness, electrophilicity index and frontier molecular orbital theory is provided. The role of MESP as a reactivity descriptor is explained in detail by emphasizing its application in quantifying substituent effect, non-covalent interactions etc. The literature comprising MESP applications in the field of inorganic chemistry and ligand design is also briefly accounted.

Computational chemistry methods are vital in understanding the fundamental aspects of chemistry. The second part of Chapter 1 deals with the basic principles and equations that govern the subatomic world to calculate and predict the molecular structure and properties. A brief account of various subfields of computational chemistry is provided. The basic theories underlying the computational chemistry methods such as *ab initio* methods, semiempirical methods, density functional theory, molecular mechanics, and molecular dynamics are briefly outlined. The basics of basis

sets, potential energy surface, molecular electrostatic potential, solvation models are also provided.

1.4 References

1. R. F. Hudson and G. Klopman, *Tetrahedron Lett.*, **1967**, *8*, 1103-1108.

2. G. Klopman, *J. Am. Chem. Soc.*, **1968**, *90*, 223-234.

3. K. Fukui, *Pure Appl. Chem.*, **1982**, *54*, 1825-1836.

4. R. G. Parr and W. T. Yang, *J. Am. Chem. Soc.*, **1984**, *106*, 4049-4050.

5. P. Politzer and J. S. Murray, *Rev. Comput. Chem.*, **1991**, 273-312.

6. M. H. Cohen, M. V. Gandugliapirovano and J. Kudrnovsky, *J. Chem. Phys.*, **1994**, *101*, 8988-8997.

7. H. Chermette, *J. Comput. Chem.*, **1999**, *20*, 129-154.

8. M. H. Cohen and A. Wasserman, *J. Phys. Chem. A*, **2007**, *111*, 2229-2242.

9. M. A. Kayala, C.-A. Azencott, J. H. Chen and P. Baldi, *J. Chem. Inf. Model.*, **2011**, *51*, 2209-2222.

10. G. Boon, F. De Proft, W. Langenaeker and P. Geerlings, *Chem. Phys. Lett.*, **1998**, *295*, 122-128.

11. P. Geerlings and F. De Proft, *Int. J. Mol. Sci.*, **2002**, *3*, 276-309.

12. R. G. Parr, R. A. Donnelly, M. Levy and W. E. Palke, *J. Chem. Phys.*, **1978**, *68*, 3801-3807.

13. R. G. Parr and L. J. Bartolotti, *J. Am. Chem. Soc.*, **1982**, *104*, 3801-3803.

14. Z. Zhou, R. G. Parr and J. F. Garst, *Tetrahedron Lett.*, **1988**, *29*, 4843-4846.

15. R. K. Roy, K. Choho, F. De Proft and P. Geerlings, *J. Phys. Org. Chem.*, **1999**, *12*, 503-509.

16. F. De Proft and P. Geerlings, *Chem. Rev.*, **2001**, *101*, 1451-1464.

17. W. Langenaeker, F. Deproft and P. Geerlings, *J. Phys. Chem.*, **1995**, *99*, 6424-6431.

18. R. K. Roy, S. Krishnamurti, P. Geerlings and S. Pal, *J. Phys. Chem. A*, **1998**, *102*, 3746-3755.

19. R. K. Roy, *J. Phys. Chem. A*, **2004**, *108*, 4934-4939.

20. P. Geerlings, A. M. Vos and R. A. Schoonheydt, *J. Mol. Struct. (THEOCHEM)*, **2006**, *762*, 69-78.

21. J. Padmanabhan, R. Parthasarathi, M. Elango, V. Subramanian, B. S. Krishnamoorthy, S. Gutierrez-Oliva, A. Toro-Labbe, D. R. Roy and P. K. Chattaraj, *J. Phys. Chem. A*, **2007**, *111*, 9130-9138.

22. S. Saha, R. Bhattacharjee and R. K. Roy, *J. Comput. Chem.*, **2013**, *34*, 662-672.

23. S. Damoun, G. Van de Woude, F. Méndez and P. Geerlings, *J. Phys. Chem. A*, **1997**, *101*, 886-893.

24. H. Hirao and T. Ohwada, *J. Phys. Chem. A*, **2003**, *107*, 2875-2881.

25. P. W. Ayers, J. S. M. Anderson and L. J. Bartolotti, *Int. J. Quantum Chem.*, **2005**, *101*, 520-534.

26. G. Koleva, B. Galabov, J. I. Wu, H. F. Schaefer, III and P. v. R. Schleyer, *J. Am. Chem. Soc.*, **2009**, *131*, 14722-14727.

27. R. K. Roy and S. Saha, *Annu. Rep. Prog. Chem., Sect. C: Phys. Chem.*, **2010**, *106*, 118-162.

28. M. Torrent-Sucarrat, F. De Proft, P. W. Ayers and P. Geerlings, *Phys. Chem. Chem. Phys.*, **2010**, *12*, 1072-1080.

29. B. Galabov, G. Koleva, H. F. Schaefer, III and P. v. R. Schleyer, *J. Org. Chem.*, **2010**, *75*, 2813-2819.

30. F. De Vleeschouwer, P. Jaque, P. Geerlings, A. Toro-Labbé and F. De Proft, *J. Org. Chem.*, **2010**, *75*, 4964-4974.

31. J. T. Muya, F. De Proft, P. Geerlings, M. T. Nguyen and A. Ceulemans, *J. Phys. Chem. A*, **2011**, *115*, 9069-9080.

32. T. Brinck, P. Carlqvist and J. H. Stenlid, *J. Phys. Chem. A*, **2016**, *120*, 10023-10032.

33. Z. Zhu, Q. Yang, Z. Xu, D. Zhao, H. Fan and Z. Yang, *Acta Phys. Chim. Sin.*, **2018**, *34*, 519-527.

34. P. K. Chattaraj and B. Maiti, *J. Phys. Chem. A*, **2001**, *105*, 169-183.

35. C. Morell, A. Grand and A. Toro-Labbe, *J. Phys. Chem. A*, **2005**, *109*, 205-212.

36. J. Oláh, T. Veszprémi, F. De Proft and P. Geerlings, *J. Phys. Chem. A*, **2007**, *111*, 10815-10823.

37. L. R. Domingo and P. Pérez, *Org. Biomol. Chem.*, **2013**, *11*, 4350-4358.

38. J. S. M. Anderson, J. Melin and P. W. Ayers, *J. Chem. Theory Comput.*, **2007**, *3*, 358-374.

39. J. Frau and D. Glossman-Mitnik, *Molecules*, **2018**, *23*, 559.

40. S. Sastre, J. Frau and D. Glossman-Mitnik, *Molecules*, **2017**, *22*, 458.

41. J. I. Martínez-Araya, G. Salgado-Morán and D. Glossman-Mitnik, *J. Phys. Chem. B*, **2013**, *117*, 6339-6351.

42. D. H. Ess, *J. Org. Chem.*, **2009**, *74*, 1498-1508.

43. Y. Huang, A. Zhong, C. Rong, X. Xiao and S. Liu, *J. Phys. Chem. A*, **2008**, *112*, 305-311.

44. G. Roos, J. Messens, S. Loverix, L. Wyns and P. Geerlings, *J. Phys. Chem. B*, **2004**, *108*, 17216-17225.

45. G. Roos, F. De Proft and P. Geerlings, *J. Phys. Chem. A*, **2005**, *109*, 652-658.

46. M. Torrent-Sucarrat, F. De Proft and P. Geerlings, *J. Phys. Chem. A*, **2005**, *109*, 6071-6076.

47. A. S. Özen, F. De Proft, V. Aviyente and P. Geerlings, *J. Phys. Chem. A*, **2006**, *110*, 5860-5868.

48. J. Moens, P. Jaque, F. De Proft and P. Geerlings, *J. Phys. Chem. A*, **2008**, *112*, 6023-6031.

49. C. Morell, V. Labet, A. Grand, P. W. Ayers, F. De Proft, P. Geerlings and H. Chermette, *J. Chem. Theory Comput.*, **2009**, *5*, 2274-2283.

50. G. Roos, P. Geerlings and J. Messens, *J. Phys. Chem. B*, **2009**, *113*, 13465-13475.

51. İ. Uğur, F. De Vleeschouwer, N. Tüzün, V. Aviyente, P. Geerlings, S. Liu, P. W. Ayers and F. De Proft, *J. Phys. Chem. A*, **2009**, *113*, 8704-8711.

52. P. Geerlings, P. W. Ayers, A. Toro-Labbé, P. K. Chattaraj and F. De Proft, *Acc. Chem. Res.*, **2012**, *45*, 683-695.

53. P. Geerlings, F. De Proft and W. Langenaeker, *Chem. Rev.*, **2003**, *103*, 1793-1874.

54. P. Geerlings and F. De Proft, *Phys. Chem. Chem. Phys.*, **2008**, *10*, 3028-3042.

55. R. G. Parr and R. G. Pearson, *J. Am. Chem. Soc.*, **1983**, *105*, 7512-7516.

56. Y. Li and J. N. S. Evans, *J. Am. Chem. Soc.*, **1995**, *117*, 7756-7759.

57. P. W. Ayers and M. Levy, *Theor. Chem. Acc.*, **2000**, *103*, 353-360.

58. L. Pauling, *J. Am. Chem. Soc.*, **1932**, *54*, 3570-3582.

59. H. O. Pritchard and H. A. Skinner, *Chem. Rev.*, **1955**, *55*, 745-786.

60. L. Pauling, *The Nature of the Chemical Bond*, Cornell University Press Ithaca, NY, **1960**.

61. R. G. Pearson, *Acc. Chem. Res.*, **1990**, *23*, 1-2.

62. L. R. Murphy, T. L. Meek, A. L. Allred and L. C. Allen, *J. Phys. Chem. A*, **2000**, *104*, 5867-5871.

63. R. S. Mulliken, *J. Chem. Phys.*, **1934**, *2*, 782-793.

64. A. L. Allred and E. G. Rochow, *J. Inorg. Nucl. Chem.*, **1958**, *5*, 264-268.

65. A. L. Allred and A. L. Hensley, *J. Inorg. Nucl. Chem.*, **1961**, *17*, 43-54.

66. L. C. Allen, *J. Am. Chem. Soc.*, **1989**, *111*, 9003-9014.

67. R. T. Sanderson, *J. Am. Chem. Soc.*, **1983**, *105*, 2259-2261.

68. W. Gordy, *Phys. Rev.*, **1946**, *69*, 604-607.

69. W. Gordy, *J. Chem. Phys.*, **1946**, *14*, 305-320.

70. R. Iczkowski and J. L. Margrave, *J. Am. Chem. Soc.*, **1961**, *83*, 3547-3551.

71. V. Tognetti, C. Morell and L. Joubert, *Chem. Phys. Lett.*, **2015**, *635*, 111-115.

72. A. R. Campanelli, A. Domenicano, F. Ramondo and I. Hargittai, *J. Phys. Chem. A*, **2004**, *108*, 4940-4948.

73. L. von Szentpály, *J. Phys. Chem. A*, **2015**, *119*, 1715-1722.

74. P. Politzer and J. S. Murray, *J. Mol. Model.*, **2018**, *24*, 214.

75. C. H. Suresh and N. Koga, *J. Am. Chem. Soc.*, **2002**, *124*, 1790-1797.

76. J. Onoda, M. Ondráček, P. Jelínek and Y. Sugimoto, *Nat. Commun.*, **2017**, *8*, 15155.

77. R. G. Pearson, *J. Am. Chem. Soc.*, **1963**, *85*, 3533-3539.

78. R. G. Pearson, *Science*, **1966**, *151*, 172-177.

79. R. G. Pearson and J. Songstad, *J. Am. Chem. Soc.*, **1967**, *89*, 1827-1836.

80. R. G. Pearson, *Inorg. Chem.*, **1988**, *27*, 734-740.

81. R. G. Pearson, *J. Chem. Educ.*, **1987**, *64*, 561-567.

82. P. K. Chattaraj, H. Lee and R. G. Parr, *J. Am. Chem. Soc.*, **1991**, *113*, 1855-1856.

83. F. Mendez and J. L. Gazquez, *J. Am. Chem. Soc.*, **1994**, *116*, 9298-9301.

84. J. L. Gazquez and F. Mendez, *J. Phys. Chem.*, **1994**, *98*, 4591-4593.

85. S. Krishnamurty, R. K. Roy, R. Vetrivel, S. Iwata and S. Pal, *J. Phys. Chem. A*, **1997**, *101*, 7253-7257.

86. W. Langenaeker, N. Coussement, F. De Proft and P. Geerlings, *J. Phys. Chem.*, **1994**, *98*, 3010-3014.

87. R. G. Parr, L. Von Szentpaly and S. B. Liu, *J. Am. Chem. Soc.*, **1999**, *121*, 1922-1924.

88. P. K. Chattaraj, U. Sarkar and D. R. Roy, *Chem. Rev.*, **2006**, *106*, 2065-2091.

89. D. R. Roy, R. Parthasarathi, V. Subramanian and P. K. Chattaraj, *QSAR Comb. Sci.*, **2006**, *25*, 114-122.

90. A. T. Maynard, M. Huang, W. G. Rice and D. G. Covell, *Proc. Natl. Acad. Sci. U.S.A.*, **1998**, *95*, 11578-11583.

91. M. Elango, R. Parthasarathi, G. K. Narayanan, A. M. Sabeelullah, U. Sarkar, N. S. Venkatasubramaniyan, V. Subramanian and P. K. Chattaraj, *J. Chem. Sci.*, **2005**, *117*, 61-65.

92. P. Bagaria and R. K. Roy, *J. Phys. Chem. A*, **2008**, *112*, 97-105.

93. M. Cases, G. Frenking, M. Duran and M. Solà, *Organometallics*, **2002**, *21*, 4182-4191.

94. K. Fukui, T. Yonezawa and H. Shingu, *J. Chem. Phys.*, **1952**, *20*, 722-725.

95. J.-L. Bredas, *Mater. Horiz.*, **2014**, *1*, 17-19.

96. J.-i. Aihara, *J. Phys. Chem. A*, **1999**, *103*, 7487-7495.

97. R. G. Pearson, *Hard and Soft Acids and Bases*, Van Nostrand Reinhold, **1973**.

98. Y. Ruiz-Morales, *J. Phys. Chem. A*, **2002**, *106*, 11283-11308.

99. B. Latha, P. Kumaresan, S. Nithiyanantham and K. Sampathkumar, *J. Mol. Struct.,* **2018**, *1152*, 351-360.

100. D. Mandal, R. Maity, H. Beg, G. Salgado-Moran and A. Misra, *Mol. Phys.*, **2018**, *116*, 515-525.

101. J. Frau and D. Glossman-Mitnik, *Front. Chem.*, **2018**, *6*.

102. B. Galabov, S. Ilieva, G. Koleva, W. D. Allen, H. F. Schaefer III and P. von R. Schleyer, *Wiley Interdiscip. Rev. Computat. Mol. Sci.*, **2013**, *3*, 37-55.

103. E. Scrocco and J. Tomasi, *Adv. Quantum Chem.*, **1978**, *11*, 115–193.

104. E. Scrocco and J. Tomasi, Berlin, Heidelberg, 1973.

105. J. S. Murray and P. Politzer, *Wiley Interdiscip. Rev.: Comput. Mol. Sci.*, **2011**, *1*, 153-163.

106. S. R. Gadre and C. H. Suresh, *J. Org. Chem.*, **1997**, *62*, 2625-2627.

107. C. K. Bagdassarian, V. L. Schramm and S. D. Schwartz, *J. Am. Chem. Soc.*, **1996**, *118*, 8825-8836.

108. C. I. Bayly, P. Cieplak, W. Cornell and P. A. Kollman, *J. Phys. Chem.*, **1993**, *97,* 10269-10280.

109. B. Pullman, D. Perahia and D. Cauchy, *Nucleic Acids Res.*, **1979**, *6*, 3821-3830.

110. A. Pullman and B. Pullman, *Q. Rev. Biophys.*, **1981**, *14*, 289-380.

111. R. Lavery and B. Pullman, *Int. J. Quantum Chem.*, **1981**, *20*, 259-272.

112. R. Lavery and B. Pullman, *Nucleic Acids Res.*, **1981**, *9*, 4677-4688.

113. S. Chidangil, M. K. Shukla and P. C. Mishra, *Mol. Model. Annu.*, **1998**, *4*, 250-258.

114. R. F. Stewart, *Chem. Phys. Lett.*, **1979**, *65*, 335-342.

115. P. Politzer and D. G. Truhlar, *Chemical Applications of Atomic and Molecular Electrostatic Potentials: Reactivity, Structure, Scattering, and Energetics of Organic, Inorganic, and Biological Systems*, Springer US, **2013**.

116. B. Pullman, *Int. J. Quantum Chem. Quantum Biol. Symp.*, **1990**, *17*, 81–92.

117. P. Politzer, L. Abrahmsen and P. Sjoberg, *J. Am. Chem. Soc.*, **1984**, *106*, 855-860.

118. F. A. Bulat, A. Toro-Labbe, T. Brinck, J. S. Murray and P. Politzer, *J. Mol. Model.*, **2010**, *16*, 1679-1691.

119. P. Politzer, J. S. Murray and T. Clark, *Phys. Chem. Chem. Phys.*, **2013**, *15*, 11178-11189.

120. P. Politzer, P. R. Laurence and K. Jayasuriya, *Environ. Health. Persp.*, **1985**, *61*, 191-202.

121. P. Politzer and J. S. Murray, *J. Mol. Struct.*, **1996**, *376*, 419-424.

122. S. R. Gadre and R. N. Shirsat, *Electrostatics of Atoms and Molecules*, Universities Press, Hyderabad, **2000**.

123. S. R. Gadre, S. S. Pundlik, A. C. Limaye and A. P. Rendell, *Chem. Commun.*, **1998**, *31*, 573–574.

124. S. R. Gadre, S. A. Kulkarni and I. H. Shrivastava, *J. Chem. Phys.*, **1992**, *96* 5253-5260.

125. S. Gadre, K. Babu and A. Rendell, *J. Phys. Chem. A*, **2000**, *104*, 8976-8982.

126. R. K. Pathak and S. R. Gadre, *J. Chem. Phys.*, **1990**, *93*, 1770-1773.

127. S. R. Gadre and I. H. Shrivastava, *J. Chem. Phys.*, **1991**, *94*, 4384-4390.

128. S. R. Gadre, S. Bapat and I. Shrivastava, *Comput. Chem.*, **1991**, *15*, 203-206.

129. S. R. Gadre, C. Koelmel and I. H. Shrivastava, *Inorg. Chem.*, **1992**, *31*, 2279-2281.

130. S. R. Gadre, S. A. Kulkarni and I. H. Shrivastava, *J. Chem. Phys.*, **1992**, *96*, 5253-5260.

131. S. R. Gadre, S. A. Kulkarni, C. H. Suresh and I. H. Shrivastava, *Chem. Phys. Lett.*, **1995**, *239*, 273-281.

132. S. R. Gadre and P. K. Bhadane, *J. Chem. Phys.*, **1997**, *107*, 5625-5626.

133. S. E. Wheeler and K. N. Houk, *J. Am. Chem. Soc.*, **2009**, *131*, 3126-3127.

134. S. E. Wheeler and K. N. Houk, *J. Chem. Theory Comput.*, **2009**, *5*, 2301-2312.

135. S. E. Wheeler and K. N. Houk, *J. Phys. Chem. A*, **2010**, *114*, 8658-8664.

136. S. E. Wheeler, *J. Am. Chem. Soc.*, **2011**, *133*, 10262-10274.

137. S. E. Wheeler, *Acc. Chem. Res.*, **2013**, *46*, 1029-1038.

138. B. Galabov and P. Bobadova-Parvanova, *J. Phys. Chem. A*, **1999**, *103*, 6793-6799.

139. B. Galabov and P. Bobadova-Parvanova, *J. Mol. Struct.*, **2000**, *550*, 93-98.

140. F. B. Sayyed and C. H. Suresh, *Tetrahedron Lett.*, **2009**, *50*, 7351-7354.

141. C. H. Suresh, P. Alexander, K. P. Vijayalakshmi, P. K. Sajith and S. R. Gadre, *Phys. Chem. Chem. Phys.*, **2008**, *10*, 6492-6499.

142. F. B. Sayyed and C. H. Suresh, *New J. Chem.*, **2009**, *33*, 2465-2471.

143. F. B. Sayyed, C. H. Suresh and S. R. Gadre, *J. Phys. Chem. A*, **2010**, *114*, 12330-12333.

144. P. K. Sajith and C. H. Suresh, *Inorg. Chem.*, **2012**, *51*, 967-977.

145. F. B. Sayyed and C. H. Suresh, *J. Phys. Chem. A*, **2011**, *115*, 9300-9307.

146. F. B. Sayyed and C. H. Suresh, *J. Phys. Chem. A*, **2011**, *115*, 5660-5664.

147. F. B. Sayyed and C. H. Suresh, *J. Phys. Chem. A*, **2012**, *116*, 5723-5732.

148. N. Mohan, C. H. Suresh, A. Kumar and S. R. Gadre, *Phys. Chem. Chem. Phys.*, **2013**, *15*, 18401-18409.

149. N. Mohan and C. H. Suresh, *J. Phys. Chem. A*, **2014**, *118*, 1697-1705.

150. K. P. Vijayalakshmi and C. H. Suresh, *New J. Chem.*, **2010**, *34*, 2132-2138.

151. C. H. Suresh and S. R. Gadre, *J. Org. Chem.*, **1999**, *64*, 2505-2512.

152. C. H. Suresh and N. Koga, *Inorg. Chem.*, **2002**, *41*, 1573-1578.

153. C. H. Suresh, *Inorg. Chem.*, **2006**, *45*, 4982-4986.

154. J. Mathew, T. Thomas and C. H. Suresh, *Inorg. Chem.*, **2007**, *46*, 10800-10809.

155. J. Mathew and C. H. Suresh, *Inorg. Chem.*, **2010**, *49*, 4665-4669.

156. J. Mathew and C. H. Suresh, *Organometallics*, **2011**, *30*, 1438-1444.

157. J. Mathew and C. H. Suresh, *Organometallics*, **2011**, *30*, 3106-3112.

158. O. Exner and S. Bohm, *Curr. Org. Chem.*, **2006**, *10*, 763-778.

159. C. H. Suresh and S. R. Gadre, *J. Am. Chem. Soc.*, **1998**, *120*, 7049-7055.

160. A. L. Ringer and C. D. Sherrill, *J. Am. Chem. Soc.*, **2009**, *131*, 4574-4575.

161. B. Galabov, V. Nikolova and S. Ilieva, *Chem. Eur. J.*, **2013**, *19*, 5149-5155.

162. G. S. Remya and C. H. Suresh, *New J. Chem.*, **2018**, *42*, 3602-3608.

163. L. P. Hammett, *Chem. Rev.*, **1935**, *17*, 125-136.

164. J. S. Murray and P. Politzer, *Chem. Phys. Lett.*, **1988**, *152*, 364-370.

165. M. Haeberlein, J. S. Murray, T. Brinck and P. Politzer, *Can. J. Chem.*, **1992**, *70*, 2209-2214.

166. M. Haeberlein and T. Brinck, *J. Phys. Chem.* , **1996**, *100*, 10116-10120.

167. C. H. Suresh and S. R. Gadre, *J. Am. Chem. Soc.*, **1998**, *120*, 7049-7055.

168. C. H. Suresh and S. R. Gadre, *J. Phys. Chem. A*, **2007**, *111*, 710-714.

169. B. Galabov, S. Ilieva and H. F. Schaefer, III, *J. Org. Chem.*, **2006**, *71*, 6382-6387.

170. E. G. Hohenstein and C. D. Sherrill, *J. Phys. Chem. A*, **2009**, *113*, 878-886.

171. S. E. Wheeler and K. Houk, *J. Chem. Theory Comput.*, **2009**, *5*, 2301-2312.

172. S. L. Cockroft, J. Perkins, C. Zonta, H. Adams, S. E. Spey, C. M. R. Low, J. G. Vinter, K. R. Lawson, C. J. Urch and C. A. Hunter, *Org. Biomol. Chem.*, **2007**, *5*, 1062-1080.

173. P. Politzer, P. Lane, K. Jayasuriya and L. N. Domelsmith, *J. Am. Chem. Soc.*, **1987**, *109*, 1899-1901.

174. C. H. Suresh, P. Alexander, K. P. Vijayalakshmi, P. Sajith and S. R. Gadre, *Phys. Chem. Chem. Phys.*, **2008**, *10*, 6492-6499.

175. F. B. Sayyed, C. H. Suresh and S. R. Gadre, *J. Phys. Chem. A*, **2010**, *114*, 12330-12333.

176. G. S. Remya and C. H. Suresh, *Phys. Chem. Chem. Phys.*, **2016**, *18*, 20615-20626.

177. P. Politzer, J. S. Murray and Z. Peralta-Inga, *Int. J. Quantum Chem.*, **2001**, *85*, 676-684.

178. Y. Ma and P. Politzer, *J. Chem. Phys.*, **2004**, *120*, 8955-8959.

179. A. S. Mahadevi and G. N. Sastry, *Chem. Rev.*, **2013**, *113*, 2100-2138.

180. E. A. Meyer, R. K. Castellano and F. Diederich, *Ang. Chem. Int. Ed.*, **2003**, *42*, 1210-1250.

181. B. W. Gung and J. C. Amicangelo, *J. Org. Chem.*, **2006**, *71*, 9261-9270.

182. P. Kollman, J. McKelvey, A. Johansson and S. Rothenberg, *J. Am. Chem. Soc.*, **1975**, *97*, 955-965.

183. S. R. Gadre and S. S. Pundlik, *J. Phys. Chem. B*, **1997**, *101*, 3298-3303.

184. B. Galabov, P. Bobadova-Parvanova, S. Ilieva and V. Dimitrova, *J. Mol. Struct. (THEOCHEM)*, **2003**, *630*, 101-112.

185. P. Bobadova-Parvanova and B. Galabov, *J. Phys. Chem. A*, **1998**, *102*, 1815-1819.

186. V. Dimitrova, S. Ilieva and B. Galabov, *J. Phys. Chem. A*, **2002**, *106*, 11801-11805.

187. C. B. Aakeröy, T. K. Wijethunga and J. Desper, *New J. Chem.*, **2015**, *39*, 822-828.

188. P. Politzer and J. S. Murray, *Cryst. Growth Des.*, **2015**, *15*, 3767-3774.

189. C. B. Aakeröy, C. L. Spartz, S. Dembowski, S. Dwyre and J. Desper, *IUCrJ*, **2015**, *2*, 498-510.

190. P. W. Kenny, *J. Chem. Soc., Perkin Trans. 2*, **1994**, 199-202.

191. P. W. Kenny, *J. Chem. Inf. Model.*, **2009**, *49*, 1234-1244.

192. M. D. Esrafili and M. Vakili, *Mol. Phys.*, **2015**, *114*, 1-8.

193. Y. Zeng, X. Zhang, X. Li, L. Meng and S. Zheng, *Chem. Phys. Chem.*, **2011**, *12*, 1080-1087.

194. S. R. Gadre and A. Kumar, *J. Chem. Sci.*, **2016**, *128*, 1519-1526.

195. P. V. Bijina, C. H. Suresh and S. R. Gadre, *J. Comput. Chem.*, **2018**, *39*, 488-499.

196. K. Sundararajan, K. Sankaran, K. S. Viswanathan, A. D. Kulkarni and S. R. Gadre, *J. Phys. Chem. A*, **2002**, *106*, 1504-1510.

197. M. M. Deshmukh, S. R. Gadre, R. Tonner and G. Frenking, *Phys. Chem. Chem. Phys.*, **2008**, *10*, 2298-2301.

198. S. D. Yeole and S. R. Gadre, *J. Phys. Chem. A*, **2011**, *115*, 12769-12779.

199. A. Kumar, S. R. Gadre, N. Mohan and C. H. Suresh, *J. Phys. Chem. A*, **2014**, *118*, 526-532.

200. S. Mecozzi, A. P. West and D. A. Dougherty, *Proc. Natl. Acad. Sci.*, **1996**, *93*, 10566-10571.

201. D. A. Dougherty, *Science*, **1996**, *271*, 163-168.

202. J. C. Ma and D. A. Dougherty, *Chem. Rev.*, **1997**, *97*, 1303-1324.

203. F. B. Sayyed and C. H. Suresh, *J. Phys. Chem. A*, **2012**, *116*, 5723-5732.

204. M. Sternberg, C. H. Suresh and F. Mohr, *Organometallics*, **2010**, *29*, 3922-3929.

205. N. Fey, A. G. Orpen and J. N. Harvey, *Coord. Chem. Rev.*, **2009**, *253*, 704-722.

206. O. Kühl, *Coord. Chem. Rev.*, **2005**, *249*, 693-704.

207. D. Cheshmedzhieva, P. Ivanova, S. Stoyanov, D. Tasheva, M. Dimitrova, I. Ivanovc and S. Ilieva, *Phys. Chem. Chem. Phys.*, **2011**, *13*, 18530-18538.

208. M. J. Ajitha and C. H. Suresh, *J. Org. Chem.*, **2012**, *77*, 1087-1094.

209. P. K. Sajith and C. H. Suresh, *Inorg. Chem.*, **2013**, *52*, 6046-6054.

210. C. H. Suresh, N. Koga and S. R. Gadre, *Organometallics*, **2000**, *19*, 3008-3015.

211. K. S. Sandhya and C. H. Suresh, *Dalton Trans.*, **2014**, *43*, 12279-12287.

212. K. S. Sandhya and C. H. Suresh, *Organometallics*, **2011**, *30*, 3888-3891.

213. K. S. Sandhya, G. S. Remya and C. H. Suresh, *Inorg. Chem.*, **2015**, *54*, 11150-11156.

214. D.-L. Wang, H.-T. Shen, H.-M. Gu and Y.-C. Zhai, *J. Mol. Struct. (THEOCHEM)*, **2006**, *776*, 47-51.

215. M. Alipour and A. Mohajeri, *J. Phys. Chem. A*, **2010**, *114*, 7417-7422.

216. J. Thyssen, T. Fleig and H. J. A. Jensen, *J. Chem. Phys.*, **2008**, *129*, 034109.

217. E. Schrödinger, *Ann. Phys.*, **1926**, *79*, 361.

218. A. Szabo and N. S. Ostlund, *Modern Quantum Chemistry: Introduction to Advanced Electronic Structure Theory*, Courier Corporation, **2012**.

219. R. Ditchfield, *Mol. Phys.*, **1974**, *27*, 789-807.

220. F. Jensen, *Introduction to Computational Chemistry*, John Wiley & Sons, **2017**.

221. V. Fock, *Z. Phys.*, **1930**, *61*, 126.

222. J. C. Slater, *Phys. Rev.*, **1930**, *35*, 210.

223. V. Fock, *Zeitschrift für Physik A Hadrons and Nuclei*, **1930**, *61*, 126-148.

224. J. C. Slater, *Phys. Rev.*, **1930**, *35*, 210-211.

225. G. G. Hall, *Proc. Royal Soc. A*, **1951**, *205*, 541-552.

226. C. C. J. Roothaan, *Rev. Mod. Phys.*, **1951**, *23*, 69-89.

227. D. C. Young, *Computational Chemistry: A Practical Guide for Applying Techniques to Real-World Problems*, Wiley-Interscience, New York, **2001**.

228. C. Møller and M. S. Plesset, *Phys. Rev.*, **1934**, *46*, 618.

229. W. Győrffy, G. Knizia and H.-J. Werner, *J. Chem. Phys.*, **2017**, *147*, 214101.

230. T. Y. Takeshita, W. A. de Jong, D. Neuhauser, R. Baer and E. Rabani, *J. Chem. Theory Comput.*, **2017**, *13*, 4605-4610.

231. S. Grimme, *J. Chem. Phys.*, **2003**, *118*, 9095-9102.

232. H. J. Werner and P. J. Knowles, *J. Chem. Phys.*, **1988**, *89*, 5803-5814.

233. R. J. Bartlett and M. Musiał, *Rev. Mod. Phys.*, **2007**, *79*, 291-352.

234. C. J. Cramer, *Essentials of Computational Chemistry: Theories and Models*, Wiley, **2013**.

235. J. Čížek, *J. Chem. Phys.*, **1966**, *45*, 4256-4266.

236. D. C. Young, *Computational Chemistry: A Practical Guide for Applying Techniques to Real World Problems*, **2001**, 19-31.

237. J. A. Pople, D. P. Santry and G. A. Segal, *J. Chem. Phys.*, **1965**, *43*, S129-S135.

238. M. J. S. Dewar and W. Thiel, *J. Am. Chem. Soc.*, **1977**, *99*, 4899-4907.

239. E. K. U. Gross and R. M. Dreizler, *Density Functional Theory*, Springer US, **2013**.

240. W. Kohn, A. D. Becke and R. G. Parr, *J. Phys. Chem.*, **1996**, *100*, 12974-12980.

241. E. Fermi, *Rend. Acad. Lincei*, **1927**, *6*, 602.

242. E. Fermi, *Z. Phys.*, **1928**, *48*, 73.

243. W. Kohn and L. J. Sham, *Phys. Rev.*, **1965**, *140*, A1133.

244. P. Hohenberg and W. Kohn, *Phys. Rev.*, **1964**, *136*, B864.

245. W. Koch and M. C. Holthausen, *A Chemist's Guide to Density Functional Theory*, John Wiley & Sons, **2015**.

246. J. K. Nørskov, F. Abild-Pedersen, F. Studt and T. Bligaard, *Proc. Natl. Acad. Sci.*, **2011**, *108*, 937-943.

247. L. H. Thomas, *Proc. Cambridge Phil. Soc.*, **1927**, *23*, 542.

248. K. Capelle, *Braz. J. Phys.*, **2006**, *36*, 1318-1343.

249. P. v. R. Schleyer, M. Manoharan, Z.-X. Wang, B. Kiran, H. Jiao, R. Puchta and N. J. R. van Eikema Hommes, *Org. Lett.*, **2001**, *3*, 2465-2468.

250. A. K. Rappé, C. J. Casewit, K. Colwell, W. Goddard Iii and W. Skiff, *J. Am. Chem. Soc.*, **1992**, *114*, 10024-10035.

251. F. Bernardi, M. Olivucci and M. A. Robb, *Chem. Soc. Rev.*, **1996**, *25*, 321-328.

252.   J. C. Slater, *Phys. Rev.*, **1951**, *81*, 385.

253.   S. H. Vosko, L. Wilk and M. Nusair, *Can. J. Phys.*, **1980**, *58*, 1200.

254.   A. D. Becke, *Phys. Rev. A*, **1988**, *38*, 3098.

255.   J. P. Perdew, *Phys. Rev.*, **1986**, *B 33*, 8822.

256.   J. P. Perdew, J. A. Chevary, S. H. Vosko, K. A. Jackson, M. R. Pederson, D. J. Singh and J. C. Fiolhais, *Phys. Rev. B*, **1992**, *46*, 6671.

257.   R. Peverati and D. G. Truhlar, *Phil. Trans. R. Soc. A*, **2014**, *372*, 20120476.

258.   Y. Zhao and D. G. Truhlar, *J. Chem. Phys.*, **2006**, *125*, 194101.

259.   Y.-S. Lin, C.-W. Tsai, G.-D. Li and J.-D. Chai, *J. Chem. Phys.*, **2012**, *136*, 154109.

260.   Y. Zhao, N. E. Schultz and D. G. Truhlar, *J. Chem. Phys.*, **2005**, *123*, 161103.

261.   R. Peverati and D. G. Truhlar, *J. Chem. Theory Comput.*, **2012**, *8*, 2310-2319.

262.   J. P. Perdew and K. Schmidt, *AIP Conference Proceedings*, **2001**, *577*, 1-20.

263.   J. P. Perdew and K. Schmidt, in *Density Functional Theory and Its Applications to Materials*, eds. V. E. Van Doren, K. Van Alseoy and P. Geerlings, AIP Press, New York, **2001**.

264.   B. G. Janesko, *J. Chem Phys.*, **2010**, *133*, 104103.

265.   B. G. Janesko, *Int. J. Quantum Chem.*, **2013**, *113*, 83.

266.   Q. Peng, F. Duarte and R. S. Paton, *Chem. Soc. Rev.*, **2016**, *45*, 6093-6107.

267.   E. R. Johnson, I. D. Mackie and G. A. DiLabio, *J. Phys. Org. Chem.*, **2009**, *22*, 1127-1135.

268.   S. Grimme, J. Antony, T. Schwabe and C. Muck-Lichtenfeld, *Org. Biomol. Chem.*, **2007**, *5*, 741-758.

269.   S. Grimme, *Wiley Interdiscip. Rev. Comput. Mol. Sci.*, **2011**, *1*, 211-228.

270.   C. Adamo and D. Jacquemin, *Chem. Soc. Rev.*, **2013**, *42*, 845-856.

271.   E. Runge and E. K. U. Gross, *Phys. Rev. Lett.*, **1984**, *52*, 997-1000.

272.   J. R. Cheeseman, G. W. Trucks, T. A. Keith and M. J. Frisch, *J. Chem. Phys.*, **1996**, *104*, 5497-5509.

273.   F. Furche and R. Ahlrichs, *J. Chem. Phys.*, **2002**, *117*, 7433-7447.

274.   R. Burcl, R. D. Amos and N. C. Handy, *Chem. Phys. Lett.*, **2002**, *355*, 8-18.

275.   M. Odelius, D. Laikov and J. Hutter, *J. Mol. Struct. (THEOCHEM)*, **2003**, *630*, 163-175.

276. A. Köhn and C. Hättig, *J. Chem. Phys.*, **2003**, *119*, 5021-5036.

277. M. E. Casida and M. Huix-Rotllant, *Annu. Rev. Phys. Chem.*, **2012**, *63*, 287-323.

278. M. A. Marques, C. A. Ullrich, F. Nogueira, A. Rubio, K. Burke and E. K. Gross, *Time-Dependent Density Functional Theory*, Springer Science & Business Media, **2006**.

279. W. D. Cornell, P. Cieplak, C. I. Bayly, I. R. Gould, K. M. Merz, D. M. Ferguson, D. C. Spellmeyer, T. Fox, J. W. Caldwell and P. A. Kollman, *J. Am. Chem. Soc.*, **1995**, *117*, 5179-5197.

280. K. Vanommeslaeghe, E. Hatcher, C. Acharya, S. Kundu, S. Zhong, J. Shim, E. Darian, O. Guvench, P. Lopes, I. Vorobyov and A. D. Mackerell Jr., *J. Comput. Chem.*, **2010**, *31*, 671-690.

281. J. P. Bowen and N. L. Allinger, *Rev. Comput. Chem.*, **1991**, 81-97.

282. P. K. Weiner and P. A. Kollman, *J. Comput. Chem.*, **1981**, *2*, 287-303.

283. V. G. S. Box, J. *Mol. Model.*, **1997**, *3*, 124-141.

284. J. Wang, R. M. Wolf, J. W. Caldwell, P. A. Kollman and D. A. Case, *J. Comput. Chem.*, **2004**, *25*, 1157-1174.

285. T. A. Halgren, *J. Am. Chem. Soc.*, **1992**, *114*, 7827-7843.

286. N. L. Allinger, Y. H. Yuh and J. H. Lii, *J. Am. Chem. Soc.*, **1989**, *111*, 8551-8566.

287. T. A. Halgren, *J. Comput. Chem.*, **1999**, *20*, 730-748.

288. K. Vanommeslaeghe, E. Hatcher, C. Acharya, S. Kundu, S. Zhong, J. Shim, E. Darian, O. Guvench, P. Lopes and I. Vorobyov, *J. Comput. Chem.*, **2010**, *31*, 671-690.

289. M. L. Kouwizjer and P. D. Grootenhuis, *J. Phys. Chem.*, **1995**, *99*, 13426-13436.

290. A. D. Mackerell Jr., *J. Comput. Chem.*, **2004**, *25*, 1584-1604.

291. M. P. Allen and D. J. Tildesley, *Computer Simulation of Liquids*, Oxford University Press, **2017**.

292. M. C. Payne, M. P. Teter, D. C. Allan, T. A. Arias and J. D. Joannopoulos, *Rev. Mod. Phys.*, **1992**, *64*, 1045-1097.

293. M. E. Tuckerman, P. J. Ungar, T. von Rosenvinge and M. L. Klein, *J. Phys. Chem.*, **1996**, *100*, 12878-12887.

294. R. Car and M. Parrinello, *Phys. Rev. Lett.*, **1985**, *55*, 2471-2474.

295. J. Doll and D. L. Freeman, *IEEE Comput. Sci. Eng.*, **1994**, *1*, 22.

296. K. Binder, D. Heermann, L. Roelofs, A. J. Mallinckrodt and S. McKay, *Comput. Phys.*, **1993**, *7*, 156-157.

297. L. C. Allen and A. M. Karo, *Rev. Mod. Phys.*, **1960**, *32*, 275-285.

298. J. C. Slater, *Phys. Rev.*, **1930**, *36*, 57-64.

299. L. C. K. Allen, A. M., *Rev. Modern. Phys.*, **1960**, *32*.

300. S. F. Boys, *Proc. R. Soc. Lond. A,* **1950**, *200*, 542.

301. D. D. Feller, E. R., *Basis Sets for Ab Initio Molecular Orbital Calculations and Intermolecular Interactions*, VCH, New York, **1990**.

302. J. B. Collins, P. v. R. Schleyer, J. S. Binkley and J. A. Pople, *J. Chem. Phys.*, **1976**, *64*, 5142-5151.

303. W. J. Hehre, R. F. Stewart and J. A. Pople, *J. Chem. Phys.*, **1969**, *51*, 2657-2664.

304. E. R. Davidson and D. Feller, *Chem. Rev.*, **1986**, *86*, 681-696.

305. R. Ditchfield, W. J. Hehre and J. A. Pople, *J. Chem. Phys.*, **1971**, *54*, 724-728.

306. M. J. Frisch, J. A. Pople and J. S. Binkley, *J. Chem. Phys.*, **1984**, *80*, 3265-3269.

307. G. Petersson and M. A. Al-Laham, *J. Chem. Phys.*, **1991**, *94*, 6081-6090.

308. J. G. Hill, *Int. J. Quantum Chem.*, **2013**, *113*, 21-34.

309. P. J. Hay and W. R. Wadt, *J. Chem. Phys.*, **1985**, *82*, 270-283.

310. C. E. Dykstra, *J. Comput. Chem.*, **1988**, *9*, 476-487.

311. J. Simons, P. Joergensen, H. Taylor and J. Ozment, *J. Phys. Chem.*, **1983**, *87*, 2745-2753.

312. T. Helgaker, E. Uggerud and H. J. A. Jensen, *Chem. Phys. Lett.*, **1990**, *173*, 145-150.

313. V. Barone, *J. Chem. Phys.*, **1994**, *101*, 10666-10676.

314. A. Matsuura, H. Sato, W. Sotoyama, A. Takahashi and M. Sakurai, *J. Mol. Struct. (THEOCHEM)*, **2008**, *860*, 119-127.

315. J. Baker and F. Chan, *J. Comput. Chem.*, **1996**, *17*, 888-904.

316. J. Baker, *J. Comput. Chem.*, **1986**, *7*, 385-395.

317. H. B. Schlegel, *J. Comput. Chem.*, **1982**, *3*, 214-218.

318. C. Peng and H. Bernhard Schlegel, *Isr. J. Chem.*, **1993**, *33*, 449-454.

319. T. A. Halgren and W. N. Lipscomb, *Chem. Phys. Lett.*, **1977**, *49*, 225-232.

320. P. Y. Ayala and H. B. Schlegel, *J. Chem. Phys.*, **1997**, *107*, 375-384.

321. C. J. Cramer and D. G. Truhlar, *Chem. Rev.*, **1999**, *99*, 2161-2200.

322.   J. Tomasi, B. Mennucci and R. Cammi, *Chem. Rev.*, **2005**, *105*, 2999-3094.

323.   S. Miertuš, E. Scrocco and J. Tomasi, *Chem. Phys.*, **1981**, *55*, 117-129.

324.   J. Tomasi, E. Cancès, C. S. Pomelli, M. Caricato, G. Scalmani, M. J. Frisch, R. Cammi, M. V. Basilevsky, G. N. Chuev and B. Mennucci, in *Continuum Solvation Models in Chemical Physics*, John Wiley & Sons, Ltd, **2007**, 1-123.

325.   R. Cammi and J. Tomasi, *J. Comput. Chem.*, **1995**, *16*, 1449-1458.

326.   V. Barone and M. Cossi, *J. Phys. Chem. A*, **1998**, *102*, 1995-2001.

327.   B. Mennucci, E. Cancès and J. Tomasi, *J. Phys. Chem. B*, **1997**, *101*, 10506-10517.

328.   A. V. Marenich, C. J. Cramer and D. G. Truhlar, *J. Phys. Chem. B*, **2009**, *113*, 6378-6396.

Chapter 2

Part A

Predicting Reduction Potentials of Mononuclear Cobalt Catalysts using MESP

Part B

Predicting Reduction Potentials of Fischer Carbene Complexes of Chromium using MESP
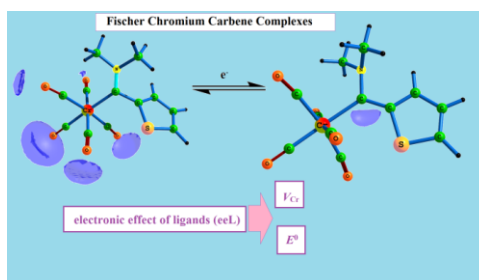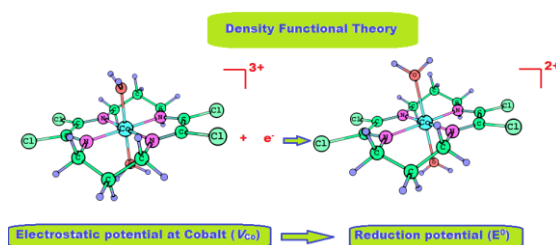
Part A: Predicting Reduction Potentials of Mononuclear Cobalt Catalysts using MESP

2.1 Abstract

*Reduction potentials (E^0) of six mononuclear cobalt catalysts (**1** − **6**) for hydrogen evolution reaction and electron donating/withdrawing effect of nine X-substituents on their macrocyclic ligand are reported at solvation effect-included B3P86/6-311+G** level of density functional theory. The electrostatic potential at the Co nucleus (V_{Co}) is found to be a powerful descriptor of the electronic effect experienced by Co from the ligand environment. The V_{Co} values vary substantially with respect to the nature of macrocycle, type of apical ligands, nature of substituent and oxidation state of the metal center. Most importantly, V_{Co} values of both the oxidized and reduced states of all the six complexes show strong linear correlation with E^0. The correlation plots between V_{Co} and E^0 provide an easy-to-interpret graphical interpretation and quantification of the effect of ligand environment on the reduction potential. Further, on the basis of a correlation between the relative V_{Co} and relative E^0 values of a catalyst with respect to the CF$_3$-substituted reference system, the E^0 of any X-substituted **1** − **6** complexes can be predicted.*

2.2 Introduction

Water splitting is considered as one of the most prominent technologies in the 21st century and significant efforts have been devoted to designing optimal electrocatalysts for hydrogen production via the hydrogen evolution reaction (HER).[1] Most of the effective water splitting electrocatalysts are still based on platinum, iridium and ruthenium, thus it is important to develop alternative metal complexes which have properties at par with that of noble metal complexes. In order to develop efficient and economically viable electrocatalysts, several studies have been carried out based on cobalt complexes over the past years.[2-7] Structural modifications of molecular cobalt

catalysts can provide imperative insights into the structure–function relationship for the hydrogen evolution reaction. Mononuclear cobalt complexes of tetraazamacrocyclic ligands are promising class of hydrogen evolving electro catalysts, known to work at modest over potential.[8-17]

Solis and Hammes-Schiffer studied the effect of substituents on tuning the reduction potentials (E^0) of cobalt diglyoxime complex referred to here as **1-X**.[18] They showed that E^0 and pK_a values of **1-X** correlate linearly to the Hammett substituent constant. The E^0 becomes more negative with increase in the electron donating character of the substituent. Theoretical calculation of E^0 to the experimental accuracy is very difficult to achieve as it demands very accurate estimation of thermodynamic parameters for both oxidized and reduced forms of the complex. This becomes even more challenging for various substituted cases as the finer substituent effects may lead to subtle variations in E^0 values. Solis and Hammes-Schiffer's work suggests that E^0 for **1-X** complex can be predicted with knowledge of substituent effect.

A MESP based analysis of reduction potentials are yet to be attempted. More than a decade ago Suresh and Koga[19] showed a strong linear relationship between V_{min} at the lone pair region of PR_3 ligands and Tolman electronic parameter. On the basis of this correlation, V_{min} has been used as a convenient electronic parameter to gauge the electron donating effect of PR_3 ligands in coordination complexes. They also derived a linear correlation between V_{min} and the experimental enthalpy change reported by Fernandez *et al.*[20] for the electrochemical couple η-Cp(CO)(PR_3)(COMe)Fe^+/η-Cp(CO)(PR_3)(COMe)Fe^0. Barring this study, a MESP based analysis of E^0 of a molecular system is yet to be reported. Herein we show that E^0 of an organometallic complex can be finely tuned by monitoring the MESP at the nucleus of the metal center. In a recent paper, Peters *et al.*[21] reported electro catalytic hydrogen evolution in acidic water for six methyl substituted cobaloxime systems, *viz.* **1-X**, **[2-X]²⁺**, **3-X**, **[4-X]³⁺**, **[5-X]³⁺** and **6-X** (Figure 2.1). These systems are selected for our study and in addition to X = CH_3, the effect of CN, CF_3, Cl, H, F, OCH_3, OH and NH_2 on the tetraazamacrocycle to modulate E^0 is considered.
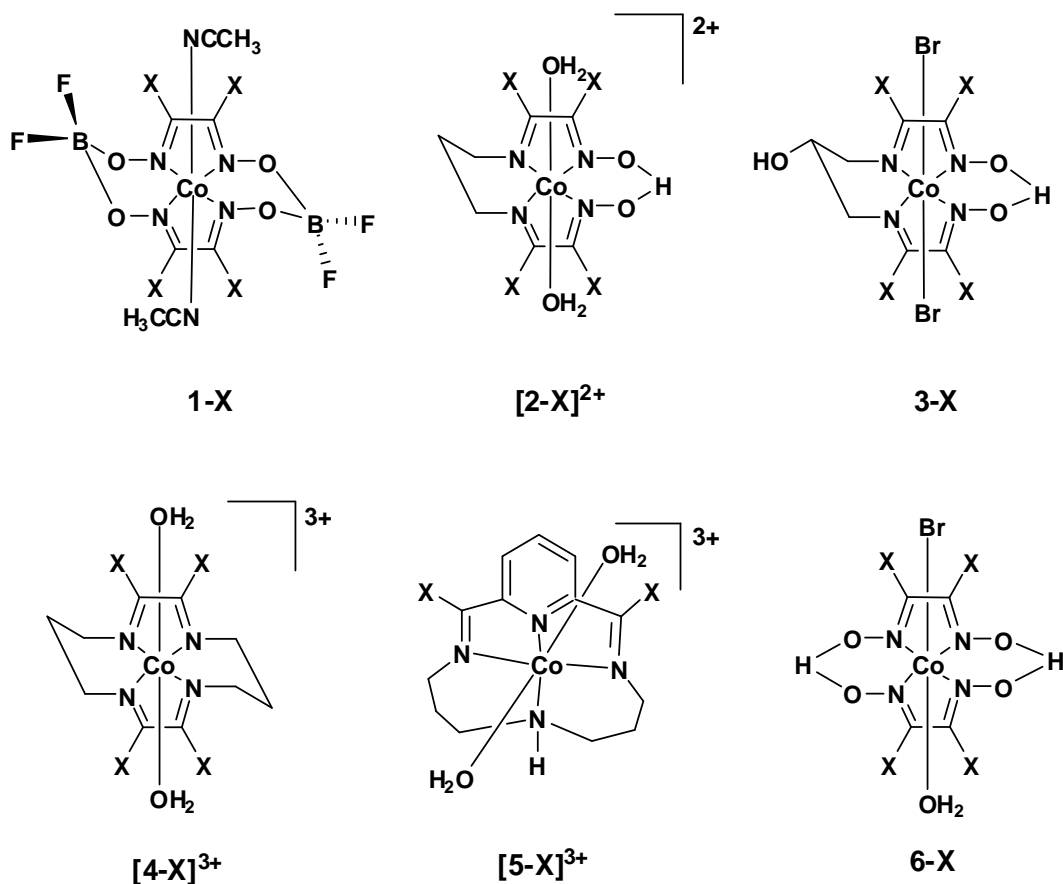
Figure 2.1 Cobalt complexes of tetraazamacrocyclic ligands (X = CN, CF$_3$, Cl, H, F, CH$_3$, OCH$_3$, OH and NH$_2$).

2.3 Computational Methodology

Isodesmic reaction method by incorporating a reference[18, 22-25] is used to calculate reduction potential (E^0). In this method, a half cell reaction with a known experimental E^0 is taken as the reference ($E^{0(ref)}$). The half cell reaction for which E^0 has to be calculated is combined with the reference to form the isodesmic reaction. E^0 is calculated using the Nernst equation, $E^0 = -\Delta G_{solv}/nF$ where F is the Faraday constant (23.06 kcal mol^{-1} V^{-1}) and n is the number of electrons involved (n = 1 for the reactions studied). In this approach the free energy contribution of electron gets cancelled.[18,25] We use the experimentally reported[10, 11] E^0 (-0.55 vs. standard calomel electrode (SCE)) of Co^{II} (dmgBF$_2$)$_2$L$_2$ (dmg = dimethylglyoxime) as $E^{0(ref)}$ in the isodesmic reaction approach (Eq. 2.1– 2.4) to calculate the reduction potential of **1-X** systems.

$$Co^{II}(dmgBF_2)_2L_2 + e^- \rightarrow [Co^I(dmgBF_2)_2L]^- + L \qquad \text{(Eq. 2.1)}$$

where L is CH_3CN

$$\textbf{1-X} + e^- \rightarrow \textbf{[1-X}'\textbf{]}^- + L \qquad \text{(Eq. 2.2)}$$

Combining (Eq. 2.1) and (Eq. 2.2) gives the isodesmic reaction

$$Co^{II}(dmgBF_2)_2L_2 + \textbf{[1-X}'\textbf{]}^- \rightarrow [Co^I(dmgBF_2)_2L]^- + \textbf{1-X} \qquad \text{(Eq. 2.3)}$$
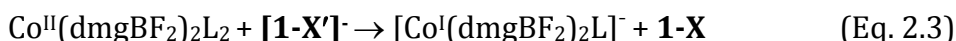
$$E^0 = -\Delta G_{solv}/nF + E^{0(ref)} \qquad \text{(Eq. 2.4)}$$

where $E^{0(ref)}$ is -0.55 V and ΔG_{solv} is the free energy change of the isodesmic reaction (Eq. 2.4). It may be noted that, a ligand loss from **1-X** leading to **[1-X′]⁻** has to be considered to develop the isodesmic scheme.

For **[2-X]²⁺**, **3-X**, **[4-X]³⁺**, **[5-X]³⁺** and **6-X** systems, Co^{III} to Co^{II} reduction occurs. The reference reaction to develop the isodesmic scheme for these systems is given in Eq. 2.5. The E^0 0.20 V vs. SCE[10] is experimentally known for this reference reaction which is used as the $E^{0(ref)}$ to calculate E^0 for **[2-X]²⁺**, **3-X**, **[4-X]³⁺**, **[5-X]³⁺** and **6-X** systems. It may be noted that the reference reaction for complexes **2 – 6** uses an experimental peak potential, which is not rigorously defined as E^0 due to reaction kinetics that can shift the peak position in the cyclic voltammetry. However, it is reasonable to assume that these related complexes would behave similarly for the non-catalytic $Co^{III/II}$ reduction. Since, no ligand loss is happening in the reference reaction, the oxidized and reduced forms of all **2 – 6** systems have been studied using full ligand environment.

$$[Co^{III}(dmgBF_2)_2L_2]^+ + e^- \rightarrow Co^{II}(dmgBF_2)_2L_2 \qquad \text{(Eq. 2.5)}$$

where L is CH_3CN.

For all computations, B3P86/6-311+G** density functional theory (DFT)[26-30] is used as implemented in the Gaussian 09[31] since a previous benchmark study by Solis and Hammes-Schiffer suggests this basis set and functional to reproduce experimental geometries.[18,23] The oxidized and reduced species were optimized in the gas phase and also verified that all are minima by vibrational frequency calculation. Complexes with unpaired electrons, *viz.* **1-X**, **[2-X]⁺**, **[3-X]⁻**, **[4-X]²⁺**, **[5-X]²⁺** and **[6-X]⁻** are computed with

the unrestricted UB3P86/6-311+G** level of theory in doublet state. Complex **[1-X′]⁻** is having Co^I metal centre and it is found to be more stable in low spin singlet state than in high spin state. The solvation free energy, ΔG_{solv} is obtained using self-consistent reaction field (SCRF) approach using 'solvation model density' (SMD) method.[32] SMD is found to be reliable in calculating free energy.[33,34] Acetonitrile is used as the solvent since most of the electrochemical experiments have been performed in this solvent. Further, $E^{0(ref)}$ values used in the isodesmic scheme correspond to experiments conducted in acetonitrile solvent. The MESP calculation is done with Gaussian 09 and V_A is directly taken from the Gaussian output file. Since the metal centre experiences the total effect of all the ligands, V_A of the cobalt nucleus (designated as V_{Co}) is analyzed for the quantification of the effects of ligands and substituents on the redox potential values.

2.4 Results and Discussion

2.4.1 Structural Details of Optimized Complexes

Figure 2.2 shows optimized structures of the oxidized and reduced forms of the complexes **1 − 6** with X = H substitution. In **1-X**, Co^{II} center is hexacoordinated while the reduced Co^I anion is pentacoordinated due to the ligand (acetonitrile) loss.[10,18] The metal center of all the oxidized and reduced forms of **2 − 5** systems is hexacoordinated as no ligand loss is observed which is desirable to develop the isodesmic scheme for $Co^{III/II}$ reduction. In the case of reduced forms of **6-X** systems wherein the X substituent is F, H, CH_3, OH, OCH_3 and NH_2, the axial ligand water gets displaced from the metal coordination sphere to form hydrogen bonded adduct with the macrocycle. In such cases, the metal center is pentacoordinated while the rest (X substituent is CN, CF_3 and Cl) show the normal hexacoordinated state of the metal center.

In all the oxidized and reduced forms of the complexes, the average value of the equatorial Co-N distances (d_1) fall in the narrow range of 1.86 – 1.96 Å. Nearly same d_1

1-H

2.236
1.891   1.891
1.891   1.891
2.236

[2-H]²⁺

1.941
1.946   1.958
1.547   1.909   1.905
1.945

3-H

2.389
1.902   1.918
1.419   1.892   1.897
2.396

[1-H′]⁻

1.921
1.857   1.858
1.858   1.858

[2-H]⁺

2.306
1.914   1.928
1.460   1.902   1.913
2.361

[3-H]⁻

2.703
1.888   1.916
1.423   1.893   1.908
2.774

[4-H]³⁺

1.942
1.939   1.939
1.941   1.941
1.942

[5-H]³⁺

1.969   1.937
1.877   1.973
1.958   1.948

6-H

1.432
2.017
1.887   1.927
1.886   1.927
2.343
1.445

[4-H]²⁺

2.344
1.929   1.929
1.929   1.929
2.344

[5-H]²⁺

2.323
1.964   1.973
1.862   1.946
2.495

[6-H]⁻

1.563
1.913
1.897
1.898   1.911
2.514
1.506

Figure 2.2 Optimized geometries of the oxidized and reduced forms of the complexes **1 − 6** with X = H, at B3P86/6-311+G** level of theory (distances in Å).

Table 2.1 Average bond length in Å between metal centre to equatorial ligand (d_1) and to axial ligand (d_2) of six complexes with various substituents. B3P86/6-311+G** DFT level of theory

Substituents	1-X d_1	1-X d_2	$[2\text{-X}]^{2+}$ d_1	$[2\text{-X}]^{2+}$ d_2	3-X d_1	3-X d_2	$[4\text{-X}]^{3+}$ d_1	$[4\text{-X}]^{3+}$ d_2	$[5\text{-X}]^{3+}$ d_1	$[5\text{-X}]^{3+}$ d_2	6-X d_1	6-X d_2
CN (ox)	1.89	2.20	1.93	1.94	1.90	2.38	1.94	1.94	1.94	1.95	1.91	2.18
CN (red)	1.86	1.91	1.92	2.32	1.90	2.65	1.93	2.33	1.94	2.41	1.89	2.52
CF₃ (ox)	1.90	2.20	1.94	1.94	1.92	2.38	1.96	1.94	1.95	1.95	1.91	2.18
CF₃ (red)	1.86	1.92	1.93	2.32	1.91	2.66	1.95	2.32	1.94	2.41	1.91	2.56
Cl (ox)	1.90	2.22	1.93	1.94	1.92	2.39	1.95	1.94	1.95	1.95	1.91	2.18
Cl (red)	1.87	1.94	1.93	2.33	1.92	2.68	1.95	2.30	1.95	2.41	1.91	2.68
F (ox)	1.89	2.24	1.93	1.95	1.90	2.40	1.94	1.94	1.94	1.95	1.91	2.18
F(red)	1.86	1.92	1.91	2.34	1.90	2.74	1.93	2.34	1.94	2.41	1.91	3.92
H (ox)	1.91	2.22	1.94	1.94	1.92	2.39	1.95	1.94	1.95	1.95	1.92	2.18
H (red)	1.91	2.18	1.93	2.33	1.92	2.70	1.95	2.34	1.95	2.40	1.92	4.02
CH₃ (ox)	1.89	2.27	1.93	1.94	1.90	2.40	1.94	1.94	1.94	1.95	1.90	2.19
CH₃(red)	1.86	1.93	1.92	2.36	1.90	2.78	1.94	2.38	1.94	2.44	1.90	3.82
OCH₃ (ox)	1.90	2.28	1.94	1.95	1.92	2.41	1.96	1.94	1.93	1.95	1.91	2.19
OCH₃(red)	1.87	1.96	1.93	2.38	1.91	2.76	1.96	2.43	1.94	2.46	1.91	3.88
OH (ox)	1.87	2.28	1.93	1.95	1.92	2.40	1.94	1.94	1.94	1.95	1.90	2.19
OH(red)	1.85	1.97	1.93	2.36	1.92	2.81	1.94	2.40	1.94	2.43	1.90	3.49
NH₂ (ox)	1.88	2.32	1.92	1.95	1.91	2.41	1.94	1.95	1.94	1.95	1.89	2.20
NH₂ (red)	1.86	1.97	1.91	2.40	1.91	2.81	1.94	2.44	1.93	2.47	1.90	3.98

values are shown by both oxidized and reduced forms of a particular case. In **1-X**, the distance from metal centre to axial ligand (d_2), $Co^I\text{-}L_{axial}$ (1.92 Å) is significantly smaller

compared to Co^{II}-L_{axial} distance (2.24 Å) which can be attributed to the reduced coordination number of the former.[10] In all other complexes where coordination number of the metal is unchanged during reduction, significant increase in d_2 is observed in the reduced forms compared to the oxidized forms (Table 2.1).

2.4.2 Reduction Potential Calculation

Table 2.2 shows calculated E^0 values of all the complexes in V vs. SCE. For **1-X**, the most electron withdrawing CN substitution gives $Co^{II/I}$ reduction potential of 0.90 V whereas for the most electron donating substituent NH_2, the reduction potential is -1.14 V. The E^0 values of CF_3, Cl, F, H, CH_3, OCH_3 and OH substituted **1-X** are 0.57, 0.00, 0.37, -0.17, -0.55, -0.88 and -0.67 V, respectively.

Table 2.2 Computed reduction potentials (E^0) of complexes **1** – **6** with various 'X' substituents (values in V vs. SCE)

X	1-X	$[2-X]^{2+}$	3-X	$[4-X]^{3+}$	$[5-X]^{3+}$	6-X
CN	0.90	0.98	-0.69	1.24	0.61	-0.22
CF_3	0.57	0.82	-0.86	1.18	0.56	-0.46
Cl	0.00	0.55	-1.07	0.89	0.44	-0.79
F	0.37	0.54	-1.10	0.87	0.42	-0.54
H	-0.17	-0.01	-1.54	0.31	0.16	-0.88
CH_3	-0.55	-0.25	-1.70	0.04	0.02	-1.06
OCH_3	-0.88	-0.15	-1.52	0.13	0.05	-1.00
OH	-0.67	-0.03	-1.55	0.30	0.14	-0.75
NH_2	-1.14	-0.58	-1.84	-0.38	-0.15	-1.13

In general, E^0 decreases as we move from electron withdrawing to electron donating substituents. This observation holds good for all the six systems studied herein and also suggests a linear correlation between Hammett substituent constant σ_p and E^0 (Figure 2.3). Earlier, Solis and Hammes-Schiffer reported such a correlation for **1-X**.[18] We also note that E^0 values obtained by us agree very well to those reported by

Solis and Hammes-Schiffer using B3P86/6-311+G** DFT in conjunction with the conductor-like polarizable continuum model (C-PCM) for solvation effects.

The mean absolute deviation of our results with values reported by Hammes-Schiffer for matching eight systems is 0.052 V.[18] The complex **6-X** shows relatively weaker correlation between σ_p and E^0 while the rest of the systems show correlation coefficient (r) above 0.94. We also note that E^0 calculated in this work does not include the effect of external acid as protonation may cause significant differences in the calculated values, particularly those having O-H-O bridges (**2**, **3** and **6**).[35] All the E^0 values of **3-X** are negative, the least negative (-0.69 V) is for CN substitution while the most negative is for NH_2 substitution (-1.84 V). The E^0 values of **[4-X]$^{3+}$** are more positive compared to other complexes. For this complex, E^0 is 1.24 V for X = CN and it decreases as the Hammett constant decreases and reaches to -0.38 V for X = NH_2. The complex **[5-X]$^{3+}$** is also showing positive E^0 except for the complex with NH_2 substitution. Similar to **3-X**, **6-X** is having negative E^0 for Co$^{III/II}$ reduction for all the nine substituents. In the case of **6-X**, CN substituent gives the least negative E^0 -0.22 V while NH_2 substituent gives the most negative E^0 -1.13 V.
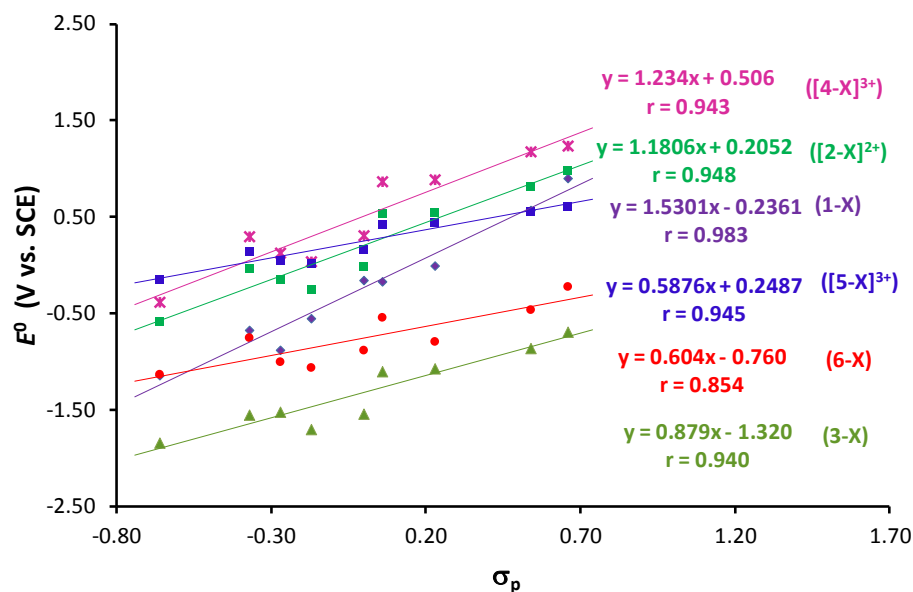
Figure 2.3 Correlation between Hammett constant (σ_p) of X-substituents and computed E^0 of X-substituted **1 − 6** complexes.

2.4.3 Molecular Electrostatic Potential Analysis

We have computed V_{Co} values for all the systems at the gas phase as well as at the solvent phase for both the oxidized and reduced forms. The trends in the gas phase V_{Co} values are very similar to the solvent phase V_{Co} values. Table 2.3 and Table 2.4 depict V_{Co} values for the oxidized and reduced complexes in the gas phase and Table 2.5 and Table 2.6 provide V_{Co} values for the oxidized and reduced complexes in the solvent respectively. As the electron donating nature of the substituent increases, V_{Co} becomes more negative suggesting a correlation between V_{Co} and E^0.

Table 2.3 Molecular electrostatic potential values (in au) at the Co nucleus (V_{Co}) of the oxidized forms of various complexes in gas phase. At B3P86/6-311+G** level of theory

X	1-X	[2-X]$^{2+}$	3-X	[4-X]$^{3+}$	[5-X]$^{3+}$	6-X
CN	-122.0721	-121.7381	-122.0401	-121.6133	-121.6480	-122.0241
CF$_3$	-122.0906	-121.7519	-122.0565	-121.6224	-121.6532	-122.0423
Cl	-122.1106	-121.7729	-122.0741	-121.6444	-121.6630	-122.0609
F	-122.1067	-121.7492	-122.0686	-121.6113	-121.6499	-122.0544
H	-122.1266	-121.7746	-122.0946	-121.6346	-121.6609	-122.0822
CH$_3$	-122.1428	-121.8053	-122.1086	-121.6748	-121.6782	-122.0962
OCH$_3$	-122.1489	-121.8199	-122.1063	-121.6961	-121.6898	-122.0924
OH	-122.1332	-121.7919	-122.0977	-121.6565	-121.6719	-122.0789
NH$_2$	-122.1556	-121.8230	-122.1156	-121.6968	-121.6890	-122.1034

All the systems show strong linear correlation between V_{Co} and E^0. The corresponding correlation plots are provided from Figure 2.4 to Figure 2.7. For the V_{Co} of the oxidized form in solvent vs. E^0 correlation plot, the r values obtained for the complexes **1-X, [2-X]$^{2+}$, 3-X, [4-X]$^{3+}$, [5-X]$^{3+}$**, and **6-X** are 0.961, 0.978, 0.968, 0.965, 0.967, and 0.980 respectively (Figure 2.6). The mean absolute deviation (MAD) of the predicted E^0 from the calculated E^0 is 0.14, 0.09, 0.08, 0.13, 0.05, and 0.04 in V for **1-X, [2-X]$^{2+}$, 3-X, [4-X]$^{3+}$, [5-X]$^{3+}$**, and **6-X** respectively. They also suggest that the

thermodynamic quantity E^0 is primarily influenced by the ligand environment around the metal centre.
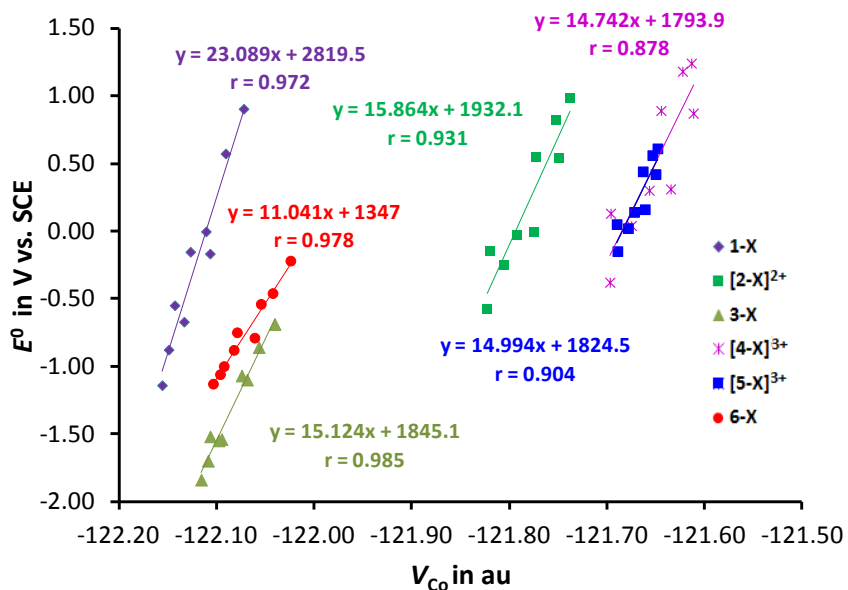
Figure 2.4 Correlation between reduction potential and molecular electrostatic potential at metal centre of oxidized form in gas phase using B3P86/6-311+G** level of theory.

Very similar results are obtained by correlating V_{Co} values of the reduced forms against the E^0 where r of the systems **[1-X′]⁻**, **[2-X]⁺**, **[3-X]⁻**, **[4-X]²⁺**, **[5-X]²⁺**, and **[6-X]⁻** is 0.972, 0.983, 0.979, 0.972, 0.979, and 0.982 respectively (Figure 2.7) while MAD of the corresponding predicted E^0 is 0.13, 0.08, 0.07, 0.12, 0.04, and 0.05 V. The V_{Co} versus E^0 correlations are remarkable considering the fact that MESP, an electronic property evaluated from one point in the molecule is useful to make a good prediction on the thermodynamic quantity E^0 of the system. MESP values also possess a thermodynamic connotation as by definition they represent the energy required to bring a unit test positive charge from infinity to the referred point. Bringing a test positive charge to the system suggests an oxidation-like process and also it implicates that MESP values are intimately related to the energetic behavior of a redox couple.

81

Table 2.4 Molecular electrostatic potential values (in au) at the Co nucleus (V_{Co}) of the reduced forms of complexes with various substitutions in gas phase. At B3P86/6-311+G** level of theory

X	$[1\text{-}X']^-$	$[2\text{-}X]^+$	$[3\text{-}X]^-$	$[4\text{-}X]^{2+}$	$[5\text{-}X]^{2+}$	$[6\text{-}X]^-$
CN	-122.1971	-121.9585	-122.2104	-121.8349	-121.8743	-122.2069
CF_3	-122.2200	-121.9756	-122.2307	-121.8475	-121.8816	-122.2285
Cl	-122.2528	-121.9993	-122.2502	-121.8754	-121.8932	-122.2438
F	-122.2614	-121.9915	-122.2547	-121.8592	-121.8884	-122.2360
H	-122.2727	-122.0321	-122.2747	-121.8754	-121.8963	-122.2612
CH_3	-122.2873	-122.0345	-122.2833	-121.9075	-121.9098	-122.2721
OCH_3	-122.2871	-122.0394	-122.2790	-121.9254	-121.9179	-122.2637
OH	-122.2869	-122.0270	-122.2761	-121.9004	-121.9057	-122.2610
NH_2	-122.3048	-122.0793	-122.2897	-121.9343	-121.9232	-122.2826
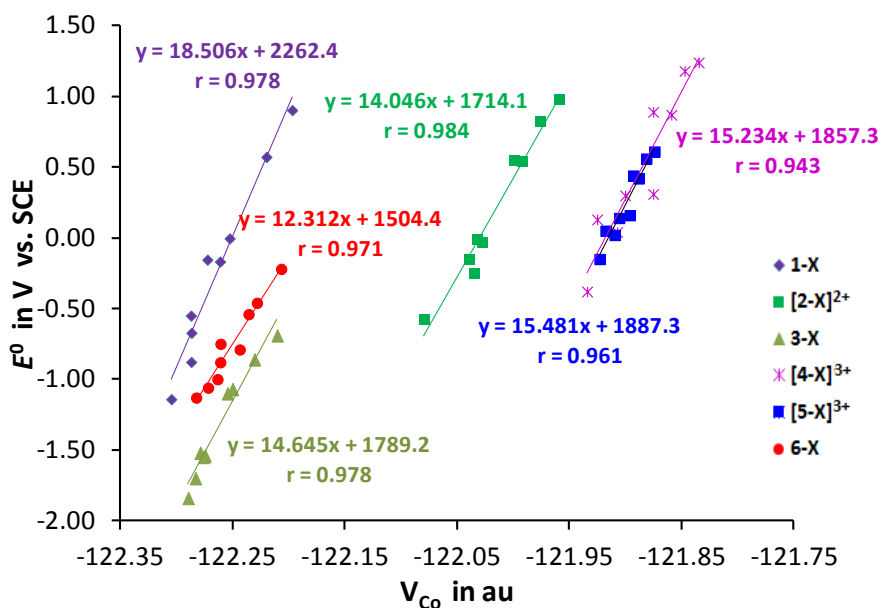
Figure 2.5 Correlation between reduction potential and molecular electrostatic potential at metal centre of reduced form in gas phase using B3P86/6-311+G** level of theory.

82

Table 2.5 Molecular electrostatic potential values (in au) at the Co nucleus (V_{Co}) of the oxidized forms of complexes with various substitutions in solvent. At B3P86/6-311+G** level of theory

X	1-X	[2-X]²⁺	3-X	[4-X]³⁺	[5-X]³⁺	6-X
CN	-122.0567	-121.6814	-122.0231	-121.5452	-121.6002	-121.9965
CF₃	-122.0871	-121.7142	-122.0492	-121.5746	-121.6144	-122.0266
Cl	-122.1141	-121.7362	-122.0711	-121.5975	-121.6248	-122.0498
F	-122.1070	-121.7223	-122.0625	-121.5788	-121.6180	-122.0414
H	-122.1396	-121.7618	-122.0931	-121.6161	-121.6345	-122.0789
CH₃	-122.1611	-121.7868	-122.1100	-121.6470	-121.6484	-122.0961
OCH₃	-122.1642	-121.7976	-122.1086	-121.6645	-121.6610	-122.0899
OH	-122.1413	-121.7715	-122.0984	-121.6295	-121.6452	-122.0722
NH₂	-122.1795	-121.8148	-122.1233	-121.6835	-121.6667	-122.1066
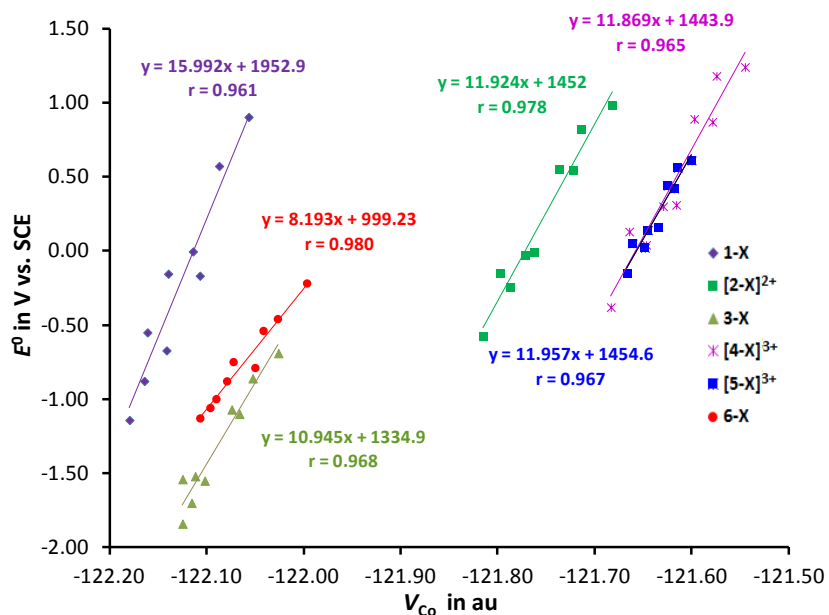
Figure 2.6 Correlation between V_{Co} and computed E^0 of oxidized forms of X-substituted **1 – 6** complexes in solvent.

Table 2.6 Molecular electrostatic potential values (in au) at the Co nucleus (V_{Co}) for the reduced forms of complexes with various substitutions in solvent. At B3P86/6-311+G** level of theory

X	[1-X]⁻	[2-X]⁺	[3-X]⁻	[4-X]²⁺	[5-X]²⁺	[6-X]⁻
CN	-122.1810	-121.9196	-122.2005	-121.7851	-121.8419	-122.1957
CF$_3$	-122.2192	-121.9534	-122.2301	-121.8171	-121.8585	-122.2271
Cl	-122.2631	-121.9804	-122.2538	-121.8464	-121.8718	-122.2484
F	-122.2673	-121.9779	-122.2528	-121.8407	-121.8716	-122.2218
H	-122.2943	-122.0108	-122.2812	-121.8708	-121.8849	-122.2602
CH$_3$	-122.3201	-122.0322	-122.2945	-121.8985	-121.8973	-122.2791
OCH$_3$	-122.3148	-122.0327	-122.2880	-121.9125	-121.9084	-122.2653
OH	-122.3063	-122.0219	-122.2829	-121.8888	-121.8971	-122.2555
NH$_2$	-122.3423	-122.0577	-122.3032	-121.9379	-121.9195	-122.2932
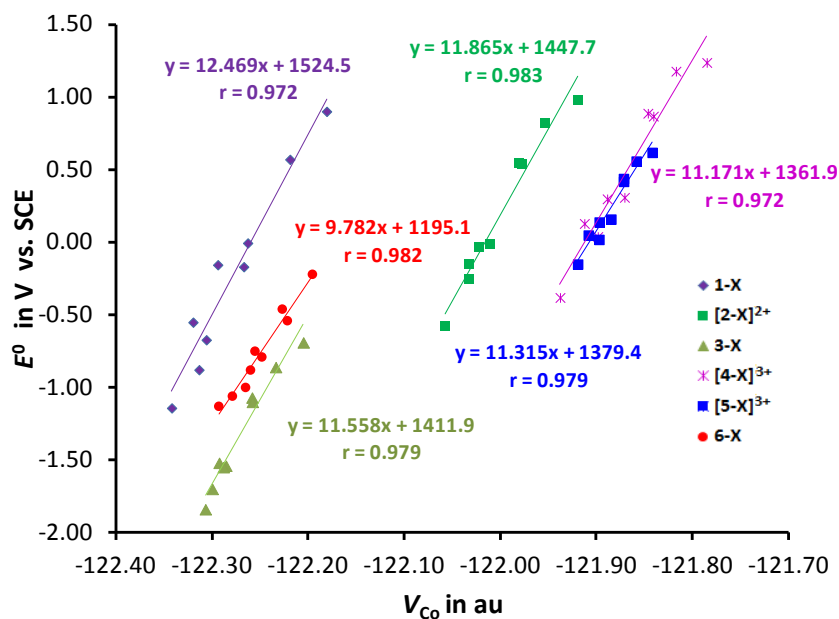
Figure 2.7 Correlation between V_{Co} and computed E^0 of reduced forms of X-substituted **1 − 6** complexes in solvent.

The correlation plots obtained for reduced states are superior to those observed for the oxidized states. This observation make sense because the process of bringing a test positive charge to the reduced state correlates more accurately to the redox couple described herein than bringing a test positive charge to the oxidized state. The correlation plots suggest that V_{Co} is very sensitive to the nature of the ligand environment and oxidation state of the metal as they fall in different regions of the plotted area.

Among all the systems, **[4-X]$^{3+}$** and **[5-X]$^{3+}$** show nearly identical correlation graphs for both oxidized and reduced forms. This indicates that the ligands though chemically very different in these systems provide nearly identical trend in ligand effect on the metal center. An inspection of the macrocyclic ligand of **[4-X]$^{3+}$** and **[5-X]$^{3+}$** shows that in both cases the ligand coordination to Co is satisfied by four nitrogen lone pairs and two water molecules. Further, two of the N-to-N connection of the macrocycle is fulfilled by the $-CH_2CH_2CH_2-$ alkyl chain in both the cases. Therefore similarity in the nature Cu-N bonding can be attributed as a reason for the similar electronic effect experienced by **[4-X]$^{3+}$** and **[5-X]$^{3+}$** leading to similar behavior for V_{Co} versus E^0 plot. The macrocycle in **[4-X]$^{3+}$** is more effective for obtaining higher reduction potential as the E^0 values of this system is almost double than that of **[5-X]$^{3+}$**.

Ligand environment of **[2-X]$^{2+}$** though identical to **[4-X]$^{3+}$**, the macrocycle of the former has $-O-H-O-$ unit for N-to-N connections compared to $-CH_2CH_2CH_2-$ unit in the latter. Since Co in **[2-X]$^{2+}$** bears less positive charge than **[4-X]$^{3+}$**, V_{Co} value of the former is more negative than the latter. Almost same amount of change in V_{Co} value of **[2-X]$^{2+}$** compared to **[4-X]$^{3+}$** is observed for all the substituents. This can be immediately noticed from the correlation plots as the correlation line obtained for **[2-X]$^{2+}$** is nearly parallel to that of **[4-X]$^{3+}$** for both oxidized and reduced forms. This result also suggests that the influence of ligand environment on E^0 is very similar for **[2-X]$^{2+}$**, **[4-X]$^{3+}$**, and **[5-X]$^{3+}$**. The E^0 values of **[2-X]$^{2+}$** lie in between that of **[4-X]$^{3+}$** and **[5-X]$^{3+}$**.

In the case of **3-X**, the macrocyclic ligand is same as that of **[2-X]$^{2+}$** except for an OH substituent present in the alkyl chain. Since **3-X** is neutral, it shows more negative V_{Co} values than **[2-X]$^{2+}$**. It is noteworthy that E^0 values of **3-X** is negative for all the

substituents. This may be attributed to anionic Br$^-$ ligands in **3-X** which can provide more electron density to the metal compared to the neutral H_2O in **[2-X]$^{2+}$**. Compared to **3-X**, **6-X** has two –O-H-O- units to make the N-to-N connectivity for the macrocycle. Further, **6-X** has one Br$^-$ and one H_2O ligand compared to two Br$^-$ in **3-X** suggesting less negative V_{Co} values for the former system compared to the latter.

The V_{Co} values indicate that the oxidized and reduced forms of **6-X** is 11 – 28 and 4 – 21 kcal/mol, respectively less negative than the corresponding values of **3-X**. The slope of the correlation line for **6-X** is 8.193 for oxidized and 9.782 for the reduced forms which are smaller than the slope of the correlation lines obtained for the oxidized and reduced forms of **3-X**, **[2-X]$^{2+}$**, **[4-X]$^{3+}$**, and **[5-X]$^{3+}$** (nearly a constant, ~11.6). This means that the second–O-H-O– bridge in **6-X** is not very electron-withdrawing, and therefore its effects on V_{Co} and thus E^0 are not so pronounced. The improvement in the E^0 values of **6-X** by 28 – 68 % compared to **3-X** can be mainly attributed to the change in the two electron donor ligands than the changes made in the macrocyclic ligand.

Among the six types of hydrogen evolving electrocatalysts studied herein, **1-X** is the most unique due to its two –O-BF$_2$-O– bridges to make the macrocyclic N-to-N connectivity. For the oxidized form of **1-X**, V_{Co} is more negative than **3-X** by 19 – 33 kcal/mol whereas the reduced form is less negative compared to **[3-X]$^-$** system by 7 – 21 kcal/mol except for X = NH$_2$ where V_{Co} is more negative by 1.1 kcal/mol. Unlike the neutral systems **3-X** and **6-X**, **1-X** shows positive E^0 values for electron withdrawing substitution on the macrocycle while the electron donating substitution yields negative E^0 values. The macrocycle of **1-X** is more sensitive to substitution than rest of the complex as it yields the highest difference of 2.04 V for the most electron withdrawing **1-CN** and the most electron donating **1-NH$_2$** systems.

2.4.4 A General Correlation for Predicting Reduction Potentials

Though the correlation equations given in Figures 2.4 to 2.7 are useful to predict the redox properties of a given type of molecular complex using the MESP value at the metal center, a general correlation approach encompassing all the set of complexes is more powerful. To derive such a correlation, we use the relative value of V_{Co} (ΔV_{Co}) and

relative value of E^0 (ΔE^0) of a given type of complex with respect to a reference X-substituted complex. For instance, in the case of **1-X** systems, with respect to **1-CF₃** system as reference, ΔE^0 of **1-NH₂** and **1-CN** are 1.71 and -0.33 V and the relative V_{Co} values (ΔV_{Co}) are 0.1232 and -0.0382 au respectively. Although one can select any X-substituted system as a reference, a screening study for all has shown that CF₃-substituded reference gives the least variation in predicting E^0 values for $\mathbf{1-6}$ systems. Further, as discussed before the data obtained for the reduced form provide better correlation than the oxidized form. The ΔE^0 and ΔV_{Co} values based on CF₃-substituted reference are given in Table 2.7 for the reduced state of $\mathbf{1-6}$ systems in solvent.

Table 2.7 The ΔE^0 (in V) and ΔV_{Co} (in au) values based on CF₃-substituded reference for the reduced state of X-substituted $\mathbf{1-6}$ complexes in solvent

Complex	CN	CF₃	Cl	F	H	CH₃	OCH₃	OH	NH₂
					ΔV_{Co}				
[1-X′]⁻	-0.0382	0.0	0.0440	0.0481	0.0751	0.1009	0.0947	0.0871	0.1232
[2-X]⁺	-0.0337	0.0	0.0270	0.0245	0.0574	0.0789	0.0793	0.0685	0.1043
[3-X]⁻	-0.0296	0.0	0.0237	0.0227	0.0510	0.0644	0.0579	0.0528	0.0731
[4-X]²⁺	-0.0321	0.0	0.0293	0.0236	0.0537	0.0814	0.0954	0.0717	0.1208
[5-X]²⁺	-0.0166	0.0	0.0132	0.0131	0.0263	0.0388	0.0499	0.0385	0.0609
[6-X]⁻	-0.0314	0.0	0.0213	-0.0053	0.0331	0.0520	0.0382	0.0284	0.0661
					ΔE^0				
1-X	-0.33	0.0	0.58	0.74	0.73	1.12	1.45	1.24	1.71
[2-X]²⁺	-0.16	0.0	0.27	0.28	0.83	1.07	0.97	0.85	1.40
3-X	-0.17	0.0	0.21	0.24	0.67	0.84	0.67	0.69	0.98
[4-X]³⁺	-0.07	0.0	0.29	0.30	0.87	1.14	1.05	0.87	1.55
[5-X]³⁺	-0.06	0.0	0.12	0.14	0.40	0.54	0.56	0.42	0.71
6-X	-0.24	0.0	0.33	0.08	0.42	0.60	0.54	0.29	0.66
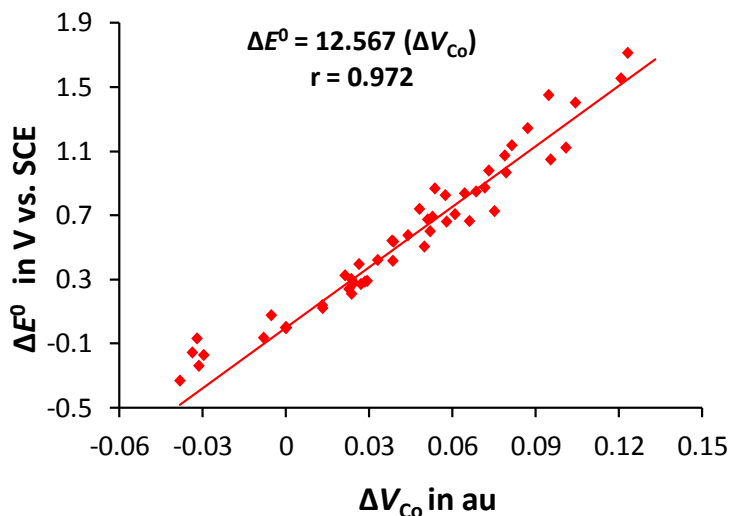
Figure 2.8 Linear correlation between the relative V_{Co} (in au) and relative computed E^0 (in V) values of the X-substituted complexes **1 − 6** with respect to those of the CF$_3$-substituted **1 − 6** complexes in reduced state.

Figure 2.8 shows a good linear correlation between ΔV_{Co} and ΔE^0 which suggests that if we know the E^0 value of CF$_3$-substituted system, E^0 of any other substituted system can be predicted solely from the electrostatic potential at the cobalt nucleus of the reduced form of the complex. As per the correlation equation in Figure 2.8, ΔE^0 of an X-substituted system is 12.567 times the ΔV_{Co}. Therefore, E^0 of the X-substituted system can be obtained by subtracting E^0 of CF$_3$-substituted system from 12.567 times ΔV_{Co} of the X-substituted system.

To further illustrate the use of this method in predicting E^0 for unknown systems, we have computed V_{Co} of **1-NO₂**, **2-COF**, **3-NO**, **4-NCO**, **5-CCl₃**, and **6-OCF₃** in reduced form and obtained values -122.1961, -121.9660, -122.1798, -121.8929, -121.8989, and -122.2202 au, respectively. These values suggest that with respect to CF$_3$-substituted system as reference, ΔV_{Co} values of **1-NO₂**, **2-COF**, **3-NO**, **4-NCO**, **5-CCl₃**, and **6-OCF₃** are -0.0231, 0.0126, -0.0503, -0.0758, 0.0404, and -0.0069 au, respectively. Hence, from the correlation equation in Figure 2.8, we can predict that E^0 values for **1-NO₂**, **2-COF**, **3-NO**, **4-NCO**, **5-CCl₃**, and **6-OCF₃** complexes are 0.86, 0.66, -0.23, 0.22, 0.05, and -0.38 V, respectively vs. SCE.

We have also computed V_{Co} values using two different methods, *viz.* the Minnesota DFT method M06L/6-311+g(d,p)[36] and Grimme's dispersion-corrected DFT method B97D/6-311+g(d,p)[37] and tested the validity of the general correlation approach presented in Figure 2.8. The V_{Co} values obtained from both these methods were more negative than B3P86/6-311+g(d,p) for all X-substituted **1** – **6** systems. Nevertheless, both the methods showed almost identical increasing trends in the negative character of V_{Co} with respect to the increasing electron donating character of the substituent. Further, their ΔV_{Co} versus ΔE^0 correlation plots were in excellent agreement with B3P86/6-311+g(d,p) results.(Figure 2.9 and Figure 2.10).
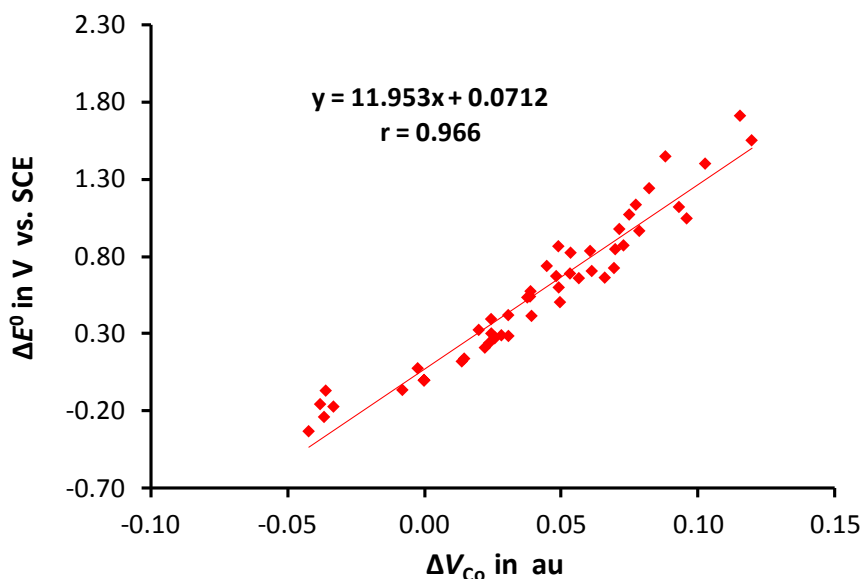
Figure 2.9 Linear correlation between ΔV_{Co} and ΔE^0 of complexes with relative values of X=CF$_3$ in reduced form. The V_{Co} is calculated at M06L/6-311+g(d,p) level of theory using B3P86/6-311+g(d,p) level optimized geometry.
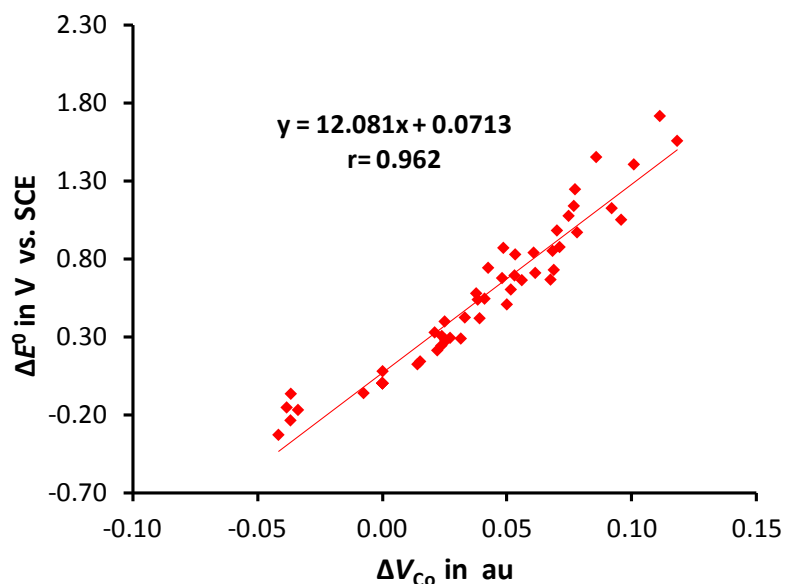
Figure 2.10 Linear correlation between ΔV_{Co} and ΔE^0 of complexes with relative values of X=CF$_3$ in reduced form. The V_{Co} is calculated B97D/6-311+g(d,p) level of theory using B3P86/6-311+g(d,p) level optimized geometry.

2.5 Conclusions

Six different mono nuclear cobalt complexes of tetraza macrocyclic ligands used as catalysts for hydrogen evolution reaction have been studied with nine different substituents using density functional theory. Their reduction potentials are calculated using isodesmic reaction. MESP at the cobalt nucleus, V_{Co} of both oxidized and reduced forms of all the complexes is also computed in gas phase and solvent. The V_{Co} is found to be very sensitive to the ligand environment and oxidation state of the complexes. All the complexes showed excellent linear correlation between V_{Co} and reduction potential E^0 for both oxidized and reduced forms. The V_{Co} versus E^0 correlations suggest that MESP is an excellent tool to predict and fine tune the reduction potential of tetraza macrocyclic cobalt complexes. The slopes of the correlation plots obtained for **[2-X]²⁺**, **3-X**, **[4-X]³⁺**, and **[5-X]³⁺** are found to be nearly a constant and suggest that the ligand environment of these complexes respond in a similar way to tune the value of E^0. Among all the complexes, the ligand environment of **6-X** comprising of two –O-H-O– bridges is the least sensitive to substituent effect on the macrocycle while that comprising of two –

O-BF$_2$-O– bridges in **1-X** is the most sensitive to substituent effect to tune E^0 values. A single correlation graph comprising of the V_{Co} and E^0 data, showing a linear relationship between the two quantities is obtained by taking their relative values with respect to a reference. This relationship is powerful to make a good prediction on the reduction potential of any type of cobalt complexes considered in this study for any substituent X. The method to predict the E^0 using MESP is very attractive considering that the calculation of the former requires computationally more demanding procedures to obtain accurate thermodynamic parameters.

Part B: Predicting Reduction Potentials of Fischer Carbene Complexes of Chromium using MESP

2.6 Abstract

Transition metal Fischer carbene complexes have ample applications in chemistry owing to their attractive redox properties which are highly sensitive to the electronic effect of ligands (eeL) and substituents. We present a systematic investigation on the reduction potentials (E^0) of a large variety of Fischer carbene complexes (FCCs) of chromium using the B3LYP/Gen1//B3LYP/Gen1/SMD density functional theory. The change in eeL due to electron donating/withdrawing substituent (R) and variations in ligand environment is quantified using topographical features of the molecular electrostatic potential (MESP). In the reduced FCC, carbene carbon showed the MESP minimum (V_{min}) indicating significant localization of the extra electron on that ligand which supports the characteristic $M^{\delta-} = C^{\delta+}$ behaviour of the metal-carbon bond in the neutral FCC. MESP at the chromium centre (V_{Cr}) showed a clear linear dependency with E^0. The change in reduction potential (ΔE^0) due to variations in ligand environment is found to be directly proportional to change in the eeL measured as ΔV_{Cr}. This relationship is verified for experimentally known FCCs and further extended to several unknown systems. Our results confirm the highly sensitive nature of the reduction potential of FCCs with respect to eeL and remote substituent effects. The MESP at the metal center clearly emerged as a direct descriptor of eeL of FCCs which can be used to make predictions on the redox activities of the complexes.

2.7 Introduction

Since their introduction in 1964 by Fischer and Maasböl, Fischer carbene complexes (FCCs) are evolved as versatile reagents in organic and organometallic

synthesis.[38-45] FCCs are often portrayed as "chemical multitalents"[46-49] owing to their potential to participate in multi component reactions (MCR).[50,51] The versatile chemical reactions of Fischer carbene complexes can be attributed to their ability to undergo transformations under mild conditions, especially their aptness for almost all types of cycloadditions.[52-54] They are efficient electrochemical probes in PNA-DNA binding in the DNA recognition.[55] Recently, FCCs are used as electron transporting layers in the fabrication of organic solar cells.[56] Though Fischer carbene complexes of groups VI - VIII are known, group VI metal carbenes, especially chromium Fischer carbene complexes exhibited the broadest applications due to their reactivity, stability and easy accessibility.[50,57]

In Fischer carbene complexes of the type $L_nM=C(XR)R'$, the metal is connected to a carbene ligand with a formal double bond, typically the metal is in low oxidation state, stabilized by π-accepting ligands such as CO and the carbene is in singlet ground state, stabilized by π-donating substituents such as OMe or NMe_2 (Figure 2.11). The nature of metal-carbene bond in FCCs is well-studied[52, 58-60] and generally explained in terms of Dewar-Chatt-Duncanson (DCD) donor-acceptor model which considers two synergistic bonding interactions, the σ-donation from the carbene lone pair to the empty d_{z^2} metal orbital and π-back-donation from an occupied d_{xz} metal atomic orbital to the formally vacant carbene p_π orbital (Figure 2.11 (b)).[60] This makes the carbene ligand electrophilic and metal centre nucleophilic ($M^{\delta-} = C^{\delta+}$). The metal carbon double bond is of special interest in organometallic chemistry since its breaking is a key step in most of the Fischer carbene reactions.[52]
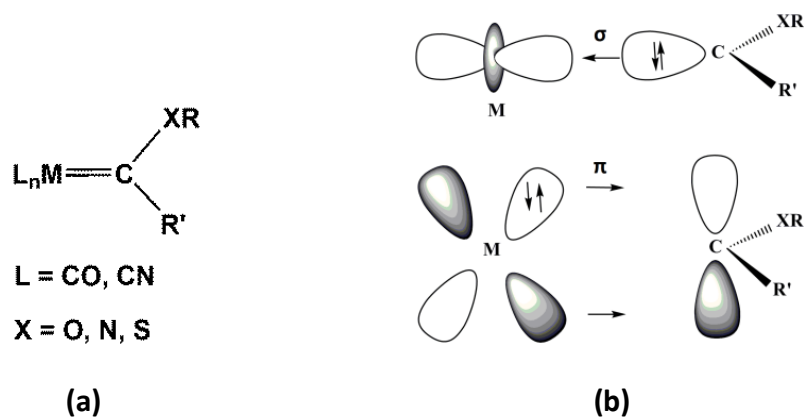
Figure 2.11 (a) General structure of Fischer carbene complex. (b) Schematic representation of the dominant orbital interactions in Fischer carbene complexes.

Reduction potential (E^0) values provide a fine measure of reactivities of FCCs, thus it is important to have reliable predictions of E^0 before synthesising the complexes, whereas only a few studies have been reported measuring the E^0 of FCCs.[61-69] The nature of carbene substituents XR and R′ have the ability to control the electrophilicity of the FCCs therefore the chemical reactivity can be tuned by systematically changing the substituents.[52] Landman and Conradie *et al*. studied the electrochemical behaviour of a series of FCCs and found that the reduction is sensitive to electrophilic nature of R′ substituent.[61] Ludvík *et al*. disclosed that even a minute change of a remote substituent ($COOCH_3$ to OCH_3) on FCC of chromium can significantly alter the electron distribution on the MC double bond and, consequently the redox properties of the complex.[70]

The major application of MESP in inorganic chemistry has been its ability to immediately characterize the electronic properties to predict the stabilities and reactivities of complexes including catalysts.[71-73] Recently, reduction potentials (E^0) of mononuclear cobalt catalysts of hydrogen evolution reaction have been predicted by using MESP at the cobalt centre (V_{Co}), where the total *electronic effect of ligands* (*eeL*) is quantified with the help of MESP.[74] The present study focuses on the quantification of *eeL* of Fischer carbene complexes using MESP analysis. It will show that reduction potentials of FCCs can be predicted with the MESP parameter used for the quantification of *eeL*.

2.8 Computational Methodology

For all the geometry optimizations, Becke's three-parameter hybrid functional B3LYP were used in conjunction with a general basis set (Gen1) consisting of 6-311++G(3df) basis set for the Cr atom and 6-311++G(d) basis set for the remaining atoms. For the reduced complexes, unrestricted UB3LYP/Gen1 was used. Optimized geometries were confirmed as energy minima by vibrational frequency calculations. Further, solvation effects (solvent = acetonitrile) were incorporated through self-consistent reaction field (SCRF) single point calculations as implemented in the SMD model.[32] At B3LYP/Gen1/SMD level (UB3LYP for open shell systems). There are computational accounts to predict redox properties of systems including transition metal complexes,[75-78] inorganic[79] and organic molecules.[22,80-83] Here the reduction potential (E^0) is calculated using the Nernst equation,

$$\Delta G^0_{red} = \Delta G^0_{solv}(R) - \Delta G^0_{solv}(O) \qquad \text{(Eq. 2.6)}$$

$$E^0_{red} = -\frac{\Delta G^0_{red}}{nF} \qquad \text{(Eq. 2.7)}$$

where F is the Faraday constant, and n is the number of electrons transferred. E^0 values are normally reported relative to a reference electrode. Here the reference electrode is standard calomel electrode (SCE) having an absolute potential of 4.199 V. Thus, to get the same reference state as in experiment, 4.199 V is subtracted from the calculated E^0 value.[84] All the DFT calculations are carried out using Gaussian 16 suite of programmes.[85]

2.9 Results and Discussion

2.9.1 Verifying E^0 with Experimentally Known Systems

The Fischer chromium carbene complexes studied by Kvapilova and Zalis *et al*. are selected for this study as a test set to validate the accuracy of the calculated E^0 values.[84] A schematic representation of the two categories (based on the ligand environment) of FCCs of chromium used by Kvapilova and Zalis *et*

al. is given in Figure 2.12. In the first category (**1a** – **1f**), apart from the carbene, the ligand environment is provided by five carbonyl groups while in the other (**2a** – **2f**), a chelating η^2-coordination from an olefin moiety in the carbene ligand is present along with four carbonyl groups. In all these complexes, the hexacoordinated Cr exists in the zero oxidation state.

1a-1f   **2a-2f**

R= (a) OCH$_3$, (b) CH$_3$, (c) H , (d) Cl , (e) COOCH$_3$, (f) CF$_3$
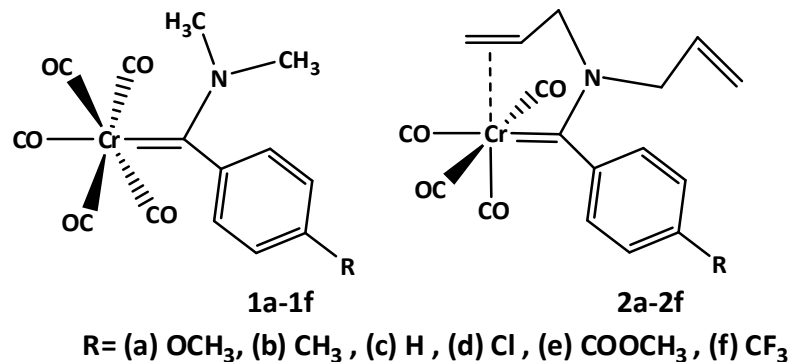
Figure 2.12 Fischer carbene complexes of chromium.

When reduction takes place, the additional electronic charge gets delocalized at the carbene ligand by maintaining the zero oxidation state of the metal centre. The optimized geometries of complexes in their neutral and reduced states (representative complexes **1a** and **1a′** in Figure 2.13), show that the reduction leads to significant changes in the geometry of the complex. For example, in **1a**, the phenyl ring shows an orthogonal arrangement with respect to the carbene π-orbital while that in the reduced form **1a′** shows a more planar arrangement. Compared to **1a**, the metal to carbene Cr-C bond is elongated by 0.092 Å in **1a′**. The nitrogen lone pair which stabilizes the electron deficient carbene centre in **1a** avoids the conjugation with this center in the more electron rich **1a′**. As a result, carbene carbon to nitrogen bond elongates from 1.323 Å in **1a** to 1.417 Å in **1a′** (Figure 2.13). The coplanarity of phenyl ring and carbene center in **1a′** and the shortening of carbene carbon to phenyl carbon distance from 1.497 Å in **1a** to 1.451 Å in **1a′** can be attributed to the conjugation of the extra electron density on the carbene center with the aromatic ring. Similar

structural changes are observed for all the other complexes (Table 2.8) when they undergo reduction.

1a   **1a′**
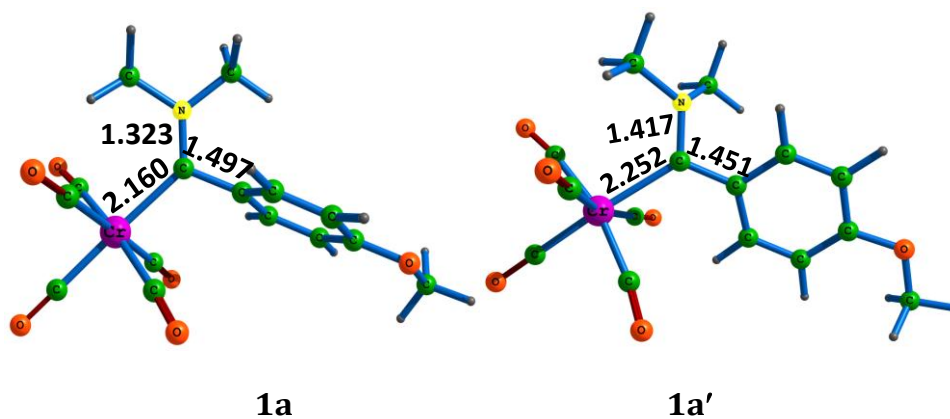
Figure 2.13 B3LYP/Gen1 level optimized structures of neutral and reduced forms Fischer carbene complexes of chromium. Distances are in Å.

Table 2.8 Bond distances in Å of oxidized and reduced complexes

Complex	Oxidized			Reduced		
	Cr-C	C-N	C-C	Cr-C	C-N	C-C
1a	2.160	1.323	1.497	2.252	1.417	1.451
1b	2.159	1.322	1.497	2.250	1.415	1.449
1c	2.158	1.322	1.497	2.251	1.412	1.449
1d	2.158	1.322	1.497	2.248	1.412	1.446
1e	2.157	1.321	1.495	2.241	1.390	1.438
1f	2.156	1.321	1.496	2.244	1.402	1.441
2a	2.106	1.324	1.487	2.226	1.425	1.439
2b	2.100	1.323	1.488	2.226	1.421	1.437
2c	2.098	1.322	1.488	2.225	1.419	1.437
2d	2.095	1.322	1.489	2.223	1.417	1.435
2e	2.097	1.321	1.486	2.218	1.391	1.430
2f	2.093	1.322	1.487	2.221	1.403	1.431

The E^0 values at B3LYP/Gen1//B3LYP/Gen1/SMD are compared with experimental cyclic voltammetry[84] values ($E^0_{(exp)}$) reported by Kvapilova and Zalis *et al.* Between E^0 and $E^0_{(exp)}$ of **1** and **2** systems given in Table 2.9, a mean absolute deviation (MAD) of 0.057 V is observed which indicates the reliability of the methodology used for calculating E^0.

Table 2.9 The calculated E^0 at B3LYP/Gen1//B3LYP/Gen1/SMD level in V vs. SCE and experimental E^0 for Fischer carbene complexes of chromium

Complex	Substituent	$E^0_{(calc)}$	$E^0_{(exp)}$
1a	OCH_3	-2.08	-2.01
1b	CH_3	-2.05	-2.00
1c	H	-2.01	-1.96
1d	Cl	-1.94	-1.83
1e	$COOCH_3$	-1.73	-1.63
1f	CF_3	-1.81	-1.75
2a	OCH_3	-2.21	-1.98
2b	CH_3	-2.17	-1.94
2c	H	-2.13	-1.93
2d	Cl	-2.04	-1.90
2e	$COOCH_3$	-1.79	-1.62
2f	CF_3	-1.89	-1.80

The complexes in category **2** show more negative E^0 than category **1** which can be attributed to the higher electron donating ability of the η^2-coordinated CC double bond than a σ-coordinated carbonyl carbon. A more negative E^0 indicates decreased tendency for reduction. From Table 2.9, it is evident that among the substituted complexes of **1** and **2**, the OCH_3 substitution gives the most negative E^0, *viz.* -2.08 and -2.21 V for **1a** and **2a**, respectively while $COOCH_3$ gives the lowest negative E^0, *viz.* -1.73 and -1.79 V, respectively for **1e** and **2e**. The

unsubstituted **1c** and **2c** (R = H) show E^0 -2.01 and -2.13 V, respectively whereas electron donating R substituents show more negative E^0 and electron withdrawing substituents show less negative E^0. In other words, electron donating group on the phenyl ring reduces the tendency of the complex to undergo reduction while electron withdrawing group increases it.

2.9.2 MESP Features

The MESP isosurface of representative systems **1c** and **2c** (R = H) along with their reduced forms **1c'** and **2c'** (radical anions) are provided in Figure 2.14 along with their (3, +3) MESP minimum (V_{min}) and MESP at the Cr atom (V_{Cr}).
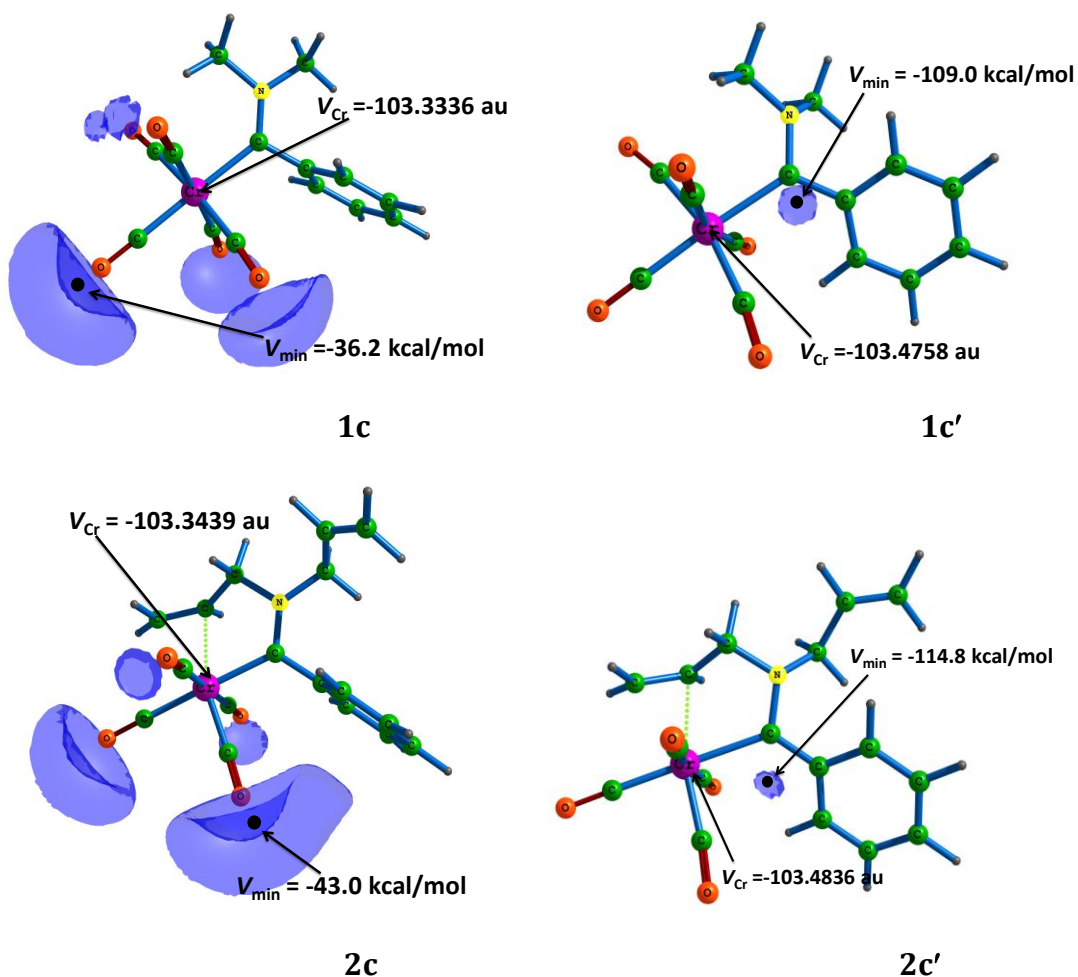
Figure 2.14 The MESP isosurface of neutral and reduced forms of Fischer carbene complexes of chromium.

In the neutral form, electron density is localized more towards the carbonyl oxygen while its carbene carbon shows electron deficiency. In **1c**, V_{min} -36.2 kcal/mol is observed at the carbonyl group positioned *trans* with respect to the carbene ligand. In general, an anionic system shows very high negative MESP than a neutral molecule due to the dominance of the electronic term over the nuclear term. For instance, V_{min} -109.0 kcal/mol observed for the anionic **1c′** is almost 3 times more negative than **1c**. Table 2.10 suggests that this observation holds good for all the reduced systems. The V_{Cr} and V_{min} values are given in Table 2.10. Formation of V_{min} over the carbon center of carbene ligand in the reduced form suggests that a major share of the electron density from reduction is localized on to the carbene carbon.

Table 2.10 Complexes **1** − **2** with corresponding V_{Cr} (in au) and V_{min} (in kcal/mol) values in acetonitrile

Complex	Substituent	V_{Cr} (neutral)	V_{Cr} (reduced)	V_{min} (neutral)	V_{min} (reduced)
1a	OCH_3	-103.3361	-103.4789	-37.1	-112.9
1b	CH_3	-103.3356	-103.4784	-36.9	-112.6
1c	H	-103.3336	-103.4758	-36.2	-109.0
1d	Cl	-103.3268	-103.4679	-34.2	-104.0
1e	$COOCH_3$	-103.3269	-103.4557	-34.2	-98.7
1f	CF_3	-103.3227	-103.4594	-33.1	-96.9
2a	OCH_3	-103.3467	-103.4867	-43.1	-116.8
2b	CH_3	-103.3460	-103.4857	-43.1	-116.5
2c	H	-103.3439	-103.4836	-43.0	-114.8
2d	Cl	-103.3372	-103.4759	-40.7	-107.8
2e	$COOCH_3$	-103.3372	-103.4615	-41.3	-109.7
2f	CF_3	-103.3329	-103.4664	-39.0	-105.0

This can be explained by invoking the basic $M^{\delta-} = C^{\delta+}$ nature of the FCCs which upon reduction accepts the electron density more towards the electrophilic carbon. The relative V_{min} values with respect to the unsubstituted system (ΔV_{min}) are given in Table 2.11. The ΔV_{min} is negative for electron donating R groups and positive for electron withdrawing R groups. The subtle variations observed in the values of V_{Cr} can also be directly related with the electron donating/withdrawing nature of R substituents. The relative V_{Cr} with respect to the unsubstituted systems (ΔV_{Cr}) measures the electron donation/withdrawal of R substituent. The reduced systems show higher magnitude for both ΔV_{min} and ΔV_{Cr} than neutral suggesting that the substituent effect is higher in the former.

Table 2.11 The ΔV_{min} and ΔV_{Cr} values in kcal/mol for neutral and reduced forms of Fischer carbene complexes of chromium

Complex	Substituent	ΔV_{min} (neutral)	ΔV_{min} (reduced)	ΔV_{Cr} (neutral)	ΔV_{Cr} (reduced)
1a	OCH_3	-0.9	-3.9	-1.6	-1.9
1b	CH_3	-0.7	-3.6	-1.3	-1.6
1c	H	0.0	0.0	0.0	0.0
1d	Cl	2.0	5.0	4.3	5.0
1e	$COOCH_3$	2.0	10.3	4.2	12.6
1f	CF_3	3.1	12.1	6.8	10.3
2a	OCH_3	-0.1	-2.0	-1.8	-1.9
2b	CH_3	-0.1	-1.7	-1.3	-1.3
2c	H	0.0	0.0	0.0	0.0
2d	Cl	2.3	7.0	4.2	4.8
2e	$COOCH_3$	1.7	5.1	4.2	13.9
2f	CF_3	4.0	9.8	6.9	10.8

2.9.3 Correlation between ΔV_{Cr} and ΔE^0

The total effect of the ligand environment is acting on the metal center. As a sensitive electronic property of the metal center, V_{Cr} reflects the total *electronic effect of the ligands* (*eeL*) environment. For instance, the increasing electron withdrawing/donating nature of the substituents appear as decreasing/increasing negative character of V_{Cr} and this behaviour parallels with the decreasing/increasing negative character of the reduction potential of the complex. In fact, ΔV_{Cr} of the reduced systems strongly correlates with the change in E^0 observed due to substitution (ΔE^0). The best fitting line for ΔV_{Cr} vs. ΔE^0 plot gives a correlation coefficient 0.992 and the corresponding Eq. 2.8 has an intercept -0.0152. The intercept may be fixed as zero as ΔV_{Cr} = 0 should corresponds to ΔE^0 = 0. Then a modified Eq. 2.9 can be written (correlation coefficient 0.987) which predicts that the change in E^0 due to substitution is 0.0222 times the ΔV_{Cr} of the reduced complex (Figure 2.15). The most remarkable observation is that even a delicate variation in E^0 can be well accounted by the substituent effect in terms of ΔV_{Cr}. Since the unsubstituted system (R = H) is the reference to calculate ΔV_{Cr} and ΔE^0, a prediction on the E^0 of an unknown systems can be made using Eq. 2.10 where $E^0{}_{(H)}$ represents the reduction potential of the unsubstituted system.

$$\Delta E^0 = 0.0234*(\Delta V_{Cr}) - 0.0152 \qquad\qquad (Eq.\ 2.8)$$

$$\Delta E^0 = 0.0222*(\Delta V_{Cr}) \qquad\qquad (Eq.\ 2.9)$$

$$E^0 = E^0(H) + 0.0222*(\Delta V_{Cr}) \qquad\qquad (Eq.\ 2.10)$$

$$\Delta E^0 = 0.0222*(\Delta V_{Cr})$$
$$r = 0.987$$
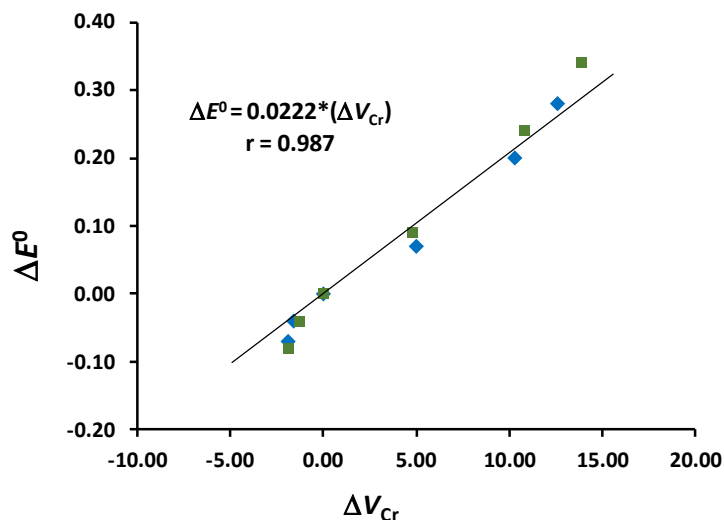
Figure 2.15 Correlation between change in MESP at Cr of reduced complex (ΔV_{Cr}) in kcal/mol and change in reduction potential (ΔE^0) in V for **1** and **2** series of complexes (complex **1** in blue and **2** in green).

Table 2.12 Complexes with corresponding V_{Cr} (in au) values in acetonitrile

R	Complex	V_{Cr}	Complex	V_{Cr}
F	**1g**	-103.4709	**2g**	-103.4787
Ph	**1h**	-103.4683	**2h**	-103.4731
Br	**1i**	-103.4677	**2i**	-103.4755
SH	**1j**	-103.4675	**2j**	-103.4749
CHCH$_2$	**1k**	-103.4661	**2k**	-103.4712
OCF$_3$	**1l**	-103.4651	**2l**	-103.4731
NC	**1m**	-103.4542	**2m**	-103.4605
CN	**1n**	-103.4496	**2n**	-103.4561

In order to examine the predictive power of Eq. 2.10, several substituted systems of **1** and **2** have been studied. The selected substituents for this purpose are F, Ph, Br, SH, CHCH$_2$, OCF$_3$, NC, and CN. Since E^0 of these complexes are

unknown, Nernst equation 2.7 is used to calculate them. Table 2.12 gives the V_{Cr} values of reduced complexes in acetonitrile. Table 2.13 depicts ΔV_{Cr} values along with the predicted E^0 using Eq. 2.10 ($E^0_{(pred)}$) and the calculated E^0 ($E^0_{(calc)}$) for the test set of complexes **1g – 1n** and **2g – 2n**. The predicted and calculated E^0 shows excellent agreement with each other. Among the substituted systems, **1g** and **2g** (R = F) show the least substituent effect and their E^0 values show only small deviation from the H-substituted systems. The highest substituent effect (highest ΔV_{Cr}) is seen for **1n** and **2n** (R = CN) and they possess the lowest negative E^0.

Table 2.13 The ΔV_{Cr} in kcal/mol, predicted $E^0_{(pred)}$ and calculated $E^0_{(calc)}$ in V vs. SCE

R	Complexes **1g – 1n**			Complexes **2g – 2n**		
	ΔV_{Cr}	$E^0_{(pred)}$	$E^0_{(calc)}$	ΔV_{Cr}	$E^0_{(pred)}$	$E^0_{(calc)}$
F	3.1	-1.94	-2.01	3.1	-2.06	-2.12
Ph	4.7	-1.91	-1.94	6.6	-1.98	-2.03
Br	5.1	-1.90	-1.94	5.1	-2.02	-2.04
SH	5.2	-1.89	-1.98	5.5	-2.01	-2.08
CHCH$_2$	6.1	-1.87	-1.88	7.8	-1.96	-1.96
OCF$_3$	6.7	-1.86	-1.94	6.6	-1.98	-2.03
NC	13.5	-1.71	-1.77	14.5	-1.81	-1.84
CN	16.5	-1.64	-1.68	17.2	-1.75	-1.73

2.9.4 Substituent Effect on FCCs with Heterocyclic Ring

In order to improve the scope of the MESP approach to E^0 prediction, we have extended the study to different set of Fischer chromium carbene complexes and the selected complexes are given in Figure 2.16. Here the substituted phenyl ring of **1** and **2** series of systems is changed to substituted heterocyclic rings (**3**, **4**, **5**, **6**, **7** and **8** series).
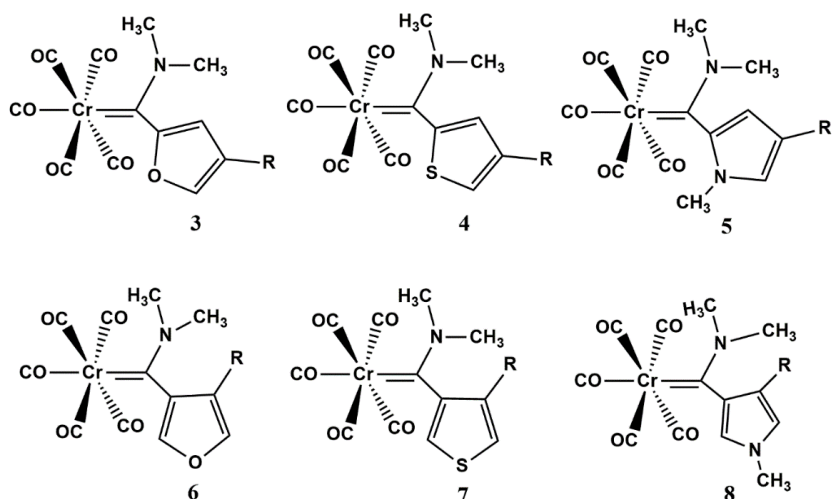
Figure 2.16 Fischer carbene complexes of chromium.

Table 2.14 The ΔV_{Cr} in kcal/mol, predicted $E^0_{(pred)}$ and calculated $E^0_{(calc)}$ in V vs. SCE of complexes **3** – **4**

R	Complexes **3a** – **3l**			Complexes **4a** – **4l**		
	ΔV_{Cr}	$E^0_{(pred)}$	$E^0_{(calc)}$	ΔV_{Cr}	$E^0_{(pred)}$	$E^0_{(calc)}$
OCH$_3$	-0.1	-1.73	-1.72	-0.3	-1.77	-1.76
CH$_3$	-1.1	-1.76	-1.75	-1.1	-1.79	-1.78
H	0.0	-1.73	-1.73	0.0	-1.76	-1.76
CHCH$_2$	1.3	-1.70	-1.72	1.6	-1.73	-1.73
SH	3.8	-1.65	-1.67	4.0	-1.67	-1.70
Br	5.1	-1.62	-1.62	5.8	-1.63	-1.64
COOCH$_3$	5.1	-1.62	-1.66	4.7	-1.66	-1.71
Cl	5.2	-1.61	-1.62	5.8	-1.63	-1.64
OCF$_3$	7.0	-1.58	-1.60	7.4	-1.60	-1.63
CF$_3$	8.1	-1.55	-1.60	8.0	-1.58	-1.64
NC	9.7	-1.51	-1.58	9.9	-1.54	-1.61
CN	11.1	-1.48	-1.57	11.1	-1.51	-1.61

Our study examines the effect of 12 different substituents, *viz.* OCH_3, CH_3, H, $CHCH_2$, SH, Br, $COOCH_3$, Cl, OCF_3, CF_3, NC, and CN on the heterocyclic ring. The unsubstituted systems (R = H) of these series (**3c**, **4c**, **5c**, **6c**, **7c**, and **8c**) are studied by Kvapilova and Zalis *et al.*[84] Tables 2.14 – 2.16 provide the ΔV_{Cr}, $E^0_{(pred)}$, and $E^0_{(calc)}$ for all the **3** – **8** series of complexes. In all the Tables, the $E^0_{(exp)}$ for the unsubstituted systems **3c** – **8c** are given in bracket. The MAD obtained for these values is 0.040 V. The magnitude and the relative ordering of $E^0_{(pred)}$ (using Eq. 2.10) agree well with the calculated $E^0_{(calc)}$.

Table 2.15 The ΔV_{Cr} in kcal/mol, predicted $E^0_{(pred)}$ and calculated $E^0_{(calc)}$ in V vs. SCE of complexes **5** – **6**

R	Complexes **5a** – **5l**			Complexes **6a** – **6l**		
	ΔV_{Cr}	$E^0_{(pred)}$	$E^0_{(calc)}$	ΔV_{Cr}	$E^0_{(pred)}$	$E^0_{(calc)}$
OCH_3	2.5	-1.98	-2.06	-5.1	-2.07	-2.09
CH_3	-0.6	-2.05	-2.06	-1.7	-2.00	-2.08
H	0.0	-2.04	-2.04	0.0	-1.96	-1.96
$CHCH_2$	2.2	-1.99	-2.02	0.5	-1.95	-2.02
SH	4.0	-1.95	-2.01	1.9	-1.92	-2.02
Br	4.6	-1.94	-1.98	1.6	-1.92	-1.99
$COOCH_3$	5.2	-1.92	-1.97	-2.6	-2.02	-2.11
Cl	4.7	-1.94	-1.98	1.3	-1.93	-1.98
OCF_3	6.5	-1.90	-1.97	3.5	-1.88	-1.92
CF_3	7.1	-1.88	-1.94	5.4	-1.84	-1.92
NC	9.1	-1.84	-1.93	6.1	-1.82	-1.85
CN	10.2	-1.81	-1.92	8.7	-1.77	-1.78

Table 2.16 The ΔV_{Cr} in kcal/mol, predicted $E^0_{(pred)}$ and calculated $E^0_{(calc)}$ in V vs. SCE of complexes **7** – **8**

R	Complexes **7a** – **7l**			Complex **8a** – **8l**		
	ΔV_{Cr}	$E^0_{(pred)}$	$E^0_{(calc)}$	ΔV_{Cr}	$E^0_{(pred)}$	$E^0_{(calc)}$
OCH$_3$	-5.5	-2.10	-2.10	-5.7	-2.44	-2.29
CH$_3$	-1.7	-2.02	-2.11	-1.5	-2.35	-2.23
H	0.0	-1.98	-1.98	0.0	-2.32	-2.14
CHCH$_2$	0.5	-1.97	-2.05	2.1	-2.28	-2.19
SH	1.7	-1.94	-2.04	1.5	-2.27	-2.21
Br	1.1	-1.96	-2.02	1.9	-2.28	-2.18
COOCH$_3$	-3.7	-2.06	-2.16	-0.2	-2.32	-2.24
Cl	0.4	-1.97	-2.01	1.5	-2.28	-2.16
OCF$_3$	2.2	-1.93	-1.94	4.0	-2.23	-2.14
CF$_3$	3.1	-1.91	-1.98	5.8	-2.19	-2.08
NC	4.6	-1.88	-1.88	7.3	-2.16	-2.02
CN	6.9	-1.83	-1.83	9.8	-1.92	-1.93

The correlation between $E^0_{(pred)}$ and $E^0_{(calc)}$ for all **1** – **8** series of systems (total 100) given in Figure 2.17 shows that $E^0_{(calc)}$ is 1.025 times $E^0_{(pred)}$. The mean absolute deviation, MAD between the two quantities is 0.033 V. In general, **8** series of systems showed the most negative E^0 (eg: -2.14 V for R = H; -2.29 V for R = OCH$_3$ and -1.93 V for R = CN) whereas the **3** series of systems showed the least negative E^0 (eg: -1.73 V for R = H; -1.74 V for R = OCH$_3$ and -1.57 V for R = CN). The data in Table 2.14 – 2.16 clearly suggest that a significant tuning of reduction potential can be achieved by the incorporation of heterocycles on the carbene center.
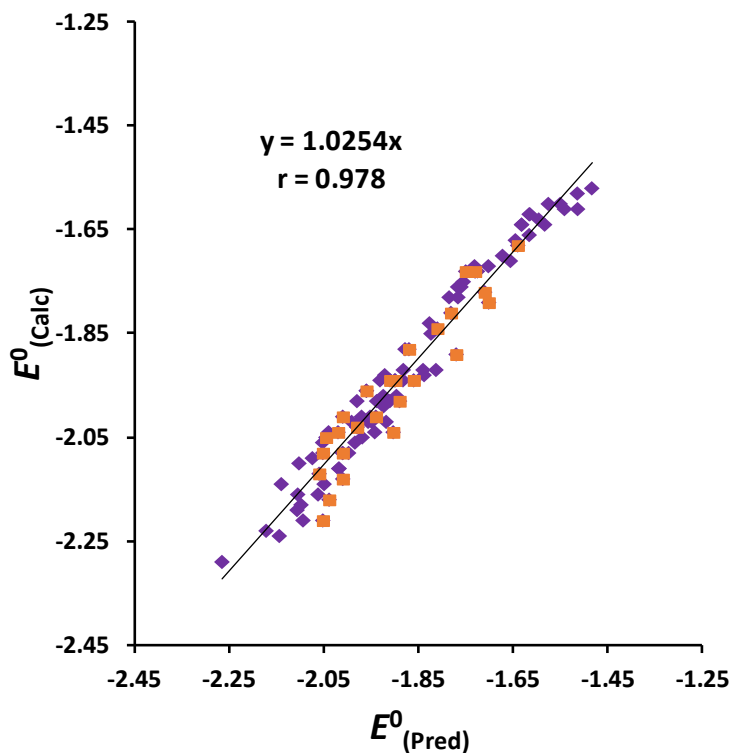
Figure 2.17 The correlation between $E^0_{(pred)}$ and $E^0_{(calc)}$ in V for all the **1** – **8** series of complexes (complexes **1** - **2** in yellow and **3** - **8** in violet).

The reduction potential is sensitive to the nature and position of heteroatom as well as nature and position of R substituent on the heterocycle. These results agree with Ludvík *et al*. who related the highly sensitive redox properties of FCCs with the remote substituent effects.

2.10 Conclusions

The redox properties of Fischer carbene complexes are intimately connected with the polarized nature of metal-carbon double bond meaning that delicate tuning of reduction potentials (E^0) can be achieved by proper structural and electronic modifications on the carbene ligand. We have elucidated the reduction potential of a large variety of Fischer carbene complexes of chromium (**1** – **8** series of systems) and found that the *electronic effect of ligands* (*eeL*) and substituent are strongly reflected on the critical features of MESP. The strong electrophilic nature of the carbene carbon of

FCC is revealed in MESP as this carbon has the most electron rich character in the reduced FCC. Further, MESP at the chromium nucleus (V_{Cr}) emerged as a sensitive quantity to understand the total *eeL* acting on it. The carbene substituent such as phenyl and aromatic heterocycles as well as remote substituents on the aromatic units deeply influence the reduction potential characteristics of FCCs. The change observed on V_{Cr} due to change in *eeL* is proportional to change observed on E^0. Hence ΔV_{Cr} is useful to forecast the influence of Fischer carbene ligands on the reduction potential of chromium complexes. The MESP parameter emerges as an excellent reactivity predictor for these organometallic complexes.

2.11 References

1.   P. Wang, G. Liang, M. R. Reddy, M. Long, K. Driskill, C. Lyons, B. Donnadieu, J. C. Bollinger, C. E. Webster and X. Zhao, *J. Am. Chem. Soc.*, **2018**, *140*, 9219-9229.

2.   V. S. Thoi, Y. Sun, J. R. Long and C. J. Chang, *Chem. Soc. Rev.*, **2013**, *42*, 2388-2400.

3.   N. Kaeffer, M. Chavarot-Kerlidou and V. Artero, *Acc. Chem. Res.*, **2015**, *48*, 1286-1295.

4.   E. S. Wiedner and R. M. Bullock, *J. Am. Chem. Soc.*, **2016**, *138*, 8309-8318.

5.   S. Varma, C. E. Castillo, T. Stoll, J. Fortage, A. G. Blackman, F. Molton, A. Deronzier and M.-N. Collomb, *Phys. Chem. Chem. Phys.*, **2013**, *15*, 17544-17552.

6.   M. van der Meer, E. Glais, I. Siewert and B. Sarkar, *Angew. Chem. Int. Ed.*, **2015**, *54*, 13792-13795.

7.   J. Wang, F. Xu, H. Jin, Y. Chen and Y. Wang, *Adv. Mater.*, **2017**, *29*, 1605838.

8.   J. L. Dempsey, B. S. Brunschwig, J. R. Winkler and H. B. Gray, *Acc. Chem. Res.*, **2009**, *42*, 1995-2004.

9.   A. Bhattacharjee, E. S. Andreiadis, M. Chavarot-Kerlidou, M. Fontecave, M. J. Field and V. Artero, *Chem. Eur. J.*, **2013**, *19*, 15166-15174.

10.   X. Hu, B. S. Brunschwig and J. C. Peters, *J. Am. Chem. Soc.*, **2007**, *129*, 8988-8998.

11.   X. Hu, B. M. Cossairt, B. S. Brunschwig, N. S. Lewis and J. C. Peters, *Chem. Commun.*, **2005**, *0*, 4723-4725.

12.   M. Razavet, V. Artero and M. Fontecave, *Inorg. Chem.*, **2005**, *44*, 4786-4795.

13. C. Baffert, V. Artero and M. Fontecave, *Inorg. Chem.*, **2007**, *46*, 1817-1824.

14. J. L. Dempsey, J. R. Winkler and H. B. Gray, *J. Am. Chem. Soc.*, **2010**, *132*, 1060-1065.

15. J. T. Muckerman and E. Fujita, *Chem. Commun.*, **2011**, *47*, 12456-12458.

16. V. Artero, M. Chavarot-Kerlidou and M. Fontecave, *Angew. Chem. Int. Ed.*, **2011**, *50*, 7238-7266.

17. S. Losse, J. G. Vos and S. Rau, *Coord. Chem. Rev.*, **2010**, *254*, 2492-2504.

18. B. H. Solis and S. Hammes-Schiffer, *J. Am. Chem. Soc.*, **2011**, *133*, 19036-19039.

19. C. H. Suresh and N. Koga, *Inorg. Chem.*, **2002**, *41*, 1573-1578.

20. A. L. Fernandez, T. Y. Lee, C. Reyes, A. Prock and W. P. Giering, *Organometallics*, **1998**, *17*, 3169-3175.

21. C. C. L. McCrory, C. Uyeda and J. C. Peters, *J. Am. Chem. Soc.*, **2012**, *134*, 3164-3170.

22. K. Arumugam and U. Becker, *Minerals*, **2014**, *4*, 345-387.

23. B. H. Solis and S. Hammes-Schiffer, *Inorg. Chem.*, **2011**, *50*, 11252-11262.

24. S. Chen, R. Rousseau, S. Raugei, M. Dupuis, D. L. DuBois and R. M. Bullock, *Organometallics*, **2011**, *30*, 6108-6118.

25. B. H. Solis and S. Hammes-Schiffer, *Inorg. Chem.*, **2014**, *53*, 6427-6443.

26. A. D. Becke, *J. Chem. Phys.*, **1993**, *98*, 5648-5652.

27. R. Krishnan, J. S. Binkley, R. Seeger and J. A. Pople, *J. Chem. Phys.*, **1980**, *72*, 650-654.

28. A. D. McLean and G. S. Chandler, *J. Chem. Phys.*, **1980**, *72*, 5639-5648.

29. P. J. Hay, *J. Chem. Phys.*, **1977**, *66*, 4377-4384.

30. J. P. Perdew, *Phys. Rev. B*, **1986**, *33*, 8822-8824.

31. M. J. Frisch, G. W. Trucks, H. B. Schlegel, G. E. Scuseria, M. A. Robb, J. R. Cheeseman, G. Scalmani, V. Barone, B. Mennucci, G. A. Petersson, H. Nakatsuji, M. Caricato, X. Li, H. P. Hratchian, A. F. Izmaylov, J. Bloino, G. Zheng, J. L. Sonnenberg, M. Hada, M. Ehara, K. Toyota, R. Fukuda, J. Hasegawa, M. Ishida, T. Nakajima, Y. Honda, O. Kitao, H. Nakai, T. Vreven, J. J. A. Montgomery, J. E. Peralta, F. Ogliaro, M. Bearpark, J. J. Heyd, E. Brothers, K. N. Kudin, V. N. Staroverov, T. Keith, R. Kobayashi, J. Normand, K. Raghavachari, A. Rendell, J. C. Burant, S. S. Iyengar, J.

Tomasi, M. Cossi, N. Rega, J. M. Millam, M. Klene, J. E. Knox, J. B. Cross, V. Bakken, C. Adamo, J. Jaramillo, R. Gomperts, R. E. Stratmann, O. Yazyev, A. J. Austin, R. Cammi, C. Pomelli, J. W. Ochterski, R. L. Martin, K. Morokuma, V. G. Zakrzewski, G. A. Voth, P. Salvador, J. J. Dannenberg, S. Dapprich, A. D. Daniels, O. Farkas, J. B. Foresman, J. V. Ortiz, J. Cioslowski and D. J. Fox, *Gaussian 09*, Revision D.01; Gaussian Inc., Wallingford CT, **2013**.

32. A. V. Marenich, C. J. Cramer and D. G. Truhlar, *J. Phys. Chem. B*, **2009**, *113*, 6378-6396.

33. J. Ho, *Phys. Chem. Chem. Phys.*, **2015**, *17*, 2859-2868.

34. M. Namazian, C. Y. Lin and M. L. Coote, *J. Chem. Theory Comput.*, **2010**, *6*, 2721-2725.

35. B. H. Solis, Y. Yu and S. Hammes-Schiffer, *Inorg. Chem.*, **2013**, *52*, 6994-6999.

36. Y. Zhao and D. G. Truhlar, *J. Chem. Phys.*, **2006**, *125*.

37. S. Grimme, *J. Comput. Chem.*, **2006**, *27*, 1787-1799.

38. E. O. Fischer and A. Maasböl, *Angew. Chem.*, **1964**, *3*, 580-581.

39. J. Barluenga, F. Aznar, A. Martin and J. T. Vazquez, *J. Am. Chem. Soc.*, **1995**, *117*, 9419-9426.

40. C. F. Bernasconi, *Chem. Soc. Rev.*, **1997**, *26*, 299-307.

41. M. A. Sierra, *Chem. Rev.*, **2000**, *100*, 3591-3638.

42. M. Gomez-Gallego, M. J. Mancheño and M. A. Sierra, *Acc. Chem. Res.*, **2005**, *38*, 44-53.

43. M. A. Sierra, M. Gomez-Gallego and R. Martinez-Alvarez, *Chem. Eur. J.*, **2007**, *13*, 736-744.

44. B. van der Westhuizen, P. J. Swarts, I. Strydom, D. C. Liles, I. Fernandez, J. C. Swarts and D. I. Bezuidenhout, *Dalton Trans.*, **2013**, *42*, 5367-5378.

45. J. W. Herndon, *Coord. Chem. Rev.*, **2013**, *257*, 2899-3003.

46. d. M. Armin, S. Heiko and D. Michael, *Angew. Chem.*, **2000**, *39*, 3964-4002.

47. Y.-T. Wu and A. de Meijere, *Metal Carbenes in Organic Synthesis*, Springer, Berlin, Heidelberg, **2004**.

48. J. Barluenga, M. A. Fernandez-Rodriguez and E. Aguilar, *J. Organomet. Chem.*, **2005**, *690*, 539-587.

49. M. A. Sierra, I. Fernandez and F. P. Cossio, *Chem. Commun.*, **2008**, *0*, 4671-4682.

50. J. Barluenga and E. Aguilar, *Adv. Organomet. Chem.*, **2017**, *67*, 1-150.

51. M. Angel Fernandez-Rodriguez, P. Garcia-Garcia and E. Aguilar, *Chem. Commun.*, **2010**, *46*, 7670-7687.

52. M. Cases, G. Frenking, M. Duran and M. Solà, *Organometallics*, **2002**, *21*, 4182-4191.

53. J. Barluenga, S. Martinez, A. L. Suarez-Sobrino and M. Tomas, *J. Am. Chem. Soc.*, **2001**, *123*, 11113-11114.

54. J. Barluenga, J. Santamaría and M. Tomás, *Chem. Rev.*, **2004**, *104*, 2259-2284.

55. C. Baldoli, P. Cerea, L. Falciola, C. Giannini, E. Licandro, S. Maiorana, P. Mussini and D. Perdicchia, *J. Organomet. Chem.*, **2005**, *690*, 5777-5787.

56. P. Vidal-Garcia, M. E. Sanchez-Vergara, R. Corona-Sanchez, O. Jimenez-Sandoval, E. G. R. Mercado, R. A. Toscano and C. Alvarez-Toledano, *Molecules*, **2018**, *23*, 751.

57. K. H. Dötz and J. Stendel, *Chem. Rev.*, **2009**, *109*, 3227-3274.

58. V. S. F. and F. Gernot, *Chem. Eur. J.*, **1998**, *4*, 1428-1438.

59. G. Frenking and N. Fröhlich, *Chem. Rev.*, **2000**, *100*, 717-774.

60. G. Frenking, M. Solà and S. F. Vyboishchikov, *J. Organomet. Chem.*, **2005**, *690*, 6178-6204.

61. M. Landman, R. Y. Liu, P. H. van Rooyen and J. Conradie, *Electrochim. Acta*, **2013**, *114*, 205-214.

62. M. Landman, R. Y. Liu, R. Fraser, P. H. van Rooyen and J. Conradie, *J. Organomet. Chem.*, **2014**, *752*, 171-182.

63. R. Gostynski, R. Fraser, M. Landman, E. Erasmus and J. Conradie, *Polyhedron*, **2017**, *127*, 323-330.

64. R. Gostynski, M. Landman and J. Conradie, *J. Nano Res.*, **2016**, *44*, 1-9.

65. S. Thompson, H. R. Wessels, R. Fraser, P. H. van Rooyen, D. C. Liles and M. Landman, *J. Mol. Struct.* , **2014**, *1060*, 111-118.

66. H. G. Raubenheimer, *Dalton Trans.*, **2014**, *43*, 16959-16973.

67. R. Metelkova, T. Tobrman, H. Kvapilova, I. Hoskovcova and J. Ludvik, *Electrochim. Acta*, **2012**, *82*, 470-477.

68. H. Kvapilova, I. Hoskovcova, M. Kayanuma, C. Daniel and S. Zalis, *J. Phys. Chem. A*, **2013**, *117*, 11456-11463.

69. R. Martinez-Alvarez, M. Gomez-Gallego, I. Fernandez, M. J. Mancheno and M. A. Sierra, *Organometallics*, **2004**, *23*, 4647-4654.

70. I. Hoskovcova, R. Zverinova, J. Rohacova, D. Dvorak, T. Tobrman, S. Zalis and J. Ludvik, *Electrochim. Acta*, **2011**, *56*, 6853-6859.

71. P. K. Sajith and C. H. Suresh, *Inorg. Chem.*, **2011**, *50*, 8085-8093.

72. J. Mathew and C. H. Suresh, *Organometallics*, **2011**, *30*, 1438-1444.

73. C. H. Suresh, N. Koga and S. R. Gadre, *Organometallics*, **2000**, *19*, 3008-3015.

74. B. A. Anjali, F. B. Sayyed and C. H. Suresh, *J. Phys. Chem. A*, **2016**, *120*, 1112-1119.

75. M. Uudsemaa and T. Tamm, *J. Phys. Chem. A*, **2003**, *107*, 9997-10003.

76. T. F. Hughes and R. A. Friesner, *J. Chem. Theory Comput.*, **2012**, *8*, 442-459.

77. S. J. Konezny, M. D. Doherty, O. R. Luca, R. H. Crabtree, G. L. Soloveichik and V. S. Batista, *J. Phys. Chem. C*, **2012**, *116*, 6349-6356.

78. G. Liang, N. J. DeYonker, X. Zhao and C. E. Webster, *J. Comput. Chem.*, **2017**, *38*, 2430-2438.

79. J. Moens, P. Geerlings and G. Roos, *Chem. Eur. J.*, **2007**, *13*, 8174-8184.

80. M. H. Baik and R. A. Friesner, *J. Phys. Chem. A*, **2002**, *106*, 7407-7412.

81. Y. Fu, L. Liu, H.-Z. Yu, Y.-M. Wang and Q.-X. Guo, *J. Am. Chem. Soc.*, **2005**, *127*, 7227-7234.

82. L. E. Roy, E. Jakubikova, M. G. Guthrie and E. R. Batista, *J. Phys. Chem. A*, **2009**, *113*, 6745-6750.

83. A. J. Fry, *Curr. Opin. Electrochem.*, **2017**, *2*, 67-75.

84. H. Kvapilova, I. Hoskovcova, J. i. Ludvik and S. Zalis, *Organometallics*, **2014**, *33*, 4964-4972.

85. M. J. Frisch, G. W. Trucks, H. B. Schlegel, G. E. Scuseria, M. A. Robb, J. R. Cheeseman, G. Scalmani, V. Barone, B. Mennucci, G. A. Petersson, H. Nakatsuji, M. Caricato, X. Li, H. P. Hratchian, A. F. Izmaylov, J. Bloino, G. Zheng, J. L. Sonnenberg, M. Hada, M. Ehara, K. Toyota, R. Fukuda, J. Hasegawa, M. Ishida, T. Nakajima, Y. Honda, O. Kitao, H. Nakai, T. Vreven, J. J. A. Montgomery, J. E. Peralta, F. Ogliaro,

M. Bearpark, J. J. Heyd, E. Brothers, K. N. Kudin, V. N. Staroverov, T. Keith, R. Kobayashi, J. Normand, K. Raghavachari, A. Rendell, J. C. Burant, S. S. Iyengar, J. Tomasi, M. Cossi, N. Rega, J. M. Millam, M. Klene, J. E. Knox, J. B. Cross, V. Bakken, C. Adamo, J. Jaramillo, R. Gomperts, R. E. Stratmann, O. Yazyev, A. J. Austin, R. Cammi, C. Pomelli, J. W. Ochterski, R. L. Martin, K. Morokuma, V. G. Zakrzewski, G. A. Voth, P. Salvador, J. J. Dannenberg, S. Dapprich, A. D. Daniels, O. Farkas, J. B. Foresman, J. V. Ortiz, J. Cioslowski and D. J. Fox, *Gaussian 16*, Revision A.03; Gaussian Inc., Wallingford CT, **2016**.

Chapter 3

Part A

Predicting Reduction Potentials of 1,3,6-Triphenyl Fulvenes using MESP

Part B

Absorption and Emission Properties of 5-Phenyl Tris(8-hydroxyquinolinato) M(III) Complexes (M = Al, Ga, In) and Correlations with MESP
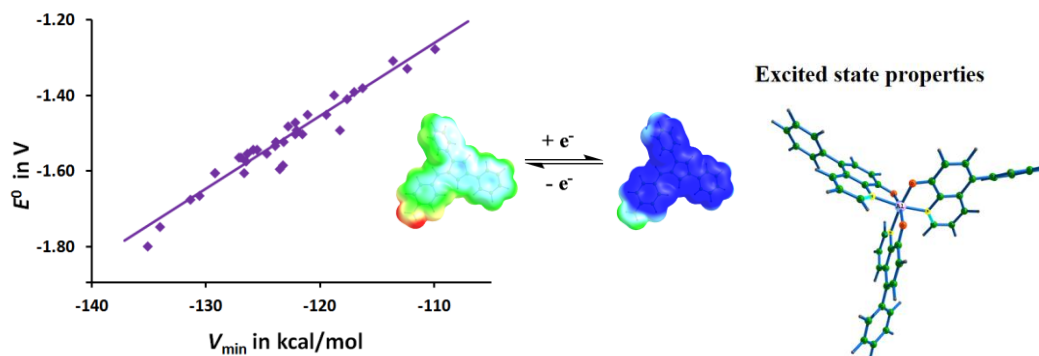
Part A: Predicting Reduction Potentials of 1,3,6-Triphenyl Fulvenes using MESP

3.1 Abstract

The influence of mono- and multiple substituent effect on the reduction potential (E^0) of 1,3,6-triphenyl fulvenes is investigated using B3LYP-SMD/6-311+G(d,p) level density functional theory. The molecular electrostatic potential (MESP) minimum at the fulvene π-system (V_{min}) and the change in MESP at any of the fulvene carbon atoms (ΔV_C) for both neutral and reduced forms are used as excellent measures of substituent effect from the para and meta positions of the 1,3 and 6-phenyl moieties. Substitution at 6-phenyl para position has led to significant change in E^0 than any other positions. By applying the additivity rule of substituent effects, an equation in ΔV_C is derived to predict E^0 for multiply substituted fulvenes. Further, E^0 is predicted for a set of 2000 hexa-substituted fulvene derivatives where the substituents and their positions in the system are chosen in a random way. The calculated E^0 agreed very well with the experimental E^0 reported by Godman et al. Predicting E^0 solely by substituent effect offers a simple and powerful way to select suitable combinations of substituents on fulvene system for light harvesting applications.

3.2 Introduction

Fulvenes are fascinating class of non aromatic, chemically reactive, cyclic conjugated systems comprising of an exo-methylene unit connected to the ring,[1-3] classified as triafulvenes, pentafulvenes, heptafulvenes etc. based on their ring size.[4-6] They are often termed as "aromatic chameleons"[7] since they can adapt to the aromaticity criteria of various electronic states by changing their electron density distribution.[8,9] The presence of an exocyclic double bond makes fulvene an interesting candidate for further development. Fulvene is highly polarizable moiety having the

dipole moment, μ = 0.42 D and the substitution significantly influences the polarity, for example, substitution of dimethyl amino group on exocyclic carbon of fulvene increases the dipole moment to 4.5 D.[7,10-13] Pentafulvenes, structural isomers of benzene, have received significant attention owing to their unique reactivity. They are having a broad range of applications varying from natural products to semiconductors.[14-19] Ottosson *et al*.[8] demonstrated that the CC exocyclic bond in polyfulvene can act as a handle, through which electronic and geometric structures can be tuned with substituents. Peloquin *et al.* synthesized 1,3,6-triphenyl fulvenes having possible applications as monomeric units in polymers and supramolecular assemblies.[20] Conjugated fulvenes have also been used as organic ligands to construct supramolecular architectures.[21, 22] Recently first metallocene-pentafulvene type complexes are synthesized and characterized.[23] Though these studies demonstrate fulvene as an excellent functional molecule, the possibility of fulvene chemistry is not yet fully unravelled.[24]

The concept of substituent effect was pioneered by the works of Hammett,[25, 26] since then several accounts on physical interpretation of substituent effects were reported.[27-32] Krygowsky and co-workers have conducted fruitful studies on substituent effects and their influence on aromaticity, hydrogen bonding etc.[33-35] The effect of different substituents on organic systems can have considerable role in determining their reactivity. Exner and Böhm carried out a number of density functional calculations on various organic compounds and validated the concept of Hammett constant.[29, 30, 36, 37] In the case of fulvenes, a study suggested that the lowest electronic states of fulvene can be varied with substituents.[12] Oziminski and Krygowsky interposed a correlation between π-electron population at carbon atoms of the ring in fulvene and benzene with substituent constant and with aromaticity index NICS.[38]

Though the first account on the redox properties of the fulvene was reported in 1946 by Wawzonek and Fan,[39] their electrochemical nature still remains as the least explored.[40] Reduction potentials of substituted fulvenes suitable for the synthesis of *ansa*-metallocenes are thoroughly investigated by Tacke *et al*.[41] There are several computational accounts[42-49] dealing with the prediction of E^0 of various molecules. Recently, Godman *et al*. have reported the synthesis and E^0 measurement of a series of

117

1,3,6-triphenyl fulvenes.[40] These systems substituted at the *para* position of 6-phenyl unit showed significant variation in E^0 with respect to the nature of the substituent. Godman *et al.*'s results prove that 1,3,6-triphenyl fulvenes are excellent systems for the study of substituent effect. In the previous chapter, we have predicted the E^0 for a series of mononuclear cobalt catalysts[50] and Fischer carbene complexes of chromium.[51] Here the study is extending to organic systems by mainly focusing on the application of MESP based analysis of substituent effect to predict the E^0. The theoretical study uses the experimental data by Godman *et al.* to validate the approach. Moreover, the study will deal with a large variety of substituents and mono- and multiple-substitution effects at *meta* and *para* positions of 1,3 and 6-phenyl units of the fulvene derivatives.

3.3 Computational Methodology

All the calculations have been carried out using Gaussian 09[52] suite of programmes employing the B3LYP-SMD/6-311+G(d,p).[53] The same level of theory is used for MESP calculation. Redox potentials were determined by using the free energy change defined in Eq. 3.1 which describes the difference between free energies of anion-radical of reduced form and neutral oxidized form in solution.[54] The Nernst equation (Eq. 3.2) then determines the standard one electron redox potentials, E^0 (in V) where the normal hydrogen electrode (NHE), the reference electrode has reduction potential[52] -4.52 V in acetonitrile solution.[54]

$$\Delta G^0_{red} = \Delta G^0_{solv}(R^{-\bullet}) - \Delta G^0_{solv}(O) \qquad \text{(Eq. 3.1)}$$

$$E^0_{red} = -\frac{\Delta G^0_{red}}{nF} + E_H \qquad \text{(Eq. 3.2)}$$

The n and F in Eq. 3.2 are the number of transferred electrons and Faraday's constant, respectively. The notations $R^{-\bullet}$ and O represent the reduced and oxidized states of the species.

3.4 Results and Discussion

3.4.1 Structural Details of Optimized Complexes

Schematic representation of the neutral and radical anionic forms of 1,3,6-triphenyl fulvene is provided in Figure 3.1. Effect of a series of substituents having electron donating to electron withdrawing nature on the *para* and *meta* positions of 1, 3 and 6-phenyl rings is characterized. The selected 35 substituents are NMe_2, NH_2, OH, OMe, Et, CH_2NH_2, Me, $SiMe_3$, Ph, SMe, H, NHCHO, CH_2OH, CH_2Cl, OCH_2F, SH, PH_2, PMe_2, F, SiH_3, CH_2F, CH_2CN, Cl, Br, C_6Cl_5, OCF_3, $CONH_2$, COOMe, COMe, $N(CF_3)_2$, OCN, CF_3, $C(CF_3)_3$, $SiCl_3$, and CN. The substituent at the 6-phenyl *para* position is denoted as R_1, 1 and 3 phenyl *para* positions as R_2 and R_3 and 6, 1 and 3 *meta* positions are represented as R_4, R_5, and R_6 respectively.
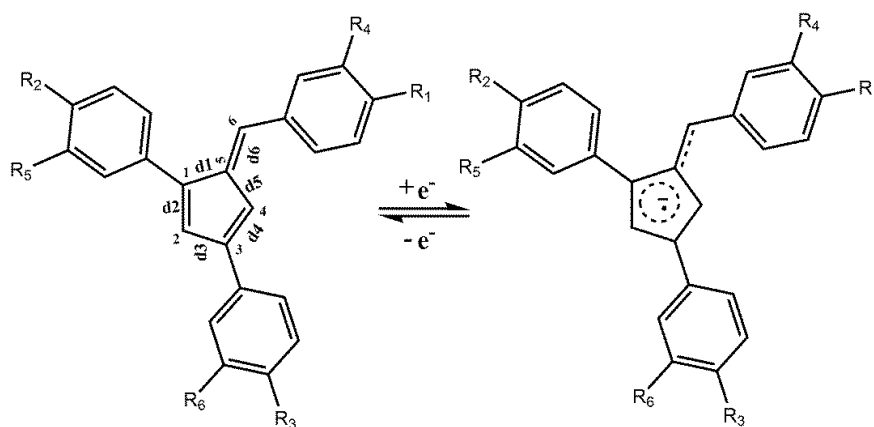
Figure 3.1 Schematic representation of the oxidised and reduced forms of 1,3,6-triphenyl fulvene along with atom numbering and bond notations.

A representative example of optimized geometries of neutral and anionic radical is given in Figure 3.2 along with the d1, d2, d3, d4, d5, and d6 bond lengths. Compared to the neutral forms, the anionic radicals show shortening of the 'formally single' d1, d3, and d5 bond lengths and lengthening of 'formally double' d2, d4, and d6 bond lengths. This suggests that the π-electron distribution in fulvene anion radical is more delocalized than the neutral form (Figure 3.2).

Table 3.1 Distances of neutral forms of 6-aryl *para* substituted 1,3-diphenyl-6-aryl fulvenes. Distances are in Å

R	d1	d2	d3	d4	d5	d6
NMe$_2$	1.481	1.369	1.460	1.378	1.450	1.375
NH$_2$	1.483	1.367	1.463	1.376	1.452	1.372
OMe	1.486	1.365	1.466	1.373	1.455	1.366
Me	1.488	1.363	1.468	1.370	1.457	1.363
Et	1.488	1.363	1.467	1.371	1.457	1.363
CH$_2$OH	1.488	1.362	1.470	1.370	1.457	1.362
CH$_2$NH$_2$	1.488	1.362	1.469	1.371	1.456	1.363
OH	1.486	1.364	1.467	1.373	1.455	1.366
Ph	1.488	1.362	1.469	1.370	1.457	1.363
H	1.489	1.363	1.469	1.370	1.458	1.362
SMe	1.487	1.364	1.468	1.372	1.455	1.365
SiMe$_3$	1.489	1.362	1.469	1.371	1.457	1.363
PMe$_2$	1.487	1.363	1.468	1.371	1.456	1.364
F	1.488	1.362	1.470	1.370	1.457	1.361
NHCHO	1.487	1.363	1.467	1.372	1.455	1.365
Br	1.489	1.361	1.471	1.370	1.458	1.361
OCH$_2$F	1.487	1.363	1.468	1.371	1.456	1.364
SH	1.487	1.363	1.469	1.372	1.456	1.364
CH$_2$F	1.489	1.361	1.471	1.370	1.458	1.361
CH$_2$Cl	1.489	1.361	1.471	1.369	1.458	1.361
SiH$_3$	1.489	1.361	1.471	1.370	1.458	1.361
PH$_2$	1.488	1.363	1.469	1.371	1.457	1.363
CH$_2$CN	1.489	1.362	1.470	1.370	1.458	1.361
Cl	1.488	1.361	1.471	1.371	1.457	1.361
C$_6$Cl$_5$	1.490	1.362	1.470	1.370	1.458	1.361
CONH$_2$	1.489	1.361	1.472	1.369	1.458	1.361
OCF$_3$	1.488	1.361	1.471	1.370	1.457	1.361
COMe	1.490	1.360	1.472	1.369	1.458	1.361
COOMe	1.490	1.360	1.472	1.369	1.458	1.360
CF$_3$	1.490	1.360	1.472	1.368	1.459	1.359
C(CF$_3$)$_3$	1.490	1.360	1.473	1.368	1.459	1.359
OCN	1.490	1.362	1.470	1.370	1.459	1.361
SiCl$_3$	1.490	1.360	1.472	1.369	1.459	1.359
N(CF$_3$)$_2$	1.490	1.360	1.472	1.369	1.459	1.359
CN	1.491	1.360	1.473	1.369	1.458	1.360
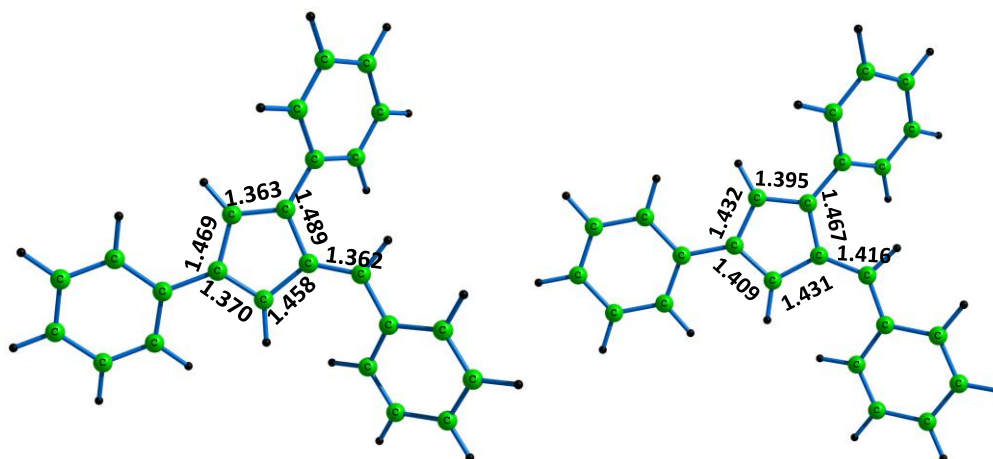
Figure 3.2 Optimized structures of neutral and anionic radical of 1,3,6-triphenyl fulvene. Bond distances in Å.

The bond lengths of 6-phenyl *para* substituted 1,3,6-triphenyl fulvenes of neutral and anionic radicals are provided in Table 3.1 and Table 3.2 respectively.

Table 3.2 Distances of anionic forms of 6-aryl *para* substituted 1,3-diphenyl-6-aryl fulvenes. Distances are in Å

R	d1	d2	d3	d4	d5	d6
NMe$_2$	1.465	1.399	1.429	1.414	1.429	1.420
NH$_2$	1.465	1.399	1.429	1.413	1.429	1.420
OMe	1.466	1.397	1.430	1.412	1.430	1.418
Me	1.466	1.396	1.431	1.410	1.431	1.417
Et	1.466	1.396	1.431	1.410	1.431	1.417
CH$_2$OH	1.466	1.395	1.432	1.408	1.431	1.416
CH$_2$NH$_2$	1.466	1.396	1.432	1.410	1.431	1.417
OH	1.465	1.398	1.430	1.412	1.430	1.418
Ph	1.466	1.395	1.433	1.407	1.432	1.416
H	1.467	1.395	1.432	1.409	1.431	1.416
SMe	1.466	1.395	1.433	1.408	1.431	1.416
SiMe$_3$	1.466	1.395	1.432	1.408	1.431	1.416
PMe$_2$	1.466	1.395	1.432	1.409	1.431	1.417
F	1.466	1.396	1.432	1.409	1.431	1.416
NHCHO	1.466	1.396	1.432	1.410	1.431	1.417
Br	1.466	1.395	1.433	1.408	1.432	1.415
OCH$_2$F	1.466	1.396	1.431	1.410	1.431	1.417
SH	1.466	1.396	1.432	1.410	1.431	1.417
CH$_2$F	1.467	1.393	1.434	1.407	1.432	1.415
CH$_2$Cl	1.467	1.392	1.435	1.405	1.432	1.414

SiH$_3$	1.467	1.393	1.434	1.407	1.432	1.415
PH$_2$	1.467	1.393	1.434	1.407	1.432	1.415
CH$_2$CN	1.467	1.395	1.433	1.408	1.431	1.415
Cl	1.466	1.394	1.433	1.408	1.431	1.415
C$_6$Cl$_5$	1.466	1.394	1.433	1.407	1.432	1.415
CONH$_2$	1.467	1.391	1.437	1.404	1.433	1.413
OCF$_3$	1.467	1.394	1.433	1.408	1.432	1.415
COMe	1.468	1.388	1.439	1.401	1.434	1.410
COOMe	1.468	1.390	1.437	1.402	1.433	1.412
CF$_3$	1.467	1.392	1.436	1.404	1.433	1.413
C(CF$_3$)$_3$	1.468	1.392	1.435	1.405	1.433	1.413
OCN	1.466	1.394	1.433	1.408	1.432	1.415
SiCl$_3$	1.468	1.390	1.437	1.402	1.433	1.412
N(CF$_3$)$_2$	1.467	1.393	1.434	1.406	1.432	1.414
CN	1.469	1.389	1.438	1.401	1.434	1.411

3.4.2 Reduction Potentials of Experimentally Known Systems

To validate the accuracy of the computed E^0 values, a comparison is made with the experimental E^0 values reported by Godman $et\ al.$[40] for the substituted 1,3,6-triphenyl fulvene derivatives (substitution is at $para$ position of 6-phenyl group; substituents are NMe$_2$, OMe, Me, Ph, H, F, Br, OCF$_3$, COOMe, and CF$_3$). Substituents on 1,3,6-triphenyl fulvene with their Hammett constant (σ_p), and experimental and calculated E^0 values are provided in Table 3.3. The calculated E^0 shows very good agreement with the experimental E^0 values. A strong linear correlation obtained between experimental and calculated E^0 is provided in the Figure 3.3. The graph implies that the slope 1.0211 of the linear equation can be used as a scaling factor to improve the accuracy of the theoretical E^0 (Table 3.3). Hereafter, only the scaled up E^0 will be provided. Compared to experimental E^0, a slight deviation in the relative ordering of E^0 can be observed in calculated E^0 for R = Ph and R = COOMe. In general, a gradual increase in E^0 is evident as we move from electron donating to electron withdrawing substituents. This has been previously noted by Godman $et\ al.$ and they showed a strong linear correlation between Hammett σ_p constant and E^0.[40]

Table 3.3 Substituents on 1,3,6-triphenyl fulvene with their Hammett σ_p constant, experimental and calculated E^0 and scaled up E^0 in V

R$_1$	σ_p	Exp. E^0	Calc. E^0	Scaled up E^0
NMe$_2$	-0.83	-1.82	-1.76	-1.80
OMe	-0.27	-1.63	-1.64	-1.67
Me	-0.07	-1.61	-1.57	-1.60
Ph	-0.01	-1.56	-1.49	-1.52
H	0.00	-1.55	-1.53	-1.56
F	0.06	-1.54	-1.52	-1.55
Br	0.23	-1.48	-1.46	-1.49
OCF$_3$	0.35	-1.46	-1.42	-1.45
COOMe	0.45	-1.39	-1.31	-1.34
CF$_3$	0.54	-1.33	-1.35	-1.38
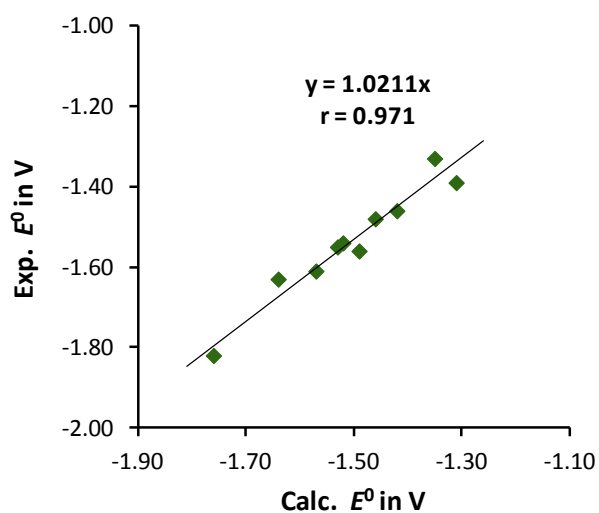
Figure 3.3 Correlation between the calculated and experimental E^0 values.

3.4.3 MESP Analysis

Figure 3.4 shows the MESP isosurface plots of neutral and radical anionic forms of 1,3,6-triphenyl fulvene. The delocalized distribution of π-electrons in both the case is evident from the MESP distribution.

(a)   (b)
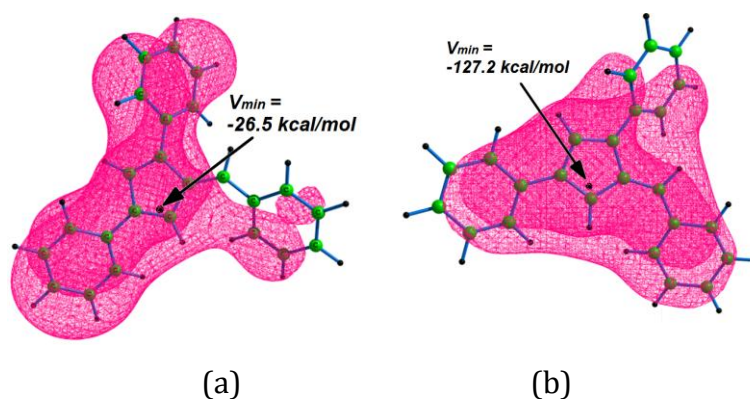
Figure 3.4 MESP isosurface plot with value -10.0 kcal/mol for (a) 1,3,6-triphenyl fulvene and another plot with value -82.0 kcal/mol for (b) the radical anion state. V_{min} values are also depicted.

Table 3.4 The V_{min} and V_C values at C4 of neutral and radical anions of 1,3,6-triphenyl fulvene upon R_1 substitution. V_{min} values in kcal/mol, V_C values in au and E^0 in V.

R_1	V_{min} neutral	V_{min} anion	V_C neutral	V_C anion	E^0
NMe$_2$	-39.9	-135.2	-14.8206	-14.9873	-1.80
NH$_2$	-35.9	-134.1	-14.8144	-14.9848	-1.75
OH	-29.5	-130.6	-14.8024	-14.9790	-1.66
OMe	-30.6	-131.4	-14.8050	-14.9808	-1.67
Et	-28.5	-129.3	-14.8004	-14.9771	-1.60
CH$_2$NH$_2$	-28.0	-126.4	-14.8003	-14.9724	-1.55
Me	-27.8	-129.3	-14.8005	-14.9775	-1.60
SiMe$_3$	-27.1	-125.9	-14.7981	-14.9724	-1.54

Ph	-25.9	-123.9	-14.7974	-14.9682	-1.52
SMe	-28.5	-123.6	-14.8012	-14.9669	-1.59
H	-26.5	-127.2	-14.7965	-14.9739	-1.56
NHCHO	-25.3	-123.3	-14.7938	-14.9661	-1.58
CH_2OH	-25.0	-125.6	-14.7950	-14.9704	-1.54
CH_2Cl	-23.5	-119.5	-14.7923	-14.9591	-1.45
OCH_2F	-26.2	-126.7	-14.7964	-14.9723	-1.60
SH	-26.6	-126.6	-14.7968	-14.9719	-1.57
PH_2	-26.8	-123.2	-14.7963	-14.9669	-1.52
PMe_2	-28.3	-127.0	-14.7991	-14.9731	-1.56
F	-23.0	-124.7	-14.7909	-14.9686	-1.55
SiH_3	-24.5	-122.8	-14.7929	-14.9666	-1.48
CH_2F	-22.9	-122.2	-14.7905	-14.9641	-1.47
CH_2CN	-24.8	-124.0	-14.7916	-14.9666	-1.53
Cl	-22.7	-122.2	-14.7889	-14.9652	-1.50
Br	-21.6	-122.1	-14.7886	-14.9647	-1.49
C_6Cl_5	-22.8	-121.6	-14.7896	-14.9636	-1.50
OCF_3	-21.5	-121.1	-14.7874	-14.9620	-1.45
$CONH_2$	-23.0	-118.8	-14.7917	-14.9592	-1.40
COOMe	-20.9	-118.7	-14.7877	-14.9533	-1.34
COMe	-21.3	-113.7	-14.7882	-14.9505	-1.31
$N(CF_3)_2$	-18.2	-117.7	-14.7822	-14.9566	-1.41
OCN	-19.1	-118.3	-14.7815	-14.9577	-1.49
CF_3	-18.4	-116.4	-14.7828	-14.9547	-1.38
$C(CF_3)_3$	-18.1	-117.1	-14.7822	-14.9554	-1.39
$SiCl_3$	-18.7	-112.4	-14.7814	-14.9481	-1.33
CN	-16.2	-110.0	-14.7775	-14.9437	-1.28

In the neutral state, phenyl units at 1 and 3 positions show more electron rich character than that at the 6 position. In both states, fulvene ring appears as the most electron rich with MESP minimum (V_{min}) located close to the C4 position. V_{min} of 1,3,6-triphenyl fulvene is -26.5 kcal/mol and that of anion is -127.2 kcal/mol. The V_{min} and V_C values at C4 of neutral and radical anions of 1,3,6-triphenyl fulvene upon R_1 substitution is provided in Table 3.4. The V_{min} data of 35 fulvene derivatives and their radical anions shows that changing the electron donating/withdrawing nature of the substituent at the *para* position of 6-phenyl unit leads to a significant increase/decrease in the magnitude of V_{min}.

With the most electron donating NMe_2 substitution at the 6-phenyl *para* position, the V_{min} value for the neutral complex becomes -39.9 kcal/mol and for the corresponding anion the magnitude of V_{min} value drastically increases to -135.2 kcal/mol. In the case of most electron withdrawing CN substituent, V_{min} becomes -16.2 kcal/mol for neutral and -110.0 kcal/mol for anion. The increasing/decreasing trend in the magnitude of V_{min} with electron donating/withdrawing nature of substituent is clearly observed (Table 3.4) in every system. Further, V_{min} shows linear correlation with E^0.
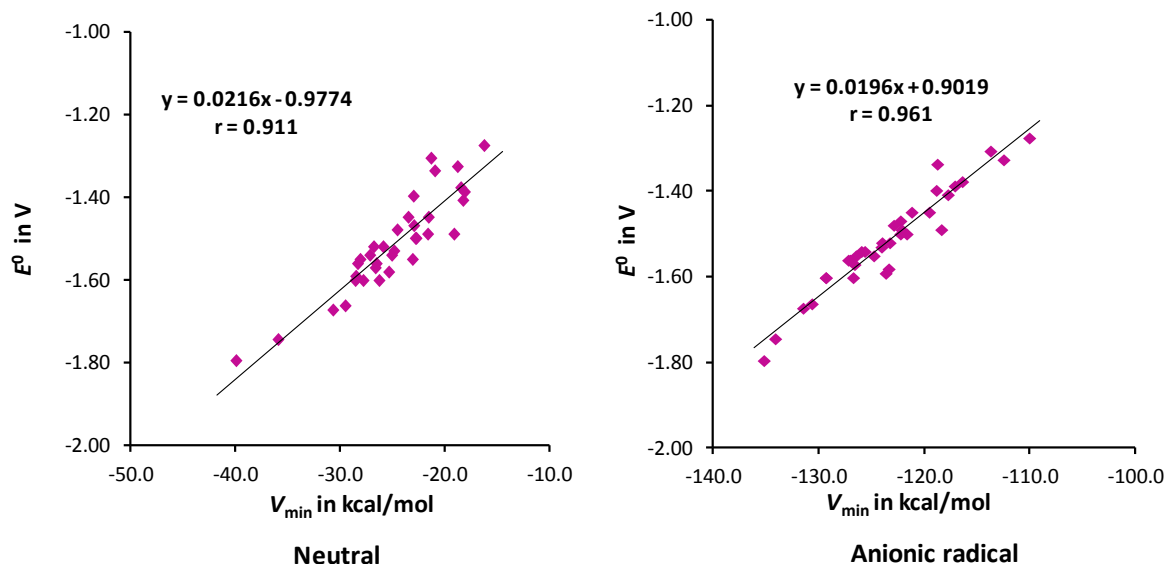
Figure 3.5 The correlation plot between V_{min} of neutral and anionic forms of 6-aryl *para* substituted 1,3-diphenyl-6-aryl fulvenes and E^0. V_{min} in kcal/mol and E^0 in V.

Neutral

Anionic radical
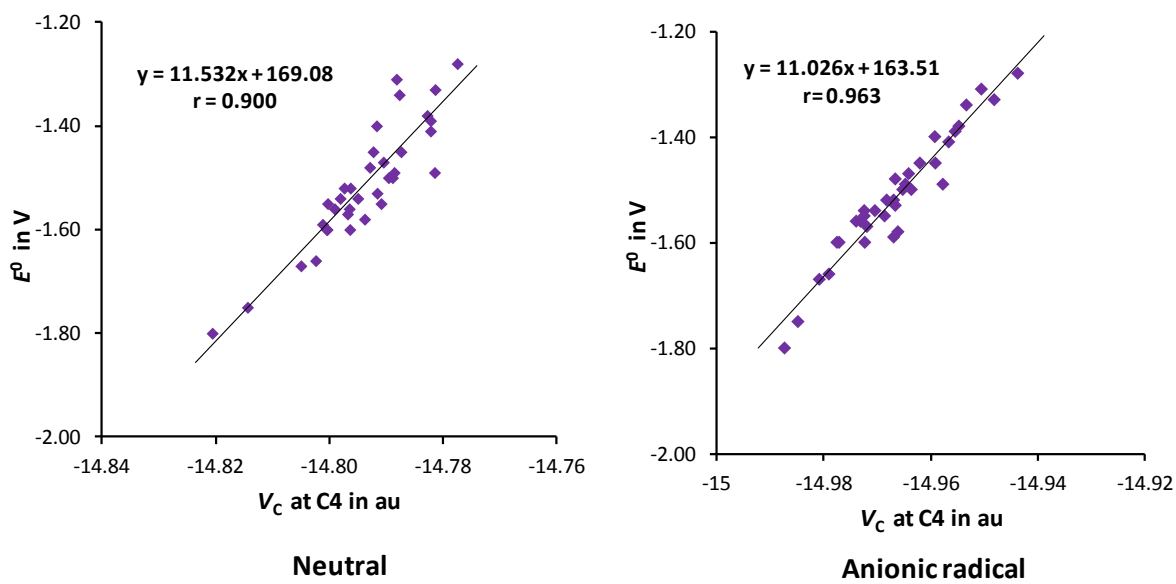
Figure 3.6 The correlation plot between V_C at the C4 position of neutral and anionic forms of 6-aryl *para* substituted 1,3-diphenyl-6-aryl fulvenes and E^0. V_C in au and E^0 in V.

The correlation coefficient, r for the neutral complex is 0.911 and for the anionic system it is 0.961 (Figure 3.5). Figure 3.6 shows the graph between V_C of neutral and anionic forms of 6-aryl *para* substituted 1,3-diphenyl-6-aryl fulvenes and E^0.

Table 3.5 The V_C values on the fulvene ring when substituent is present on the 6-aryl *para* position of neutral forms of 1,3-diphenyl-6-aryl fulvene(V_C values are in au).

R	C1	C2	C3	C4	C5	C6
NMe_2	-14.8094	-14.8225	-14.8094	-14.8206	-14.8016	-14.7743
NH_2	-14.8030	-14.8160	-14.8026	-14.8144	-14.7943	-14.7681
OH	-14.7924	-14.8048	-14.7922	-14.8050	-14.7823	-14.7586
OMe	-14.7878	-14.7990	-14.7866	-14.8005	-14.7770	-14.7572
Et	-14.7878	-14.7993	-14.7869	-14.8004	-14.7771	-14.7574
CH_2NH_2	-14.7823	-14.7939	-14.7812	-14.7950	-14.7701	-14.7507
Me	-14.7870	-14.7984	-14.7857	-14.8003	-14.7763	-14.7571
$SiMe_3$	-14.7902	-14.8027	-14.7898	-14.8024	-14.7794	-14.7557

Ph	-14.7848	-14.7962	-14.7837	-14.7974	-14.7730	-14.7538
SMe	-14.7838	-14.7950	-14.7827	-14.7965	-14.7721	-14.7535
H	-14.7886	-14.8006	-14.7880	-14.8012	-14.7773	-14.7557
NHCHO	-14.7853	-14.7966	-14.7838	-14.7981	-14.7740	-14.7562
CH$_2$OH	-14.7863	-14.7979	-14.7856	-14.7991	-14.7751	-14.7552
CH$_2$Cl	-14.7794	-14.7914	-14.7784	-14.7909	-14.7659	-14.7449
OCH$_2$F	-14.7833	-14.7962	-14.7824	-14.7938	-14.7702	-14.7470
SH	-14.7769	-14.7888	-14.7758	-14.7886	-14.7626	-14.7431
PH$_2$	-14.7848	-14.7968	-14.7838	-14.7964	-14.7727	-14.7509
PMe$_2$	-14.7848	-14.7968	-14.7838	-14.7968	-14.7727	-14.7513
F	-14.7788	-14.7900	-14.7768	-14.7905	-14.7653	-14.7475
SiH$_3$	-14.7793	-14.7910	-14.7786	-14.7923	-14.7661	-14.7474
CH$_2$F	-14.7804	-14.7917	-14.7790	-14.7929	-14.7677	-14.7499
CH$_2$CN	-14.7841	-14.7958	-14.7831	-14.7963	-14.7721	-14.7523
Cl	-14.7790	-14.7910	-14.7788	-14.7916	-14.7656	-14.7453
Br	-14.7774	-14.7892	-14.7760	-14.7889	-14.7634	-14.7436
C$_6$Cl$_5$	-14.7776	-14.7892	-14.7765	-14.7896	-14.7638	-14.7450
OCF$_3$	-14.7772	-14.7890	-14.7772	-14.7917	-14.7636	-14.7449
CONH$_2$	-14.7760	-14.7881	-14.7751	-14.7874	-14.7615	-14.7408
COOMe	-14.7746	-14.7862	-14.7739	-14.7882	-14.7600	-14.7425
COMe	-14.7754	-14.7864	-14.7735	-14.7877	-14.7608	-14.7448
N(CF$_3$)$_2$	-14.7710	-14.7827	-14.7698	-14.7828	-14.7549	-14.7371
OCN	-14.7706	-14.7823	-14.7693	-14.7822	-14.7544	-14.7366
CF$_3$	-14.7715	-14.7840	-14.7706	-14.7815	-14.7552	-14.7341
C(CF$_3$)$_3$	-14.7697	-14.7813	-14.7685	-14.7814	-14.7533	-14.7361
SiCl$_3$	-14.7708	-14.7827	-14.7696	-14.7822	-14.7546	-14.7362
CN	-14.7664	-14.7783	-14.7648	-14.7775	-14.7487	-14.7312

Table 3.6 The V_C values on the fulvene ring when substituent is present on the 6-aryl *para* position of anionic radicals of 1,3-diphenyl-6-aryl fulvene. V_C values are in au.

R	C1	C2	C3	C4	C5	C6
NMe$_2$	-14.9697	-14.9763	-14.9704	-14.9873	-14.9699	-14.9558
NH$_2$	-14.9674	-14.9743	-14.9684	-14.9848	-14.9672	-14.9521
OH	-14.9630	-14.9703	-14.9644	-14.9808	-14.9623	-14.9472
OMe	-14.9596	-14.9665	-14.9603	-14.9775	-14.9595	-14.9458
Et	-14.9594	-14.9662	-14.9600	-14.9771	-14.9592	-14.9458
CH$_2$NH$_2$	-14.9525	-14.9599	-14.9535	-14.9704	-14.9517	-14.9376
Me	-14.9551	-14.9624	-14.9558	-14.9724	-14.9542	-14.9402
SiMe$_3$	-14.9616	-14.9690	-14.9630	-14.9790	-14.9605	-14.9445
Ph	-14.9508	-14.9580	-14.9513	-14.9682	-14.9503	-14.9358
SMe	-14.9557	-14.9626	-14.9563	-14.9739	-14.9555	-14.9429
H	-14.9504	-14.9575	-14.9505	-14.9669	-14.9491	-14.9351
NHCHO	-14.9547	-14.9614	-14.9550	-14.9724	-14.9545	-14.9417
CH$_2$OH	-14.9553	-14.9625	-14.9562	-14.9731	-14.9548	-14.9411
CH$_2$Cl	-14.9523	-14.9599	-14.9532	-14.9686	-14.9500	-14.9343
OCH$_2$F	-14.9501	-14.9583	-14.9514	-14.9661	-14.9475	-14.9305
SH	-14.9481	-14.9559	-14.9490	-14.9647	-14.9460	-14.9307
PH$_2$	-14.9557	-14.9631	-14.9565	-14.9723	-14.9539	-14.9387
PMe$_2$	-14.9545	-14.9621	-14.9557	-14.9719	-14.9534	-14.9381
F	-14.9469	-14.9542	-14.9471	-14.9641	-14.9459	-14.9324
SiH$_3$	-14.9422	-14.9497	-14.9424	-14.9591	-14.9411	-14.9268
CH$_2$F	-14.9488	-14.9560	-14.9493	-14.9666	-14.9483	-14.9350
CH$_2$CN	-14.9489	-14.9562	-14.9497	-14.9669	-14.9483	-14.9344
Cl	-14.9497	-14.9575	-14.9507	-14.9666	-14.9479	-14.9329
Br	-14.9485	-14.9562	-14.9494	-14.9652	-14.9465	-14.9313

C$_6$Cl$_5$	-14.9469	-14.9546	-14.9477	-14.9636	-14.9450	-14.9301
OCF$_3$	-14.9394	-14.9475	-14.9412	-14.9592	-14.9393	-14.9244
CONH$_2$	-14.9457	-14.9536	-14.9467	-14.9620	-14.9428	-14.9273
COOMe	-14.9310	-14.9392	-14.9322	-14.9505	-14.9311	-14.9162
COMe	-14.9357	-14.9430	-14.9355	-14.9533	-14.9352	-14.9221
N(CF$_3$)$_2$	-14.9378	-14.9457	-14.9383	-14.9547	-14.9355	-14.9211
OCN	-14.9386	-14.9467	-14.9393	-14.9554	-14.9362	-14.9221
CF$_3$	-14.9427	-14.9511	-14.9436	-14.9577	-14.9388	-14.9219
C(CF$_3$)$_3$	-14.9312	-14.9392	-14.9316	-14.9481	-14.9289	-14.9148
SiCl$_3$	-14.9403	-14.9484	-14.9411	-14.9566	-14.9374	-14.9222
CN	-14.9268	-14.9352	-14.9271	-14.9437	-14.9245	-14.9096

The correlation plots give r value 0.900 for neutral and 0.963 for radical anion states. Though all the carbon centers on fulvene can show correlation similar to V_C at C4 with E^0 (Figure 3.7), the V_C data of C4 position is discussed as one of the most sensitive positions of the fulvene ring. Compared to the neutral system, V_C of anion shows stronger correlation with E^0 and the relationship predicts that reduction potential of 1,3,6-triphenyl fulvene with a substituent (R) at *para* position of 6-phenyl can be written as

$$E^0 = 11.026(V_C) + 163.51 \qquad \text{(Eq. 3.3)}$$

This equation can be transformed to

$$\Delta E^0 = 0.0176(\Delta V_C) - 0.0369 \qquad \text{(Eq. 3.4)}$$

where ΔE^0 represents the difference between E^0 of 1,3,6-triphenyl fulvene (unsubstituted) and that of substituted system while ΔV_C represents the difference between the corresponding V_C values. The significance of Eq. 3.4 is that it predicts the increase or decrease in E^0 due to the substituent effect in terms of the MESP quantity ΔV_C.
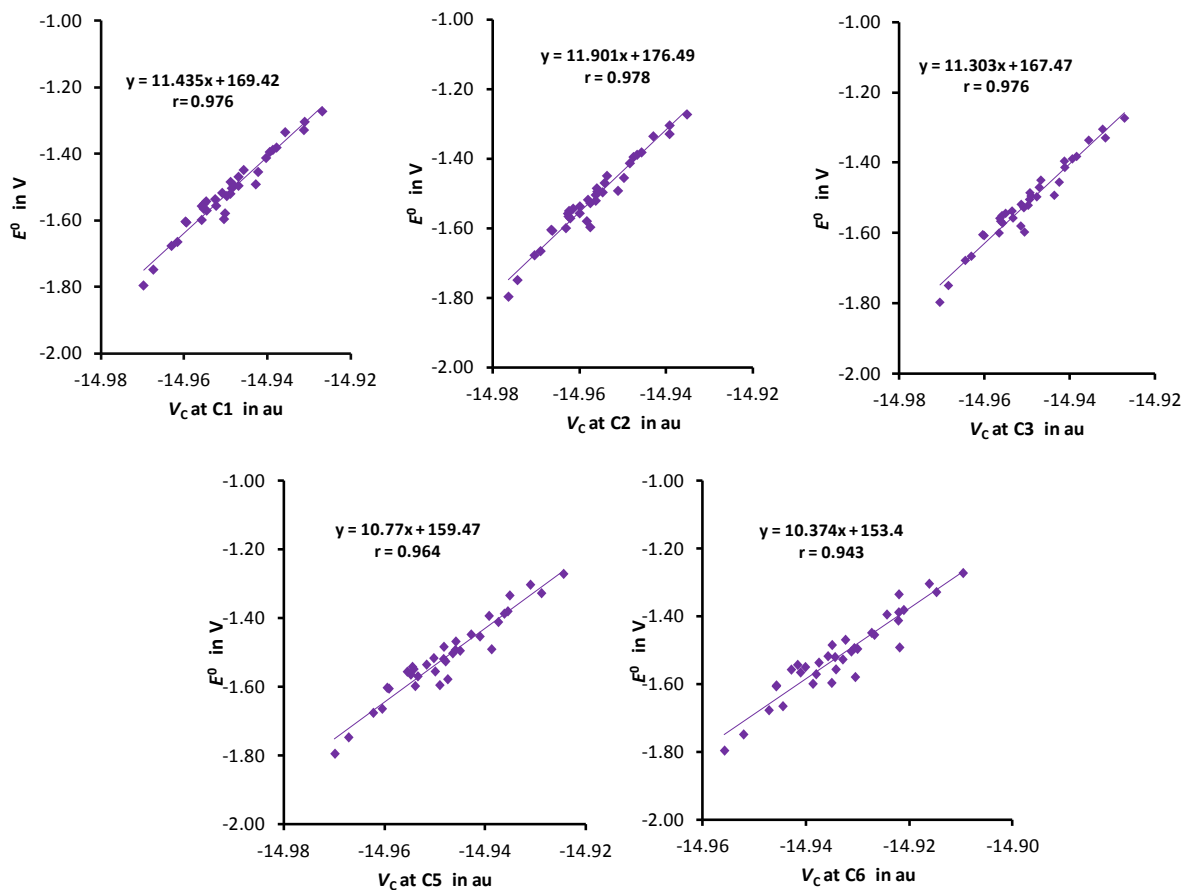
Figure 3.7 The correlation plot between V_C (at various carbon atoms of fulvene ring) of anion systems of 6-aryl *para* substituted 1,3-diphenyl-6-aryl fulvenes and E^0. V_C in au and E^0 in V.

3.4.4 E^0 vs. V_C for a Large Set of Substituted Fulvenes

The MESP approach to E^0 is extended to other R substituted 1,3,6-triphenyl fulvene systems where R occupies 1-phenyl *para* (R_2), 3-phenyl *para* (R_3), 6-phenyl *meta* (R_4), 1-phenyl *meta* (R_5) and 3-phenyl *meta* (R_6) positions.

131

Table 3.7 E^0 in V for 1,3,6-triphenyl fulvene systems where R is at positions 1-phenyl *para* (R_2), 3-phenyl *para* (R_3), 6-phenyl *meta* (R_4), 1-phenyl *meta* (R_5) and 3-phenyl *meta* (R_6)

R	R_2	R_3	R_4	R_5	R_6
NMe_2	-1.62	-1.67	-1.62	-1.59	-1.59
NH_2	-1.61	-1.66	-1.59	-1.57	-1.57
OH	-1.59	-1.61	-1.54	-1.55	-1.54
OMe	-1.59	-1.62	-1.56	-1.55	-1.55
Et	-1.57	-1.59	-1.58	-1.57	-1.57
CH_2NH_2	-1.57	-1.57	-1.58	-1.56	-1.56
Me	-1.57	-1.58	-1.57	-1.56	-1.56
$SiMe_3$	-1.56	-1.55	-1.58	-1.56	-1.57
Ph	-1.55	-1.54	-1.55	-1.55	-1.55
SMe	-1.59	-1.58	-1.55	-1.55	-1.54
H	-1.56	-1.56	-1.56	-1.56	-1.56
NHCHO	-1.55	-1.56	-1.52	-1.52	-1.52
CH_2OH	-1.54	-1.54	-1.55	-1.54	-1.54
CH_2Cl	-1.52	-1.51	-1.52	-1.52	-1.54
OCH_2F	-1.56	-1.58	-1.53	-1.52	-1.53
SH	-1.56	-1.56	-1.52	-1.52	-1.53
PH_2	-1.54	-1.54	-1.54	-1.53	-1.55
PMe_2	-1.56	-1.55	-1.57	-1.55	-1.55
F	-1.55	-1.55	-1.48	-1.52	-1.50
SiH_3	-1.53	-1.52	-1.53	-1.53	-1.54
CH_2F	-1.52	-1.50	-1.52	-1.54	-1.53
CH_2CN	-1.54	-1.54	-1.52	-1.52	-1.54
Cl	-1.53	-1.52	-1.47	-1.52	-1.51
Br	-1.52	-1.52	-1.47	-1.51	-1.50
C_6Cl_5	-1.53	-1.52	-1.51	-1.51	-1.52
OCF_3	-1.52	-1.50	-1.46	-1.51	-1.50
$CONH_2$	-1.50	-1.47	-1.51	-1.51	-1.52
COOMe	-1.47	-1.43	-1.49	-1.53	-1.52
COMe	-1.47	-1.42	-1.49	-1.51	-1.52
$N(CF_3)_2$	-1.50	-1.47	-1.45	-1.49	-1.49

OCN	-1.52	-1.51	-1.43	-1.48	-1.48
CF_3	-1.48	-1.46	-1.45	-1.50	-1.50
$C(CF_3)_3$	-1.48	-1.46	-1.46	-1.49	-1.49
$SiCl_3$	-1.46	-1.42	-1.45	-1.49	-1.50
CN	-1.44	-1.39	-1.43	-1.48	-1.47

In Table 3.7, E^0 of all these systems are depicted and in Table 3.8, V_C values at C4 of the corresponding anions are given. The data in Table 3.7 suggest that compared to R_1 derivative, the substitution effect by any of the *meta* or other *para* positions of phenyl rings on E^0 is minor. E^0 in the ranges -1.62 to -1.44, -1.67 to -1.39, and -1.62 to -1.43 V are observed for R_2, R_3 and R_4 systems, respectively whereas E^0 in the ranges -1.59 to -1.48 and -1.59 to -1.47 V are obtained for R_5 and R_6 systems, respectively. In all the cases, the most negative E^0 is due to NMe_2 and the least negative is due to CN substitutions. V_C values (Table 3.8) and E^0 follow very similar trend. This can be immediately noticed in V_C versus E^0 plots given in Figure 3.8 for R_2, R_3, R_4, R_5, and R_6 systems.

Table 3.8 MESP values in au at C4 (V_C) for anionic radicals of 1,3,6-triphenyl fulvenes where R is at positions 1-phenyl *para* (R_2), 3-phenyl *para* (R_3), 6-phenyl *meta* (R_4), 1-phenyl *meta* (R_5) and 3-phenyl *meta* (R_6)

R	R_2	R_3	R_4	R_5	R_6
NMe_2	-14.9838	-14.9860	-14.9819	-14.9797	-14.9817
NH_2	-14.9815	-14.9834	-14.9795	-14.9767	-14.9787
OH	-14.9766	-14.9773	-14.9724	-14.9750	-14.9713
OMe	-14.9779	-14.9792	-14.9746	-14.9729	-14.9736
Et	-14.9764	-14.9768	-14.9762	-14.9753	-14.9759
CH_2NH_2	-14.9751	-14.9762	-14.9778	-14.9733	-14.9740
Me	-14.9764	-14.9770	-14.9759	-14.9753	-14.9759
$SiMe_3$	-14.9736	-14.9729	-14.9743	-14.9742	-14.9743
Ph	-14.9711	-14.9699	-14.9718	-14.9726	-14.9723
SMe	-14.9694	-14.9734	-14.9730	-14.9695	-14.9705
H	-14.9739	-14.9739	-14.9739	-14.9739	-14.9739

NHCHO	-14.9677	-14.9654	-14.9646	-14.9649	-14.9632
CH$_2$OH	-14.9705	-14.9702	-14.9712	-14.9692	-14.9689
CH$_2$Cl	-14.9659	-14.9638	-14.9668	-14.9692	-14.9672
OCH$_2$F	-14.9728	-14.9719	-14.9699	-14.9698	-14.9692
SH	-14.9715	-14.9710	-14.9685	-14.9684	-14.9678
PH$_2$	-14.9690	-14.9678	-14.9698	-14.9716	-14.9693
PMe$_2$	-14.9733	-14.9721	-14.9731	-14.9726	-14.9719
F	-14.9691	-14.9674	-14.9653	-14.9667	-14.9651
SiH$_3$	-14.9684	-14.9671	-14.9690	-14.9709	-14.9694
CH$_2$F	-14.9670	-14.9656	-14.9673	-14.9698	-14.9677
CH$_2$CN	-14.9679	-14.9661	-14.9667	-14.9673	-14.9649
Cl	-14.9664	-14.9643	-14.9635	-14.9662	-14.9633
Br	-14.9661	-14.9639	-14.9635	-14.9658	-14.9631
C$_6$Cl$_5$	-14.9665	-14.9645	-14.9653	-14.9671	-14.9651
OCF$_3$	-14.9636	-14.9609	-14.9612	-14.9634	-14.9602
CONH$_2$	-14.9618	-14.9609	-14.9631	-14.9630	-14.9621
COOMe	-14.9595	-14.9570	-14.9654	-14.9673	-14.9673
COMe	-14.9561	-14.9546	-14.9603	-14.9632	-14.9610
N(CF$_3$)$_2$	-14.9599	-14.9562	-14.9585	-14.9622	-14.9577
OCN	-14.9610	-14.9568	-14.9566	-14.9620	-14.9563
CF$_3$	-14.9587	-14.9553	-14.9589	-14.9632	-14.9592
C(CF$_3$)$_3$	-14.9585	-14.9554	-14.9592	-14.9636	-14.9588
SiCl$_3$	-14.9535	-14.9500	-14.9567	-14.9625	-14.9574
CN	-14.9493	-14.9455	-14.9528	-14.9596	-14.9535
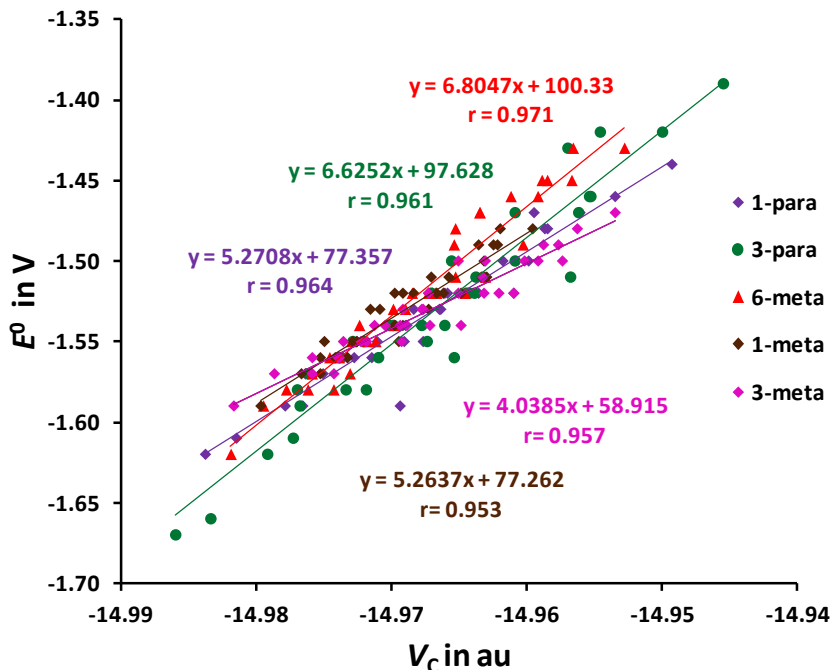
Figure 3.8 Correlation plot between V_C of 1,3,6-triphenyl fulvene radical anions and E^0 with R at various positions. V_C in au and E^0 in V.

The slopes of the linear plots in Figure 3.8 fall in the range 4.0385 to 6.8047 which is significantly smaller than the slope 11.026 observed for R_1 systems given in Eq. 1.3 meaning that substituting at R_1 position is very effective for tuning E^0 of the fulvene derivatives while a significantly reduced effect can be injected if R occupies *meta* position of 6-phenyl as well as *meta* or *para* positions of other phenyl rings.

Since the substituent effect in R_2, R_3, R_4, R_5, and R_6 systems are small and nearly same, we consider the average V_C and average E^0 for these systems to derive a general correlation equation for all these positions. The correlation plot given in Figure 3.9 suggests that the reduction potential of R_2, R_3, R_4, R_5, and R_6 systems can be predicted as

$$E^0 = 5.6082(V_C) + 82.413 \qquad \text{(Eq. 3.5)}$$

Eq. 3.5 can be transformed to Eq. 3.6 by the parameters ΔE^0 (average change in reduction potential) and ΔV_C (average change in MESP) for R_2, R_3, R_4, R_5, and R_6 substitutions.

$$\Delta E^0 = 0.0089(\Delta V_C) - 0.0036 \qquad \text{(Eq. 3.6)}$$

By fixing the very small value of intercept in Eq. 1.6 to zero leads to

$$\Delta E^0 = 0.0085(\Delta V_C) \qquad \text{(Eq. 3.7)}$$
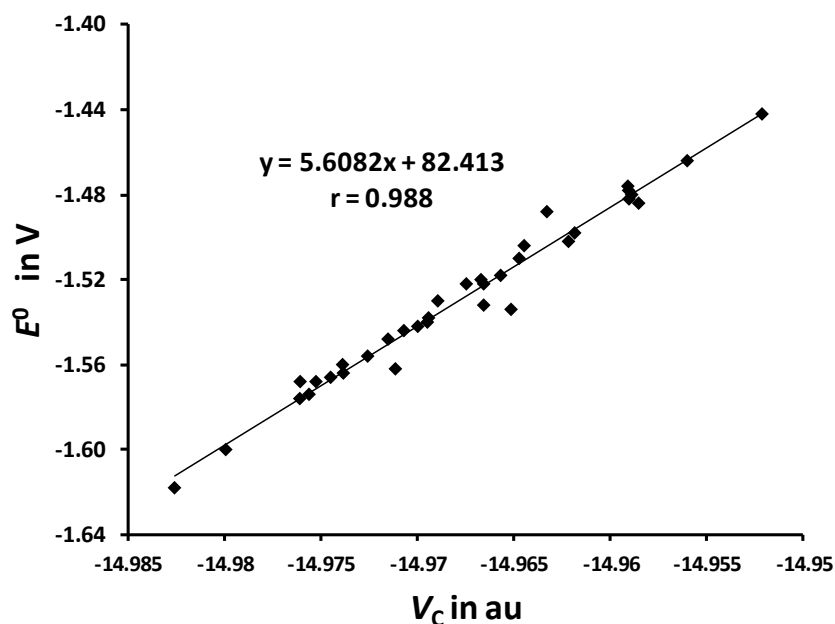
Figure 3.9 Correlation plot between average V_C and average E^0 (average values of R_2, R_3, R_4, R_5, and R_6 substitutions) of 1,3,6-triphenyl fulvenes.

Eq. 3.7 is useful to predict E^0 of any R_2, R_3, R_4, R_5, and R_6 systems provided that E^0 of the unsubstituted system, 1,3,6-triphenyl fulvene is known.

3.4.5 Predicting E^0 of Multiply Substituted Fulvenes

Contribution of substituent effect at 6-phenyl *para* position to change the reduction potential is known from Eq. 3.4 while that due to any other *para* and *meta* position of the phenyl rings is known from Eq. 3.7.

Hence, in a multiply substituted system with one 6-phenyl *para* substitution and '*n*' other substitutions, the total substituent effect contribution towards the change in reduction potential can be written by combining Eq. 3.4 and Eq. 3.7 as:

$$\Delta E^0 = 0.0176\left(\Delta V_C^{6-\text{para}}\right) + 0.0085 \sum_{i=1}^{n} \Delta V_C^{\text{others}} - 0.0369 \qquad \text{(Eq. 3.8)}$$

where $\Delta V_C^{6-\text{para}}$ is the change in MESP at C4 due to 6-phenyl *para* substitution and $\Delta V_C^{\text{others}}$ is that expected due to any other substitution. Table 3.9 depicts these quantities for all the 35 substituents which are derived from the V_C values given in Tables 3.4 and 3.8, respectively. Eq. 3.8 is derived on the basis of the additivity property of substituent effect.[55] Using Eq. 3.8, E^0 of any multiply substituted 1,3,6-triphenyl fulvene systems can be predicted where substituents occupy *meta* and *para* positions of the three phenyl rings.

To test the applicability of Eq. 3.8 to predict E^0, a random selection of 6 substituents from the set of 35 substituents is made to create 2000 hexa substituted fulvene derivatives. Among the 6 substituents, one occupies the R_1 position and the rest are populated in any random manner in five other positions, *viz.* R_2, R_3, R_4, R_5, and R_6 positions. The predicted E^0 values fall in the range -0.85 to -1.85 V for the 2000 systems. Further, to validate the accuracy of the MESP approach to predict the reduction potential, E^0 of a representative set of multiply substituted fulvene derivatives is calculated. Table 3.10 provides the predicted and calculated E^0 for these systems and they show very good agreement with mean absolute deviation 0.031 V.

Table 3.9 The relative MESP values (ΔV_C) for R substituted 1,3,6-triphenyl systems when R is at R_1 position and average ΔV_C for other positions (R_2, R_3, R_4, R_5, and R_6) in kcal/mol

R	$\Delta V_C^{6-\text{para}}$	$\Delta V_C^{\text{others}}$	R	$\Delta V_C^{6-\text{para}}$	$\Delta V_C^{\text{others}}$
NMe_2	-8.4	-5.5	F	3.3	4.5
NH_2	-6.9	-3.8	SiH_3	4.6	3.1
OH	-3.2	-0.4	CH_2F	6.1	4.0
OMe	-4.4	-1.1	CH_2CN	4.6	4.6
Et	-2.0	-1.4	Cl	5.5	5.7
CH_2NH_2	0.9	-0.9	Br	5.8	5.9
Me	-2.3	-1.4	C_6Cl_5	6.5	5.1
$SiMe_3$	0.9	0.0	OCF_3	7.5	7.6
Ph	3.6	1.5	$CONH_2$	9.2	7.4
SMe	4.4	1.7	COOMe	12.9	6.7
H	0.0	0.0	COMe	14.7	9.3
NHCHO	4.9	5.5	$N(CF_3)_2$	10.9	9.4
CH_2OH	2.2	2.4	OCN	10.2	9.6
CH_2Cl	9.3	4.6	CF_3	12.0	9.3
OCH_2F	1.0	2.0	$C(CF_3)_3$	11.6	9.3
SH	1.2	2.8	$SiCl_3$	16.2	11.2
PH_2	4.4	2.8	CN	19.0	13.7
PMe_2	0.5	0.8			

Table 3.10 Substituents at six different positions in a multiply substituted fulvene system and the predicted and calculated E^0 (bold) values in V.

Trial No.	R_1	R_2	R_3	R_4	R_5	R_6	E^0	E^0
1	CN	CN	CN	Br	$SiCl_3$	Br	-0.85	**-0.86**
2	COOMe	$C(CF_3)_3$	CH_2F	CN	PH_2	CH_2CN	-1.10	**-1.05**
3	CF_3	F	SiH_3	OH	$C(CF_3)_3$	NHCHO	-1.22	**-1.24**
4	Cl	SiH_3	$C(CF_3)_3$	COOMe	CH_2CN	SH	-1.30	**-1.28**
5	F	NMe_2	CN	Me	NHCHO	PMe_2	-1.45	**-1.42**
6	Me	COOMe	NH_2	NH_2	Me	SMe	-1.68	**-1.64**
7	NMe_2	$N(CF_3)_2$	NH_2	CH_2CN	NH_2	NH_2	-1.76	**-1.66**
8	NMe_2	NMe_2	NMe_2	CH_2OH	CH_2NH_2	OMe	-1.85	**-1.77**

Table 3.11 Substituents at six different positions in a multiply substituted fulvene system and the predicted and calculated E^0 (bold) values in V.

Trial No.	R_1	R_2	R_3	R_4	R_5	R_6	E^0	E^0
1	CN	Br	CN	Br	CN	$SiCl_3$	-0.85	**-0.90**
2	COOMe	$C(CF_3)_3$	CH_2F	CH_2CN	CN	PH_2	-1.10	**-1.12**
3	CF_3	OH	F	NHCHO	$C(CF_3)_3$	SiH_3	-1.22	**-1.30**
4	Cl	$C(CF_3)_3$	COOMe	SiH_3	SH	CH_2CN	-1.30	**-1.26**
5	F	PMe_2	NHCHO	Me	CN	NMe_2	-1.45	**-1.51**
6	Me	SMe	COOMe	NH_2	Me	NH_2	-1.68	**-1.58**
7	NMe_2	NH_2	CH_2CN	$N(CF_3)_2$	NH_2	NH_2	-1.76	**-1.63**
8	NMe_2	CH_2NH_2	OMe	CH_2OH	NMe_2	NMe_2	-1.85	**-1.83**

Since the small contribution of substituent effect for all positions other than R_1 is considered to be same to derive Eq. 3.8, the predicted E^0 for the fulvene system will remain identical for any combination of a given set of substituents at these positions. In order to verify this feature, another test set of multiply substituted 1,3,6-triphenyl fulvene systems are made from the systems given in Table 3.10 by shuffling the substituents at positions other than R_1. Table 3.11 provides the

rearranged positions of the substituents as well as the predicted and calculated E^0. The calculated values again show good agreement with the predicted values with a mean absolute deviation 0.063 V.

3.5 Conclusions

The quantification of the effect of substituents on tuning the reduction potential, E^0 for a series of 1,3,6-triphenyl fulvenes has been achieved at B3LYP-SMD/6-311+G(d,p) level DFT. The change in MESP minimum at the fulvene π-system or the change in MESP at any of the fulvene carbon atoms is found to be very sensitive to the nature of the substituent attached at the *para* or *meta* positions of the 1,3 and 6-phenyl moieties. The reduced form of the fulvene derivative, a radical anion has also exhibited MESP features similar to that of the neutral form and the change in MESP at its C4 position due to substitution (ΔV_C) has been used as a sensitive parameter to find correlations with E^0. The substituent attached at the *para* position of 6-phenyl unit is the most influential on E^0 while the effect of other *para* and *meta* positions is moderate. The strong linear correlations observed between V_C and E^0 for all mono substituted systems, *viz*, R_2, R_3, R_4, R_5, and R_6 positions, led to the derivation of a general equation (Eq. 3.8) to predict E^0 of multiply substituted systems solely from substituent effects measured in terms of ΔV_C. This equation works on the basis of the additivity rule of substituent effects and also considers the moderate effect of substituents other than R_1 in a unified way. The predicted E^0 of a randomly generated several hexa substituted fulvene derivatives agreed very well with the calculated values. The strength of Eq. 3.8 is that it can instantly generate E^0 of all possible multiply substituted combinations (*meta* and *para*) of fulvene derivatives. As a test case, E^0 of 2000 hexa substituted combinations have been reported here. This study proves that MESP analysis offers an effective approach to the quantification of substituent effect and can be applied to tune the reduction potential of light harvesting molecules.

Part B: Absorption and Emission Properties of 5-Phenyl Tris(8-hydroxyquinolinato) M(III) Complexes (M = Al, Ga, In) and Correlations with MESP

3.6 Abstract

A series of 5-phenyl substituted tris(8-hydroxyquinolinato) M(III) complexes (Mq3) of aluminium, gallium and indium are investigated using B3LYP/SMD/BS1 level of density functional theory (DFT) for the ground state properties and the time-dependent version of DFT (TDDFT) is used for their absorption and emission properties. The effect of different substituents, ranging from electron withdrawing to electron donating nature has been analyzed. A comparison between the ground state energy of mer and fac isomers of all the complexes revealed that the mer configuration is always more most stable than fac. Hence only mer complexes have been considered for a systematic study on their absorption and emission properties. The substituent effect is significantly reflected at the fluorescence maximum (λ_F) values whereas the effect is moderate at the absorption maximum (λ_{abs}) values. The molecular electrostatic potential (MESP) at the metal centre and the most electron rich region indicated by MESP minimum (V_{min}), located at the oxygen of phenoxide ring exhibit excellent correlations with the λ_F and Stokes shift (λ_F - λ_{abs}) values. The λ_F values are highly sensitive to the electron withdrawing and donating substituents and a red shift is observed from electron withdrawing to electron donating substituents (NMe$_2$ to CN) as well as from lighter metal to heavier metal (Al to Ga). The study suggests the use of Stokes shift as an experimental quantity to measure the excited state substituent effect while the V_{min} or V_M emerge as theoretical quantities to measure the same.

3.7 Introduction

The first efficient organic light emitting diode (OLED) was constructed by Tang and VanSlyke at Kodak in 1987 with a double organic layer structure consisting of tris (8-hydroxyquinolinato) aluminium (III) (Alq3) as emitter.[56-60] Thereupon, Alq3 and other group III metal chelates of gallium and indium have received significant attention as electroluminescent materials due to their distinctive electron transport and emissive properties.[60-70] In the Mq3 complex, the trivalent metal coordinated to three bidentate 8-hydroxyquinolinate ligands ($M(C_9H_6NO)_3$) forms an octahedral complex having two geometric isomers, meridional (*mer*) and facial (*fac*) (Figure 3.10). The *mer* isomer consists of three oxygen and three nitrogen atoms in perpendicular planes of the octahedron and its three quinoline ligands are not in equivalent positions and belongs to C_1 symmetry point group. The *fac* isomer has three equivalent bidentate quinoline ligands around the central M(III) atom; three oxygen and three nitrogen atoms are located on the opposite faces of the distorted octahedron having C_{3v} symmetry.

mer   *f ac*
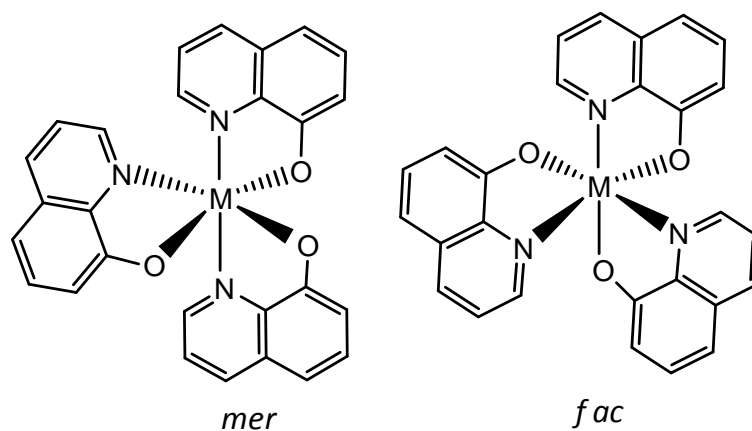
Figure 3.10 The meridional (*mer*) and facial (*fac*) isomers of Mq3 complex.

The first accurate assessment of structure and energy of *mer* and *fac* forms of Alq3 using density functional theory has been carried out by Curioni *et al.*,[71] they demonstrated *mer* isomer as the energetically stable form. Later, Zhang and Frenking,[72] and several others backed this study by confirming *mer* isomer as the preferred form of Alq3.[73-75] The free 8-hydroxyquinoline (8-HQ) is known to be weakly luminescent due to fast excited state intramolecular proton transfer while coordinating with suitable metal

cation leads to distinct fluorescence spectra.[76,77] The π-π^* charge transfer from the electron rich phenoxide ring (HOMO) to the electron deficient pyridyl ring (location of the LUMO) is responsible for the light emission thus emissive colour can be tuned by substituting the ligand with electron withdrawing or donating groups.[57,78-80] The introduction of aromatic substituents on Alq3 skeleton seems to improve its electronic properties such as ionization potential, energy gap, electron affinity etc. Anzenbacher *et al.*[79] demonstrated that the effective colour tuning from blue to red is possible by substituting electron withdrawing to electron donating aromatic rings at the C5 positions of the quinolinate ring in Alq3 complex. Studies also showed that the nature of the metal ion has a role in determining the emission colour, efficiency, stability and evaporability of the metal complex.[81,82] Though a large number of studies have been devoted to the electron distribution of the HOMO/LUMO orbitals of Alq3,[83,84] a MESP based analysis of Mq3 complexes has not yet carried out. Cheshmedzhieva and Ilieva *et. al.*[85] studied the spectral features of substituted aryl hydrazones and established a linear correlation of fluorescence values with MESP at the naphthalimide nitrogen in excited states of aryl hydrazones. Herein, an attempt is made to rationalize the absorption and fluorescence spectral characteristics of Mq3 complexes with the use of MESP analysis.

3.8 Computational Methodology

For all the ground-state (S^0) gas-phase optimizations, Becke's three-parameter hybrid functional (B3LYP) density functional theory (DFT) is used. For absorption spectra calculation, time-dependent DFT (TDDFT) is used in conjunction with self consistent reaction field (SCRF) method SMD to incorporate solvation effects of dichloromethane. Lowest singlet excite state (S^1) is also optimized with TDDFT method in combination with SCRF. The basis set 6-31g(d) is used for Al and for all the nonmetal atoms while for Ga and In, LANL2DZ basis set is used. The level of theory used for the absorption and emission calculation is abbreviated as B3LYP/SMD/BS1 where BS1 stands for the mixed basis set used. Gaussian 16 package is used for all the calculations.[86]

3.9 Results and Discussion

The selected complexes for the study are depicted in Figure 3.11. In all the cases, the 8-hydroxyquinolinate ligands are substituted at the 5th position with *para*-substituted phenyl units (Figure 3.11). The selected substituent (R) groups are CN, CF$_3$, COMe, COOMe, CHO, OCF$_3$, Cl, F, H, OCH$_3$, OH, NH$_2$, and NMe$_2$. The corresponding complex is abbreviated as ***mer*-Mq3-R**.
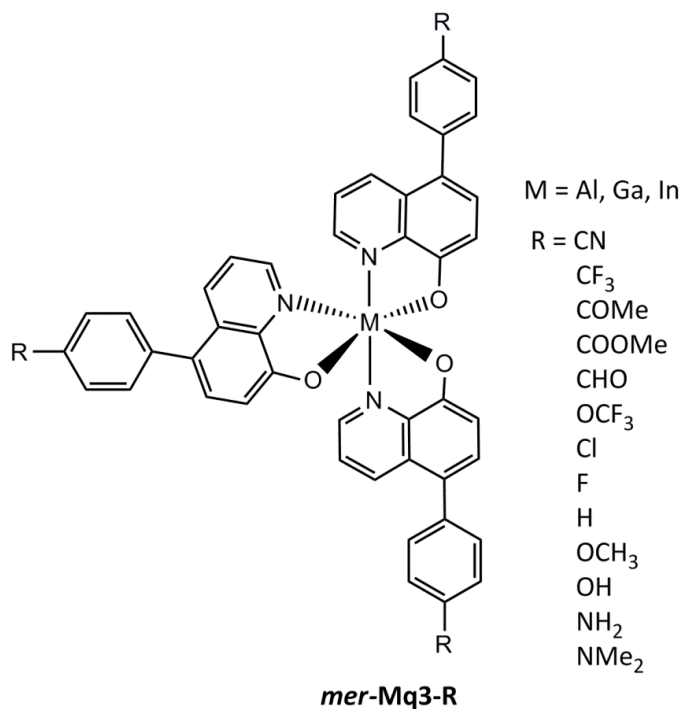
Figure 3.11 The selected complexes for the study.

3.9.1 *mer* and *fac* Isomers of Mq3-R

The *mer* isomers of Al and Ga complexes are widely accepted as the most stable forms compared to their *fac* isomers.[71,72,74,87,88] The ground state energy comparison between *mer* and *fac* isomers of **Alq3-R**, **Gaq3-R**, and **Inq3-R** complexes reveal that the *mer* isomers are always more stable than their *fac* isomers (Tables 3.12 – 3.14) which is in agreement with the existing literature data.[89,90] The *mer* isomers of **Alq3-R** and **Gaq3-R** are ~5 kcal/mol more stable than their *fac* isomers and the *mer* isomers of **Inq3-R** are ~4 kcal/mol more stable than their *fac* isomers. The stable *mer* isomers are considered for further studies.

Table 3.12 The ground state energy comparison between *mer* and *fac* isomers of **Alq3-R** complexes.

R	*mer*-**Alq3-R** (au)	*fac*-**Alq3-R** (au)	ΔE (kcal/mol)
CN	-2642.2614	-2642.2528	5.4
CF$_3$	-3376.6436	-3376.6352	5.3
COMe	-2823.4733	-2823.4651	5.1
COOMe	-3049.1712	-3049.1630	5.1
CHO	-2705.5060	-2705.4975	5.3
OCF$_3$	-3602.2965	-3602.2877	5.5
Cl	-3744.3180	-3744.3096	5.3
F	-2663.2291	-2663.2209	5.2
H	-2365.5295	-2365.5214	5.1
OCH$_3$	-2709.0972	-2709.0890	5.1
OH	-2591.1776	-2591.1693	5.2
NH$_2$	-2531.5891	-2531.5807	5.3
NMe$_2$	-2767.4299	-2767.4219	5.0

Table 3.13 The ground state energy comparison between *mer* and *fac* isomers of **Gaq3-R** complexes.

R	*mer*-**Gaq3-R** (au)	*fac*-**Gaq3-R** (au)	ΔE (kcal/mol)
CN	-2401.7673	-2401.7594	5.0
CF$_3$	-3136.1488	-3136.1409	4.9
COMe	-2582.9792	-2582.9714	4.8
COOMe	-2808.6737	-2808.6663	4.7
CHO	-2465.0134	-2465.0058	4.8
OCF$_3$	-3361.7983	-3361.7915	4.3
Cl	-3503.8218	-3503.8141	4.8

F	-2422.7411	-2422.7335	4.8
H	-2125.0434	-2125.0359	4.7
OCH_3	-2468.6062	-2468.5988	4.7
OH	-2350.6882	-2350.6805	4.8
NH_2	-2291.1000	-2291.0923	4.8
NMe_2	-2526.9369	-2526.9296	4.6

Table 3.14 The ground state energy comparison between *mer* and *fac* isomers of **Inq3-R** complexes.

R	*mer*-**Inq3-R** (au)	*fac*-**Inq3-R** (au)	ΔE (kcal/mol)
CN	-2401.5806	-2401.5739	4.2
CF_3	-3135.9621	-3135.9555	4.1
COMe	-2582.7925	-2582.7860	4.1
COOMe	-2808.4870	-2808.4809	3.9
CHO	-2464.8267	-2464.8203	4.0
OCF_3	-3361.6117	-3361.6061	3.5
Cl	-3503.6351	-3503.6287	4.0
F	-2422.5544	-2422.5481	4.0
H	-2124.8568	-2124.8506	3.9
OCH_3	-2468.4196	-2468.4134	3.9
OH	-2350.5016	-2350.4952	4.0
NH_2	-2290.9134	-2290.9070	4.0
NMe_2	-2526.7503	-2526.7443	3.8

3.9.2 Ground State Geometries of *mer*-Mq3-R Complexes

The ground state optimized geometries of **mer-Mq3-H** complexes (unsubstituted) are given in Figure 3.12. The selected bond distances of all the optimized complexes of **mer-Alq3-R**, **mer-Gaq3-R**, and **mer-Inq3-R** are provided in

Tables 3.15, 3.16, and 3.17 respectively. The distances between the metal and oxygen are labeled as d1, d2, and d3 and the metal nitrogen bonds are labeled as d4, d5, and d6.

In ***mer*-Al-H**, d6 distance 2.123 Å corresponding to Al-N bond *trans* with respect to Al-O bond is the longest whereas the remaining two Al-N distances show comparatively smaller values (2.063 and 2.083 Å). The shortest bond distance is observed for d2 (1.855 Å) corresponds to an Al-O bond which is orienting *trans* with respect to the longest Al-N bond, while the other two Al-O bonds show comparatively larger and more similar values (1.883 and 1.880 Å)(Figure 3.12).
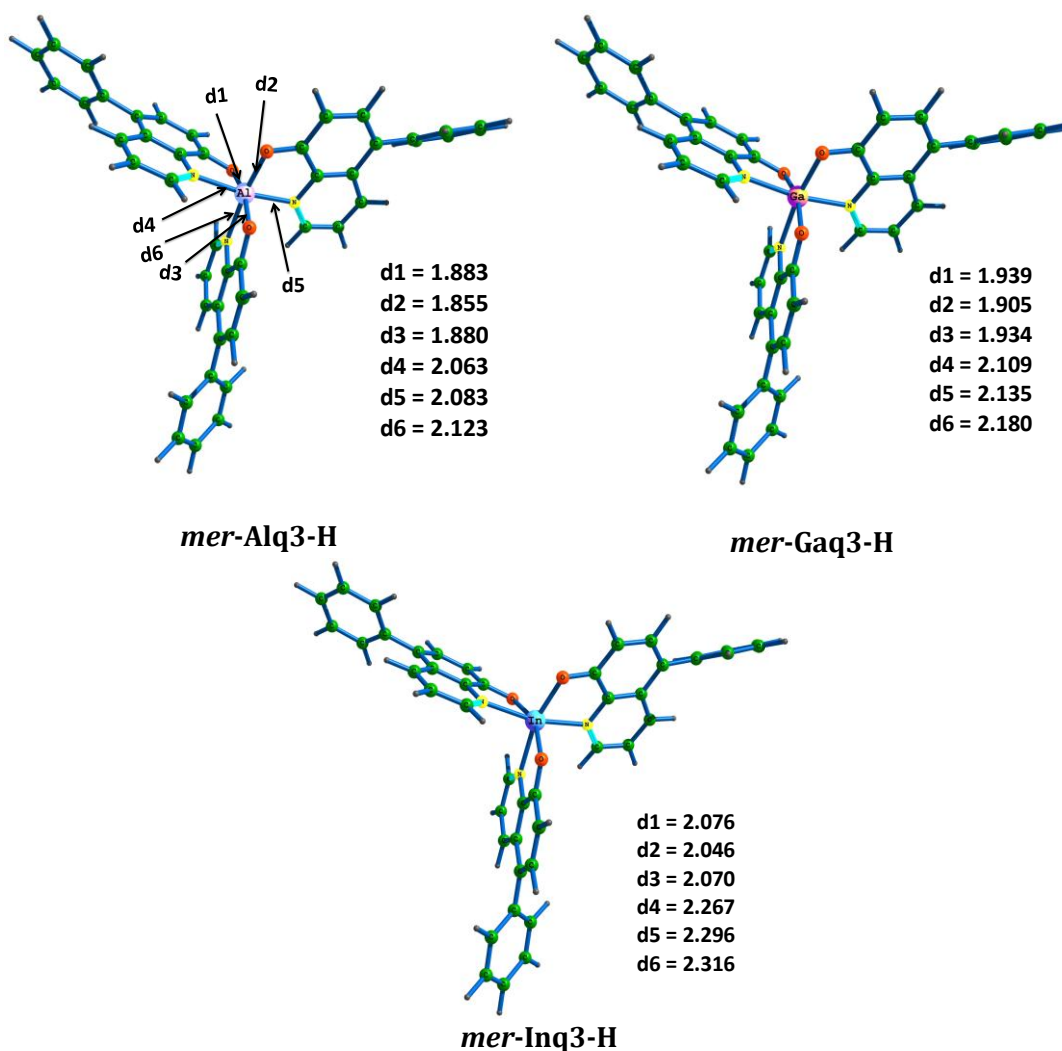
Figure 3.12 Gas phase optimized ground state geometries of ***mer*-Mq3-H** complexes. Bond lengths are in Å. oxygen (orange), nitrogen (yellow), carbon (green), and hydrogen (ash).

Very similar trend in M-O and M-N bond distances is observed for the ground state geometries of the *mer* complexes of Ga and In. However, the bond distances show higher values due to the increase in the size of the metal atoms, *viz.* Ga-O and Ga-N bond lengths are nearly 0.05 Å longer and In-O and In-N bond lengths are nearly 0.20 Å longer than that of Al-O and Al-N bonds. The conclusions drawn on d2 (shortest bond) and d6 (longest bond) remain same for all the substituted **mer-Mq3-R** systems (Tables 3.15 – 3.17).

Table 3.15 Bond distances and sum of the bond distances of ground state geometries of **mer-Alq3-R** complexes (values are in Å). Hammett constants are also given.

		Ground state geometry						
R	σ_p	Al-O_1 (d1)	AlO_2 (d2)	Al-O_3 (d3)	Al-N_1 (d4)	Al-N_2 (d5)	Al-N_3 (d6)	$\sum_{i=1}^{6} d_i$
CN	0.66	1.882	1.856	1.879	2.063	2.083	2.121	11.884
CF_3	0.54	1.882	1.856	1.879	2.063	2.083	2.122	11.885
COMe	0.50	1.882	1.856	1.879	2.062	2.082	2.122	11.883
COOMe	0.45	1.882	1.856	1.879	2.062	2.083	2.122	11.884
CHO	0.42	1.883	1.856	1.879	2.063	2.082	2.121	11.884
OCF_3	0.35	1.883	1.856	1.878	2.063	2.083	2.122	11.885
Cl	0.23	1.882	1.855	1.879	2.063	2.083	2.123	11.885
F	0.06	1.882	1.855	1.879	2.063	2.083	2.124	11.886
H	0.00	1.883	1.855	1.880	2.063	2.083	2.123	11.887
OCH_3	-0.27	1.883	1.855	1.880	2.063	2.083	2.124	11.888
OH	-0.37	1.883	1.855	1.880	2.063	2.083	2.124	11.888
NH_2	-0.66	1.883	1.855	1.879	2.063	2.083	2.124	11.887
NMe_2	-0.83	1.883	1.855	1.879	2.063	2.083	2.125	11.888

In all the cases, bond distances show negligible variation with respect to the nature of R group. Sum of the bond distances around the metal center, $\sum_{i=1}^{6} d_i$ is also depicted in Tables 3.15 – 3.17. This quantity is slightly more sensitive than individual bond lengths and in general, $\sum_{i=1}^{6} d_i$ increases/decreases with respect to the electron donating/withdrawing character of the substituent. In all the cases, the d6 (the longest M-N bond distance) is more sensitive compared to other individual distances. In the case of **mer-Alq3-R**, the d6 value changes reasonably with the Hammett σ_p substituent constant, whereas the effect becomes lesser for **mer-Gaq3-R** and **mer-Inq3-R** (Figure 3.13).

Table 3.16 Bond distances and sum of the bond distances of ground state geometries of **mer-Gaq3-R** complexes (values are in Å)

	Ground state geometry						
R	Ga-O_1 (d1)	Ga-O_2 (d2)	Ga-O_3 (d3)	Ga-N_1 (d4)	Ga-N_2 (d5)	Ga-N_3 (d6)	$\sum_{i=1}^{6} d_i$
CN	1.939	1.905	1.934	2.109	2.134	2.178	12.199
CF$_3$	1.939	1.905	1.935	2.109	2.134	2.178	12.200
COMe	1.939	1.905	1.934	2.109	2.134	2.179	12.200
COOMe	1.939	1.905	1.934	2.109	2.134	2.179	12.200
CHO	1.939	1.906	1.934	2.108	2.134	2.178	12.199
OCF$_3$	1.939	1.905	1.934	2.109	2.135	2.180	12.202
Cl	1.939	1.905	1.934	2.109	2.135	2.180	12.202
F	1.939	1.904	1.934	2.109	2.135	2.181	12.202
H	1.939	1.905	1.934	2.109	2.135	2.180	12.202
OCH$_3$	1.939	1.905	1.934	2.110	2.135	2.181	12.204
OH	1.940	1.904	1.934	2.109	2.135	2.181	12.203
NH$_2$	1.940	1.905	1.934	2.109	2.135	2.181	12.204
NMe$_2$	1.940	1.904	1.934	2.110	2.135	2.182	12.205

Table 3.17 Bond distances and sum of the bond distances of ground state geometries of *mer*-**Inq3_R** complexes (values are in Å)

	Ground state geometry						
R	In-O_1 (d1)	In-O_2 (d2)	In-O_3 (d3)	In-N_1 (d4)	In-N_2 (d5)	In-N_3 (d6)	$\sum_{i=1}^{6} d_i$
CN	2.076	2.046	2.070	2.267	2.295	2.315	13.069
CF_3	2.076	2.046	2.071	2.267	2.295	2.314	13.069
COMe	2.076	2.046	2.070	2.267	2.295	2.315	13.069
COOMe	2.076	2.046	2.070	2.266	2.295	2.315	13.068
CHO	2.076	2.046	2.070	2.266	2.295	2.315	13.068
OCF_3	2.076	2.046	2.070	2.267	2.296	2.316	13.071
Cl	2.076	2.046	2.070	2.267	2.296	2.316	13.071
F	2.076	2.046	2.070	2.267	2.296	2.316	13.071
H	2.076	2.046	2.070	2.267	2.296	2.316	13.071
OCH_3	2.076	2.046	2.070	2.268	2.296	2.316	13.072
OH	2.076	2.045	2.070	2.267	2.296	2.317	13.071
NH_2	2.076	2.046	2.070	2.267	2.296	2.316	13.071
NMe_2	2.076	2.046	2.070	2.267	2.296	2.316	13.071
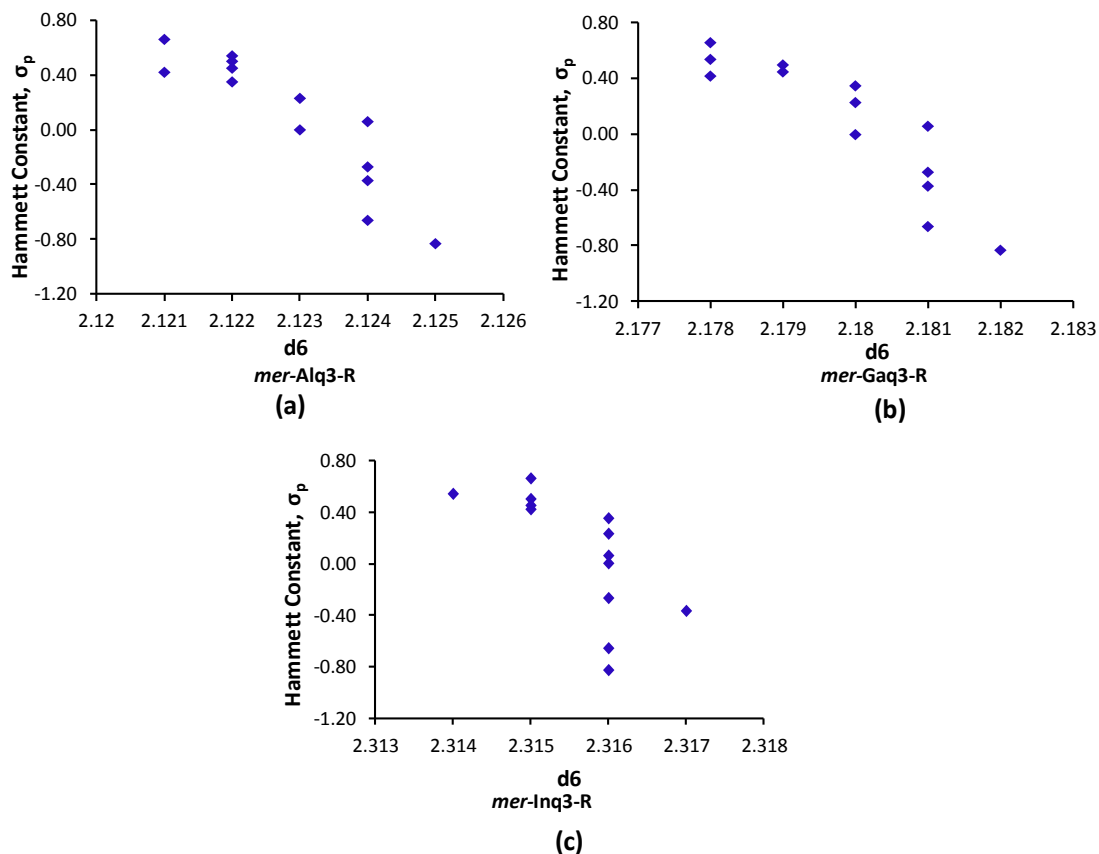
Figure 3.13 Graph between d6 (longest M-N bond distance) and Hammett constant (σ_p) of (a) *mer*-**Alq3-R**, (b) *mer*-**Gaq3-R**, and (c) *mer*-**Inq3-R**.

3.9.3 First Excited State Geometries of *mer*-**Mq3-R* Complexes**

First excited state geometries of *mer*-**Mq3-H*** complexes are shown in Figure 3.14. In general, excitation results in noticeable changes in geometry particularly for M-O and M-N bond lengths. For example the d1 distance 1.883 Å in *mer*-**Alq3-H** is changed to 1.961 Å in the excited state *mer*-**Alq3-H***, the d2 and d3 distances 1.855 and 1.880 Å, respectively changed to 1.868 Å, whereas the two of the Al-N distances decreased and the third one increased.

d1 = 1.961
d2 = 1.868
d3 = 1.868
d4 = 1.978
d5 = 2.105
d6 = 2.094

mer-Alq3-H*

d1 = 2.045
d2 = 1.917
d3 = 1.922
d4 = 2.003
d5 = 2.155
d6 = 2.157

mer-Gaq3-H*

d1 = 2.079
d2 = 2.157
d3 = 2.081
d4 = 2.288
d5 = 2.166
d6 = 2.283

mer-Inq3-H*
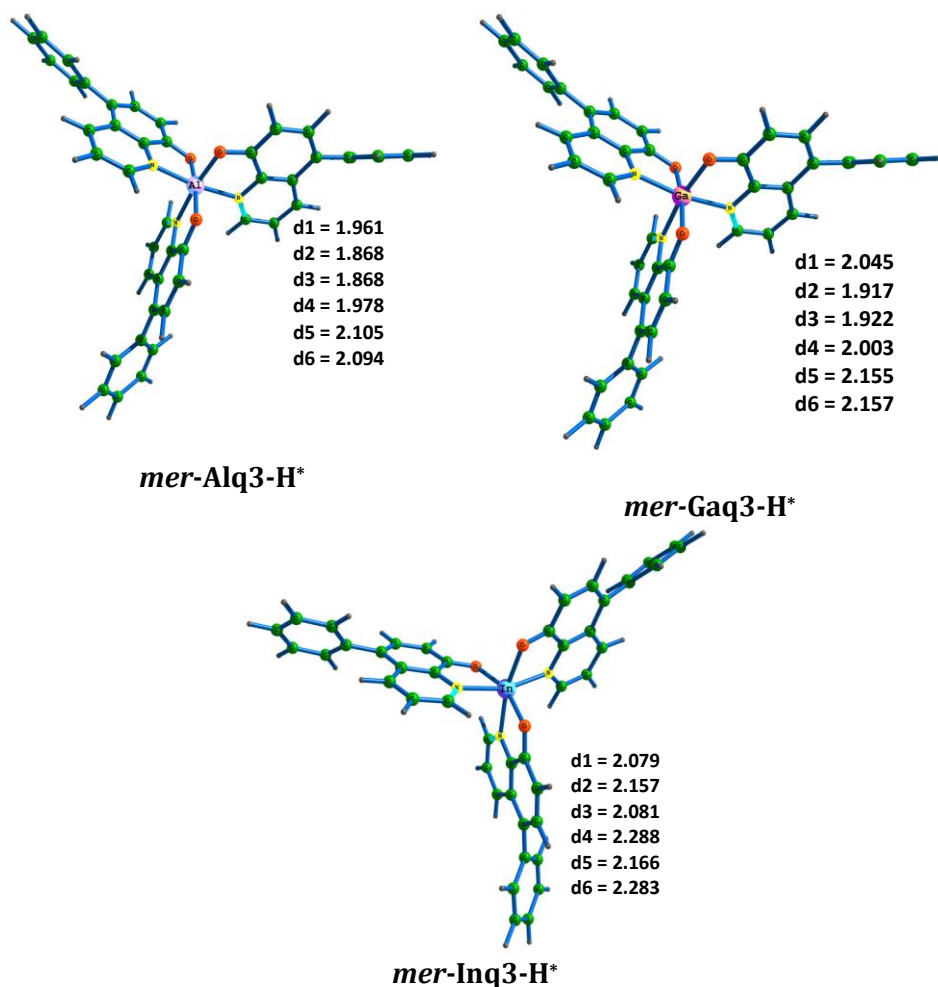
Figure 3.14 B3LYP/SMD/BS1 level optimized geometry of the first excited state of **mer-Mq3-H** complexes. Bond lengths are in Å.

The bond distances of all the excited state geometries are provided in Tables 3.18 – 3.20. Similar to the ground state geometry, the d6 is more sensitive among all the distances, whereas here excellent correlations with the Hammett substituent constant, σ_p values are present (Figure 3.15). This indicates that the excited state geometry is more sensitive to substituent effect compared to its ground state geometry.

Table 3.18 Bond distances and their sum of first excited state geometries of *mer*-**Alq3-R** complexes (values are in Å)

R	Al-O_1 (d1)	AlO_2 (d2)	Al-O_3 (d3)	Al-N_1 (d4)	Al-N_2 (d5)	Al-N_3 (d6)	$\sum_{i=1}^{6} d_i$
			Excited state geometry				
CN	1.961	1.868	1.869	1.981	2.102	2.088	11.869
CF$_3$	1.963	1.867	1.867	1.979	2.104	2.089	11.869
COMe	1.959	1.868	1.868	1.980	2.104	2.090	11.869
COOMe	1.960	1.868	1.868	1.980	2.104	2.091	11.871
CHO	1.958	1.868	1.868	1.982	2.103	2.088	11.867
OCF$_3$	1.962	1.867	1.867	1.978	2.105	2.092	11.871
Cl	1.960	1.868	1.868	1.979	2.104	2.093	11.872
F	1.959	1.868	1.868	1.978	2.105	2.095	11.873
H	1.961	1.868	1.868	1.978	2.105	2.094	11.874
OCH$_3$	1.948	1.869	1.871	1.977	2.109	2.101	11.875
OH	1.950	1.869	1.871	1.977	2.108	2.100	11.875
NH$_2$	1.933	1.876	1.872	1.976	2.113	2.106	11.876
NMe$_2$	1.928	1.878	1.873	1.976	2.115	2.109	11.879

Table 3.19 Bond distances and their sum of first excited state geometries of *mer*-**Gaq3-R** complexes (values are in Å)

R	Ga-O_1 (d1)	Ga-O_2 (d2)	Ga-O_3 (d3)	Ga-N_1 (d4)	Ga-N_2 (d5)	Ga-N_3 (d6)	$\sum_{i=1}^{6} d_i$
			Excited state geometry				
CN	2.046	1.918	1.922	2.006	2.154	2.151	12.197
CF$_3$	2.044	1.918	1.923	2.006	2.154	2.152	12.197

COMe	2.048	1.917	1.922	2.004	2.154	2.152	12.197
COOMe	2.045	1.917	1.923	2.005	2.153	2.152	12.195
CHO	2.043	1.918	1.923	2.008	2.153	2.151	12.196
OCF_3	2.042	1.918	1.923	2.004	2.156	2.155	12.198
Cl	2.044	1.918	1.922	2.004	2.156	2.155	12.199
F	2.042	1.917	1.922	2.003	2.157	2.158	12.199
H	2.045	1.917	1.922	2.003	2.155	2.157	12.199
OCH_3	2.027	1.919	1.926	2.003	2.160	2.163	12.198
OH	2.030	1.919	1.925	2.003	2.162	2.160	12.199
NH_2	2.005	1.931	1.923	2.002	2.165	2.169	12.195
NMe_2	1.999	1.933	1.924	2.003	2.167	2.171	12.197

Table 3.20 Bond distances and their sum of first excited state geometries of *mer*-**Inq3-R** complexes (values are in Å)

	Excited state geometry						
R	In-O_1 (d1)	In-O_2 (d2)	In-O_3 (d3)	In-N_1 (d4)	In-N_2 (d5)	In-N_3 (d6)	$\sum_{i=1}^{6} d_i$
CN	2.079	2.160	2.081	2.286	2.168	2.281	13.055
CF_3	2.079	2.157	2.081	2.287	2.168	2.282	13.054
COMe	2.078	2.161	2.080	2.287	2.167	2.281	13.054
COOMe	2.078	2.158	2.080	2.287	2.168	2.281	13.052
CHO	2.079	2.157	2.081	2.285	2.169	2.282	13.053
OCF_3	2.078	2.154	2.081	2.289	2.167	2.282	13.051
Cl	2.078	2.157	2.081	2.288	2.166	2.283	13.053
F	2.079	2.155	2.081	2.288	2.166	2.284	13.053
H	2.079	2.157	2.081	2.288	2.166	2.283	13.054

OCH$_3$	2.081	2.142	2.083	2.305	2.165	2.287	13.054
OH	2.082	2.144	2.081	2.287	2.165	2.290	13.049
NH$_2$	2.085	2.123	2.085	2.294	2.167	2.295	13.049
NMe$_2$	2.086	2.117	2.086	2.297	2.166	2.296	13.048
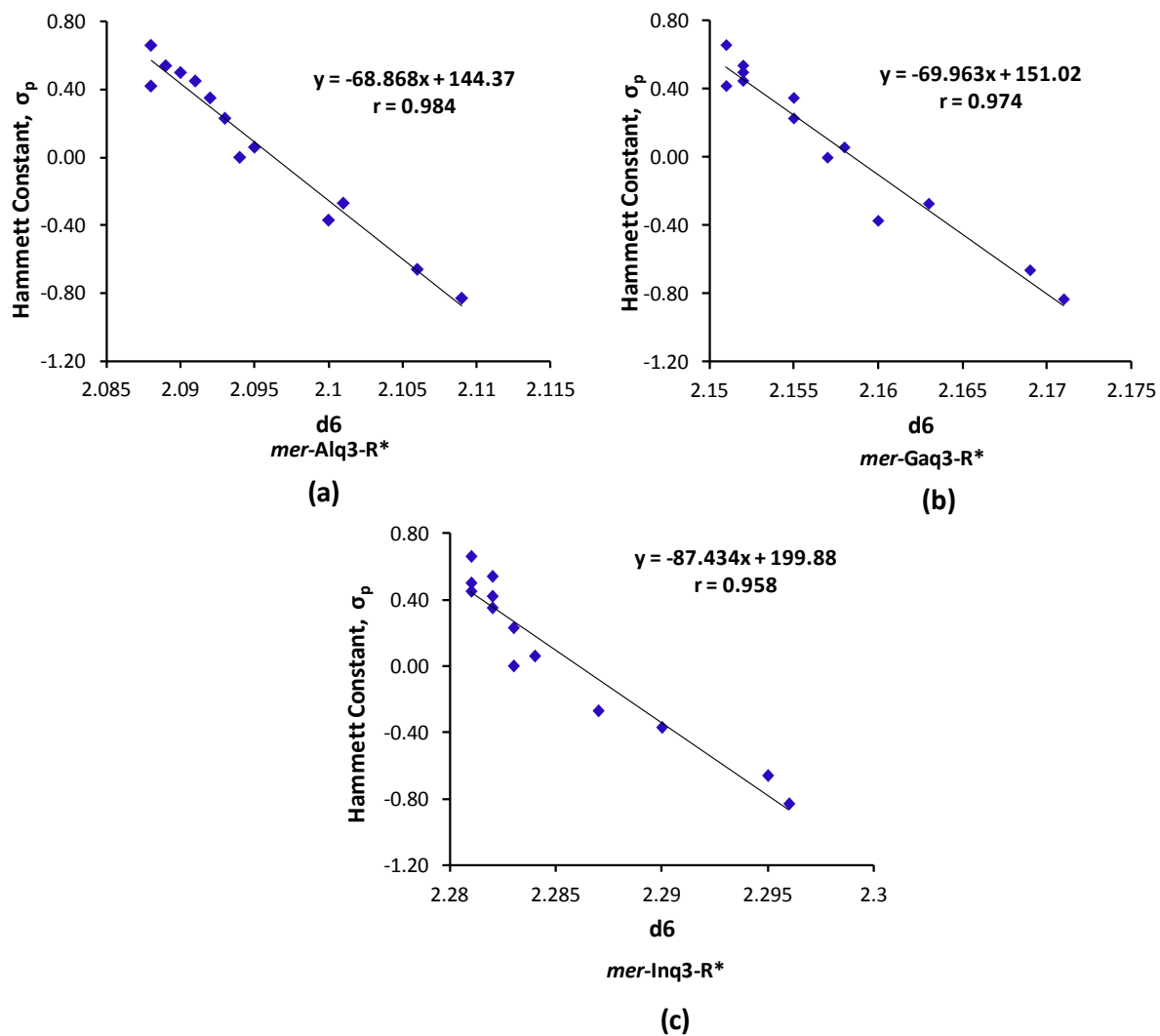
Figure 3.15 Correlation between d6 (longest M-N bond distance) and Hammett constant (σ_p) for (a) *mer*-**Alq3-R***, (b) *mer*-**Gaq3-R***, and (c) *mer*-**Inq3-R***.

3.9.4 MESP Features of *mer*-Mq3-R Complexes

For all the **mer-Mq3-R** complexes, the anionic character of the ligand is centered on oxygen atoms of phenoxide ring which can be revealed with molecular electrostatic potential (MESP) topography. The MESP shows the minimum (V_{min}) at the oxygen centers and among the three oxygen centers, the one *trans* to the nitrogen atom (Figure 3.16) has the most negative value. The V_{min} value for this oxygen center in the ground and excited state geometries of all the **mer-Mq3-R** complexes (substituents are arranged in the order of Hammett constant) are provided in Table 3.21. The most negative V_{min} corresponds to NMe$_2$ group and less negative for CN group. The V_{min} values corresponding to **mer-Alq3-NMe₂**, **mer-Gaq3-NMe₂** and **mer-Inq3-NMe₂** are -82.3, -82.6, and -79.8 respectively whereas for **mer-Alq3-CN**, **mer-Gaq3-CN**, and **mer-Inq3-CN** the values are -65.2, -65.8, and -65.7 kcal/mol respectively.

mer-Alq3-NMe₂*

mer-Gaq3-F*
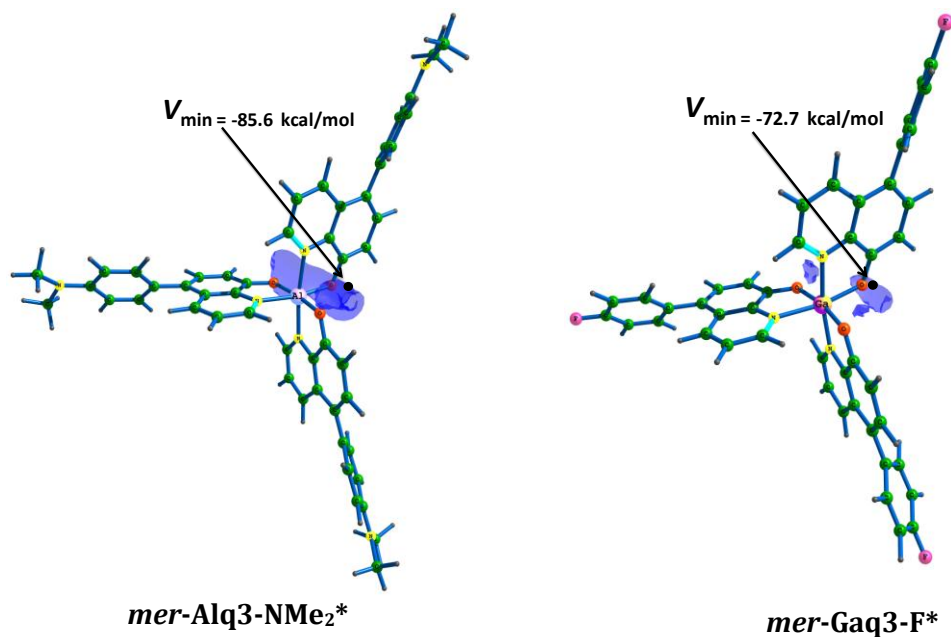
Figure 3.16 MESP features of singlet excited state optimized structures of representative **mer-Mq3-R** complexes.

Table 3.21 The $V_{\min}$ values obtained for ground and singlet excited state geometries of **mer-Mq3-R** complexes in kcal/mol

	Ground state geometry			Excited state geometry		
R	*mer-* Alq3-R	*mer-* Gaq3-R	*mer-* Inq3-R	*mer-* Alq3-R*	*mer-* Gaq3-R*	*mer-* Inq3-R*
CN	-65.2	-65.8	-65.7	-67.3	-67.8	-67.3
CF$_3$	-65.0	-65.0	-64.1	-66.5	-67.0	-66.5
COMe	-66.5	-66.2	-63.9	-68.1	-67.0	-67.7
COOMe	-67.2	-67.4	-65.6	-68.8	-68.4	-69.2
CHO	-63.7	-64.2	-61.7	-64.2	-65.5	-65.1
OCF$_3$	-67.4	-69.0	-66.3	-68.3	-70.1	-70.7
Cl	-66.9	-67.6	-65.5	-68.8	-68.9	-70.2
F	-70.7	-71.2	-68.6	-72.8	-72.7	-72.8
H	-74.5	-74.5	-72.2	-76.7	-76.2	-77.0
OCH$_3$	-77.2	-76.7	-74.6	-78.9	-79.5	-77.1
OH	-76.4	-76.6	-75.1	-78.5	-78.4	-79.4
NH$_2$	-80.6	-80.9	-78.4	-84.1	-84.3	-85.2
NMe$_2$	-82.3	-82.6	-79.8	-85.6	-85.6	-85.4

The change in $V_{\min}$ due to substitution ($\Delta V_{\min}$) - the difference between the $V_{\min}$ of a substituted complex and unsubstituted reference complex (**mer-Mq3-H**) - is depicted in Table 3.22 for ground and excited state geometries of the complexes. $\Delta V_{\min}$ provides a quantification of the substituent effect as it correlates strongly with the Hammett σ_p constant (Figure 3.17).

Table 3.22 The $\Delta V_{\min}$ values for the ground and first excited state geometries of **mer-Mq3-R** complexes in kcal/mol

	Ground state geometry			Excited state geometry		
R	Alq3-R	Gaq3-R	Inq3-R	Alq3-R*	Gaq3-R*	Inq3-R*
CN	9.3	8.8	6.5	9.5	8.3	9.7
CF$_3$	9.5	9.5	8.1	10.2	9.2	10.5
COMe	8.0	8.4	8.2	8.7	9.1	9.2

COOMe	7.3	7.1	6.5	8.0	7.7	7.8
CHO	10.8	10.4	10.4	12.6	11.8	11.9
OCF$_3$	7.1	5.6	5.8	8.4	6.1	6.3
Cl	7.7	7.0	6.7	8.0	7.3	6.8
F	3.8	3.3	3.5	3.9	3.5	4.2
H	0.0	0.0	0.0	0.0	0.0	0.0
OCH$_3$	-2.6	-2.1	-2.4	-2.2	-3.4	-2.1
OH	-1.9	-2.0	-3.0	-1.7	-2.3	-2.4
NH$_2$	-6.1	-6.4	-6.2	-7.4	-8.1	-8.2
NMe$_2$	-7.8	-8.0	-7.6	-8.8	-9.5	-8.4
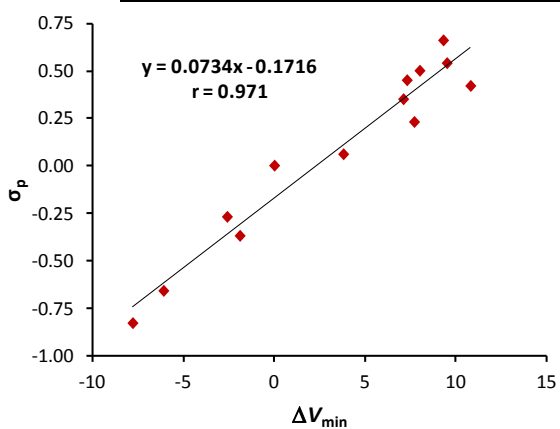
Ground state geometry

$y = 0.0734x - 0.1716$
$r = 0.971$

Excited state geometry

$y = 0.066x - 0.1667$
$r = 0.967$

(a)

Ground state geometry

$y = 0.0751x - 0.1573$
$r = 0.975$

Excited state geometry

$y = 0.0665x - 0.1209$
$r = 0.967$
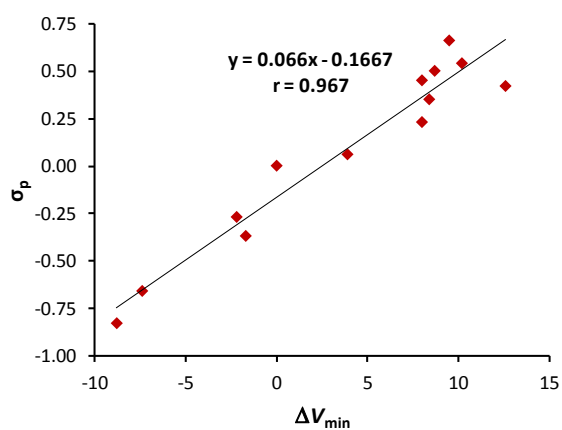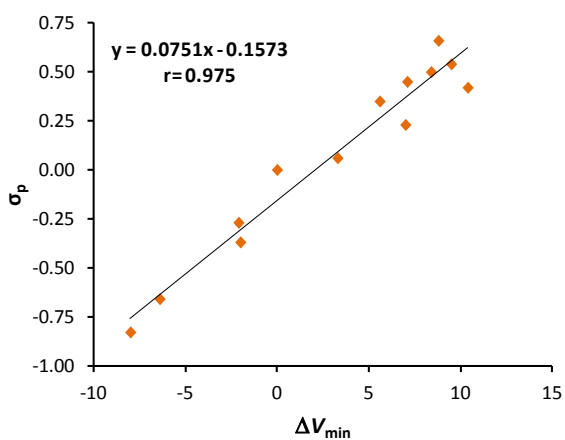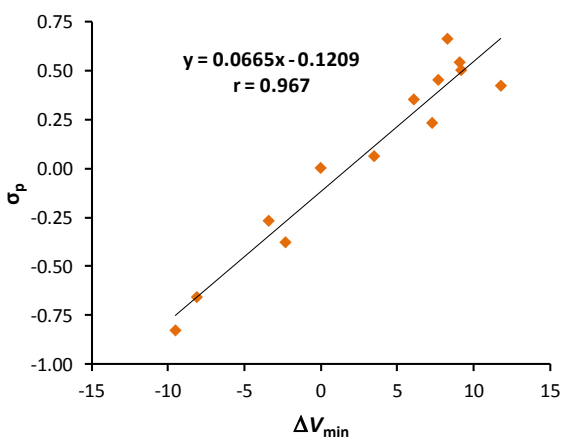
(b)
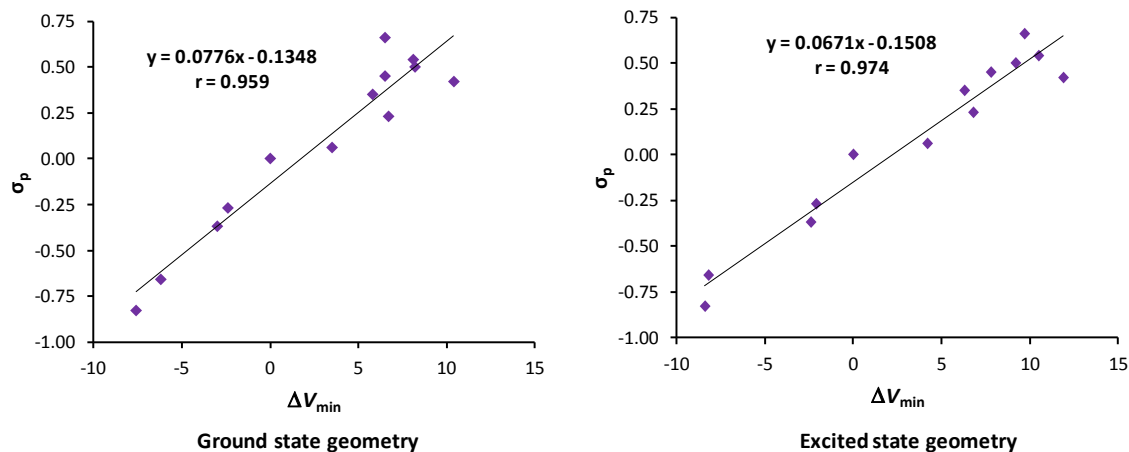
(c)

Figure 3.17 Correlation between ΔV_{min} (in kcal/mol) measured for the ground and first excited state geometries of (a) ***mer*-Alq3-R** (b) ***mer*-Gaq3-R and** (c) ***mer*-Inq3-R** complexes with Hammett constant, σ_p.

Table 3.23 The ΔV_M values for the ground and first excited state geometries of ***mer*-Mq3-R** complexes in kcal/mol

R	Ground state geometry			Excited state geometry		
	ΔV_{Al}	ΔV_{Ga}	ΔV_{In}	ΔV_{Al}	ΔV_{Ga}	ΔV_{In}
CN	16.9	16.8	16.6	17.6	17.7	20.0
CF$_3$	9.8	9.8	9.7	10.4	10.4	11.7
COMe	9.0	8.7	8.6	9.6	9.3	11.7
COOMe	7.8	7.7	7.6	8.2	8.2	10.7
CHO	11.9	12.0	11.9	12.9	12.9	15.4
OCF$_3$	7.3	6.2	6.0	8.1	6.4	8.6
Cl	7.1	7.0	6.9	7.3	7.3	9.6
F	3.7	3.6	3.6	3.6	3.6	5.9
H	0.0	0.0	0.0	0.0	0.0	0.0
OCH$_3$	-3.3	-3.3	-3.3	-4.2	-4.3	-1.9
OH	-2.6	-2.5	-2.5	-3.4	-3.4	-0.9
NH$_2$	-7.4	-7.5	-7.3	-10.2	-10.5	-8.0
NMe$_2$	-9.3	-9.3	-9.1	-11.7	-11.9	-9.5

159

The MESP at the metal centre, V_M is also analyzed as a sensitive measure of electron rich/deficient character of the metal center due to changes in the ligand environment. The change V_M with respect to the unsubstituted system (ΔV_M) is provided in Table 3.23 for ground and excited state geometries. This change in MESP values is considered as the contribution of the substituent. Like ΔV_{min}, strong linear correlations are observed between σ_p and ΔV_M values of all the ***mer*-Mq3-R** complexes (Figures 3.18).
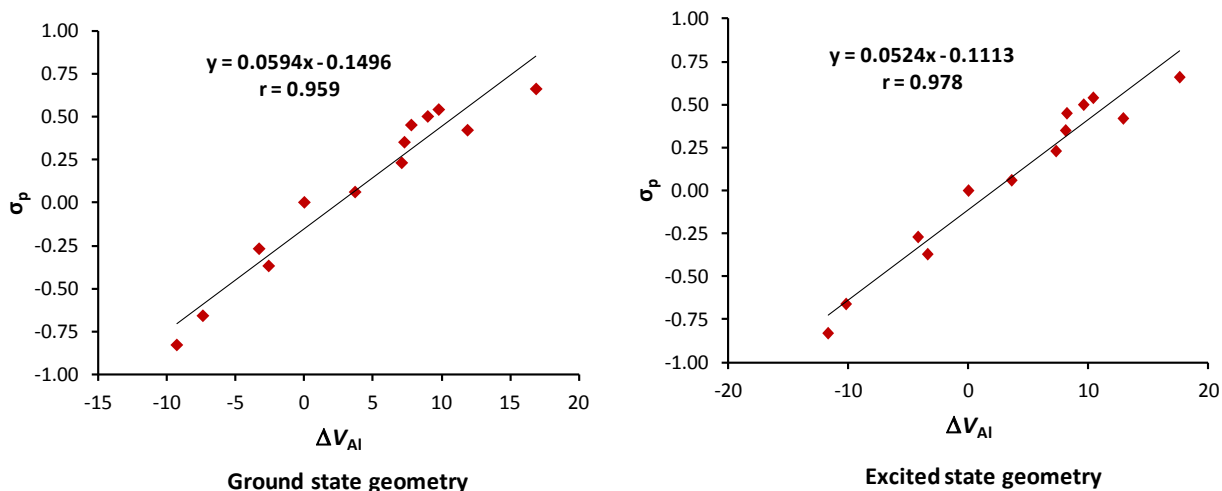
(a)
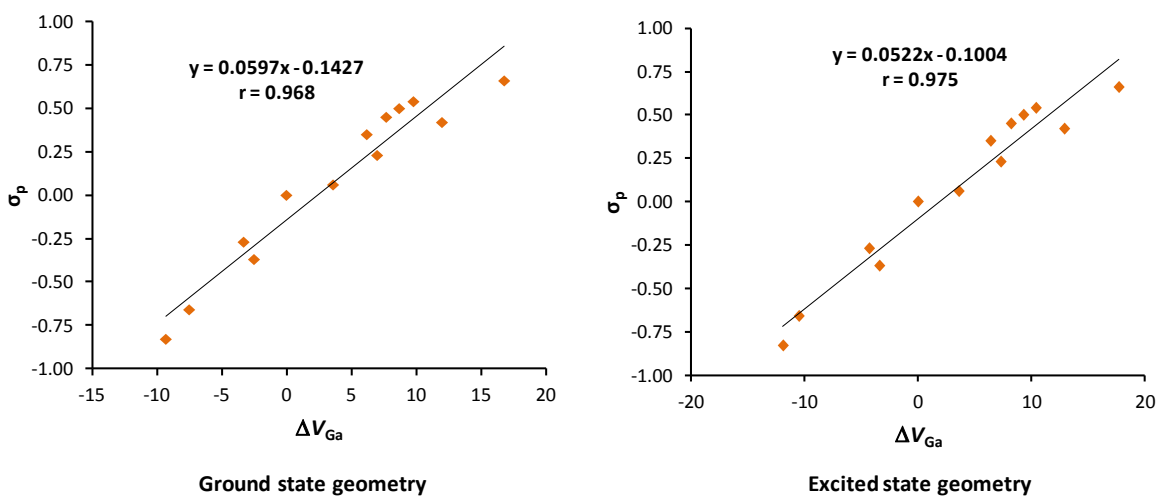
(b)
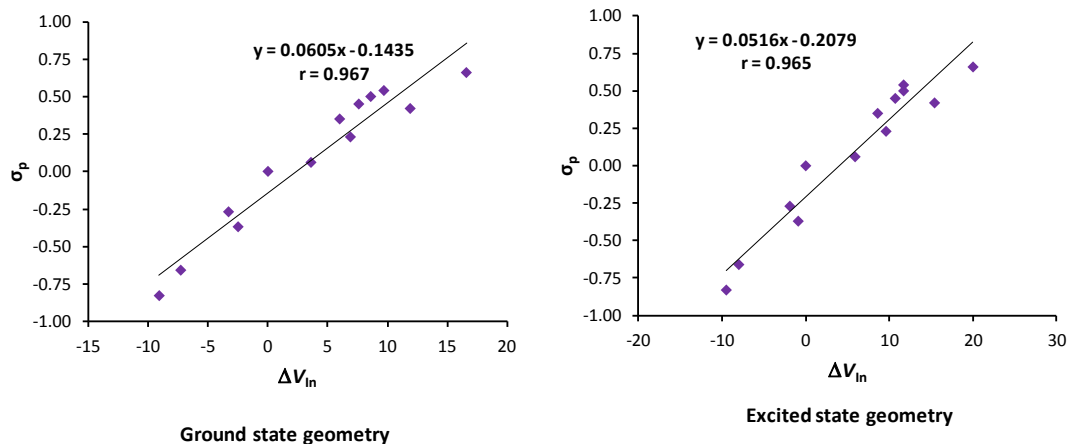
(c)

Figure 3.18 Correlation between ΔV_{In} (in kcal/mol) measured for the ground and first excited state geometries of (a) **_mer_-Alq3-R** (b) **_mer_-Gaq3-R and** (c) **_mer_-Inq3-R** complexes with Hammett constant, σ_p.

3.9.5 Absorption Maximum (λ_{abs}) of _mer_-Mq3-R Complexes

The absorption maximum (λ_{abs}) values of all the **_mer_-Mq3-R** complexes are provided in Table 3.24 along with the oscillator strength (f) values.

Table 3.24 The absorption maximum (λ_{abs}) values (in nm) and corresponding oscillator (f) strength of **_mer_-Mq3-R** complexes

	mer-Alq3-R		_mer_-Gaq3-R		_mer_-Inq3-R	
R	λ_{abs}	f	λ_{abs}	f	λ_{abs}	f
CN	417	0.252	418	0.316	416	0.363
CF$_3$	421	0.167	417	0.211	415	0.244
COMe	421	0.262	422	0.341	420	0.391
COOMe	416	0.233	420	0.300	418	0.340
CHO	422	0.318	422	0.440	421	0.490
OCF$_3$	420	0.144	421	0.196	419	0.222
Cl	420	0.156	420	0.204	418	0.233
F	422	0.135	422	0.181	420	0.206

H	422	0.138	422	0.183	420	0.208
OCH$_3$	433	0.140	434	0.193	432	0.218
OH	433	0.132	433	0.190	431	0.210
NH$_2$	452	0.148	449	0.197	447	0.218
NMe$_2$	470	0.151	467	0.201	465	0.225

The λ_{abs} shows a clear red shift in all the cases where the substituent is of electron donating character while it is largely unaffected by nature of the electron withdrawing substituents (Figures 3.19). From CN to H substitution, the shift in absorption value is only 5 nm in the case of **mer-Alq3-R** (Figure 3.20) and merely 4 nm each for **mer-Gaq3-R** and **mer-Inq3-R**. (Figures 3.21 and 3.22).
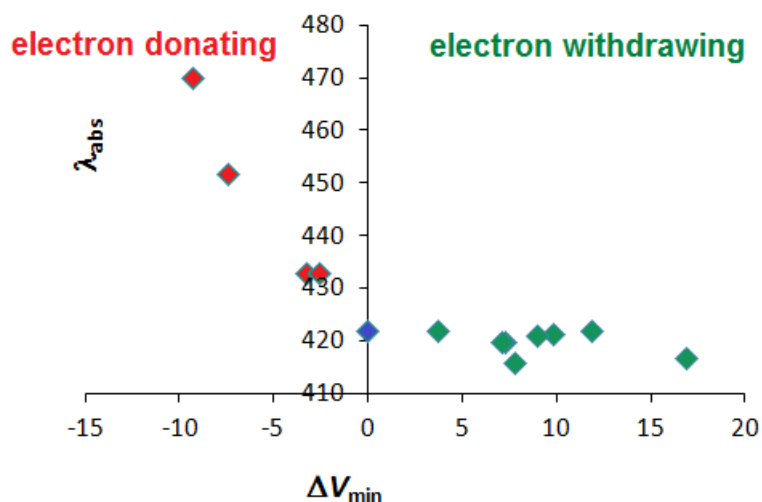
Figure 3.19 Graph between ΔV_{min} of ground state geometries and λ_{abs} of **mer-Alq3-R** complexes.

The CHO substituent gives the most intense band having oscillator strength (f) values of 0.318, 0.440, and 0.490 respectively for **mer-Alq3-R**, **mer-Gaq3-R**, and **mer-Inq3-R**. Among all the substituents, the F and H substitution provide less intense bands, this trend is equivalent in all the **mer-Mq3-R** complexes.
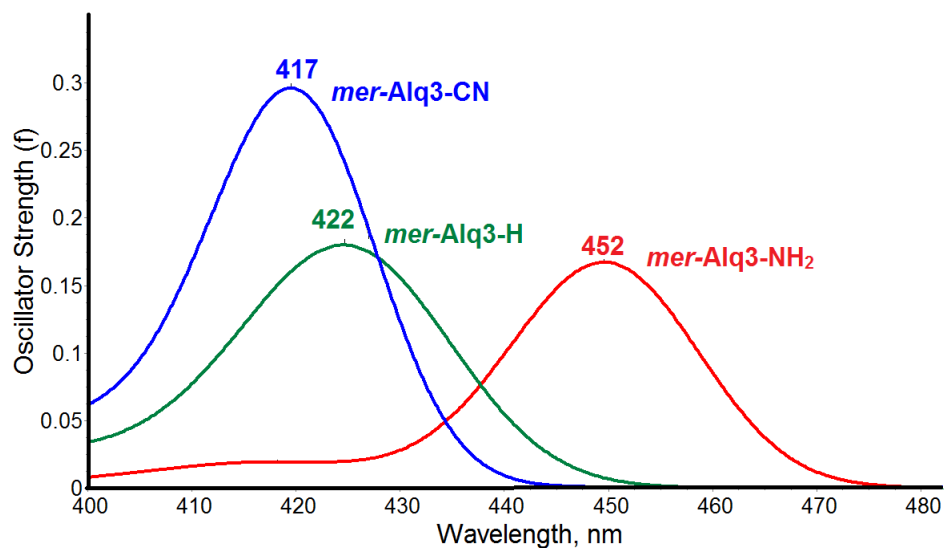
Figure 3.20 The TD absorption spectra of ***mer*-Alq3-R**.
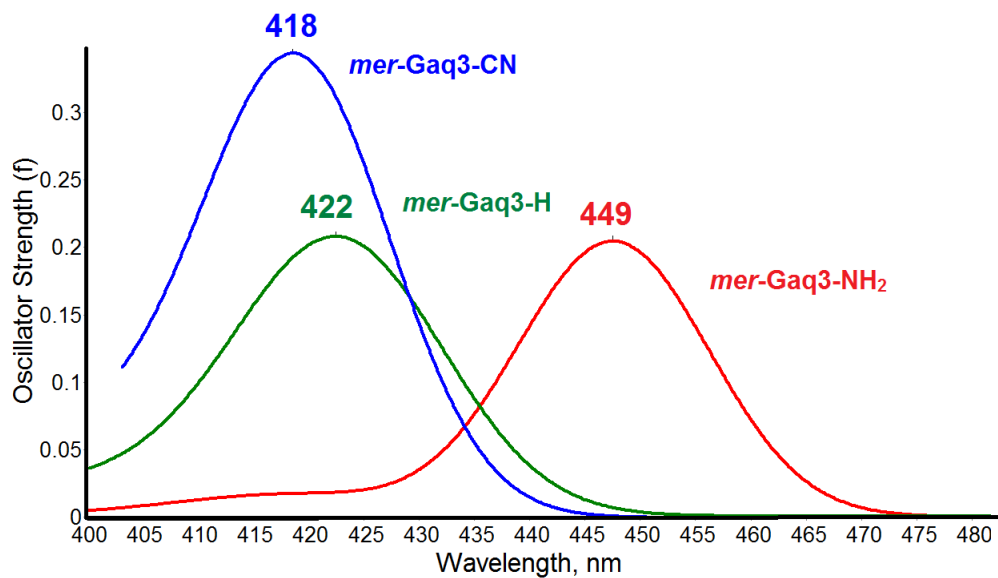
Figure 3.21 The TD absorption spectra of ***mer*-Gaq3-R**.
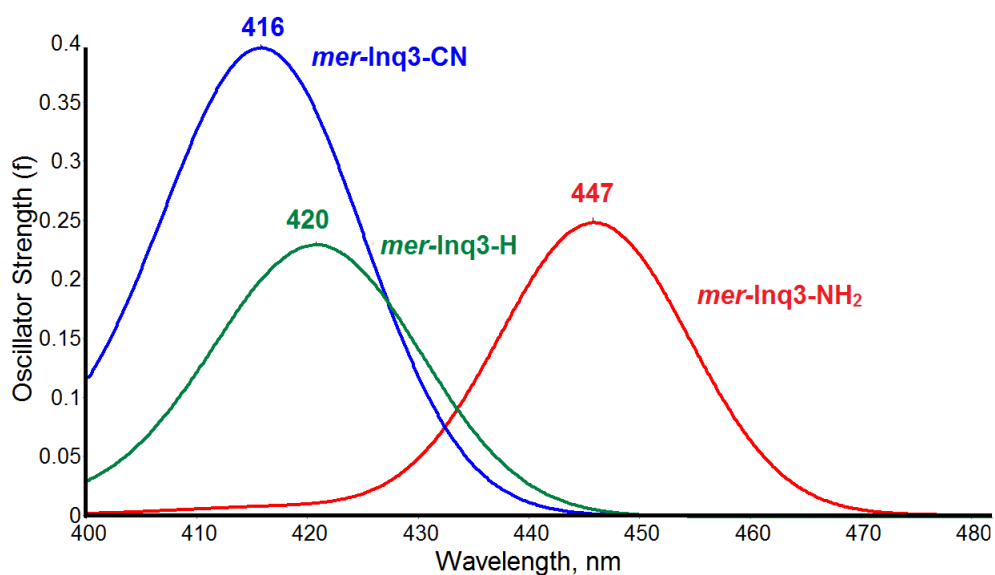
Figure 3.22 The TD absorption spectra of ***mer*-Inq3-R**.

The longest wavelength absorption is due to HOMO to LUMO π-π* transition of the electrons. The HOMO is mainly centered on one of the 8-hydroxyquinolinato moieties which is characterized by the presence of the shortest M-O bond (this bond is *trans* to the longest M-N bond). Similarly the LUMO is mainly centered on one of the 8-hydroxyquinolinato moieties which is characterized by the presence of the longest M-N bond (Figure 3.23)
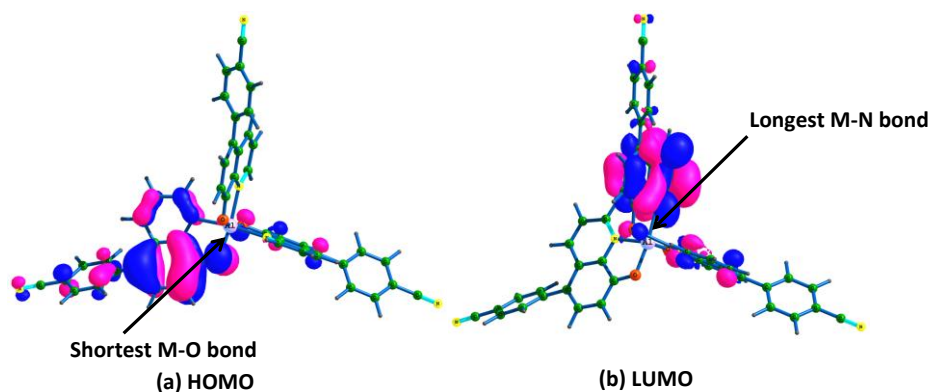
Figure 3.23 (a) HOMO and (b) LUMO of the ***mer*-Alq3-CN** complex.

3.9.6 Fluorescence Maximum (λ_F) of Experimentally Known Systems

Anzenbacher *et al.*[79] reported fluorescence properties of a large variety of C5-substituted tris(8-hydroxyquinolinato) aluminium(III) complexes. These systems (**1a** – **1n**) are depicted in Table 3.25. In order to check the reliability of the TDDFT method to reproduce the fluorescence maximum (λ_F) values reported by Anzenbacher *et al.*, these ***mer*-Alq3-R** systems are studied.

Table 3.25 *mer*-Alq3-R complexes with corresponding experimental and TDDFT calculated fluorescence values (λ_F) in nm (solvent = dichloromethane)
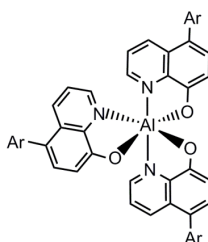
Name	Ar	$\lambda_{F(Exp)}$	$\lambda_{F(TDDFT)}$	Name	Ar	$\lambda_{F(Exp)}$	$\lambda_{F(TDDFT)}$
1a		490	485	1h		541	555
1b		501	504	1i		545	561
1c		513	463	1j		538	585
1d		516	516	1k		551	588
1e		530	529	1l		564	603
1f		534	536	1m		564	612
1g		537	545	1n		612	671

For Alq3 complex without the C5 substitution, the calculated λ_F value is 531 nm which agrees very well with the λ_F 526 nm reported by Anzenbacher *et al*. For all the substituted systems, the experimental λ_F ($\lambda_{F(Exp)}$) values range from 490 to 612 nm and the corresponding TDDFT values ($\lambda_{F(TDDFT)}$) range from 485 to 671 nm (Table 3.25). The mean absolute deviation (MAD) is 26 nm and the linear correlation (correlation coefficient = 0.943) observed between these quantities (Figure 3.24) indicates that the method used to compute fluorescence is reliable.

In general, aryl substituents with electron donating groups show higher values for λ_F than those containing electron withdrawing groups which indicates that the methodical colour tuning can be achieved by systematically changing electron withdrawing aryl moieties to aryl moieties substituted with electron donating groups.[ref]
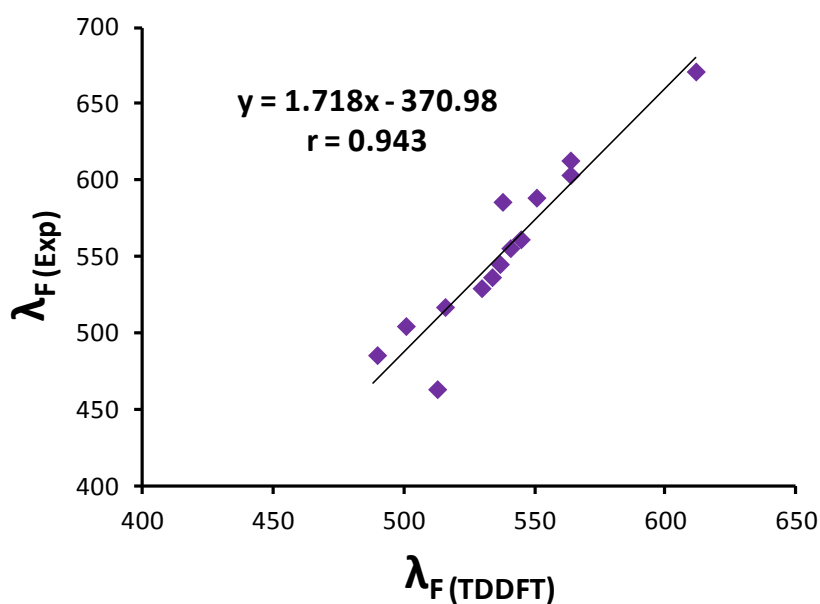
Figure 3.24 Correlation between TDDFT calculated fluorescence and experimental fluorescence values. Values are in nm.

3.9.7 Fluorescence Maximum (λ_F) of *mer*-Mq3-R complexes

The fluorescence maximum (λ_F) values of all the **mer-Mq3-R** complexes are provided in Table 3.26 along with the corresponding oscillator strength (*f*) values. The λ_F values steadily increase from electron withdrawing to electron donating group (CN

to NMe$_2$) and the substituent effect is noticeably larger compared to λ_{abs} values. From CN to H a shift in λ_F value of 25 nm is observed whereas as previously explained the change in λ_{abs} value is $\sim$ 5 nm.

All the metals; Al, Ga and In behave in a similar way with the change in substituent. For **mer-Alq3-R**, **mer-Gaq3-R** and **mer-Inq3-R** the λ_F values are in the ranges 536 – 671, 547 – 680, and 554 – 684, respectively.

Table 3.26 The fluorescence maximum (λ_F) values (in nm) and corresponding oscillator (*f*) strength of **mer-Mq3-R** complexes

	mer-Alq3-R		mer-Gaq3-R		mer-Inq3-R	
R	λ_F	*f*	λ_F	*f*	λ_F	*f*
CN	536	0.168	547	0.159	554	0.150
CF$_3$	543	0.123	554	0.117	561	0.110
COMe	545	0.173	555	0.162	561	0.152
COOMe	545	0.157	555	0.147	562	0.139
CHO	540	0.202	550	0.189	557	0.177
OCF$_3$	552	0.114	575	0.110	581	0.104
Cl	555	0.120	567	0.115	573	0.108
F	566	0.108	577	0.103	584	0.098
H	561	0.109	571	0.104	578	0.099
OCH$_3$	603	0.119	613	0.114	618	0.108
OH	599	0.113	609	0.109	616	0.103
NH$_2$	664	0.125	674	0.121	677	0.117
NMe$_2$	671	0.140	680	0.137	684	0.132

For the **mer-Alq3-NMe$_2$** complex, λ_F is 671 nm, when the metal changes to Ga, λ_F value is red shifted to 680 nm. In the case of **mer-In-NMe$_2$**, λ_F value further red-shifted to 684 nm. In organic-metallic chelates, the increase in emission wavelength can be due

to heavy atom effect *i.e.*, as the metal size increases the covalent nature of metal ligand bonding increases.[91,63,92]

       As observed in the case of λ_{abs} values, the CHO substituent gives the most intense band having *f* values of 0.202, 0.189, and 0.177 respectively for **mer-Alq3-CHO**, **mer-Gaq3-CHO**, and **mer-Inq3-CHO**. Similarly, the F and H substitution results in less intense bands.
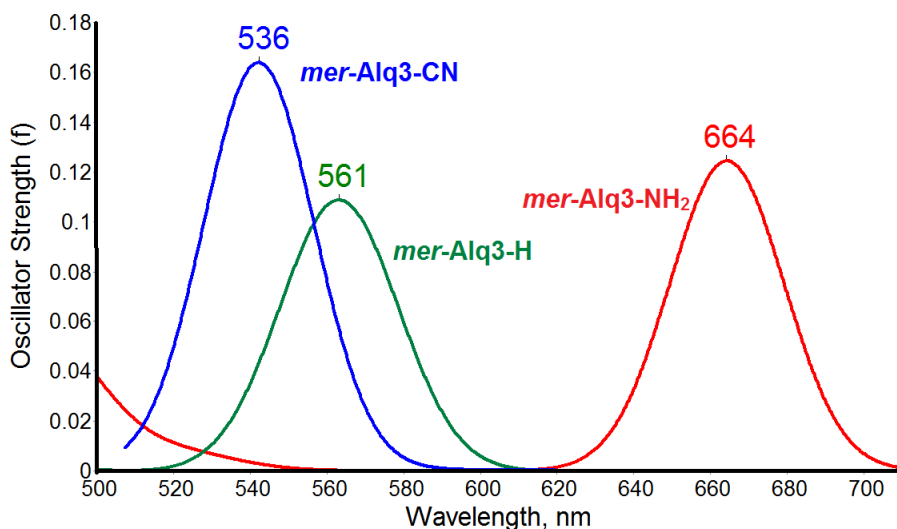
Figure 3.25 The TD emission spectra of **mer-Alq3-R**.
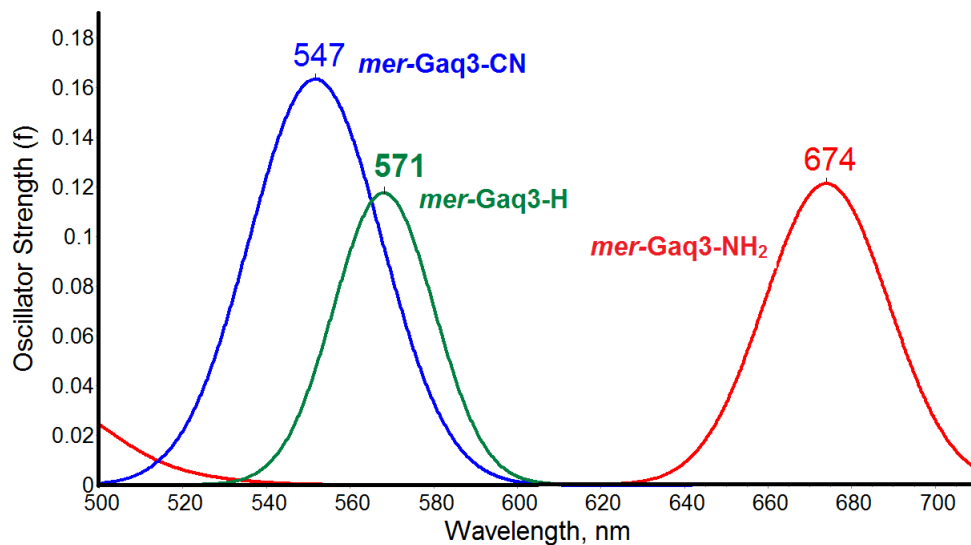
Figure 3.26 The TD emission spectra of **mer-Gaq3-R**.

Figure 3.25 consists of the TD emission spectra of some representative systems. *viz.* **mer-Alq3-CN**, **mer-Alq3-H**, and **mer-Al-NH₂**. Similarly, the Figures 3.26 and 3.27 provide the TD emission spectra of **mer-Gaq3-R**, **mer-Inq3-R**.
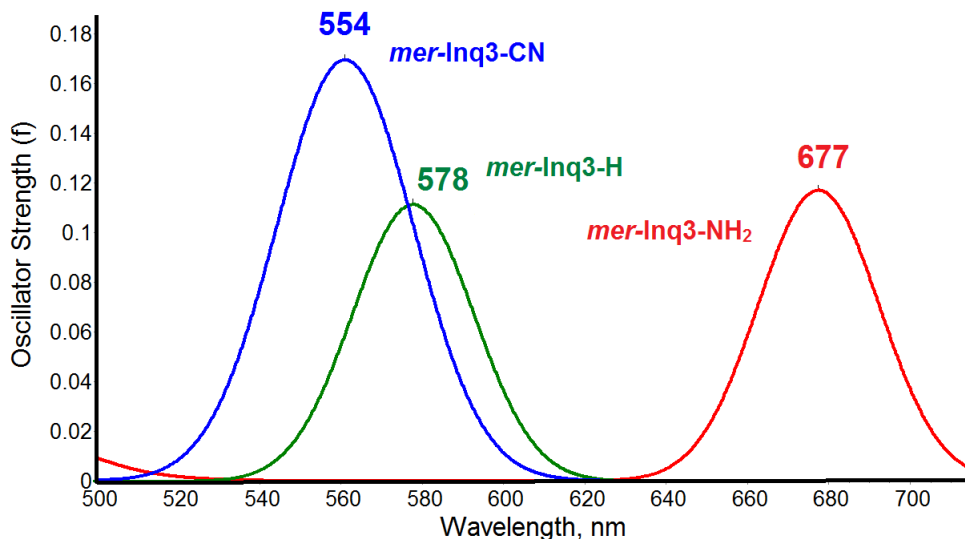
Figure 3.27 The TD emission spectra of **mer-Inq3-R**.

Table 3.27 provides the difference in λ_F with respect to the unsubstituted system (R = H), $\Delta\lambda_F$ for all the **mer-Mq3-R** complexes. The correlation between ΔV_{Al} (kcal/mol) of ground state and excited state geometries with the $\Delta\lambda_F$ (nm) of **mer-Mq3-R** complexes is provided in Figure 3.28.

The MESP values measured for the excited state geometries provide better correlations compared to that measured for the ground state geometries (r values 0.915 and 0.934 respectively). In all the cases, the unsubstituted or the H substituted system is the highest deviated system in the correlation line.

Table 3.27 The difference in λ_F with respect to the unsubstituted system (R = H), $\Delta\lambda_F$ for the *mer*-**Mq3-R** complexes (values are in nm)

R	*mer*-**Alq3-R** $\Delta\lambda_F$	*mer*-**Gaq3-R** $\Delta\lambda_F$	*mer*-**Inq3-R** $\Delta\lambda_F$
CN	-25	-25	-24
CF3	-18	-17	-17
COMe	-16	-16	-17
COOMe	-16	-16	-16
CHO	-21	-21	-22
OCF3	-9	3	3
Cl	-6	-5	-5
F	6	6	5
H	0	0	0
OCH3	42	41	39
OH	38	38	38
NH2	103	103	99
NMe2	110	108	105

Ground state geometry: $y = -5.3412x + 35.396$ $r = 0.915$

Excited state geometry: $y = -4.7809x + 32.204$ $r = 0.934$
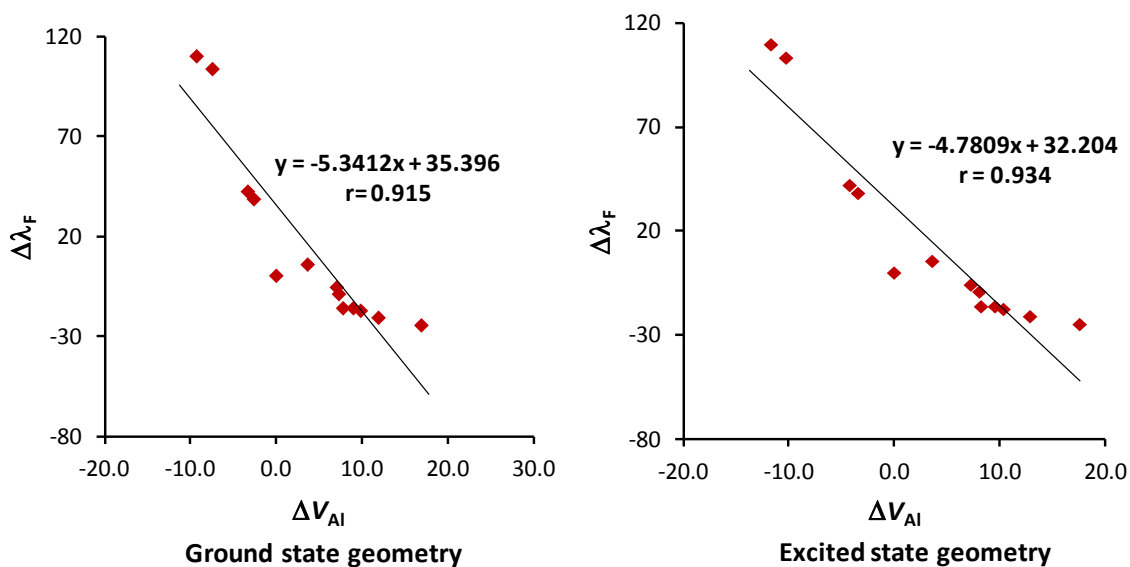
(a)
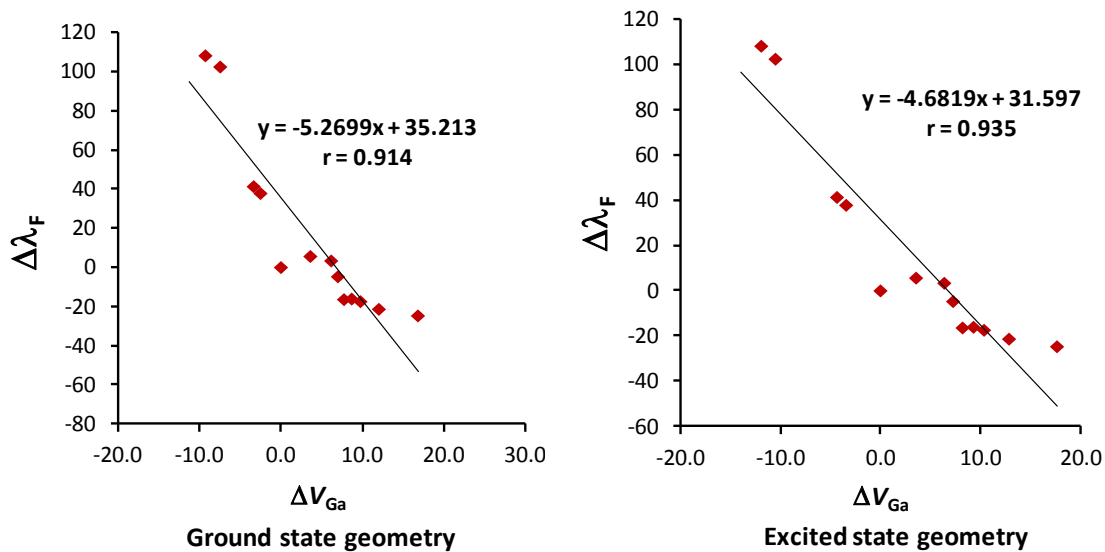
(b)
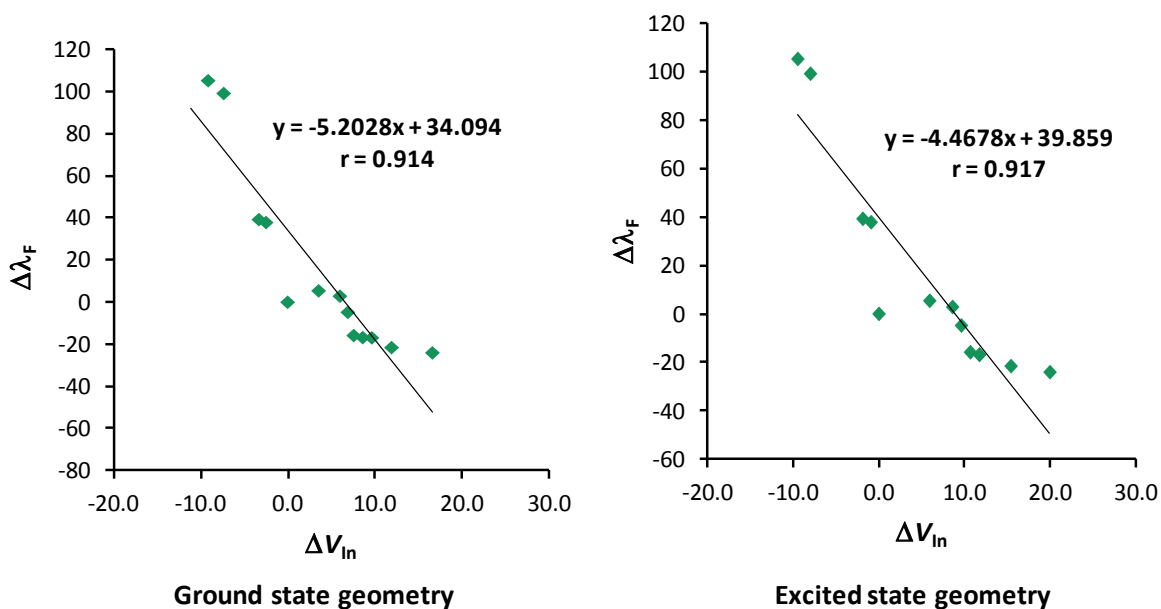
(c)

Figure 3.28 The correlation between ΔV_M (kcal/mol) measured for the ground and excited state geometries with the $\Delta\lambda_F$ (nm) of (a) *mer*-**Alq3-R** (b) *mer*-**Gaq3-R and** (c) *mer*-**Inq3-R**.

(a) *mer*-Alq3-R

(b) *mer*-Gaq3-R

(c)
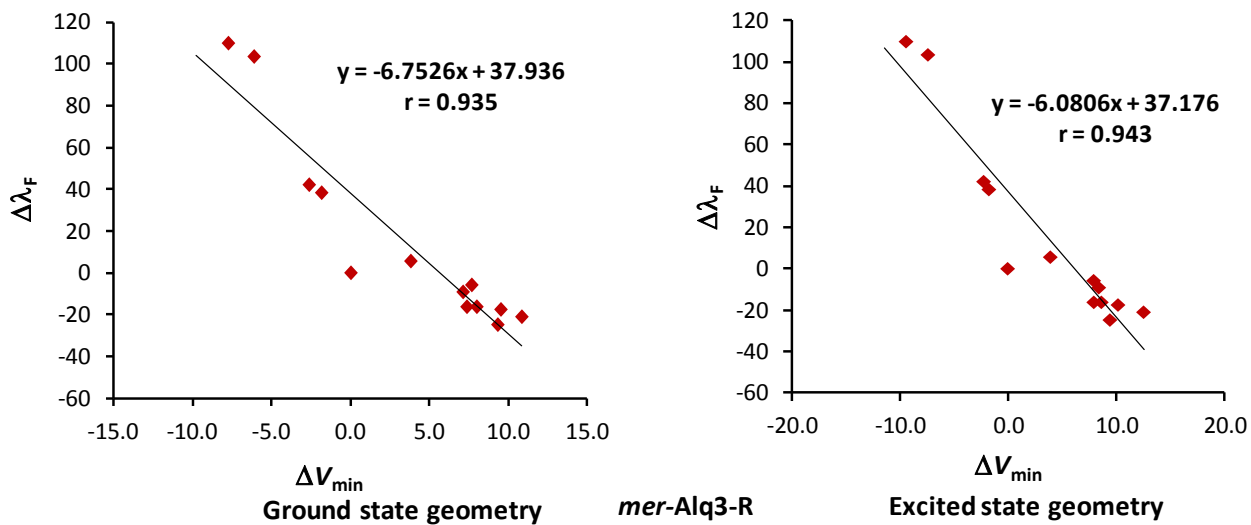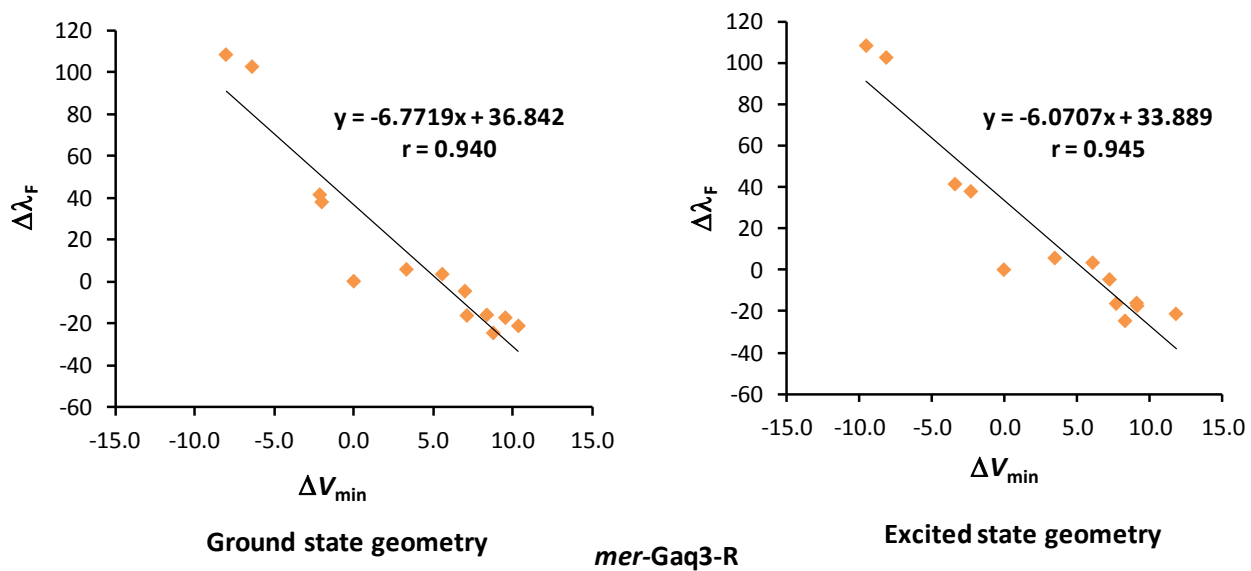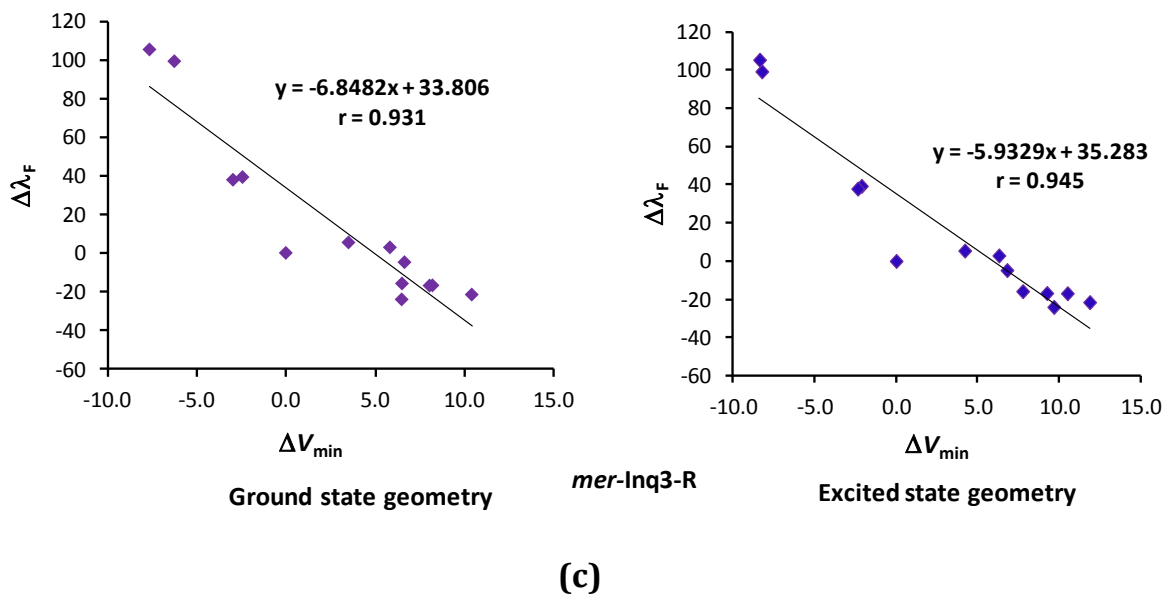
Figure 3.29 The correlation between ΔV_{min} (kcal/mol) measured for the ground state and excited state geometries with the $\Delta \lambda_F$ (nm) of (a) **mer-Alq3-R** (b) **mer-Gaq3-R and** (c) **mer-Inq3-R**.

The correlation plots between ΔV_{min} values measured for the ground and excited state geometries of the **mer-Mq3-R** complexes with the corresponding $\Delta \lambda_F$ values are provided in Figure 3.29.

3.9.8 Stokes Shift of *mer*-Mq3-R Complexes

Table 3.28 provides the difference between the maximum values of absorption and emission (Stokes shift, $(\lambda_F - \lambda_{abs})$) for all the **mer-Mq3-R** complexes. The $(\lambda_F - \lambda_{abs})$ values are in the ranges 119 – 212, 129 – 225, and 139 – 231 nm respectively for **mer-Alq3-R**, **mer-Gaq3-R** and **mer-Inq3-R**. For all the **mer-Mq3-R** complexes, the Stokes shift is found to be maximum when R = NH2.

The Stokes shift values are found to be in good correlation with the ΔV_M and the ΔV_{min} values. In fact better correlations compared to that of $\Delta \lambda_F$ values are observed. The correlation between ΔV_M (kcal/mol) measured for the ground state and excited state geometries of all the **mer-Mq3-R** complexes with the corresponding $(\lambda_F - \lambda_{abs})$ values are illustrated in Figure 3.30.

173

Table 3.28 The difference between absorption maximum and emission maximum (Stokes shift) for the ***mer*-Mq3-R** complexes (values are in nm)

R	*mer*-Alq3-R $(\lambda_F - \lambda_{abs})$	*mer*-Gaq3-R $(\lambda_F - \lambda_{abs})$	*mer*-Inq3-R $(\lambda_F - \lambda_{abs})$
CN	119	129	139
CF$_3$	122	137	146
COMe	124	134	142
COOMe	129	135	144
CHO	118	128	136
OCF$_3$	132	154	162
Cl	135	146	155
F	144	155	163
H	139	149	158
OCH$_3$	170	179	186
OH	166	176	185
NH$_2$	212	225	231
NMe$_2$	201	213	219

(a)

(b)

(c)
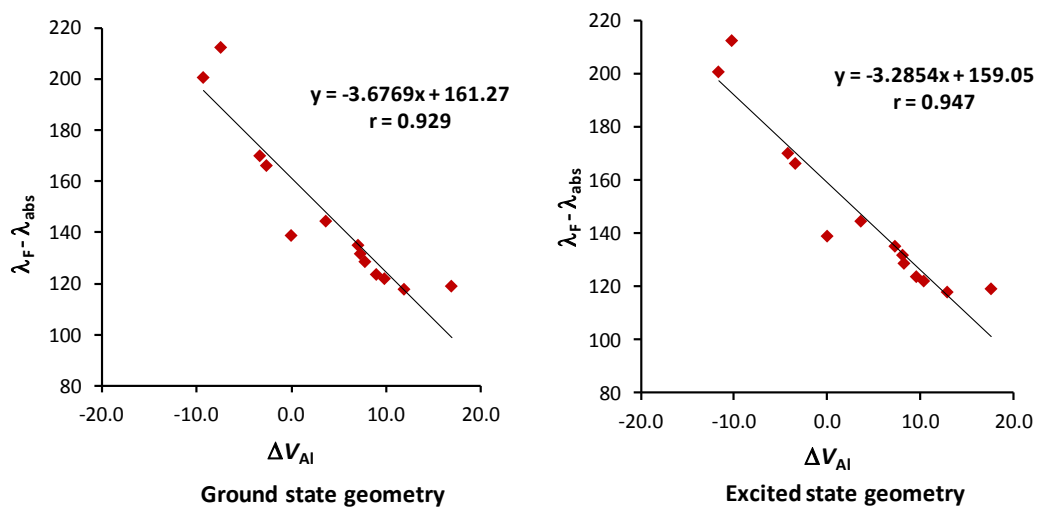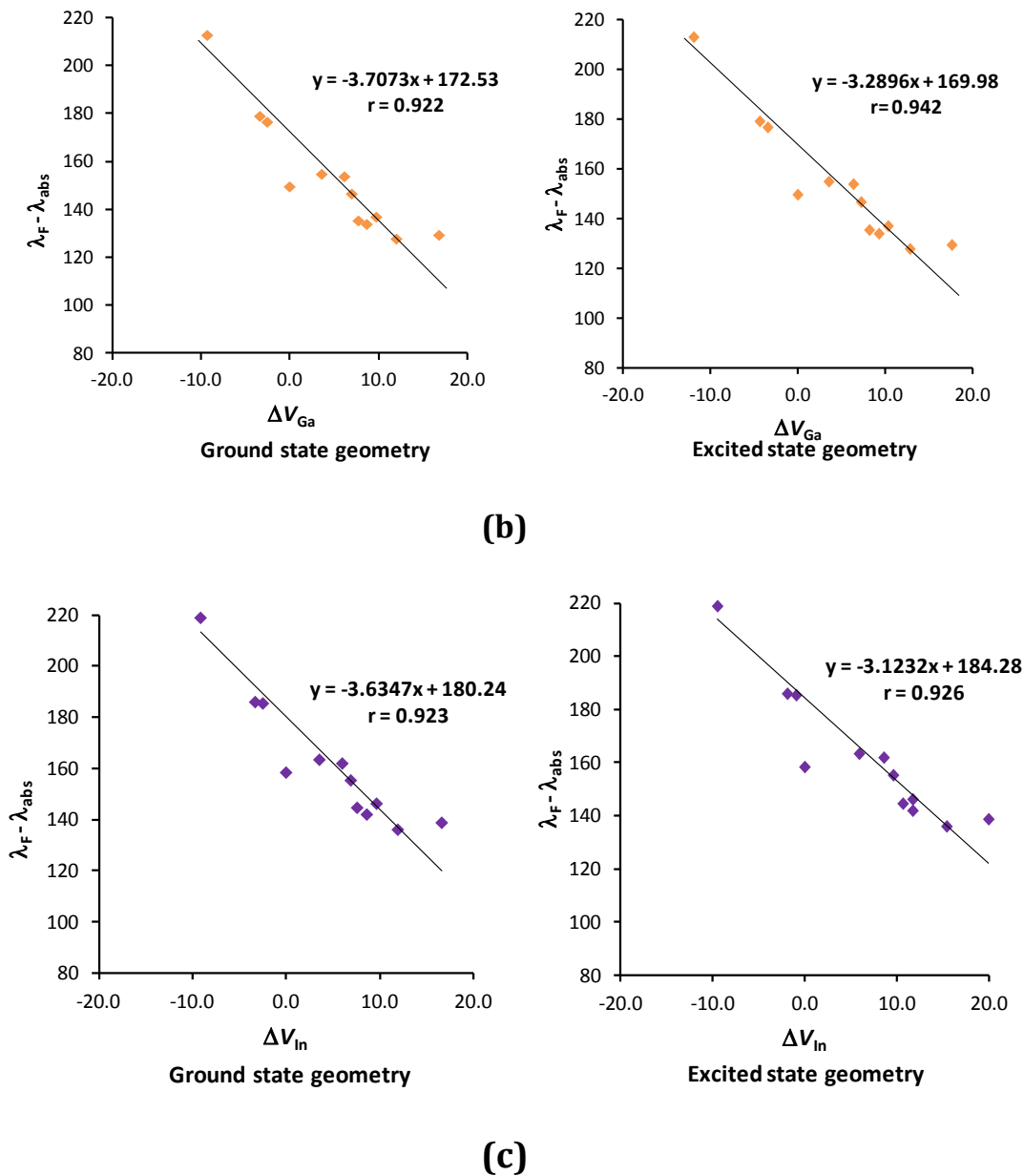
Figure 3.30 The correlation between ΔV_M (kcal/mol) of ground state and excited state geometries with the λ_F -λ_{abs} (nm) of (a) *mer*-**Alq3-R** (b) *mer*-**Gaq3-R and** (c) *mer*-**Inq3-R**.

As observed previously, the MESP values measured at the excited state geometries provide better correlation compared to that measured at the ground state geometries. The ΔV_{Al} for ground state geometry vs. (λ_F - λ_{abs}) plot gives correlation coefficient of 0.929 whereas the corresponding plot for excited state geometry provide

an r value of 0.947. Similarly, for **mer-Gaq3-R** complexes the r values obtained with ΔV_{Ga} of ground and excited state geometries are 0.922 and 0.942 respectively. The slope of all the **mer-Mq3-R** complexes are nearly same which suggests that the substituent effect is similar in all the three metals *i.e.*, Al, Ga, and In.

Figure 3.31 provides the correlation plots of ΔV_{min} (kcal/mol) of ground and excited state geometries of all the **mer-Mq3-R** complexes with the corresponding λ_F - λ_{abs} values. Compared to the ΔV_M vs. (λ_F -λ_{abs}) plots, the ΔV_{min} vs. (λ_F -λ_{abs}) plots give better correlations. For **mer-Alq3-R**, the r values are 0.948 and 0.952 respectively for the ground and excited state geometries. The r values are 0.943, 0.950 and 0.937, 0.954 respectively for ground and excited state geometries of **mer-Gaq3-R** and **mer-Inq3-R**.

(a)

176
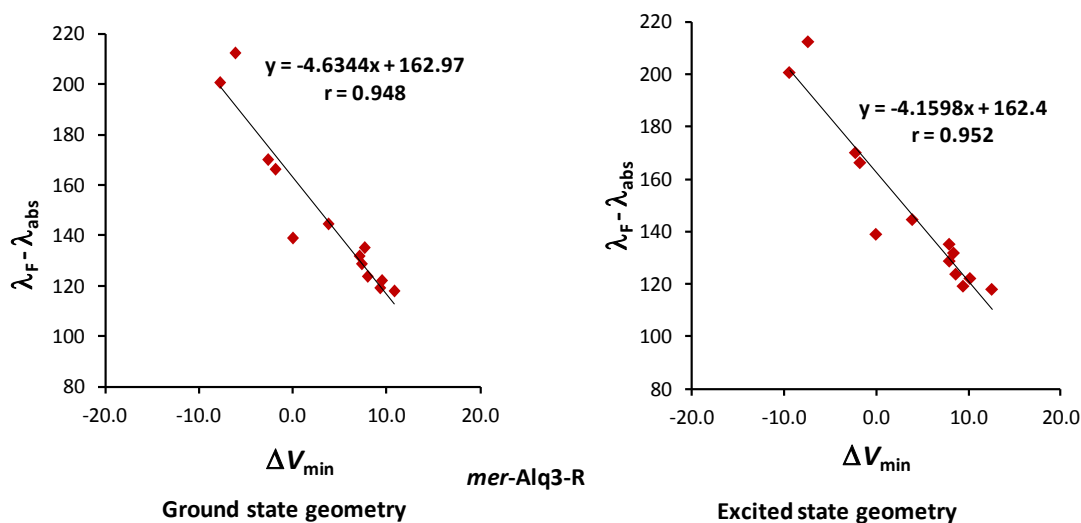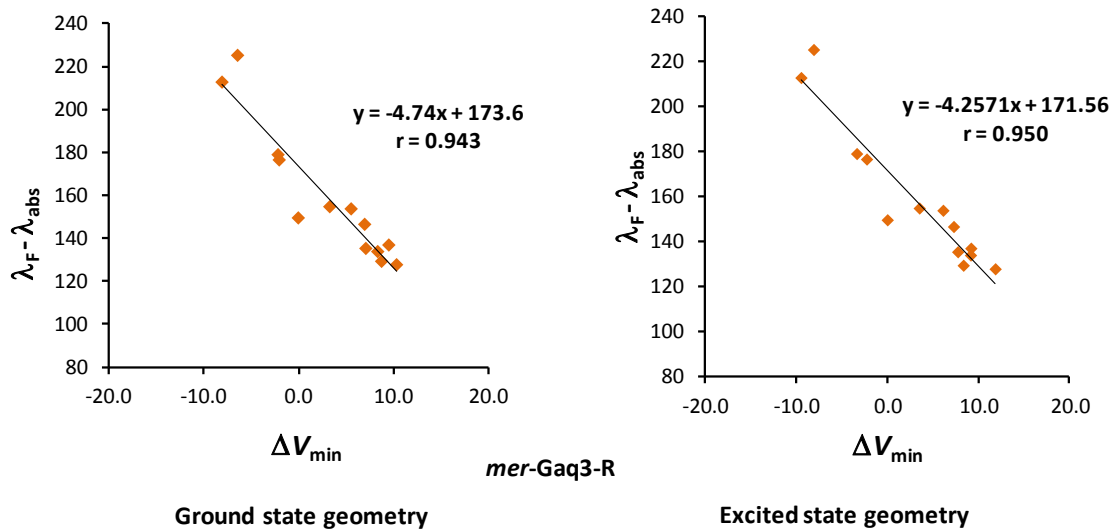
(b)
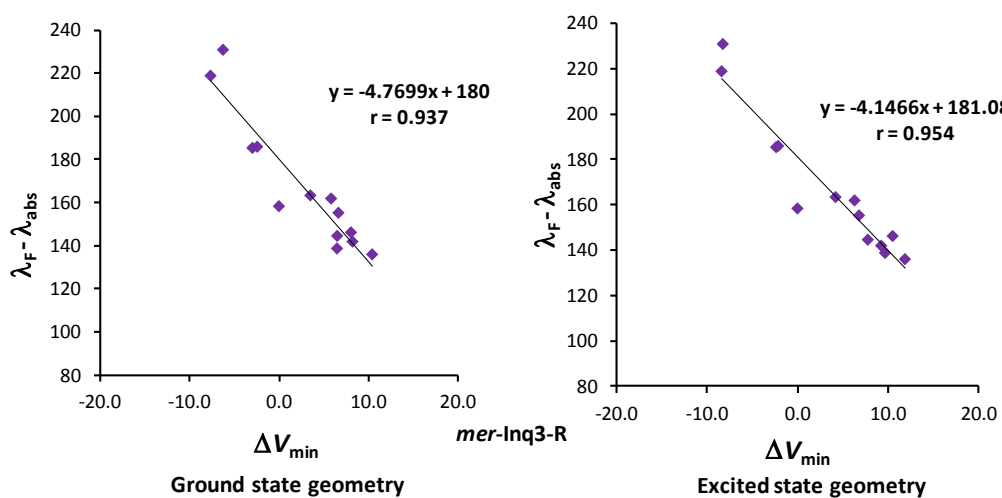
(c)

Figure 3.31 The correlation between ΔV_{min} (kcal/mol) of ground state and excited state geometries with the λ_F -λ_{abs} (nm) of (a) **_mer_-Alq3-R** (b) **_mer_-Gaq3-R and** (c) **_mer_-Inq3-R**.

3.10 Conclusions

A DFT study for the ground state properties and TDDFT study for the excited state properties have been conducted for group 13 metal complexes of 5-phenyl substituted tris(8-quinolinolate). The energy comparison between the ground state optimized

geometries of *mer* and *fac* isomers of **Mq3-R** complexes reveal that the *mer* isomers are always more stable. This is attributed to the less *trans* effect in *mer* isomers compared to their *fac* isomers. The distance between the metal and nitrogen atom which is *trans* to the oxygen atom (d6) is found to be more sensitive to the substituent effect and excellent correlations are observed between d6 of excited state geometries with the corresponding Hammett substituent constants, σ_p. The subtle structural changes invoked by the introduction of electron withdrawing and donating groups at the 5-phenyl position of the ***mer*-Mq3-R** complexes reveal that the substituent effects strongly influence fluorescence maximum (λ_F) values whereas such effects have only minor influence on absorption maximum (λ_{abs}) values. All the metals exhibited excellent flourescence tunability with various substituents. The TDDFT calculated λ_F values of known systems of ***mer*-Alq3-R** complexes agreed very well with that of experimental values reported by Anzenbacher *et al.* The electronic features of ground and excited state geometries are quantified with the use of MESP minimum (V_{min}) and MESP at the metal centre(V_M). The MESP parameters showed excellent linear correlations with the fluorescence values (λ_F) and Stokes shift (λ_F - λ_{abs}) values. In all the cases, the correlations of MESP values measured for the excited state geometries are found to be superior compared to that calculated for the groud state geometries. This study unambiguously proves that substituent effect on an S^1 state geomerty is very high compared to that on an S^0 state. The strong correlation observed between Stokes shift and substituent parameter suggests that the determination of the fomer quantity provides an experimental way to quantify the substituent effect in exctired states while the latter quantity emerges as a simple theoretical measure of the same.

3.11 References

1.   P. Baron, R. Brown, F. Burden, P. Domaille and J. Kent, *J. Mol. Spectrosc.*, **1972**, 43, 401-410.

2.   H. Ottosson, K. Kilså, K. Chajara, M. C. Piqueras, R. Crespo, H. Kato and D. Muthas, *Chem. Eur. J.*, **2007**, 13, 6998-7005.

3.	H. Hopf and M. S. Sherburn, *Cross Conjugation: Modern Dendralene, Radialene and Fulvene Chemistry*, Wiley, **2016**.

4.	A. P. Scott, I. Agranat, P. U. Biedermann, N. V. Riggs and L. Radom, *J. Org. Chem.*, **1997**, 62, 2026-2038.

5.	B. Halton, *Eur. J. Org. Chem.*, **2005**, 2005, 3391-3414.

6.	K. Najafian, P. von Rague Schleyer and T. T. Tidwell, *Org. Biomol. Chem.*, **2003**, 1, 3410-3417.

7.	H. Möllerstedt, M. C. Piqueras, R. Crespo and H. Ottosson, *J. Am. Chem. Soc.*, **2004**, 126, 13938-13939.

8.	C. Dahlstrand, B. O. Jahn, A. Grigoriev, S. Villaume, R. Ahuja and H. Ottosson, *J. Phys. Chem. C*, **2015**, 119, 25726-25737.

9.	C. Dahlstrand, M. Rosenberg, K. Kilså and H. Ottosson, *J. Phys. Chem. A*, **2012**, 116, 5008-5017.

10.	M. Rosenberg, C. Dahlstrand, K. Kilså and H. Ottosson, *Chem. Rev.*, **2014**, 114, 5379-5425.

11.	F. Feixas, E. Matito, J. Poater and M. Solà, *Chem. Soc. Rev.*, **2015**, 44, 6434-6451.

12.	C. Dahlstrand, K. Yamazaki, K. Kilså and H. Ottosson, *J. Org. Chem.*, **2010**, 75, 8060-8068.

13.	B. T. Stępień, T. M. Krygowski and M. K. Cyrański, *J. Org. Chem.*, **2002**, 67, 5987-5992.

14.	B.-C. Hong, F.-L. Chen, S.-H. Chen, J.-H. Liao and G.-H. Lee, *Org. Lett.*, **2005**, 7, 557-560.

15.	B. Enk, H. Kopacka, K. Wurst, T. Müller and B. Bildstein, *Organometallics*, **2009**, 28, 5575-5586.

16.	T. L. Andrew, J. R. Cox and T. M. Swager, *Org. Lett.*, **2010**, 12, 5302-5305.

17.	E. Aqad, P. Leriche, G. Mabon, A. Gorgues and V. Khodorkovsky, *Org. Lett.*, **2001**, 3, 2329-2332.

18.	K. Kondo, H. Goda, K. Takemoto, H. Aso, T. Sasaki, K. Kawakami, H. Yoshida and K. Yoshida, *J. Mater. Chem. A*, **1992**, 2, 1097-1102.

19.	E. Shurdha, B. K. Repasy, H. A. Miller, K. Dees, S. T. Iacono, D. W. Ball and G. J. Balaich, *RSC Adv.*, **2014**, 4, 41989-41992.

20. A. J. Peloquin, R. L. Stone, S. E. Avila, E. R. Rudico, C. B. Horn, K. A. Gardner, D. W. Ball, J. E. B. Johnson, S. T. Iacono and G. J. Balaich, *J. Org. Chem.*, **2012**, 77, 6371-6376.

21. Y.-B. Dong, Y. Geng, J.-P. Ma and R.-Q. Huang, *Organometallics*, **2006**, 25, 447-462.

22. Y.-B. Dong, P. Wang, R.-Q. Huang and M. D. Smith, *Inorg. Chem.*, **2004**, 43, 4727-4739.

23. F. Jaroschik, M. Penkhues, B. Bahlmann, E. Nicolas, M. Fischer, F. Massicot, A. Martinez, D. Harakat, M. Schmidtmann, R. Kokkuvayil Vasu, J.-L. Vasse and R. Beckhaus, *Organometallics*, **2017**, 36, 2004-2013.

24. A. D. Finke, O. Dumele, M. Zalibera, D. Confortin, P. Cias, G. Jayamurugan, J.-P. Gisselbrecht, C. Boudon, W. B. Schweizer, G. Gescheidt and F. Diederich, *J. Am. Chem. Soc.*, **2012**, 134, 18139-18146.

25. L. P. Hammett, **1940**.

26. L. P. Hammett, *J. Am. Chem. Soc.*, **1937**, 59, 96-103.

27. C. Hansch, A. Leo and R. Taft, *Chem. Rev.*, **1991**, 91, 165-195.

28. T. Siodła, W. P. Oziminski, M. Hoffmann, H. Koroniak and T. M. Krygowski, *J. Org. Chem.*, **2014**, 79, 7321-7331.

29. O. Exner and S. Böhm, *J. Org. Chem.*, **2002**, 67, 6320-6327.

30. O. Exner and S. Bohm, *Phys. Chem. Chem. Phys.*, **2004**, 6, 3864-3871.

31. B. Galabov, S. Ilieva and H. F. Schaefer, *J. Org. Chem.*, **2006**, 71, 6382-6387.

32. B. Galabov, V. Nikolova and S. Ilieva, *Chem. Eur. J.*, **2013**, 19, 5149-5155.

33. M. K. Cyrañski, T. M. Krygowski, A. R. Katritzky and P. v. R. Schleyer, *J. Org. Chem.*, **2002**, 67, 1333-1338.

34. T. M. Krygowski and B. T. Stępień, *Chem. Rev.*, **2005**, 105, 3482-3512.

35. T. M. Krygowski, J. E. Zachara-Horeglad and M. Palusiak, *J. Org. Chem.*, **2010**, 75, 4944-4949.

36. O. Exner and S. Böhm, *Chem. Eur. J.*, **2003**, 9, 4718-4723.

37. O. Exner and S. Böhm, *J. Phys. Org. Chem.*, **2004**, 17, 124-130.

38. W. P. Oziminski and T. M. Krygowski, *J. Mol. Model.*, **2011**, 17, 565-572.

39. S. Wawzonek and J. W. Fan, *J. Am. Chem. Soc.*, **1946**, 68, 2541-2544.

40. N. P. Godman, S. K. Adas, K. M. Hellwig, D. W. Ball, G. J. Balaich and S. T. Iacono, *J. Org. Chem.*, **2016**, 81, 9630-9638.

41. M. Tacke, S. Fox, L. Cuffe, J. Dunne, F. Hartl and T. Mahabiersing, *J. Mol. Struct.*, **2001**, 559, 331-339.

42. A. V. Marenich, J. Ho, M. L. Coote, C. J. Cramer and D. G. Truhlar, *Phys. Chem. Chem. Phys.*, **2014**, 16, 15068-15106.

43. S. J. Konezny, M. D. Doherty, O. R. Luca, R. H. Crabtree, G. L. Soloveichik and V. S. Batista, *J. Phys. Chem. C*, **2012**, 116, 6349-6356.

44. K. Arumugam and U. Becker, *Minerals*, **2014**, 4, 345-387.

45. J. Ho, *Phys. Chem. Chem. Phys.*, **2015**, 17, 2859-2868.

46. M. H. Baik and R. A. Friesner, *J. Phys. Chem. A*, **2002**, 106, 7407-7412.

47. R. I. Zubatyuk, L. Gorb, O. V. Shishkin, M. Qasim and J. Leszczynski, *J. Comput. Chem.*, **2010**, 31, 144-150.

48. H. Kim, J. Park and Y. S. Lee, *J. Comput. Chem.*, **2015**, 36, 33-41.

49. G. Liang, N. J. DeYonker, X. Zhao and C. E. Webster, *J. Comput. Chem.*, **2017**, 38, 2430-2438.

50. B. A. Anjali, F. B. Sayyed and C. H. Suresh, *J. Phys. Chem. A*, **2016**, 120, 1112-1119.

51. B. A. Anjali and C. H. Suresh, *New J. Chem.*, **2018**, 42, 18217-18224.

52. M. J. Frisch, G. W. Trucks, H. B. Schlegel, G. E. Scuseria, M. A. Robb, J. R. Cheeseman, G. Scalmani, V. Barone, B. Mennucci, G. A. Petersson, H. Nakatsuji, M. Caricato, X. Li, H. P. Hratchian, A. F. Izmaylov, J. Bloino, G. Zheng, J. L. Sonnenberg, M. Hada, M. Ehara, K. Toyota, R. Fukuda, J. Hasegawa, M. Ishida, T. Nakajima, Y. Honda, O. Kitao, H. Nakai, T. Vreven, J. J. A. Montgomery, J. E. Peralta, F. Ogliaro, M. Bearpark, J. J. Heyd, E. Brothers, K. N. Kudin, V. N. Staroverov, T. Keith, R. Kobayashi, J. Normand, K. Raghavachari, A. Rendell, J. C. Burant, S. S. Iyengar, J. Tomasi, M. Cossi, N. Rega, J. M. Millam, M. Klene, J. E. Knox, J. B. Cross, V. Bakken, C. Adamo, J. Jaramillo, R. Gomperts, R. E. Stratmann, O. Yazyev, A. J. Austin, R. Cammi, C. Pomelli, J. W. Ochterski, R. L. Martin, K. Morokuma, V. G. Zakrzewski, G. A. Voth, P. Salvador, J. J. Dannenberg, S. Dapprich, A. D. Daniels, O. Farkas, J. B. Foresman, J. V. Ortiz, J. Cioslowski and D. J. Fox, *Gaussian 09*, Revision D.01; Gaussian Inc., Wallingford CT, **2013**.

53. A. V. Marenich, C. J. Cramer and D. G. Truhlar, *J. Phys. Chem. B*, **2009**, 113, 6378-6396.

54. L. K. Sviatenko, L. Gorb, F. C. Hill, D. Leszczynska and J. Leszczynski, *Chem. Heterocycl. Compd.*, **2014**, 50, 311-318.

55. F. B. Sayyed and C. H. Suresh, *New J. Chem*, **2009**, 33, 2465-2471.

56. C. W. Tang and S. A. VanSlyke, *Appl. phys. lett.*, **1987**, 51, 913-915.

57. Y. S. Zhao, C. Di, W. Yang, G. Yu, Y. Liu and J. Yao, *Adv. Funct. Mater.*, **2006**, 16, 1985-1991.

58. H. Sasabe and J. Kido, *J. Mater. Chem. C*, **2013**, 1, 1699-1707.

59. A. Curioni and W. Andreoni, *J. Am. Chem. Soc.*, **1999**, 121, 8216-8220.

60. A. P. Kulkarni, C. J. Tonzola, A. Babel and S. A. Jenekhe, *Chem. Mater.*, **2004**, 16, 4556-4573.

61. M. Brinkmann, B. Fite, S. Pratontep and C. Chaumont, *Chem. Mater.*, **2004**, 16, 4627-4633.

62. Y. Shirota and H. Kageyama, *Chem. Rev.*, **2007**, 107, 953-1010.

63. L. S. Sapochak, A. Padmaperuma, N. Washton, F. Endrino, G. T. Schmett, J. Marshall, D. Fogarty, P. E. Burrows and S. R. Forrest, *J. Am. Chem. Soc.*, **2001**, 123, 6300-6307.

64. J. Wang, K. D. Oyler and S. Bernhard, *Inorg. Chem.*, **2007**, 46, 5700-5706.

65. S.-H. Liao, J.-R. Shiu, S.-W. Liu, S.-J. Yeh, Y.-H. Chen, C.-T. Chen, T. J. Chow and C.-I. Wu, *J. Am. Chem. Soc.*, **2009**, 131, 763-777.

66. C. F. R. A. C. Lima, R. J. S. Taveira, J. C. S. Costa, A. M. Fernandes, A. Melo, A. M. S. Silva and L. M. N. B. F. Santos, *Phys. Chem. Chem. Phys.*, **2016**, 18, 16555-16565.

67. Y.-W. Yu, C.-P. Cho and T.-P. Perng, *Nanoscale Res. Lett.*, **2009**, 4, 820.

68. I. Hernández and W. P. Gillin, *J. Phys. Chem. B*, **2009**, 113, 14079-14086.

69. J. C. S. Costa, C. Lima and L. Santos, *J. Phys. Chem. C*, **2014**, 118, 21762-21769.

70. D. Singh, V. Nishal, S. Bhagwan, R. K. Saini and I. Singh, *Mater. Des.*, **2018**, 156, 215-228.

71. A. Curioni, M. Boero and W. Andreoni, *Chem. Phys. Lett.*, **1998**, 294, 263-271.

72. J. Zhang and G. Frenking, *Chem. Phys. Lett.*, **2004**, 394, 120-125.

73. C.-K. Tai, Y.-M. Chou and B.-C. Wang, *J. Lumin.*, **2011**, 131, 169-176.

74. G. P. Kushto, Y. Iizumi, J. Kido and Z. H. Kafafi, *J. Phys. Chem. A*, **2000**, 104, 3670-3680.

75. M. Amati and F. Lelj, *J. Phys. Chem. A*, **2003**, 107, 2560-2569.

76. E. Bardez, I. Devol, B. Larrey and B. Valeur, *J. Phys. Chem. B*, **1997**, 101, 7786-7793.

77. M. L. Ramos, L. L. G. Justino, A. I. N. Salvador, A. R. E. de Sousa, P. E. Abreu, S. M. Fonseca and H. D. Burrows, *Dalton Trans.*, **2012**, 41, 12478-12489.

78. R. Pohl and P. Anzenbacher, *Org. Lett.*, **2003**, 5, 2769-2772.

79. V. A. Montes, R. Pohl, J. Shinar and P. Anzenbacher, *Chem. Eur. J.*, **2006**, 12, 4523-4535.

80. A. Irfan and J. Zhang, *Theor. Chem. Acc.*, **2009**, 124, 339-344.

81. C. H. Chen and J. Shi, *Coord. Chem. Rev.*, **1998**, 171, 161-174.

82. C. Bizzarri, E. Spuling, D. M. Knoll, D. Volz and S. Bräse, *Coord. Chem. Rev.*, **2018**, 373, 49-82.

83. M. Sugimoto, M. Anzai, K. Sakanoue and S. Sakaki, *Appl. phys. lett.*, **2001**, 79, 2348-2350.

84. B. C. Lin, C. P. Cheng, Z.-Q. You and C.-P. Hsu, *J. Am. Chem. Soc.*, **2005**, 127, 66-67.

85. D. Cheshmedzhieva, P. Ivanova, S. Stoyanov, D. Tasheva, M. Dimitrova, I. Ivanov and S. Ilieva, *Phys. Chem. Chem. Phys.*, **2011**, 13, 18530-18538.

86. M. J. Frisch, G. W. Trucks, H. B. Schlegel, G. E. Scuseria, M. A. Robb, J. R. Cheeseman, G. Scalmani, V. Barone, B. Mennucci, G. A. Petersson, H. Nakatsuji, M. Caricato, X. Li, H. P. Hratchian, A. F. Izmaylov, J. Bloino, G. Zheng, J. L. Sonnenberg, M. Hada, M. Ehara, K. Toyota, R. Fukuda, J. Hasegawa, M. Ishida, T. Nakajima, Y. Honda, O. Kitao, H. Nakai, T. Vreven, J. J. A. Montgomery, J. E. Peralta, F. Ogliaro, M. Bearpark, J. J. Heyd, E. Brothers, K. N. Kudin, V. N. Staroverov, T. Keith, R. Kobayashi, J. Normand, K. Raghavachari, A. Rendell, J. C. Burant, S. S. Iyengar, J. Tomasi, M. Cossi, N. Rega, J. M. Millam, M. Klene, J. E. Knox, J. B. Cross, V. Bakken, C. Adamo, J. Jaramillo, R. Gomperts, R. E. Stratmann, O. Yazyev, A. J. Austin, R. Cammi, C. Pomelli, J. W. Ochterski, R. L. Martin, K. Morokuma, V. G. Zakrzewski, G. A. Voth, P. Salvador, J. J. Dannenberg, S. Dapprich, A. D. Daniels, O. Farkas, J. B.

Foresman, J. V. Ortiz, J. Cioslowski and D. J. Fox, *Gaussian 16*, Revision A.03; Gaussian Inc., Wallingford CT, **2016**.

87.   R. L. Martin, J. D. Kress, I. H. Campbell and D. L. Smith, *Phys. Rev. B*, **2000**, 61, 15804-15811.

88.   G. Gahungu and J. P. Zhang, *J. Mol. Struct. (THEOCHEM)*, **2005**, 755, 19-30.

89.   L. S. Sapochak, A. Ranasinghe, H. Kohlmann, K. F. Ferris and P. E. Burrows, *Chem. Mater.*, **2004**, 16, 401-406.

90.   M. Seitz, E. G. Moore and K. N. Raymond, *Inorg. Chem.*, **2008**, 47, 8665-8673.

91.   B. J. Chen, X. W. Sun and Y. K. Li, *Appl. Phys. Lett.*, **2003**, 82, 3017-3019.

92.   P. E. Burrows, L. S. Sapochak, D. M. McCarty, S. R. Forrest and M. E. Thompson, *Appl. phys. lett.*, **1994**, 64, 2718-2720.

Interpreting Oxidative Addition of Ph-X (X = CH₃, F, Cl, Br) to Monoligated Pd (0) Catalysts using MESP

Molecular electrostatic potential at Pd
predicts activation energy

Pd-L + Ar-X ⟶ L-Pd-Ar ⟶ L-Pd-Ar ⟶ L-Pd-Ar

L= phosphines   X = Br, Cl, F, Me
    NHCs
    alkenes
    alkynes
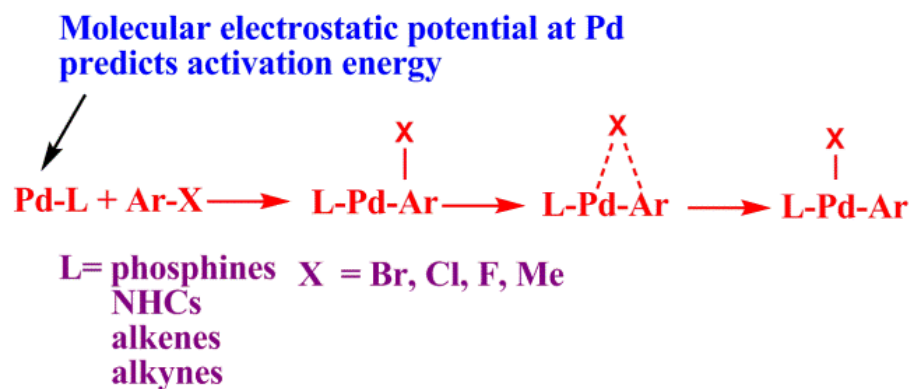
4.1 Abstract

A B3LYP density functional theory (DFT) study on the oxidative addition of halogenobenzenes and toluene to monoligated zerovalent palladium catalysts (Pd-L) has been carried out using the 'L' ligands phosphines, N-heterocyclic carbenes (NHC), alkynes and alkenes. The electron deficiency of the under-coordinated Pd in Pd-L is quantified in terms of the molecular electrostatic potential at the metal center (V_{Pd}) which showed significant variation with respect to the nature of the L ligand. Further, a strong linear correlation between ΔV_{Pd} and the activation barrier (E_{act}) of the reaction is established. The correlation plots between ΔV_{Pd} and E_{act} suggests that a priori prediction on the ability of the palladium complex to undergo oxidative addition is possible from V_{Pd} analysis. In general, as the electron donating nature of ligand increases, the suitability of Pd(0) catalyst to undergo oxidative addition increases. V_{Pd} measures the electron rich/deficient nature of the metal center and provides a quantitative measure of the reactivity of the catalyst. By tuning V_{Pd} value, efficient catalysts can be designed.

4.2 Introduction

Palladium catalysts have emerged as invaluable tools for organometallic synthesis, mainly in cross coupling reactions such as Heck,[1] Negishi,[2] Suzuki-Miyaura,[3] Stille,[4] Sonogashira,[5] etc. to form carbon-carbon and carbon-hetero atom bonds.[7-11] Generally, the initial step of the catalytic cycle comprises of an oxidative addition of electrophilic aryl halide to zerovalent palladium center (Pd(0)), generating a Pd(II) aryl halo complex, which is often observed as the rate limiting step.[12,13] Hence, activation energy (E_{act}) for the oxidative addition becomes a key thermodynamic parameter to be tuned for the successful design of efficient catalysts, and several experimental[14,15] and computational[16-22] studies have been devoted to such attempts. Many of the developed Pd(0) catalysts are found to be most effective with two-electron donating phosphines[15,23,24] and N-heterocyclic carbenes (NHCs),[25-29] while a few studies have

been reported for Pd(0) complexes of alkenes[30] and alkynes.[31,32] In the catalyst design strategy, the choice of ligands in Pd(0) systems can have a considerable impact on the reaction pathway, as the fine tuning of E_{act} is often achieved by a balanced mix of steric and electronic effect exerted by the ligand on the metal center which effectively determines the kinetic aspects of the reaction.[33]

Oxidative addition of aryl halides (Ar-X) to Pd(0) complexes has gained considerable interest in both experimental[34,35] and theoretical[20,36-38] studies owing to its wide range of applications in modern organic synthesis. Aryl bromides, iodides and triflates are the general substrates used in this category, whereas chlorides are found to be generally unreactive,[7] and thus efforts have been made to make them more reactive.[7,12,34,39] Mechanistic studies in this area are pioneered by the works of Hartwig,[14,35,39] Amatore,[40] and Norrby.[16,17,32,41] Various studies identified either the presence of coordinatively unsaturated 14-electron complex with two donor ligands (PdL$_2$) or the one ligand dissociated 12-electron complex (PdL) as the major species in solution, based on their ligand size.[42] As per the typical mechanisms summarized in Scheme 4.1, the active form of the catalyst PdL$_2$, either interacts with the Ar-X directly and follows an associative pathway to give the oxidation product, or it dissociates to PdL and react with Ar-X to form a σ-adduct. In the σ-adduct, C-X bond is activated and eventually breaks to form the oxidative addition product. Kozuch et al. have shown that the tri-coordinated anionic Pd intermediate (Pd^{0}L$_2$Cl$^-$) formed by introducing anions such as chlorides is more susceptible to an oxidative addition of aryl halides than the regular Pd^{0}L$_2$ catalyst.[43,44] Senn and Ziegler have investigated the oxidative addition of phenyl halides to bidentate phosphines.[22] A density functional theory (DFT) study conducted by Ahlquist and Norrby on oxidative addition of aryl chlorides to monoligated Pd(0) has gained much attention recently.[16] Hartwig et al. studied the mechanism for oxidative addition of haloarenes to trialkylphosphine Pd(0) complexes and evaluated the steric properties of ligands.[14]

Scheme 4.1 Associative and dissociative pathways of oxidative addition.
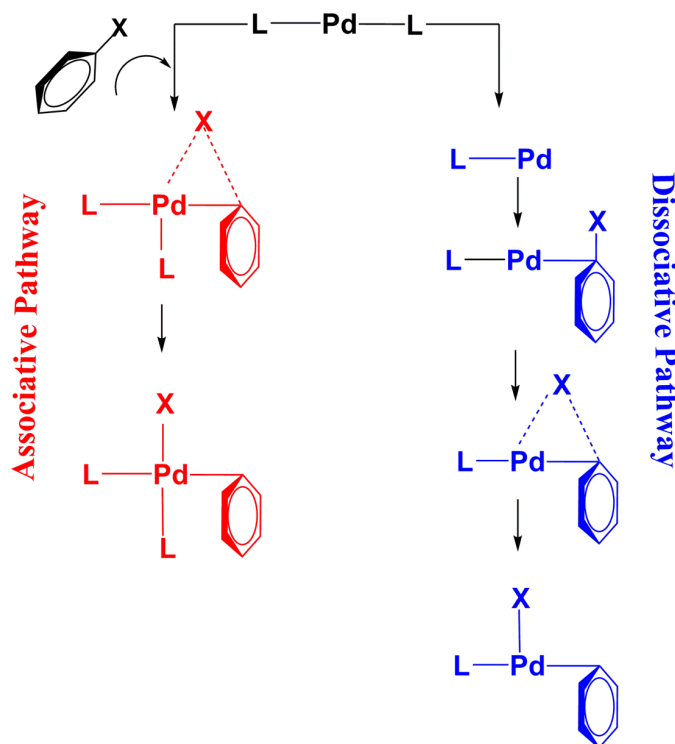
Numerous studies show that the use of hindered phosphines as ligands for palladium complexes has significantly improved the catalytic activity.[45] In the case of Pd-phosphine complexes, Hartwig et al.[46], Mitchell and Baird[47], Harvey et al.[20] and Brown and Jutand[15] has demonstrated that even small changes to PR$_3$ ligands can influence the mechanism of the reaction substantially, showing equilibria between PdL$_4$, PdL$_3$, PdL$_2$, as well as a preference for associative displacement pathways for the oxidative addition step. The present study focuses only on the reactivity of the monoligated PdL complexes (L = phosphines, N-heterocyclic carbenes, alkynes and alkenes) in the dissociative pathway and use molecular electrostatic potential (MESP) analysis as a tool to understand the subtle variations in the energetics of the oxidative addition of Ph-X (X = F, Cl, Br and CH$_3$) to Pd(0).

MESP has been made a significant impact in predicting stabilities and reactivities of diverse organometallic catalysts including first-generation Grubbs olefin metathesis catalysts,[48] pincer catalysts,[49] metal hydrides of Mo, W, Mn, Re, Fe and Ru which are applicable as water splitting catalysts[50] etc. In the previous chapters, the reduction

potential (E^0) values of mononuclear cobalt catalysts,[51] Fischer carbene complexes of chromium,[52] and 1,3,6-triphenyl fulvenes[53] are predicted.

In organometallic complexes, metal center plays the pivotal role in executing a reaction and a single parameter that explains the reactivity of the metal center is yet to be established with respect to a correlation with the activation barrier of the reaction. Further, the question of how the selectivity of a ligand influences the performance of the metal center in the rate determining step of a reaction remains unanswered. For the first time, we provide a mechanistic interpretation of the oxidative addition of aryl halides to Pd(0) solely based on the MESP at the Pd center which undergoes delicate changes with respect to changes in ligand environment. MESP is an electronic property and the quantification of it on the metal center provides an easy measure of the activation barrier of the oxidative addition. Thus a novel use of MESP is unraveled in this work which will also establish this quantity as an excellent electronic parameter for the direct quantification of the chemical reactivity.

The oxidative addition of aryl bromide, aryl chloride, aryl fluoride and toluene to Pd(0) centers ligated with phosphines, N-heterocyclic carbenes, alkenes and alkynes has been carried out. As there is an increasing tendency to replace traditional phosphines with NHCs in organic synthesis, this work will also enable the comparison of the suitability of phosphine and NHC ligands. Several groups have tried to make Pd-phosphines and Pd-NHCs more bulky in order to ease oxidative addition, however, the molecular design strategies were not based on a quantitative measure for the electron rich/deficient character of the metal center. MESP at Pd(0) gives a convenient measure of the ability of Pd(0) to undergo oxidative addition and its calculation is available with many computational software. Our findings will pave the way for developing a rational design strategy for making efficient ligands in oxidative addition.

4.3 Computational Methodology

All the molecules are optimized using B3LYP density functional with 6-31+G(d,p) basis set for all the atoms except for Pd, for Pd Lanl2DZ basis set is used. Frequency and MESP calculations have also been carried out at the same level of theory. A minimum

189

energy structure shows zero imaginary frequency and a transition state is characterized with one imaginary frequency along the bond breaking/forming direction of the oxidative addition. The energy profiles of the computed mechanisms are derived from the total energy of the complexes.

Selection of 50 ligands from four categories leads to the study of 250 complexes (including transition states) for elucidating the mechanism of the oxidative addition toluene and aryl halides. Hence, a total of 750 complexes are analyzed in this study. In order to understand the effect of solvation (solvent = THF) and dispersion, the reaction of aryl bromide with a selected set of 15 phosphine coordinated complexes is also described at B3LYP-D3/SMD/BS1 level[54] using the self-consistent reaction field (SCRF) approach with "solvation model density" (SMD) method.[55] We have also tested SDD basis set for Pd along with dispersion and solvation (B3LYP-D3/BS2) corrections for the test systems. All the calculations have been carried out using Gaussian 09 suite of programmes.[56]

4.4 Results and Discussion

4.4.1 Ligands and MESP Features

The selected sets of ligands are depicted in Figure 4.1. The abbreviation $ImNX_2Y_2$ is used for naming the NHC ligands, where ImN represents the imidazole core unit while X and Y represent the N and C substituents, respectively. In Figure 4.2, MESP isosurface at -20.0 kcal/mol (-0.0319 au) is plotted for a representative set of optimized ligands along with their MESP minimum (a (3, +3) critical point), V_{min} in kcal/mol. This figure also depicts MESP value in a.u. at the nucleus of phosphorous (V_P) for phosphines, at the carbene carbon (V_C) for NHC, at the alkyne carbon (V_C) and at the alkene carbon (V_C).
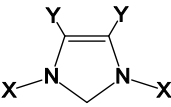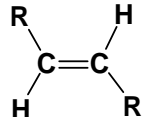
Phosphines	PCy_3, $PtBu_3$, $PiPr_3$, PMe_3, PEt_3, $P(SiMe_3)_3$, $PHMePh$, PPh_3, PH_3, $P(Ph-F)_3$, $P(thiophene)_3$, $P(Ph-Cl)_3$, $P(SMe)_3$, $P(Ph-CF_3)_3$, PH_2CF_3, PCl_2Ph, PCl_2Me, PCl_3, $P(CF_3)_3$, PF_3.
	X, Y = Me, H; H, H; Me, COOMe; Me, F; Me, Cl; H, F; Me, CF_3; CF_3, H; Me, CN; Me, NO_2.
$R-C{\equiv}C-R$	R= NH_2, NMe_2, Me, $SiMe_3$, Et, Ph, H, Br, Cl, F.
	R= Me, Et, H, $SiMe_3$, Ph, Cl, Br, F, CF_3, CN.

Figure 4.1 Schematic representation of ligands selected for the study.

The MESP value at the nucleus is very high compared to the V_{min}. Hence, in Tables 4.1, 4.2, 4.3 and 4.4, the relative values of V_P and V_C with respect to the respective unsubstituted systems PH_3, $ImNH_2H_2$, C_2H_2 and CH_2CH_2 are reported along with V_{min} and ΔV_{min} values (usually, the term 'unsubstituted' indicates that the substituent is H). ΔV_{min} is the difference between the V_{min} of the ligand and that of the unsubstituted reference ligand. The notations used for the relative values for phosphorus and carbon nuclei are ΔV_P and ΔV_C, respectively. Among the phosphines, PCy_3 shows the most negative V_{min} (-43.1 kcal/mol) followed by $PtBu_3$ (-42.4 kcal/mol). V_{min} of $PiPr_3$, PMe_3 and PEt_3 (~-40.0 kcal/mol) lie very close to PCy_3 whereas a significant reduction in negative character of V_{min} is observed from PPh_3 (-30.7 kcal/mol). The ligands PCl_3, PCF_3 and PF_3 do not have V_{min} indicating the highly electron withdrawing nature of their P-substituents (Table 4.1). Similarly, the ligands PH_2CF_3, PCl_2Ph and PCl_2Me show substantial decrease in the negative character of V_{min} suggesting the electron deficient nature of those ligands.[57]
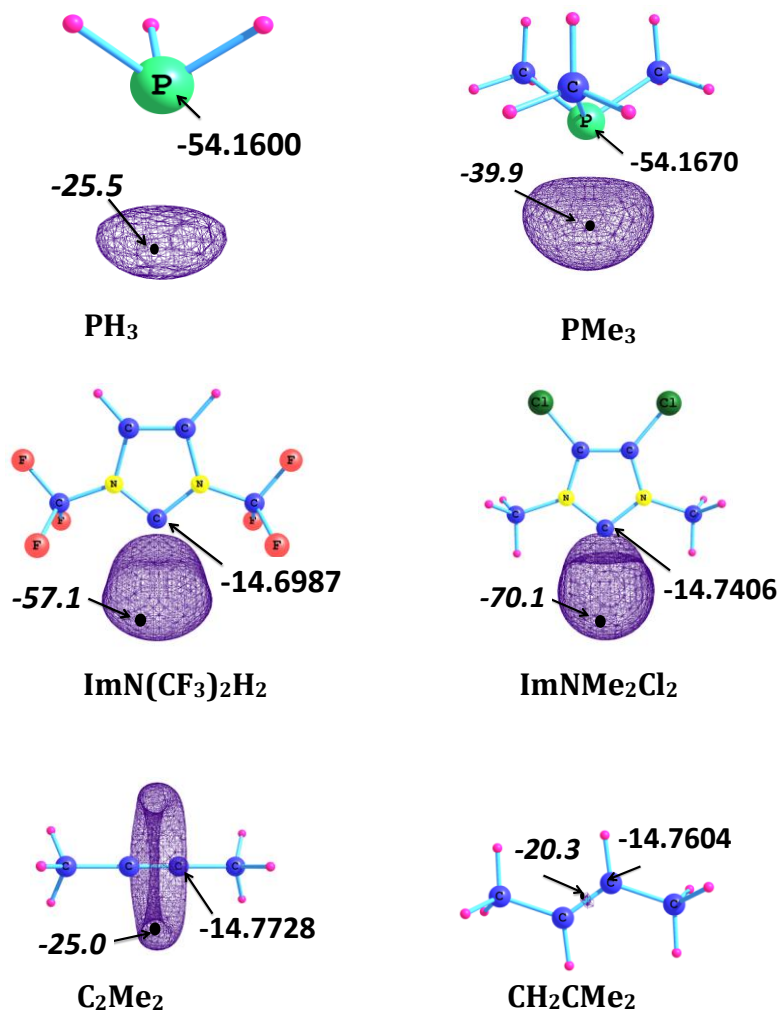
Figure 4.2 Representation of MESP isosurface at -20.0 kcal/mol. V_{min} in kcal/mol, V_C and V_P in au.

For a particular ligand, the negative sign of ΔV_{min} indicates the electron donating nature and the positive sign indicates the electron withdrawing nature. A trend very similar to V_{min} is observed for ΔV_P, ΔV_N and ΔV_C for most of the ligands (Tables 4.1 – 4.4). Nearly a two-fold increase in the negative character V_{min} is observed for NHC compared to phosphines which suggests that lone pair of NHC is more electron rich and more donating towards coordination bonds than phosphine. A detailed elucidation of MESP analysis for several phosphines and NHCs are stated elsewhere.[58,59]

Table 4.1 The V_{min}, ΔV_{min}, ΔV_P of phosphine ligands (in kcal/mol)

Ligand	V_{min}	ΔV_{min}	ΔV_P
PCy$_3$	-43.1	-17.6	-12.0
PtBu$_3$	-42.4	-16.9	-8.7
PiPr$_3$	-40.5	-15.0	-10.6
PMe$_3$	-39.9	-14.3	-4.4
PEt$_3$	-39.7	-14.1	-9.2
P(SiMe$_3$)$_3$	-35.5	-10.0	-33.9
PHMePh	-32.1	-6.5	0.2
PPh$_3$	-30.7	-5.1	5.4
PH$_3$	-25.5	0.0	0.0
P(Ph-F)$_3$	-23.8	1.8	14.4
P(thiophene)$_3$	-23.8	1.8	20.9
P(Ph-Cl)$_3$	-21.5	4.1	16.6
P(SMe)$_3$	-17.7	7.8	33.9
P(Ph-CF$_3$)$_3$	-14.0	11.5	25.2
PH$_2$CF$_3$	-9.3	16.2	23.8
PCl$_2$Ph	-6.8	18.7	60.5
PCl$_2$Me	-6.3	19.2	61.3
PCl$_3$	nil	nil	92.5
P(CF$_3$)$_3$	nil	nil	59.5
PF$_3$	nil	nil	129.7

Table 4.2 The V_{min}, ΔV_{min}, ΔV_C of NHC ligands (in kcal/mol)

Ligand	V_{min}	ΔV_{min}	ΔV_C
$ImNMe_2H_2$	-82.1	-1.3	-8.1
$ImNH_2H_2$	-80.8	0.0	0.0
$ImNMe_2COOMe_2$	-72.1	8.7	2.9
$ImNMe_2F_2$	-70.7	10.1	6.2
$ImNMe_2Cl_2$	-70.1	10.7	5.5
$ImNH_2F_2$	-68.5	12.3	16.6
$ImNMe_2(CF_3)_2$	-63.0	17.8	13.7
$ImN(CF_3)_2H_2$	-57.1	23.7	31.8
$ImNMe_2CN_2$	-55.7	25.1	23.9
$ImNMe_2NO_2$	-51.2	29.6	29.5

Table 4.3 The V_{min}, ΔV_{min}, ΔV_C of alkynes (in kcal/mol)

Ligand	V_{min}	ΔV_{min}	ΔV_C
$C_2(NH_2)_2$	-30.4	-12.3	-1.6
$C_2(NMe_2)_2$	-27.2	-9.1	-6.1
C_2Me_2	-25.0	-6.9	-16.1
$C_2(SiMe_3)_2$	-24.8	-6.7	-30.6
C_2Et_2	-24.6	-6.5	-18.4
C_2Ph_2	-19.2	-1.1	-6.0
C_2H_2	-18.1	0.0	0.0
C_2Br_2	-7.9	10.2	31.8
C_2Cl_2	-6.9	11.2	37.8
C_2F_2	nil	nil	71.7

Very recently, Suresh, Gadre and co-workers have shown that MESP V_{min} characterizes lone pairs in molecules.[60,61] In the case of alkyne ligands, amino substituted $C_2(NH_2)_2$ and $C_2(NMe_2)_2$ show the most negative V_{min} whereas the severe withdrawing effect of F substituents in C_2F_2 leads to disappearance of negative MESP region for the CC triple bond. Similarly, alkyl substituted alkenes show the most electron rich double bonds ($V_{min} \sim$ -20 kcal/mol) while CF_3 and CN substituted cases do not exhibit V_{min}. The ΔV_C follow a trend similar to that of ΔV_{min} for electron withdrawing substituents whereas alkyl and silyl substituted systems appear more electron rich than amino substituted systems in ΔV_C than ΔV_{min}.

Table 4.4 The V_{min}, ΔV_{min}, ΔV_C of alkenes (in kcal/mol)

Ligand	V_{min}	ΔV_{min}	ΔV_C
CH_2CMe_2	-20.3	-1.4	-4.9
CH_2CEt_2	-19.5	-0.6	-6.6
CH_2CH_2	-18.9	0.0	0.0
$CH_2C(SiMe_3)_2$	-17.8	1.10	-13.0
CH_2CPh_2	-15.2	3.7	3.9
CH_2CCl_2	-7.5	11.4	49.0
CH_2CBr_2	-7.1	11.8	46.7
CH_2CF_2	-0.8	18.1	64.3
$CH_2(CF_3)_2$	nil	nil	44.5
$CH_2(CN)_2$	nil	nil	64.7

The discrepancy may be due to the difference in the through space and through bond interactions of the alkyl and amino groups; the former is mainly through bond active *via* inductive effect while the through space effect of the lone pair on the amino group may strongly influence the absolute value of V_{min} for the CC π-bond.

4.4.2 Dissociation of Pd-L from PdL$_2$

As stated in the introduction, in the monoligated pathway, the substrate is oxidatively added to a 12-electron active catalyst (PdL), which is formed by the dissociation of the 14-electron bis-ligated complex (PdL$_2$).

Table 4.5 Phosphine ligands and the corresponding MESP values at Pd of PdL$_2$ and PdL in au and the difference between V_{Pd2} and V_{Pd1} in kcal/mol

Ligand	V_{Pd1}	V_{Pd2}	V_{Pd2} - V_{Pd1}
PCy$_3$	-16.4359	-16.4374	-0.93
PtBu$_3$	-16.4354	-16.4382	-1.76
PiPr$_3$	-16.4328	-16.4358	-1.87
PMe$_3$	-16.4281	-16.4315	-2.18
PEt$_3$	-16.4309	-16.4339	-1.89
P(SiMe$_3$)$_3$	-16.4368	-16.4410	-2.64
PHMePh	-16.4174	-16.4244	-4.37
PPh$_3$	-16.4197	-16.4249	-3.23
PH$_3$	-16.4104	-16.4222	-7.42
P(Ph-F)$_3$	-16.4018	-16.4131	-7.12
P(thiophene)$_3$	-16.4105	-16.4174	-4.33
P(Ph-Cl)$_3$	-16.3983	-16.4105	-7.64
P(SMe)$_3$	-16.3959	-16.4063	-6.54
P(Ph-CF$_3$)$_3$	-16.3826	-16.3991	-10.37
PH$_2$CF$_3$	-16.3737	-16.3962	-14.12
PCl$_2$Ph	-16.3694	-16.3853	-9.98
PCl$_2$CH$_3$	-16.3556	-16.3837	-17.62
PCl$_3$	-16.3347	-16.3644	-18.67
PCF$_3$	-16.3346	-16.3652	-19.21
PF$_3$	-16.3259	-16.3629	-23.22

The MESP values at the Pd nucleus of PdL$_2$ and PdL are designated as V_{Pd1} and V_{Pd2}. The V_{Pd1} and V_{Pd2} values of phosphine, NHC, alkyne and alkene ligated complexes are given in Tables 4.5 – 4.8.

Table 4.6 NHC ligands and the corresponding MESP values at Pd of PdL$_2$ and PdL in au and the difference between V_{Pd2} and V_{Pd1} in kcal/mol

Ligand	V_{Pd1}	V_{Pd2}	V_{Pd2} - V_{Pd1}
ImNMe$_2$H$_2$	-16.4477	-16.4423	3.35
ImNH$_2$H$_2$	-16.4462	-16.4395	4.18
ImNMe$_2$COOMe$_2$	-16.4299	-16.4311	-0.73
ImNMe$_2$F$_2$	-16.4276	-16.4300	-1.49
ImNMe$_2$Cl$_2$	-16.4286	-16.4308	-1.37
ImNH$_2$F$_2$	-16.4233	-16.4257	-1.54
ImNMe$_2$(CF$_3$)$_2$	-16.4104	-16.4189	-5.37
ImN(CF$_3$)$_2$H$_2$	-16.4139	-16.4168	-1.82
ImNMe$_2$CN$_2$	-16.3950	-16.4088	-8.60
ImNMe$_2$NO$_2$	-16.3853	-16.4012	-10.00

Table 4.7 Alkyne ligands and the corresponding MESP values at Pd of PdL$_2$ and PdL in au the difference between V_{Pd2} and V_{Pd1} in kcal/mol

Ligand	V_{Pd1}	V_{Pd2}	V_{Pd2} - V_{Pd1}
C$_2$(NH$_2$)$_2$	-16.3618	-16.4104	-30.5
C$_2$(NMe$_2$)$_2$	-16.3715	-16.4175	-28.9
C$_2$Me$_2$	-16.3761	-16.4107	-21.7
C$_2$(SiMe$_3$)$_2$	-16.3824	-16.4147	-20.3
C$_2$Et$_2$	-16.3755	-16.4099	-21.5
C$_2$Ph$_2$	-16.3535	-16.3927	-24.6
C$_2$H$_2$	-16.3502	-16.3958	-28.6

C_2Br_2	-16.2936	-16.3579	-40.3
C_2Cl_2	-16.2877	-16.3556	-42.6
C_2F_2	-16.2512	-16.3387	-54.9

Table 4.8 Alkene ligands and the corresponding MESP values at Pd of PdL_2 and PdL in au the difference between V_{Pd2} and V_{Pd1} in kcal/mol

Ligand	V_{Pd1}	V_{Pd2}	V_{Pd2} - V_{Pd1}
CH_2CMe_2	-16.4017	-16.4169	-9.51
CH_2CEt_2	-16.4008	-16.4162	-9.65
CH_2CH_2	-16.3864	-16.4106	-15.18
$CH_2C(SiMe_3)_2$	-16.3843	-16.4070	-14.29
CH_2CPh_2	-16.3893	-16.4058	-10.37
CH_2CCl_2	-16.3407	-16.3709	-19.00
CH_2CBr_2	-16.3376	-16.3687	-19.51
CH_2CF_2	-16.3485	-16.3743	-16.21
$CH_2(CF_3)_2$	-16.3086	-16.3554	-29.32
$CH_2(CN)_2$	-16.2946	-16.3442	-31.14

The negative character of these quantities decreases with increase in electron withdrawing power of the ligand. The relative values of V_{Pd1} and V_{Pd2} with respect to the unsubstituted systems (ΔV_{Pd1} and ΔV_{Pd2}) are useful to make a quick comparison of the electron donating/withdrawing power of the ligands. Tables 4.9, 4.10, 4.11 and 4.12 depict these MESP parameters along with the Pd-P distance d1 for PdL_2, Pd-P distance d2 for PdL, and dissociation energy of L from PdL_2 (E_{dis}) for phosphines, NHCs, alkynes and alkenes, respectively.

Table 4.9 Pd-P distances (Å), relative MESP values (kcal/mol) and phosphine dissociation energy (kcal/mol) of Pd(0) catalysts

Ligand	d1	d2	ΔV_{Pd1}	ΔV_{Pd2}	E_{dis}
PCy_3	2.341	2.241	-16.0	-9.5	31.8
$PtBu_3$	2.365	2.259	-15.7	-10.0	30.4
$PiPr_3$	2.342	2.239	-14.1	-8.5	30.9
PMe_3	2.321	2.219	-11.1	-5.9	31.1
PEt_3	2.329	2.227	-12.9	-7.4	30.6
$P(SiMe_3)_3$	2.351	2.260	-16.5	-11.8	27.4
PHMePh	2.316	2.215	-4.4	-1.4	29.9
PPh_3	2.328	2.230	-5.9	-1.7	29.8
PH_3	2.302	2.206	0.0	0.0	26.8
$P(Ph-F)_3$	2.328	2.228	5.1	5.7	30.1
$P(thiophene)_3$	2.320	2.220	-0.1	3.0	29.0
$P(Ph-Cl)_3$	2.327	2.227	7.6	7.3	29.8
$P(SMe)_3$	2.308	2.206	9.1	10.0	26.8
$P(Ph-CF_3)_3$	2.325	2.223	17.5	14.5	29.0
PH_2CF_3	2.295	2.192	23.0	16.3	25.5
PCl_2Ph	2.301	2.192	25.7	23.2	25.2
PCl_2CH_3	2.285	2.186	34.4	24.2	26.6
PCl_3	2.288	2.181	47.5	36.3	21.3
$P(CF_3)_3$	2.286	2.177	47.6	35.8	22.3
PF_3	2.269	2.154	53.0	37.2	22.3

In both PdL_2 and PdL complexes, Pd-P bond length is the highest for $PtBu_3$ ligated complex and the lowest for PF_3 ligated complex which suggest that Pd-P distance increases with electron donating and bulky ligands. When the ligand is more electron donating, ΔV_{Pd} values become more negative. The PCy_3, $PtBu_3$ and $P(SiMe_3)_3$ complexes show more negative ΔV_{Pd2} and ΔV_{Pd1} values. The electron richness of the metal center is directly proportional to its tendency to undergo oxidative addition. The E_{dis} is more or

less same for Pd(0) complexes coordinated with alkyl/phenyl substituted phosphines whereas it decreases with increasing electron withdrawing effect by other ligands. A contradictory correlation aspect can be immediately noted between d1 or d2 distances and E_{dis}. The Pd-P bond shortening leads to a decrease in bond strength. In the case of alkyl/phenyl substituted phosphines, steric effect may be retarding the closer approach of the ligand to the metal whereas the electron rich nature of the ligand compensate it by providing more electron sharing in Pd-P bond. In the case of electron withdrawing ligands, the Pd-P bond is inherently weak due to the diminished electron density while the reduced steric effect decreases the bond length. In addition, the back bonding effect from metal to ligand may also influence the bond strength.

Table 4.10 Pd-C distances (Å), relative MESP values (kcal/mol) and NHC dissociation energy (kcal/mol) of Pd(0) catalysts

Ligand	d1	d2	ΔV_{Pd1}	ΔV_{Pd2}	E_{dis}
$ImNMe_2H_2$	2.053	1.971	-0.9	-1.7	41.3
$ImNH_2H_2$	2.031	1.951	0.0	0.0	40.9
$ImNMe_2COOMe_2$	2.051	1.971	10.2	5.3	41.3
$ImNMe_2F_2$	2.050	1.971	11.7	6.0	41.5
$ImNMe_2Cl_2$	2.051	1.971	11.1	5.5	41.4
$ImNH_2F_2$	2.027	1.949	14.4	8.7	41.0
$ImNMe_2(CF_3)_2$	2.050	1.971	22.5	12.9	41.5
$ImN(CF_3)_2H_2$	2.031	1.951	20.3	14.3	36.2
$ImNMe_2CN_2$	2.044	1.962	32.1	19.3	41.1
$ImNMe_2NO_2$	2.044	1.963	38.3	24.1	40.8

From Table 4.10 it is evident that the Pd-C distances of Pd coordinated to NHCs fall on a narrow range of 2.03 - 2.05 Å for d1 and 1.95 - 1.97 Å for d2. The most negative ΔV_{Pd1} and ΔV_{Pd2} are observed when the coordinating ligand is $ImNMe_2H_2$, indicating the

high electron donating character of CH_3 substituent at the N atom of NHC. Except for $ImN(CF_3)_2H_2$, all the dissociation energy fall in the narrow range of 40.8 – 41.5 kcal/mol.

Table 4.11 Pd-C distances (Å), relative MESP values (kcal/mol) and alkyne dissociation energy (kcal/mol) of Pd(0) catalysts

Ligand	d1	d2	ΔV_{Pd1}	ΔV_{Pd2}	E_{dis}
$C_2(NH_2)_2$	2.085	2.077	-7.3	-9.1	32.9
$C_2(NMe_2)_2$	2.089	2.092	-13.4	-13.7	33.6
C_2Me_2	2.128	2.096	-16.2	-9.4	28.2
$C_2(SiMe_3)_2$	2.167	2.138	-20.2	-11.9	29.3
C_2Et_2	2.132	2.099	-15.9	-8.9	28.1
C_2Ph_2	2.114	2.083	-2.1	1.9	28.6
C_2H_2	2.114	2.083	0.0	0.0	30.2
C_2Br_2	2.070	2.046	35.5	23.8	30.8
C_2Cl_2	2.064	2.041	39.3	25.2	31.0
C_2F_2	2.033	2.020	62.2	35.8	34.9

In the case of alkyne complexes, the Pd-C distance in both Pd-L_2 and Pd-L is higher when $C_2(SiMe_3)_2$ is employed as a ligand. This is due the steric influence of bulky $SiMe_3$ substituent. The Pd-C_1 and Pd-C_2 distances of all the PdL complexes are same except that of Pd($C_2(NMe_2)_2$), in this case, Pd-C_1 is 2.133 Å and Pd-C_2 is 2.051 Å. The average of the two Pd-C distances is given in Table 4.11. Although the MESP parameters clearly distinguish the electron rich ligands from electron deficient ones, the E_{dis} values do not show a correlation pattern with these parameters or a pattern with the Pd-P bond distance data. This indicates that in addition to the σ donating electronic effect from ligands, binding of the ligand to the metal is influenced by steric effect and back bonding effect arising from interaction of filled metal d-orbitals and π*-orbital of alkyne.

Table 4.12 Pd-C distances (Å), relative MESP values (kcal/mol) and alkene dissociation energy (kcal/mol) of Pd(0) catalysts

Ligand	d1	d2	ΔV_{Pd1}	ΔV_{Pd2}	E_{dis}
CH_2CMe_2	2.240	2.155	-9.6	-4.0	21.5
CH_2CEt_2	2.238	2.158	-9.0	-3.5	21.9
CH_2CH_2	2.223	2.140	0.0	0.0	25.2
$CH_2C(SiMe_3)_2$	2.241	2.163	1.3	2.2	21.4
CH_2CPh_2	2.247	2.166	-1.8	3.0	20.4
CH_2CCl_2	2.195	2.101	28.7	24.9	17.7
CH_2CBr_2	2.186	2.096	30.6	26.3	20.2
CH_2CF_2	2.210	2.099	23.8	22.8	16.1
$CH_2(CF_3)_2$	2.196	2.113	48.8	34.6	18.6
$CH_2(CN)_2$	2.218	2.130	57.6	41.6	17.3

Among the PdL_2 complexes of alkenes, the Cl, Br, F, CF_3, and CN systems show two different Pd-C bond lengths while the rest of the systems show same bond length for all the four Pd-C bonds. Two examples, *viz*. $Pd(CH_2CMe_2)_2$ and $Pd(CH_2CCl_2)_2$ are shown in Figure 4.3 to illustrate this geometric feature. For those showing different Pd-C bond lengths, the average bond distance is given in Table 4.12. Overall, the dissociation energies of alkenes (16.1 – 25.2 kcal/mol) are found to be significantly smaller than other sets of ligands.
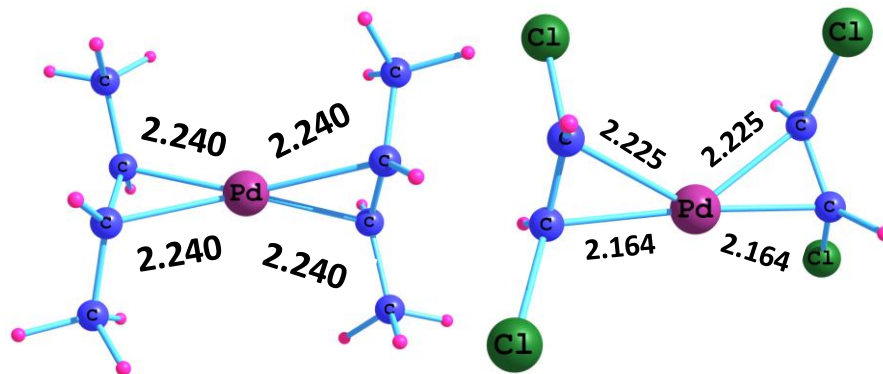
Figure 4.3 Optimized structures of Pd(CH$_2$CMe$_2$)$_2$ and Pd(CH$_2$CCl$_2$)$_2$. Distances in Å.

4.4.3 Oxidative addition of Ph-Br, Ph-Cl, Ph-F, and Ph-Me

A typical energy profile diagram for the oxidative addition of Ph-X to Pd(P*t*Bu$_3$) is given in Figure 4.5. Pd(P*t*Bu$_3$) in the reaction is generated by dissociating P*t*Bu$_3$ from Pd(P*t*Bu$_3$)$_2$. The adduct of Ph-X and Pd(P*t*Bu$_3$) (**I$_1$**) subsequently passes through a transition state **TS$_1$** to form a tri-coordinated product **P$_1$**. In the cases of Ph-Br and Ph-Cl, **I$_1$** is formed as a result of η^2-type coordination of Pd to one of the ortho CC bonds of the arene ring whereas in the case of Ph-F and Ph-Me, the η^2-type coordination of Pd occurs on one of the meta CC bonds (Figure 4.4). The Pd-C and Pd-P distances in **P$_1$** for aryl halides is found to be 1.98 and 2.51 Å, respectively while those of toluene are 2.02 and 2.49 Å, respectively. The activation energy (E$_{act}$) of oxidative addition of substrates follows the order Ph-F $\approx$ Ph-Me >> Ph-Cl > Ph-Br. Compared to the strong C-C and C-F bonds, the weaker C-Cl and C-Br bonds cleave with significantly less energy. The E$_{act}$ data for all the Pd(PR$_3$) complexes are provided in Table 4.13. In general, electron rich phosphines such as alkyl substituted show lower E$_{act}$ than those with electron withdrawing substituents.
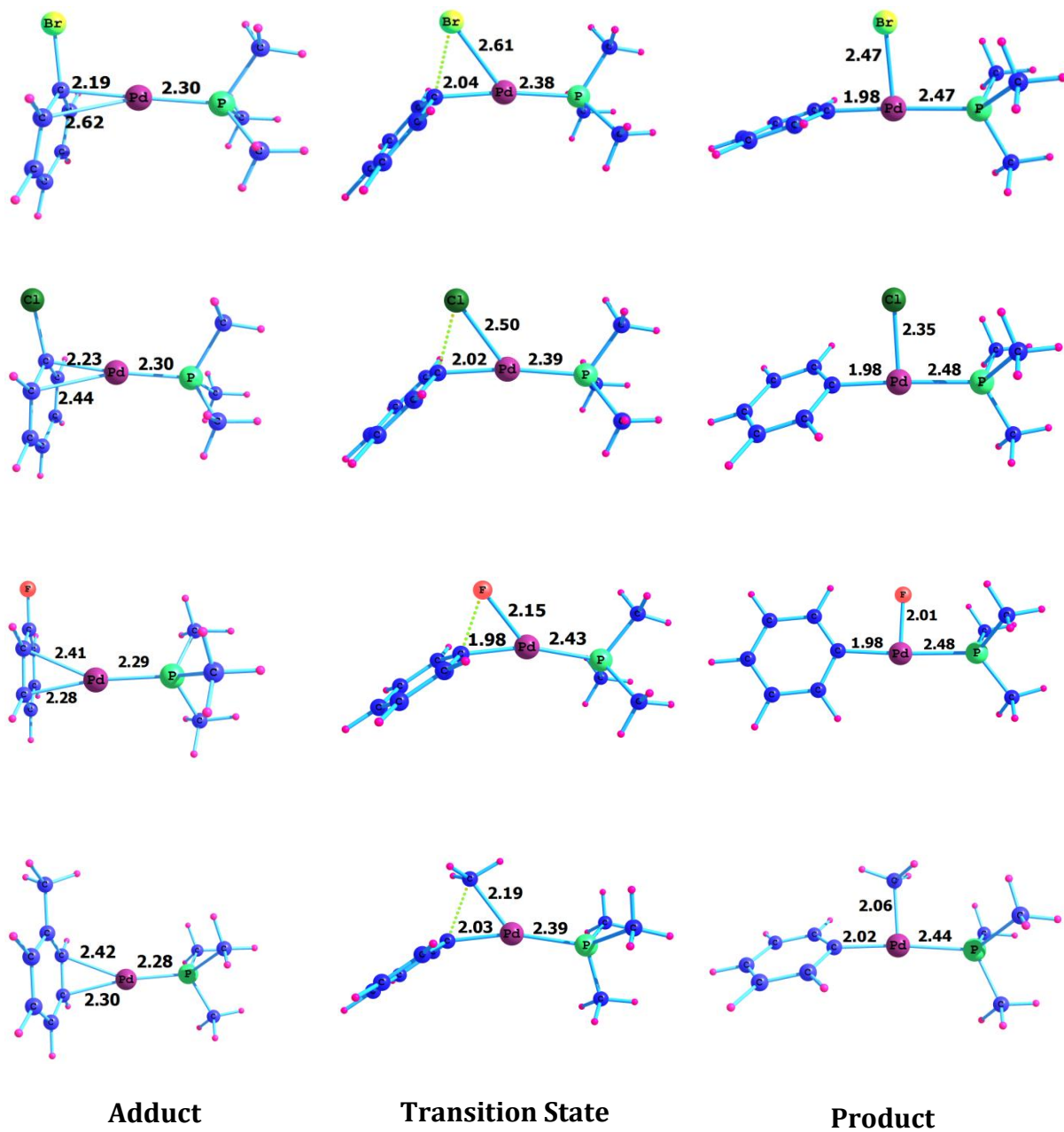
Figure 4.4 Optimized structures of **I₁**, **TS₁** and **P₁** on adding Ph-Br, Ph-Cl, Ph-F, and Ph-Me. The bond distances are given in Å.
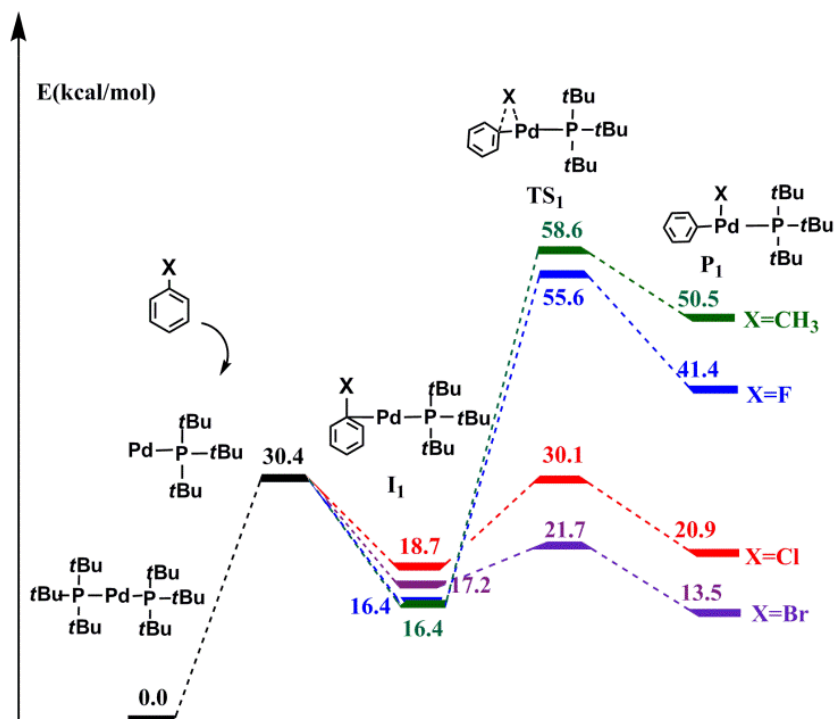
Figure 4.5 Illustration of the energy profile describing the oxidative addition of Ph-X to Pd(P*t*Bu₃).

Table 4.13 Phosphine ligands and the corresponding energy barriers on addition of Ph-X to Pd(phosphine)

Ligand	E_{act} on adding Ph-Br	E_{act} on adding Ph-Cl	E_{act} on adding Ph-F	E_{act} on adding Ph-Me
PCy₃	4.7	11.6	39.9	41.8
P*t*Bu₃	4.6	11.4	39.2	42.2
PiPr₃	4.6	11.8	40.1	42.2
PMe₃	5.5	12.6	41.2	43.3
PEt₃	5.0	12.3	40.7	43.0
P(SiMe₃)₃	4.7	12.0	40.2	39.6
PHMePh	5.3	12.5	41.0	43.7
PPh₃	5.2	12.4	40.7	43.5

PH$_3$	6.6	13.8	43.4	44.1
P(Ph-F)$_3$	5.5	12.8	41.1	44.5
P(thiophene)$_3$	5.5	12.7	40.9	43.5
P(Ph-Cl)$_3$	5.8	13.1	41.5	44.4
P(SMe)$_3$	6.6	13.8	42.1	45.1
P(Ph-CF$_3$)$_3$	6.4	13.2	43.2	45.1
PH$_2$CF$_3$	8.1	15.3	45.1	46.2
PCl$_2$Ph	7.9	15.3	43.6	46.5
PCl$_2$CH$_3$	8.2	15.7	45.3	48.4
PCl$_3$	10.8	18.3	48.2	47.2
P(CF$_3$)$_3$	11.3	18.9	48.3	41.8
PF$_3$	11.9	19.2	48.8	42.2

Table 4.14 NHC ligands and the corresponding energy barriers on addition of Ph-X to Pd(NHC)

Ligand	E$_{act}$ on adding Ph-Br	E$_{act}$ on adding Ph-Cl	E$_{act}$ on adding Ph-F	E$_{act}$ on adding Ph-Me
ImNMe$_2$H$_2$	4.6	11.4	39.0	38.6
ImNH$_2$H$_2$	4.7	11.7	39.1	39.8
ImNMe$_2$COOMe$_2$	4.9	12.1	39.6	39.5
ImNMe$_2$F$_2$	5.0	12.0	39.9	39.5
ImNMe$_2$Cl$_2$	5.0	11.9	39.9	39.4
ImNH$_2$F$_2$	5.2	12.3	39.9	40.7
ImNMe$_2$(CF$_3$)$_2$	5.3	12.4	40.5	40.1

ImN(CF₃)₂H₂	5.1	12.5	41.8	41.1
ImNMe₂CN₂	5.7	12.9	41.7	40.7
ImNMe₂NO₂	6.0	13.3	43.1	41.3

Energy profile diagram for the oxidative addition of Ph-X to the active catalyst Pd(ImNMe₂H₂) is given in Figure 4.6. The E_{dis} of NHC in Pd(ImNMe₂H₂)₂ is 41.3 kcal/mol. The mono ligated complex forms an adduct **I₂** with Ph-X which subsequently passes through a transition state **TS₂** to form the product **P₂**. The adduct formation of substrate with Pd(NHC) leads to more energy lowering than that with Pd(PR₃) whereas E_{act} data given in Table 4.14 show that NHC ligation is more favorable for the reaction than PR₃ ligation. The E_{act} for the substrate addition follows the order Ph-F ≈ Ph-Me >> Ph-Cl > Ph-Br. The maximum E_{act} is observed for ImNMe₂NO₂, the least donating NHC ligand to Pd.
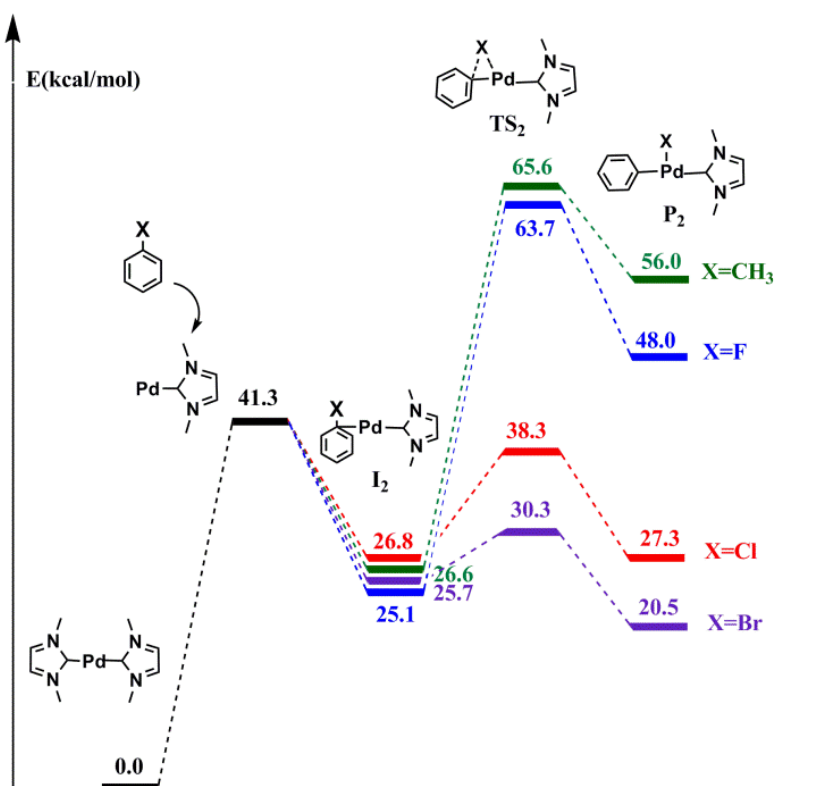
Figure 4.6 Illustration of the energy profile describing the oxidative addition of Ph-X to Pd(ImNMe₂H₂).

207
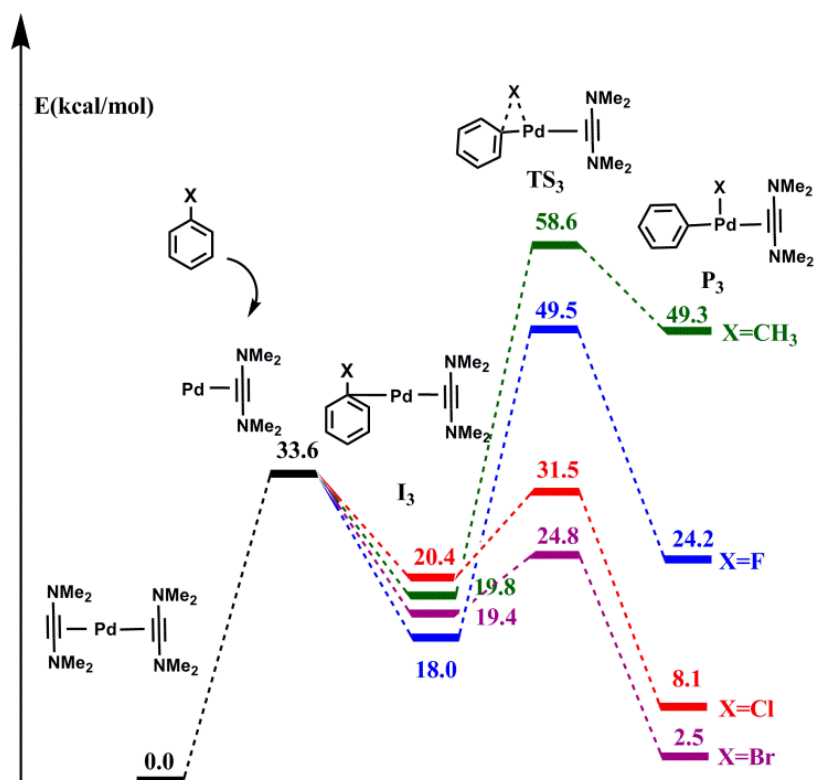
Figure 4.7 Illustration of the energy profile describing the oxidative addition of Ph-X to Pd(C$_2$(NMe$_2$)$_2$).

Table 4.15 Alkyne ligands and the corresponding energy barriers on addition of Ph-X to Pd(alkynes)

Ligand	E$_{act}$ on adding Ph-Br	E$_{act}$ on adding Ph-Cl	E$_{act}$ on adding Ph-F	E$_{act}$ on adding Ph-Me
C$_2$(NH$_2$)$_2$	5.9	11.9	32.6	39.1
C$_2$(NMe$_2$)$_2$	5.4	11.1	31.5	38.8
C$_2$Me$_2$	5.6	12.8	33.8	39.4
C$_2$(SiMe$_3$)$_2$	4.9	12.0	35.0	39.6
C$_2$Et$_2$	5.6	12.9	34.1	39.8
C$_2$Ph$_2$	7.1	13.6	34.9	41.2
C$_2$H$_2$	7.2	14.2	35.8	40.9

C$_2$Br$_2$	10.9	15.9	36.8	45.4
C$_2$Cl$_2$	11.2	16.1	36.9	45.6
C$_2$F$_2$	12.7	17.6	37.8	46.8

Energy profile diagram for oxidative addition of Ph-X to the active catalyst Pd(C$_2$(NMe$_2$)$_2$) is given in Figure 4.7. The E$_{dis}$ of Pd(C$_2$(NMe$_2$)$_2$)$_2$ is 33.6 kcal/mol. For Ph-Br, Ph-Cl, Ph- F and Ph-Me, the adduct **I$_3$** formation takes place respectively at relative energies 19.4, 20.4, 18.0 and 19.8 kcal/mol. With respect to **I$_3$**, the oxidative addition is significantly exothermic for Ph-Cl and Ph-Br whereas the reaction is highly endothermic for Ph-Me and Ph-F. All E$_{act}$ values for adding Ph-X to Pd-alkynes are given in Table 4.15.
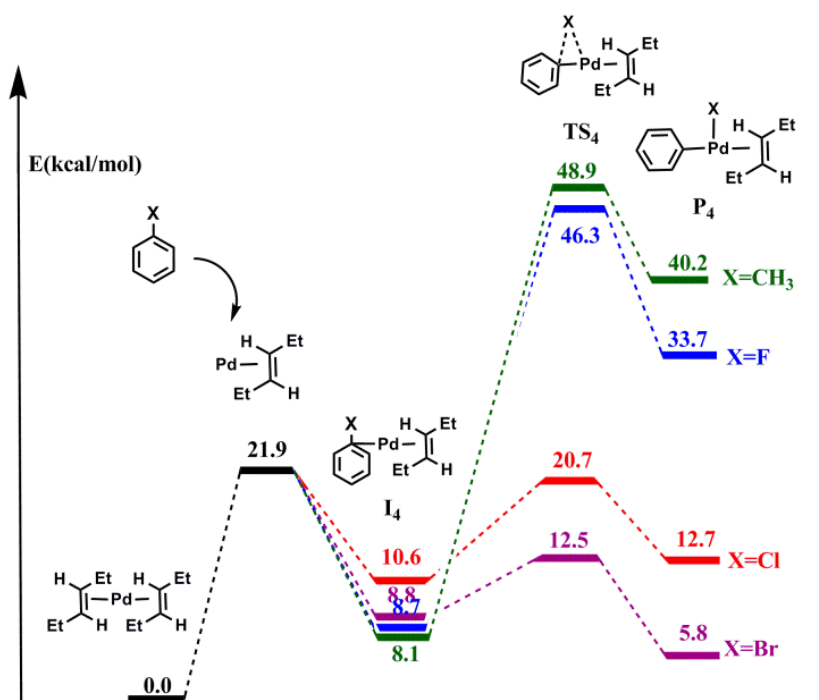
Figure 4.8 Illustration of the energy profile describing the oxidative addition of Ph-X to Pd(CH$_2$CEt$_2$).

The presence of F substituent in alkyne ligand gives the highest E$_{act}$ in all the four cases of additions, *viz.*, 12.7, 17.6, 37.8 and 46.8 for Ph-Br, Ph-Cl, Ph-F and Ph-Me, respectively. Among all, the alkyne with NMe$_2$ substituent gives the least E$_{act}$, *viz.,* 5.4,

11.1, 31.5 and 38.8 kcal/mol, respectively for Ph-Br, Ph-Cl, Ph-F and Ph-Me which are even less than that of phosphine complexes except for the case of Ph-Br. These results support the findings of Ahlquist et al. that alkynes are excellent ligands for Pd(0) complexes for oxidative addition reactions.[32]

Table 4.16 Alkene ligands and the corresponding energy barriers on addition of Ph-X to Pd(alkenes)

Ligand	E_{act} on adding Ph-Br	E_{act} on adding Ph-Cl	E_{act} on adding Ph-F	E_{act} on adding Ph-Me
CH_2CMe_2	4.7	11.1	39.2	41.6
CH_2CEt_2	3.7	10.2	37.6	40.8
CH_2CH_2	5.8	12.3	40.2	43.0
$CH_2C(SiMe_3)_2$	5.6	12.0	39.4	43.1
CH_2CPh_2	5.3	11.9	39.4	42.6
CH_2CCl_2	9.1	15.6	43.5	44.9
CH_2CBr_2	9.4	15.9	43.8	45.1
CH_2CF_2	8.7	15.3	43.4	45.1
$CH_2(CF_3)_2$	12.1	18.4	46.4	46.9
$CH_2(CN)_2$	12.5	18.8	47.0	48.0

Energy profile diagram for oxidative addition of Ph-X to a representative Pd-alkene complex, Pd(CH_2CEt_2) is given in Figure 4.8. The E_{dis} is 21.9 kcal/mol for this complex. Association of Ph-X to the mono ligated complex leads to the formation of the adduct **I₄**. The adduct formation stabilizes the complex by 8 - 11 kcal/mol. The oxidative addition of Ph-F and Ph-Me are highly endothermic and passes through high energy transition states (**TS₄**) whereas moderate values of E_{act}, *viz.* 10.1 and 13.7 kcal/mol are observed for the cleavage of Ph-Cl and Ph-Br bonds, respectively. Table 4.16 depicts the E_{act} values for adding the four substrates to the Pd(alkene) complex.

The least E_{act} is obtained for Pd(CH$_2$CEt$_2$) complex, *viz.* 3.7, 10.2, 37.6 and 40.8 kcal/mol, respectively for Ph-Br, Ph-Cl, Ph-F, and Ph-Me. Alkenes with electron donating ligands appear as excellent ligands for palladium. The presence of substituents CF$_3$ and CN makes the ligand electron deficient leading to high E_{act} values. The relative energies of all adduct systems (**I$_1$** - **I$_4$**), transition states (**TS$_1$** - **TS$_4$**) and the product complexes (**P$_1$** - **P$_4$**) are provided in Table 4.17 – 4.20.

Table 4.17 Phosphines and corresponding relative energies of adduct (**I$_1$**), transition state (**TS$_1$**) and product (**P$_1$**) on adding different substrates to Pd(phosphines) (energies are given in kcal/mol)

Ligand	Ph-Br			Ph-Cl			Ph-F			Ph-Me		
	I$_1$	**TS$_1$**	**P$_1$**	**I$_1$**	**TS$_1$**	**P$_1$**	**I$_1$**	**TS$_1$**	**P$_1$**	**I$_1$**	**TS$_1$**	**P$_1$**
PCy$_3$	18.7	23.4	14.8	20.3	31.9	22.4	17.9	57.7	43.6	17.9	59.7	52.1
PtBu$_3$	17.2	21.7	13.5	18.7	30.1	20.9	16.4	55.6	41.4	16.4	58.6	50.5
PiPr$_3$	18.1	22.7	14.8	19.5	31.3	22.2	17.1	57.2	43.4	17.0	59.2	51.6
PMe$_3$	18.2	23.7	15.7	19.4	32.0	22.5	17.0	58.2	44.2	16.8	60.1	51.6
PEt$_3$	24.1	29.0	15.5	19.0	31.3	22.6	16.7	57.3	43.9	16.6	59.6	51.5
P(SiMe$_3$)$_3$	14.1	18.8	9.9	15.4	27.3	17.3	13.1	53.2	37.7	14.7	54.4	47.1
PHMePh	17.1	22.3	14.7	18.3	30.8	22.6	15.7	56.7	44.2	15.4	59.1	50.8
PPh$_3$	17.1	22.3	14.7	18.7	31.0	22.3	16.1	56.8	43.0	15.7	59.2	50.7
PH$_3$	12.9	19.5	13.2	13.9	27.7	20.1	11.4	54.8	42.2	10.8	54.9	47.2
P(Ph-F)$_3$	17.5	23.0	15.7	19.0	31.8	23.3	16.4	57.5	43.8	15.7	60.2	51.9
P(thiophene)$_3$	16.2	21.7	15.1	17.7	30.4	22.5	15.0	55.9	42.8	15.1	58.6	50.4
P(Ph-Cl)$_3$	17.3	23.0	15.8	18.8	31.8	23.6	16.3	57.7	44.0	15.6	60.0	52.0
P(SMe)$_3$	13.9	20.5	15.1	15.2	29.0	22.0	12.5	54.6	42.4	11.9	57.0	49.0
P(Ph-CF$_3$)$_3$	17.1	23.5	15.7	17.8	31.4	23.4	15.1	58.2	43.6	14.3	59.4	52.0
PH$_2$CF$_3$	12.4	20.5	15.0	13.7	29.0	22.0	10.8	55.9	43.9	9.6	55.8	49.2
PCl$_2$Ph	11.9	19.8	15.4	13.2	28.4	22.4	10.6	54.2	42.7	10.9	55.9	48.8
PCl$_2$CH$_3$	13.4	21.5	16.0	14.5	30.2	22.9	11.8	57.1	44.3	11.9	57.2	50.1
PCl$_3$	7.8	18.6	15.1	9.1	27.3	22.3	6.3	54.5	44.6	5.9	52.3	46.4
PCF$_3$	8.9	20.2	17.6	10.3	29.3	25.2	8.2	56.5	47.1	6.2	54.6	49.9
PF$_3$	8.5	20.4	17.9	9.6	28.9	25.0	7.7	56.5	47.6	6.5	53.7	48.9

Table 4.18 NHCs and corresponding relative energies of adduct (I_2), transition state (TS_2) and product (P_2) on adding different substrates to Pd(NHCs) (energies are given in kcal/mol)

Ligand	Ph-Br			Ph-Cl			Ph-F			Ph-Me		
	I_2	TS_2	P_2	I_2	TS_2	P_2	I_2	TS_2	P_2	I_2	TS_2	P_2
ImNMe$_2$H$_2$	25.7	30.3	20.5	26.8	38.3	27.3	25.1	63.7	48.0	26.6	65.6	56.0
ImNH$_2$H$_2$	25.7	30.4	16.8	26.7	38.4	23.4	24.7	64.5	43.0	26.2	65.2	56.1
ImNMe$_2$COOMe$_2$	26.0	30.9	21.6	27.1	39.2	29.0	25.4	64.8	49.8	26.6	66.2	57.0
ImNMe$_2$F$_2$	26.1	31.1	22.1	27.2	39.2	28.9	25.3	64.8	49.5	26.5	66.5	57.3
ImNMe$_2$Cl$_2$	25.9	30.8	21.8	27.0	38.9	28.6	25.1	64.5	49.3	26.3	66.3	56.9
ImNH$_2$F$_2$	25.9	31.1	17.7	27.0	39.3	24.3	24.9	65.6	43.2	26.0	65.9	57.1
ImNMe$_2$(CF$_3$)$_2$	26.3	31.6	23.2	27.5	39.9	30.2	25.5	65.6	50.8	26.6	67.1	58.3
ImN(CF$_3$)$_2$H$_2$	21.6	26.7	19.2	22.9	35.3	26.5	20.4	61.5	48.3	21.3	63.1	54.1
ImNMe$_2$CN$_2$	26.1	31.8	23.9	27.3	40.1	30.8	25.3	65.9	51.2	26.1	67.8	58.8
ImNMe$_2$NO$_2$	25.9	31.9	24.4	27.1	40.4	31.7	25.0	66.2	51.7	24.2	67.3	59.2

Table 4.19 Alkynes and corresponding relative energies of adduct (I_3), transition state (TS_3) and product (P_3) on adding different substrates to Pd(alkynes) (energies are given in kcal/mol)

Ligand	Ph-Br			Ph-Cl			Ph-F			Ph-Me		
	I_3	TS_3	P_3	I_3	TS_3	P_3	I_3	TS_3	P_3	I_3	TS_3	P_3
C$_2$(NH$_2$)$_2$	18.8	24.7	13.9	19.7	31.6	9.1	17.2	49.8	40.2	18.7	57.9	49.9
C$_2$(NMe$_2$)$_2$	19.4	24.8	2.5	20.4	31.5	8.1	18.0	49.5	24.2	19.8	58.6	49.3
C$_2$Me$_2$	13.1	18.7	10.7	14.0	26.9	17.3	11.6	45.4	24.2	12.8	52.2	43.9
C$_2$(SiMe$_3$)$_2$	13.9	18.7	4.7	15.1	27.1	9.6	12.7	47.7	26.6	14.0	53.6	45.5
C$_2$Et$_2$	13.1	18.7	10.9	14.1	27.0	17.6	11.7	45.8	38.7	12.9	52.6	44.3
C$_2$Ph$_2$	13.6	20.7	12.5	15.1	28.6	19.8	12.8	47.7	40.5	13.5	54.7	46.9
C$_2$H$_2$	15.7	23.0	9.1	16.9	31.1	13.8	14.3	50.1	31.2	15.1	56.1	49.4
C$_2$Br$_2$	15.9	26.8	12.8	17.8	33.6	17.5	16.1	53.0	34.5	13.8	59.2	54.4
C$_2$Cl$_2$	16.6	27.8	14.4	18.5	34.6	19.0	16.8	53.7	35.8	14.5	60.1	55.6
C$_2$F$_2$	20.3	33.0	20.3	22.2	39.7	24.8	20.8	58.5	40.9	18.2	64.9	61.6

212

Table 4.20 Alkenes and corresponding relative energies of adduct (**I₄**), transition state (**TS₄**) and product (**P₄**) on adding different substrates to Pd(alkenes) (energies are given in kcal/mol)

Ligand	Ph-Br			Ph-Cl			Ph-F			Ph-Me		
	I_4	TS_4	P_4	I_4	TS_4	P_4	I_4	TS_4	P_4	I_4	TS_4	P_4
CH_2CMe_2	7.1	11.8	5.0	8.8	20.0	11.7	6.4	45.6	33.0	6.3	47.9	39.1
CH_2CEt_2	8.8	12.5	5.8	10.6	20.7	12.7	8.7	46.3	33.7	8.1	48.9	40.2
CH_2CH_2	10.8	16.7	12.2	12.6	24.8	18.9	10.7	50.9	40.3	9.6	52.6	45.3
$CH_2C(SiMe_3)_2$	7.6	13.2	7.9	9.6	21.6	15.2	6.8	46.2	35.5	6.1	49.2	42.8
CH_2CPh_2	6.1	11.5	4.4	8.1	20.0	11.5	6.1	45.5	32.5	5.0	47.6	38.3
CH_2CCl_2	3.7	12.8	9.0	5.6	21.2	15.7	3.9	47.3	36.7	2.4	47.3	40.6
CH_2CBr_2	5.7	15.1	11.5	7.6	23.5	18.2	5.6	49.5	40.0	4.2	49.3	42.5
CH_2CF_2	2.5	11.2	6.7	4.3	19.5	13.4	2.5	45.9	35.0	1.2	46.3	38.7
$CH_2(CF_3)_2$	3.3	15.4	13.9	5.5	24.0	21.2	3.9	50.2	42.7	1.8	48.7	44.8
$CH_2(CN)_2$	1.6	14.1	13.0	3.7	22.6	20.1	2.0	48.9	41.7	-0.9	47.1	43.6

4.4.4 Correlation Plot of ΔV_{Pd2} vs. E_{act}

Figure 4.9 depicts ΔV_{Pd2} versus E_{act} correlation plots corresponding to phosphines, NHCs, alkynes and alkenes. All cases show excellent linear correlations which strongly suggests that MESP at palladium nucleus serves as an effective electronic parameter for predicting E_{act}. From the linear equations in the graph, the unknown E_{act} of a ligand can be calculated by knowing the ΔV_{Pd} value. The E_{act} increases with increase in ΔV_{Pd2} value (from negative to positive), meaning that improving the electron density at Pd nucleus by appropriate ligation can improve the efficiency of oxidative addition. It is evident from the correlation that, all the ligands behave in a similar fashion with respect to the substrates since the slope of the graph is fairly close for most of them.
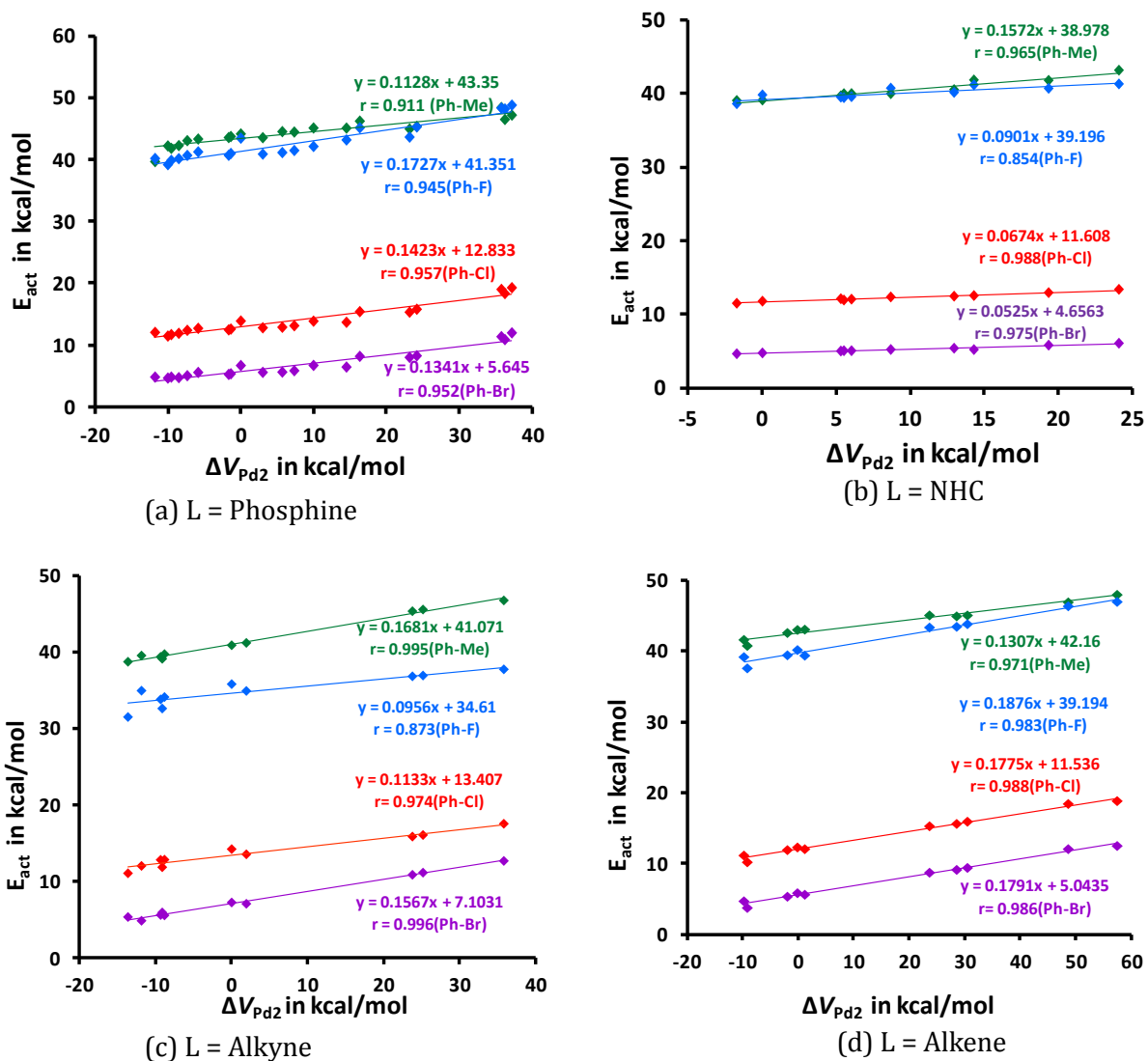
Figure 4.9 The correlation between activation barrier (E_act) and relative MESP at the Pd nucleus of Pd-L (ΔV_{Pd2}). (a) L = Phosphine (b) L = NHC (c) L = alkyne (d) L = alkene

Among all the substrates, Ph-Me is the most difficult to cleave by oxidative addition followed by Ph-F. In Pd(phosphine), Pd(NHC) and Pd(akene), complexes, Ph-Me and Ph-F show similar reactivity towards oxidative addition whereas in Pd(alkyne), reactivity of Ph-F is significantly higher than that of Ph-Me. The Pd(alkyne) complex formed with electron rich ligands emerged as the most promising systems for activating Ph-F bonds under oxidative addition conditions.

4.4.5 Benchmark Study

A benchmark study has been carried out to understand the effect of solvation (solvent = THF) and dispersion, for that the reaction of aryl bromide with a selected set of 15 phosphine coordinated complexes are selected. Table 4.21 and Table 4.22 provide E_{act} and ΔV_{Pd2} values in kcal/mol calculated at B3LYP-D3/BS1 and B3LYP-D3/BS2 level of theory respectively. Figure 4.10 and Figure 4.11 gives the corresponding correlation plots between E_{act} and ΔV_{Pd2} values. The results for the tested systems show close similarity to the B3LYP/BS1 results.

y = 0.084x + 6.0203
r = 0.982

Figure 4.10 The correlation between dispersion-corrected activation barrier (E_{act}) and relative MESP at the Pd nucleus of Pd(phosphine). Solvent used is THF. At B3LYP/6-31+G(d,p) basis set for all atoms except Pd, and Lanl2DZ basis set for Pd.

Table 4.21 Dispersion corrected and solvation incorporated (solvent=THF), E_{act} and V_{Pd2} values in kcal/mol (at B3LYP/6-31+G(d,p) basis set for all atoms except Pd, and Lanl2DZ basis set for Pd)

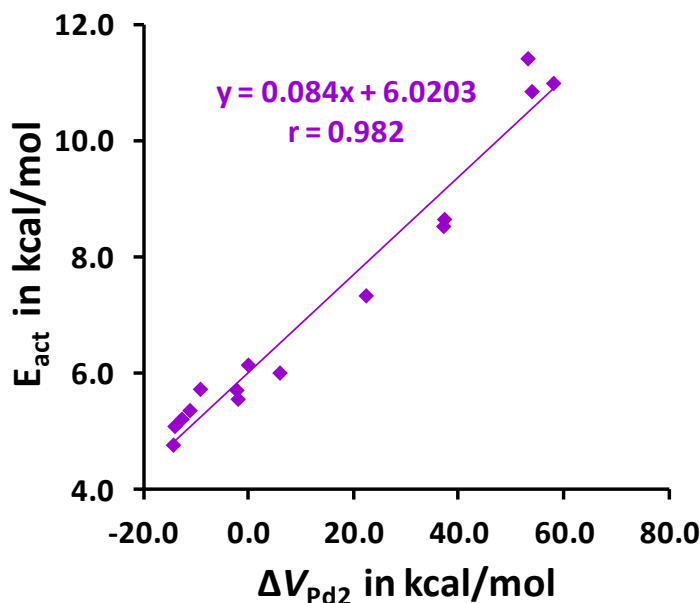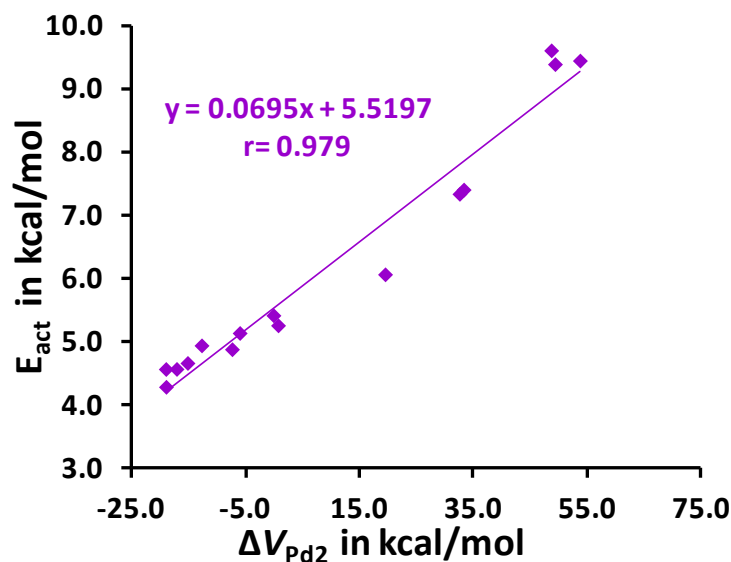| Ligand	Dispersion Corrected	
	E_{act}	ΔV_{Pd2}
PCy$_3$	5.1	-14.0
PtBu$_3$	4.8	-14.3
PiPr$_3$	5.2	-12.6
PMe$_3$	5.7	-9.1
PEt$_3$	5.4	-11.1
PHMePh	5.7	-2.2
PPh$_3$	5.6	-2.0
PH$_3$	6.1	0.0
P(thiophene)$_3$	6.0	6.0
PH$_2$CF$_3$	7.3	22.4
PCl$_2$Ph	8.5	37.2
PCl$_2$CH$_3$	8.7	37.3
PCl$_3$	11.0	58.1
PCF$_3$	10.8	54.0
PF$_3$	11.4	53.2

Figure 4.11 The correlation between dispersion-corrected activation barrier (E_{act}) and relative MESP at the Pd nucleus of Pd(phosphine). Solvent used is THF. At B3LYP/6-31+G(d,p) basis set for all atoms except Pd, and SDD basis set for Pd.

Table 4.22 Dispersion corrected and solvation incorporated (solvent=THF), E_{act} and V_{Pd2} values in kcal/mol. At B3LYP/6-31+G(d,p) basis set for all atoms except Pd, and SDD basis set for Pd

Ligand	Dispersion Corrected	
	E_{act}	ΔV_{Pd2}
PCy$_3$	4.5	-18.9
PtBu$_3$	4.3	-18.9
PiPr$_3$	4.6	-17.0
PMe$_3$	4.9	-12.6
PEt$_3$	4.6	-15.1
PHMePh	5.1	-5.9
PPh$_3$	4.9	-7.3
PH$_3$	5.4	0.0
P(thiophene)$_3$	5.2	0.8

PH$_2$CF$_3$	6.0	19.6
PCl$_2$Ph	7.3	32.7
PCl$_2$CH$_3$	7.4	33.4
PCl$_3$	9.4	53.9
PCF$_3$	9.4	49.5
PF$_3$	9.6	48.8

4.5 Conclusions

In summary, we have investigated the C-Br, C-Cl, C-F and C-C bond breaking *via* oxidative addition on monoligated palladium catalysts. MESP derived parameters V_{min} and V_{Pd} emerge as good measures to characterize the electron rich/poor character of the ligands and the complexes. Steric effect influences the absolute value of V_{min} to some extent while V_{Pd} reflects mostly the overall electronic effect of the ligand environment at the nucleus. Both MESP parameters undergo subtle variations with respect to change in the ligand environment. With respect to a reference complex - typically the complex coordinated with the unsubstituted ligand - the observed change in V_{Pd} (ΔV_{Pd}) gives a measure of electron donation to- or electron withdrawal from the metal center. A linear correlation is established between MESP at the Pd center and E$_{act}$. Ligands of electron donating nature favour oxidative addition reaction. Thus, use of ligands showing strong electron rich character can be proposed as a common strategy for designing efficient catalysts susceptible for oxidative addition. Alkenes and alkynes have shown excellent ligand property to oxidative addition by Pd(0). Though the high energy barrier observed for adding Ph-F and Ph-Me is suggesting a non-feasible reaction, the ΔV_{Pd} versus E$_{act}$ correlations aid us to develop feasible oxidative additions by tuning V_{Pd} *via* appropriate ligands. In summary, the MESP based electronic parameter V_{Pd} emerges as an easy tool for fine tuning the reactivity of the Pd(0) catalysts.

4.6 References

1. C. Amatore and A. Jutand, *Acc. Chem. Res.*, **2000**, *33*, 314-321.

2. E. Negishi, *Acc. Chem. Res.*, **1982**, *15*, 340-348.

3. N. Miyaura, K. Yamada and A. Suzuki, *Tetrahedron Lett.*, **1979**, *20*, 3437-3440.

4. J. K. Stille, *Angew. Chem. Int. Ed.*, **1986**, *25*, 508-524.

5. Z. Novák, A. Szabó, J. Répási and A. Kotschy, *J. Org. Chem.*, **2003**, *68*, 3327-3329.

6. M. García-Melchor, A. A. C. Braga, A. Lledós, G. Ujaque and F. Maseras, *Acc. Chem. Res.*, **2013**, *46*, 2626-2634.

7. A. F. Littke and G. C. Fu, *Angew. Chem. Int. Ed.*, **2002**, *41*, 4176-4211.

8. N. Marion and S. P. Nolan, *Acc. Chem. Res.*, **2008**, *41*, 1440-1449.

9. H. Li, C. C. Johansson Seechurn and T. J. Colacot, *ACS Catal.*, **2012**, *2*, 1147-1164.

10. P. G. Gildner and T. J. Colacot, *Organometallics*, **2015**, *34*, 5497-5508.

11. A. Molnár, *Chem. Rev.*, **2011**, *111*, 2251-2320.

12. U. Christmann and R. Vilar, *Angew. Chem. Int. Ed.*, **2005**, *44*, 366-374.

13. L. J. Goossen, D. Koley, H. L. Hermann and W. Thiel, *Organometallics*, **2005**, *24*, 2398-2410.

14. F. Barrios-Landeros, B. P. Carrow and J. F. Hartwig, *J. Am. Chem. Soc.*, **2009**, *131*, 8141-8154.

15. E. Galardon, S. Ramdeehul, J. M. Brown, A. Cowley, K. K. Hii and A. Jutand, *Angew. Chem. Int. Ed.*, **2002**, *114*, 1838–1841.

16. M. Ahlquist and P.-O. Norrby, *Organometallics*, **2007**, *26*, 550-553.

17. M. Ahlquist, P. Fristrup, D. Tanner and P.-O. Norrby, *Organometallics*, **2006**, *25*, 2066-2073.

18. L. Xue and Z. Lin, *Chem. Soc. Rev.*, **2010**, *39*, 1692-1705.

19. S. Sakaki, M. Ogawa, Y. Musashi and T. Arai, *Inorg. Chem.*, **1994**, *33*, 1660-1665.

20. C. L. McMullin, J. Jover, J. N. Harvey and N. Fey, *Dalton Trans.*, **2010**, *39*, 10833-10836.

21. C. L. McMullin, N. Fey and J. N. Harvey, *Dalton Trans.*, **2014**, *43*, 13545-13556.

22. H. M. Senn and T. Ziegler, *Organometallics*, **2004**, *23*, 2980-2988.

23. K. W. Anderson, R. E. Tundel, T. Ikawa, R. A. Altman and S. L. Buchwald, *Angew. Chem. Int. Ed.*, **2006**, *45*, 6523-6527.

24. B. C. Hamann and J. F. Hartwig, *J. Am. Chem. Soc.*, **1998**, *120*, 7369-7370.

25. M. G. Organ, S. Avola, I. Dubovyk, N. Hadei, E. A. B. Kantchev, C. J. O'Brien and C. Valente, *Chem. Eur. J.*, **2006**, *12*, 4749-4755.

26. E. Peris and R. H. Crabtree, *Coord. Chem. Rev.*, **2004**, *248*, 2239-2246.

27. F. E. Hahn and M. C. Jahnke, *Angew. Chem. Int. Ed.*, **2008**, *47*, 3122-3172.

28. A. C. Hillier, G. A. Grasa, M. S. Viciu, H. M. Lee, C. Yang and S. P. Nolan, *J. Org. Chem.*, **2002**, *653*, 69-82.

29. M.-T. Lee and C.-H. Hu, *Organometallics*, **2004**, *23*, 976-983.

30. I. J. S. Fairlamb, *Org. Biomol. Chem.*, **2008**, *6*, 3645-3656.

31. S. Cacchi, M. Felici and B. Pietroni, *Tetrahedron Lett.*, **1984**, *25*, 3137-3140.

32. M. Ahlquist, G. Fabrizi, S. Cacchi and P.-O. Norrby, *Chem. Commun.*, **2005**, *0*, 4196-4198.

33. K. J. Bonney and F. Schoenebeck, *Chem. Soc. Rev.*, **2014**, *43*, 6609-6638.

34. D. W. Old, J. P. Wolfe and S. L. Buchwald, *J. Am. Chem. Soc.*, **1998**, *120*, 9722-9723.

35. L. M. Alcazar-Roman, J. F. Hartwig, A. L. Rheingold, L. M. Liable-Sands and I. A. Guzei, *J. Am. Chem. Soc.*, **2000**, *122*, 4618-4630.

36. A. Ariafard and Z. Lin, *Organometallics*, **2006**, *25*, 4030-4033.

37. K. C. Lam, T. B. Marder and Z. Lin, *Organometallics*, **2007**, *26*, 758-760.

38. Z. Li, Y. Fu, Q.-X. Guo and L. Liu, *Organometallics*, **2008**, *27*, 4043-4049.

39. F. Barrios-Landeros and J. F. Hartwig, *J. Am. Chem. Soc.*, **2005**, *127*, 6944-6945.

40. C. Amatore and A. Jutand, *J. Org. Chem.*, **1999**, *576*, 254-278.

41. M. Ahlquist, G. Fabrizi, S. Cacchi and P.-O. Norrby, *J. Am. Chem. Soc.*, **2006**, *128*, 12785-12793.

42. A. K. d. K. Lewis, S. Caddick, F. G. N. Cloke, N. C. Billingham, P. B. Hitchcock and J. Leonard, *J. Am. Chem. Soc.*, **2003**, *125*, 10066-10073.

43. S. Kozuch, C. Amatore, A. Jutand and S. Shaik, *Organometallics*, **2005**, *24*, 2319-2330.

44. S. Kozuch, S. Shaik, A. Jutand and C. Amatore, *Chem. Eur. J.*, **2004**, *10*, 3072-3080.

45. C. A. Fleckenstein and H. Plenio, *Chem. Soc. Rev.*, **2010**, *39*, 694-711.

46. J. F. Hartwig and F. Paul, *J. Am. Chem. Soc.*, **1995**, *117*, 5373-5374.

47. E. A. Mitchell, P. G. Jessop and M. C. Baird, *Organometallics*, **2009**, *28*, 6732-6738.

48. J. Mathew and C. H. Suresh, *Organometallics*, **2011**, *30*, 1438-1444.

49. K. S. Sandhya, G. S. Remya and C. H. Suresh, *Inorg. Chem.*, **2015**, *54*, 11150-11156.

50. K. S. Sandhya and C. H. Suresh, *Dalton Trans.*, **2014**, *43*, 12279-12287.

51. B. A. Anjali, F. B. Sayyed and C. H. Suresh, *J. Phys. Chem. A*, **2016**, *120*, 1112-1119.

52. B. A. Anjali and C. H. Suresh, *New J. Chem.*, **2018**, *42*, 18217-18224.

53. B. A. Anjali and C. H. Suresh, *J. Comput. Chem.*, **2018**, *39*, 881-888.

54. S. Grimme, *J. Comput. Chem.*, **2006**, *27*, 1787-1799.

55. A. V. Marenich, C. J. Cramer and D. G. Truhlar, *J. Phys. Chem. B*, **2009**, *113*, 6378-6396.

56. M. J. Frisch, G. W. Trucks, H. B. Schlegel, G. E. Scuseria, M. A. Robb, J. R. Cheeseman, G. Scalmani, V. Barone, B. Mennucci, G. A. Petersson, H. Nakatsuji, M. Caricato, X. Li, H. P. Hratchian, A. F. Izmaylov, J. Bloino, G. Zheng, J. L. Sonnenberg, M. Hada, M. Ehara, K. Toyota, R. Fukuda, J. Hasegawa, M. Ishida, T. Nakajima, Y. Honda, O. Kitao, H. Nakai, T. Vreven, J. J. A. Montgomery, J. E. Peralta, F. Ogliaro, M. Bearpark, J. J. Heyd, E. Brothers, K. N. Kudin, V. N. Staroverov, T. Keith, R. Kobayashi, J. Normand, K. Raghavachari, A. Rendell, J. C. Burant, S. S. Iyengar, J. Tomasi, M. Cossi, N. Rega, J. M. Millam, M. Klene, J. E. Knox, J. B. Cross, V. Bakken, C. Adamo, J. Jaramillo, R. Gomperts, R. E. Stratmann, O. Yazyev, A. J. Austin, R. Cammi, C. Pomelli, J. W. Ochterski, R. L. Martin, K. Morokuma, V. G. Zakrzewski, G. A. Voth, P. Salvador, J. J. Dannenberg, S. Dapprich, A. D. Daniels, O. Farkas, J. B. Foresman, J. V. Ortiz, J. Cioslowski and D. J. Fox, *Gaussian 09*, Revision D.01; Gaussian Inc., Wallingford CT, **2013**.

57. J. Mathew, T. Thomas and C. H. Suresh, *Inorg. Chem.*, **2007**, *46*, 10800-10809.

58. C. H. Suresh and N. Koga, *Inorg. Chem.*, **2002**, *41*, 1573-1578.

59. M. J. Ajitha and C. H. Suresh, *J. Org. Chem.*, **2012**, *77*, 1087-1094.

60. A. Kumar, S. R. Gadre, N. Mohan and C. H. Suresh, *J. Phys. Chem. A*, **2014**, *118*, 526-532.

61. N. Mohan, C. H. Suresh, A. Kumar and S. R. Gadre, *Phys. Chem. Chem. Phys.*, **2013**, *15*, 18401-18409.

List of Publications

(i) Articles in journals

1. Correlation and Prediction of Redox Potentials of Hydrogen Evolution Mononuclear Cobalt Catalysts *via* Molecular Electrostatic Potential: A DFT Study. **B. A. Anjali**, F. B Sayyed, C. H. Suresh, *J. Phys. Chem. A,* **2016**, 120, 1112-1119.

2. Interpreting Oxidative Addition of Ph–X (X = CH$_3$, F, Cl, and Br) to Monoligated Pd(0) Catalysts using Molecular Electrostatic Potential. **B. A. Anjali** and C. H. Suresh, *ACS Omega,* **2017**, 2, 4196-4206.

3. Predicting Reduction Potentials of 1,3,6-Triphenyl Fulvenes Using Molecular Electrostatic Potential Analysis of Substituent Effects. **B. A. Anjali** and C. H. Suresh, *J. Comput. Chem.,* **2018**, 39, 881-888.

4. Electronic Effect of Ligands vs. Reduction Potentials of Fischer Carbene Complexes of Chromium: A Molecular Electrostatic Potential Analysis. **B. A. Anjali** and C. H. Suresh, *New J. Chem.,* **2018**, 42, 18217-18224.

5. Absorption and Emission Properties of 5-Phenyl Tris(8-hydroxyquinolinato) M(III) Complexes (M = Al, Ga, In) and Correlations with Molecular Electrostatic Potential. **B. A. Anjali** and C. H. Suresh. (to be submitted)

(ii) Published contributions to academic conferences

1. Presented a poster entitled "Predicting Redox Potentials of Hydrogen Evolution Cobalt Catalysts using Molecular Electrostatic Potential" at the Modeling Chemical and Biological (Re) Activity (MCBR4) meeting, Heidelberg University, Germany. February 2015.

2. Presented a poster entitled "Oxidative Addition of Aryl Halides to Monoligated Palladium (0) Catalysts: A DFT Study" at the Theoretical

Chemistry Symposium, University of Hyderabad, Hyderabad, India. December 2016.

3. Presented a paper entitled Interpreting "Oxidative Addition of Ph–X (X= CH_3, F, Cl, and Br) to Monoligated Pd (0) Catalysts using Molecular Electrostatic Potential" at the 30th Kerala Science Congress, Govt. Brennen College, Thalassery, Kerala, India, January 2018.